Trace element interactions in nutrient transfer during early development and later in life

Dissertation

Zur Erlangung des Doktorgrades
der Naturwissenschaften (Dr. rer. nat.) im Fachbereich Chemie
der Mathematisch-Naturwissenschaftlichen Fakultät
der Bergischen Universität Wuppertal

vorgelegt von
Vivien Michaelis
aus Wuppertal
– 2022 –

Dekan:in: ..... Prof. Dr. Stefan F. Kirsch

Erste:r Gutachter:in: ..... Prof. Dr. Julia Bornhorst

Zweite:r Gutachter:in: ..... Prof. Dr. Martin Simon

Tag der mündlichen Prüfung: 26.10.2022

“I am among those who think that science has great beauty.
A scientist in his laboratory is not only a technician: he is also a child placed before natural phenomena which impress him like a fairy tale.”

(Marie Curie)

Für meine Familie

Introductory remarks to the structure of the dissertation

This semi-cumulative dissertation is mainly based on first- or co-authorship publications published in or submitted to peer-reviewed journals (chapter 4 – 6) and therefore include remarks and suggestions of all first- or co-authors involved in manuscript preparation or reviewer and journal editor comments obtained during the peer-reviewing process. Furthermore, chapter 3 focuses on unpublished data of method development of the applied cell culture system. Since the introduction of each publication gives a more detailed overview about the state of research, chapter 1 and 2 will give general background information about the entirety of the project, whereas chapter 7 will summarize the project following a general discussion and outlook.

For reasons of clarity and comprehensibility it was chosen to combine all publications, unpublished data and applied bibliography. However, the original structure and style of each publication was altered in order to give a consistent structure, and is rewritten in American English. Despite the standard of each journal, differences and inconsistency in abbreviations, nomenclature and structure might be apparent. The reference of each publication is clearly highlighted at the beginning of each chapter.

The entire thesis contains nomenclature of human genes and proteins. Whereas human genes are spelled in italicized capital letter (e.g. *ACTB* for human β-actin) proteins are spelled in non-italicized capital letters (e.g. FTH for human ferritin heavy chain) and mice genes in italicized first capital letter (e.g. *Dmt1* for mouse divalent metal transporter 1).

Table of Contents

Figure and Table Legends

Figures

Figures – Supplementary Material

Tables

Tables – Supplementary Material

List of Abbreviations

(v/v)	volume fraction
(w/v)	weight fraction
[Zn^{2+}]	labile zinc
3R	Refinement, Reduction and Replacement
5-HT	5-hydroxytryptamine
8OHdG	8-hydroxyguanosine
8oxodG	8-oxo-7,8-dihydro-2′-guanine
A	area of microporous insert
ABC	ATP binding cassette
Ac-DEVD-AFC	N-acetyl-asp-glu-val-asp-7-amino-4-trifluoromethylcoumarin
ACP	average total acid phosphatase
ACTB	gene encoding human β-actin
AD	Alzheimer's disease
AFB1	Aflatoxin B1
AFC	7-amino-4-trifluoromethylcoumarin
AI	adequate intake
ALT	alanine transaminase
AMP	adenosine monophosphate
AMPA	α-amino-3-hydroxy-5-methyl-4-isoxazole-propionic acid/kainate channel
AP sites	apurinic/ apyrimidinic sites
apo-Tf	unbound transferrin
ARE	antioxidant response element
AST	aspartate transaminase
ATP	adenosine triphosphate
ATP13A2	ATPase 13A2
Aβ	amyloid beta
BBB	blood-brain barrier
BCA	bicinchoninic acid
B-CSF-B	blood-cerebrospinal fluid barrier
BER	base excision repair
BHT	butylated hydroxytoluene
BSA	bovine serum albumin
c_0	concentration at the start of incubation
Ca	calcium

cAMP	cyclic AMP
Carboxy-DCFH-DA	5-(&6)-carboxy-2',7'-dichloro-dihydrofluorescein-diacetate
CAT	catalase
CDG	congenital disorders of glycosylation
cDNA	complementary DNA
CE-ICP-MS	capillary electrophoresis chromatography-inductively coupled plasma mass spectrometry
CNS	central nervous system
CSF	cerebrospinal fluid
Cu	copper
CuZnSOD	copper-zinc superoxide dismutase
CYP450	cytochrome P450
DART	Developmental and Reproductive Toxicity
dC	deoxycytidine
DcytB	duodenal cytochrome B
DGE	German Nutrition Society
DMEM	Dulbecco's Modified Eagle's Medium
DMT1	divalent metal transporter
DNA	deoxyribonucleic acid
dsDNA	double-stranded DNA
EC	endothelial growth medium
ECL	enhanced chemiluminescence
EFSA	European Food Safety Authority
ELISA	enzyme-linked immunosorbent assay
Em	emission
ERK	extracellular signal-regulated kinase
ESI+	electrospray ionization in positive ion mode
EtHg	ethyl mercury
Ex	extinction
F	fluorescence
FCS	fetal calf serum
Fe	iron
FGR	fetal growth restriction
F_{min}	minimal fluorescence
F_{max}	maximal fluorescence
FPN	ferroportin

FTH	ferritin heavy chain
FTL	ferritin light chain
GDNF	glial-derived neurotrophic factor
GLUT1	glucose transporter 1
GPx	glutathione peroxidase
GST	glutathione-S-transferase
hCG	human chorionic gonadotropin
HFE	homeostatic iron regulator
Hg	mercury
HIF	hypoxia-inducible factor
HMOX1	heme oxygenase 1
HPEC	human venous endothelial cells
HPVEC	human placental vascular endothelial cells
HRP	horseradish peroxidase
HUVEC	human umbilical vein cells
IB	incubation buffer
ICP-MS/MS	inductively coupled plasma-tandem mass spectrometry
ICP-OES	inductively coupled plasma-optical emission spectrometry
IRE	iron responsive element
IREB	iron responsive element binding protein
IRP	iron regulatory protein
IS	internal standard
IVNAA	*in vivo* neutron activation analysis
JNK	c-Jun terminal kinase
K_D	dissociation constant
KEAP	Kelch-like ECH-associated protein 1-nuclear factor
LA:DGLA	linolenic acid:dihomo-ɣ-linolenic acid ratio
LDH	lactate dehydrogenase
L-glu	L-glutamine
LUHMES	Lund human mesencephalic cells
MAPK	mitogen-activated protein kinase
MB	measurement buffer
MeHg	methyl mercury
MEM	Eagle's minimum essential medium
Mn	manganese
MnSOD	manganese superoxide dismutase

MRI	magnetic resonance imaging
mRNA	messenger RNA
MT	metallothionein
MTF1	metal regulatory transcription factor 1
mTOR	mammalian target of rapamycin
NAC	N-acetyl cysteine
NADH	nicotinamide adenine dinucleotide
NaFlu	sodium fluorescein
NEA	Non-essential amino acids
NF-κB	Nuclear Factor kappa B
NOAEL	no observed adverse effect level
Nrf2	Nuclear Factor Erythroid 2-related Factor 2
NTBI	non-transferrin bound iron
OECD	Organization for Economic Co-operation and Development
P	permeability
PAR	Poly(ADP-ribose)
PARylation	Poly(ADP-ribosyl)ation
PBCEC	porcine brain capillary endothelial cells
PBS	phosphate buffered saline
PD	Parkinson's disease
PE	preeclampsia
Pen/Strep	penicillin/ streptomycin
PFA	para-formaldehyde
PN	parenteral nutrition
PRI	Population Reference Intake
QQQ	triple quadrupole
RNA	ribonucleic acid
RONS	reactive oxygen and nitrogen species
ROS	reactive oxygen species
RPMI	Roswell Park Memorial Institute
RT	room temperature
rt	retention time
RT-qPCR	real-time quantitative polymerase chain reaction
s	seconds
SD	standard deviation
SDS-PAGE	sodium dodecyl sulfate-polyacrylamide gel electrophoresis

Se	selenium
SEC-DRP-ICP-MS	size exclusion chromatography-inductively coupled plasma-dynamic reaction cell-mass spectrometry
SLC	solute carrier protein family
SOD	superoxide dismutase
SPCA1	Ca^{2+}-ATPase isoform 1
ssDNA	single-stranded DNA
sTfR	soluble transferrin
t	time
TE	trace element
TEER	transepithelial electrical resistance
Tf	transferrin
TfR	transferrin receptor
TIMS-ToF	trapped ion mobility spectrometry-time of flight mass spectrometry
TNF-α	tumor necrosis factor alpha
TPEN	N,N,N',N'-tetrakis(2-pyridinylmethyl)-1,2-ethanediamine
TrxR	thioredoxin reductase
T-TBS	Tris buffered saline containing 0.1 % Tween® 20
UL	upper limit
UTR	untranslated region
WHO	World Health Organization
ZIP	Zrt-/ Irt-like protein
Zn	zinc
ZnT	zinc transporter
ZO-1	zonula occludens-1
ZPP	zinc protoporphyrin
ZSI	zinc status index
ΔQ	basolateral trace element amount

Summary

Trace elements (TE), such as manganese (Mn), iron (Fe), and zinc (Zn) are often considered regarding their essentiality and their role as important co-factors maintaining regulating processes involved in macronutrient metabolism, hematopoiesis, anti-inflammatory, and anti-oxidative defense mechanisms. Although essential, (chronic) overexposure has been shown to adversely affect human health. Mn, Fe, and Zn accumulation in brain tissue of patients suffering from neurodegenerative diseases have been associated with the pathogenesis of Parkinson's (PD) and Alzheimer's disease (AD). Furthermore, metal overexposure, leading to impaired fetal (neuro)development and adverse pregnancy outcomes became also a rising concern. Whereby one of the main discussed pathways includes the generation of reactive oxygen species (ROS), resulting as the cause or consequence of disrupted metal homeostasis.

Several institutions like the European Food Safety Authority (EFSA) or the German Nutrition Society (DGE) have evaluated data on Mn, Fe, and Zn uptake, distribution, and excretion to assess TE intake recommendations for the general population. As food does contain a mixture of the TEs in different bioavailable and non-bioavailable forms, the effect of TE mixtures and TE interactions in metal bioavailability is of central importance. This rather represents the nutrition scenario of the general population than isolated Mn, Fe, and Zn uptake. However, to date data on TE interrelations in the general population but also in micronutrient acquisition for the developing fetus is scarce. Therefore, this thesis aims to elucidate fundamentals in TE transfer and interactions as well as potential organ- and cell-specific differences in metal bioavailability. For this, several *in vitro* models were utilized to unveil a potential reciprocal impact on three physiological different organs, specifically the placenta, the liver, and the brain.

To investigate micronutrient transfer across placental barrier-building cells, a Transwell®-based *in vitro* system of human villous trophoblasts was established. Human villous trophoblasts were modeled by using the BeWo b30 cell line, which resembles a trophoblast-like phenotype regarding polarization, barrier formation, and expression of a variety of transporters involved in TE homeostasis. Barrier characteristics such as integrity and permeability were determined by measuring the transepithelial electrical resistance (TEER), the exclusion of sodium fluorescein, and immunocytochemical staining of the tight junction proteins γ-catenin, zonula occludens-1, and the microtubule protein tubulin. Due to the

absence of contact inhibition in BeWo b30 cells, the formation of a monolayer had to be monitored precisely to obtain a reliable, reproducible *in vitro* system.

Using the established BeWo b30 Transwell® system facilitated the investigation of Mn transfer across the trophoblasts of the placental barrier due to the simplicity of the monolayer and short culture times. Since data on placental Mn transfer relies on rodent data and extrapolations from placenta-independent studies, comparing transfer kinetics with the further clarified placental Fe transfer was advantageous to reveal similarities and differences between these two TEs. Mn and Fe transfer, as well as cellular Mn and Fe amounts, were assessed via inductively coupled plasma-based spectrometry. In a mechanistic approach, gene and protein expression of TE transport-, storage-, and oxidative stress-associated genes revealed potential mechanisms of Mn and/or Fe transfer across the trophoblast layer. While Mn transfer has been shown to be time- but not concentration-dependent (normalized to the applied dose), Fe transfer showed clear concentration-dependent effects. Concurrent Mn and Fe exposure revealed increased Fe transfer and decreased Mn transfer combining a 10-fold less Fe concentration with Mn. Hereby, Mn was highly affecting the protein expression of the Fe storage proteins ferritin heavy and light chain.

Since the liver is predominantly involved in metal homeostasis by regulating distribution to other compartments and organs, it is one of the main targets of metal-induced toxicity. While impaired liver function has been associated with Mn accumulation, due to disturbed hepatobiliary Mn excretion, Zn is known to serve as a cytoprotective, antioxidative, and anti-inflammatory micronutrient. However, the role of Zn in liver Mn homeostasis and vice versa is widely unknown. Utilizing the human hepatoma cell line HepG2 offered the ability to investigate hepatocyte-specific alterations in Mn and Zn bioavailability and cytotoxicity *in vitro*. For this Mn and Zn cytotoxicity and bioavailability were determined after short- and long-term Zn preincubation in HepG2 cells via inductively coupled plasma-based spectrometry and cytotoxicity markers such as cell number, metabolic activity as well as apoptosis and necrosis markers, specifically caspase-3 activation and lactate dehydrogenase (LDH) release. The underlying study revealed protective effects of Zn on Mn cytotoxicity in terms of enhanced cell count, decreased caspase-3 activation, and LDH release. This may be attributed to the decreased Mn bioavailability in HepG2 cells after concurrent exposure with Zn. While alterations in gene expression do not fully explain decreased Mn bioavailability, they hint at the potential induction of antioxidative defense mechanisms, since metallothionein (MT)

expression was upregulated after single Mn treatment. Fluorescence probe-based assessment of labile “free” Zn as a potential novel Zn biomarker, supported the notion of Mn-induced Zn binding to MTs.

Due to their high metabolic turnover, neurons are highly susceptible to metal-induced oxidative stress resulting in neuronal damage and consequently neuronal death, one of the hallmarks of neurodegenerative diseases. Hereby, *in vivo* as well as *in vitro* studies have revealed enhanced Mn accumulation in the dopamine-rich areas of the brain, making dopaminergic neurons one of the main targets of Mn-induced neurotoxicity. As exact neurotoxic pathways and Mn-induced effects on neuronal DNA damage response and neurite outgrowth are rarely characterized, the last study revealed potential alterations in genome integrity in differentiated dopaminergic-like Lund human mesencephalic neurons (LUHMES). Furthermore, including this study in the context of this thesis offered the opportunity to get a wide overview of organ- or cell-specific alteration in metal bioavailability.

In summary, studies conducted in this thesis emphasized the relevance of cellular TE interrelations in TE transfer and distribution but also revealed a lack of knowledge regarding different metal mixtures and underlying mechanisms including the role of metal transporters. Even if cellular metal homeostasis is tightly regulated, *in vitro* studies conducted in this thesis revealed that different TEs do not only adversely affect the uptake of the other but also inherit protective effects towards TE-induced toxicity. Although TE interactions across the placental barrier have not been the focus of current research so far, and mechanisms of TE interactions in other tissues and organs are still unclarified further investigations on interrelated effects are urgently needed. This may improve the estimation of micronutrient intake recommendations for the general population but also sensitive populations like the expecting mother and her developing fetus.

Chapter 1 – Motivation and Scope of the Thesis

1.1. Motivation of the Thesis

Essential trace elements (TE) such as manganese (Mn), iron (Fe), and zinc (Zn) are required for the maintenance of a plethora of physiological processes in human metabolism. Whereas Mn, Fe, and Zn are mainly serving as co-factors for a variety of enzymes involved in macronutrient metabolism, antioxidative defense, and immune function. In order to sustain health, TE intake recommendations or requirements for the general population but also sensitive populations like pregnant women are proposed by authorities like the European Food Safety Authority (EFSA) or the German Society of Nutrition (DGE). Data considered for those recommendations are mainly based on TE bioavailability, gastrointestinal absorption, and excretion. Due to the ubiquitous occurrence of the TEs in drinking water and nutrition, following a balanced nutrition lifestyle is sufficient for an adequate nutrient supply [1-4].

Although essential, chronic overexposure of Mn, Fe as well as Zn may also lead to detrimental health effects leading among others to neurodegeneration or impaired organ function during development and later in life. Adverse effects of Mn, Fe, and Zn in excess are much better established for the general population, but the availability of data considering pregnant women is limited. While lots of studies focused on alterations in fetal development during deficiency, little is known about the consequences for the developing fetus and the health of pregnant women in case of overexposure. Furthermore, as recently reviewed by Smith *et al.* pregnant women are mostly excluded from studies on nutrition status due to the increased risk for adverse outcomes in fetal development. However, these studies would provide important data, which need to be considered during the assessment of micronutrient requirements [5-7]. Latest proposals for micronutrient requirements during pregnancy are mainly based on data extrapolated on weight gain or based on rodent data due to the limited availability of exact biomarkers reflecting fetal but also maternal nutrient supply. Nevertheless, data availability on micronutrient status and biomarkers do only account for single TE and do not consider uptake interactions of micronutrient mixtures [2-4]. Many studies have shown that transporters involved in Mn, Fe, and Zn influx or efflux are not specifically transferring one TE but all that accomplish transporter characteristics such as oxidation state or proton symport. Since all TEs discussed in this thesis are naturally occurring in mixtures and are involved in similar metabolic pathways in the human body, regulatory interactions seem likely [8-10]. Their exact role in nutrient supply but also potential negative outcomes due to an altered TE homeostasis during development and later in life are rarely characterized until today.

Therefore, data compiled in this thesis should provide first fundamentals of transfer modes, and the role of TE interactions in cellular metal homeostasis, as well as mechanistic investigations on metal-induced adverse effects in the three different physiological organs the placenta, the liver, and the brain. Potential outcomes on intracellular TE supply should reveal to which extent pathways in TE homeostasis are positively or negatively affected by other TEs present in the environment.

1.2. Scope of the thesis

This thesis is based on the following

- Development of an *in vitro* system of human villous trophoblasts modeling the placental barrier
- Investigating alterations in Mn and Fe transfer across the trophoblasts layer in regard to transfer interactions
- The role of Zn in Mn uptake and cytotoxicity in HepG2 cells
- Potential organ- and cell-specific differences in metal bioavailability

Chapter 2 – General Background Information

2.1. The essential trace elements

TEs are referred to as "trace" elements since they are occurring in very low quantities. To date, 11 different metals are widely accepted as TEs, namely chromium (Cr), cobalt (Co), copper (Cu), fluorine (F), Fe, iodine (I), Mn, molybdenum (Mo), selenium (Se), vanadium (V), and Zn. By definition, all of these TEs are present in concentrations of about 50 mg/ kg body weight or lower, except for Fe, with 60 mg/kg body weight. TEs inherit important functions in the human body because they are essential structural components of vitamins, hormones, or co-factors in metalloenzymes. Due to their essentiality, physiological concentrations are tightly regulated by absorption, excretion, and distribution mechanisms and disturbance in this underlying metal homeostasis has been associated with detrimental health issues [11,12]. Therefore, the following paragraph will focus on the physiology of the three TEs Mn, Fe, and Zn and will highlight similarities, differences, and interactions between their homeostases.

2.1.1. Manganese

Mn, a transition metal, is one of the most abundant elements in the earth's crust and is therefore occurring ubiquitously in the environment in several minerals in the form of oxides, carbonates, and silicates [13,14]. Furthermore, it is used in different industrial processes such as the production of dry cell batteries, and steel, but can also be found in fuel oil additives and antiknock agents [14]. Mn is a component of Maneb and Mancozeb, pesticides used in agricultural settings, and contrast agents for medical magnetic resonance imaging (MRI) due to its paramagnetic properties [15].

Mn is also known as an essential TE, involved in a variety of processes in human metabolism, contributing as a co-factor in the pyruvate carboxylase or arginase, among other transferases, hydrolases, and oxidoreductases, and in the Mn-dependent, antioxidative enzyme superoxide dismutase (MnSOD) [16]. In living organisms, Mn is commonly abundant in the divalent or trivalent oxidation state (Mn(II), Mn(III)). In addition, other physiological relevant species are among the ionic forms, Mn(II)-citrate and Mn(III)-transferrin but also Mn bound to serum albumin or α2-macroglobulin [8].

The primary route of Mn uptake for the general population is dietary consumption. Mn-rich foods include nuts, grains, rice, tea, and drinking water. Mn is added to infant formula and foods or parenteral nutrition (PN) in considerable concentrations as an essential micronutrient [3,17]. Additionally, daily supplements with varying Mn levels are one of the many Mn sources.

However, due to the lack of a no observed effect level (NOAEL) from animal studies and limited data available from human studies, an upper limit (UL) of Mn exposure has not been set so far [3,8,18]. The EFSA proposed an adequate intake (AI) of 3 mg Mn/ day for the general adult population [3]. The AI for young infants aged from 7 to 11 months is much lower (0.02 – 0.5 mg/ day) due to their not fully developed excretion metabolism [3,19].

In the gastrointestinal tract, 3 – 5 % Mn is resorbed actively in the small intestine or by passive diffusion (fig. 1) [18]. Involved in this process are active transport mechanisms including membrane-bound metal transporters. Initially, the divalent metal transporter 1 (DMT1) was suggested to be the major contributor to intestinal Mn absorption. However, the lack of DMT1 expression in the intestine of mice did not show altered Mn levels compared to wild-type animals, which suggests that the role of DMT1 in intestinal Mn transport is rather low [20]. Therefore, transport systems like the transferrin receptor (TfR) or two representatives of the Zrt-/ Irt-like family proteins ZIP8 and ZIP14 are more important in facilitating intestinal Mn transport. Nevertheless, those transporters are not exclusively transporting Mn but a variety of other metals like Zn, Fe, Cu, or calcium (Ca). Mn efflux from the intestine into the blood is predominantly mediated by proteins of the solute carrier family member 2, namely SLC40A1 (Ferroportin, FPN), expressed on the basolateral surface of the enterocytes, or SLC30A2 (ZnT10) [8,21]. Discussed in Mn export is also the cation transporting ATPase 13A2 (ATP13A2/PARK9) and the secretory pathway Ca^{2+}-ATPase isoform 1 (SPCA1) [8,22]. In blood plasma, divalent or trivalent Mn is conjugated to transferrin (Tf), citrate, or albumin and distributed to other tissues like the liver. Organs with the highest Mn levels are among the liver, the pancreas, bone, kidney, and brain [8].

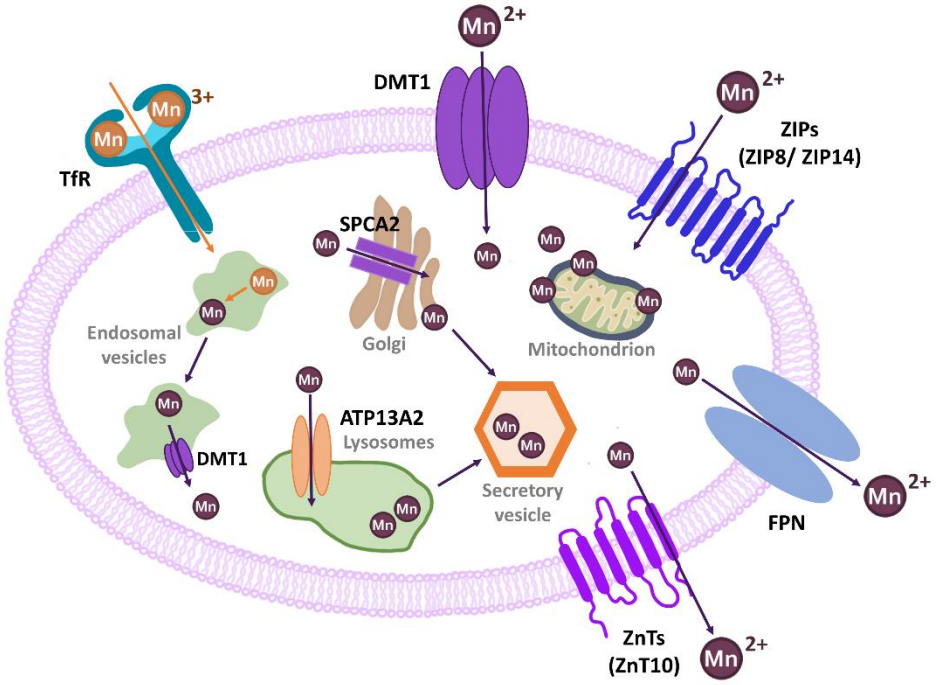

Figure 1: Cellular Mn homeostasis (adapted and modified from [22]).

2.1.1.1. Homeostasis, deficiency, and overexposure

In the human body, the liver has been regarded to be serving as the main regulatory organ in Mn homeostasis since it is able to regulate systemic Mn levels through endogenous gut losses. Small Mn amounts, which are needed for physiological processes remain in the blood plasma [8]. Excess Mn is sequestered by hepatocytes and bound to bile. This conjugate can then be excreted in the feces. In hepatocytes, the membrane transporters like DMT1, TfR, ZIP14, ZIP8, and the citrate transporter are expressed, strictly regulating Mn homeostasis [23-25]. Exact Mn transport expression patterns in hepatocytes are discussed in more detail in chapter 2.6.1 – Trace element transport and storage in liver and brain and chapter 5 – The Impact of Zinc on Manganese Cytotoxicity and Bioavailability in HepG2 cells. However, alterations in transporter gene expression are often caused due to inherited mutations in transporter-associated genes but also interactions with other TEs can disturb Mn homeostasis [26,27].

Maintaining Mn homeostasis is of central importance in preventing deficiency or overexposure. However, as Mn is ubiquitously occurring in food, Mn deficiency has rarely been observed in humans [3,28]. Moreover, Mn is entering the environment by anthropogenic sources such as exhaust gas emission and the inadequate disposal of dry-cell batteries leading to Mn polluted air and soil. Drinking water with a high Mn burden occurs in rural areas but also in highly industrialized countries like Australia, Bangladesh, and China, further

highlighting its ubiquitous appearance [29-31]. Since Mn is increasingly used in the industrial and agricultural setting, smelters, welders, miners, and agricultural workers are at increased risk of inhalative Mn overexposure from Mn-rich dusts, fumes, or the application of Mn-containing pesticides like Maneb and Mancozeb. In this case, Mn is taken up through the lung epithelium readily entering the blood circulation. After the transport to the olfactory bulb, it is directly taken up by the brain, bypassing the efficient homeostasis in the liver and the regulation by the blood-brain barriers (BBB, blood-cerebrospinal fluid barrier (B-CSF-B)) [8,32,33]. People with hepatic dysfunction and neonates are also at increased risk for Mn overexposure due to the not fully developed or perturbed hepatobiliary Mn excretion system. This is a present concern in neonates additionally receiving infant formula, and for patients dependent on PN where Mn is applied in considerable concentrations [8,17,34].

Mn overexposure and Mn accumulation in the brain has been associated with the symptomatology often referred to as "Manganism" or "Mn-induced Parkinsonism". Common symptoms are cognitive deficits and perturbed motor functions also resembling those seen in idiopathic Parkinson's disease (PD). Despite the variety of mutual symptoms, PD and Mn-induced parkinsonism cases differ regarding the manifestation of dystonia, resting tremor, and motor function, such as balance. Additionally, while PD is associated with the progressive loss of dopaminergic neurons in the *substantia nigra pars compacta*, in the initial phase of manganism neuronal dysfunction is rather located in the *globus pallidus* [22,35-39]. Many studies focused on molecular mechanisms underlying Mn-induced neurotoxicity. One of the proposed mechanisms includes the formation of reactive oxygen and nitrogen species (RONS) via Fenton or Fenton-like reactions, which are able to target macromolecules like DNA and proteins. This has been shown to result in oxidative DNA damage leading to neuronal apoptotic cell death. Other related mechanisms include mitochondrial disturbance, endoplasmic reticulum stress, neuroinflammation pathways, and interactions in the neurotransmitter metabolism, which may be the cause or consequence of Mn-induced oxidative stress [40,41]. Some of those are discussed in further detail in chapter 6 – Mechanistic studies on the adverse effect of manganese overexposure in differentiated LUHMES cells.

While in healthy individuals the efficient Mn homeostasis protects from Mn deficiency or overexposure, genetic variants (mutations) in transporter-associated genes can affect whole body Mn levels and Mn-dependent enzyme activity. It has been shown that patients carrying a mutation in *SLC39A8* (ZIP8) have lower hepatic *ZIP8* expression causing low blood Mn levels.

Patients additionally developed severe Mn deficiency, neurological as well as skeletal defects, and increased biomarkers of type II congenital disorders of glycosylation (CDG) [24,42]. A study by Lin *et al.* revealed that *ZIP8*, expressed in hepatocytes, is highly modulating whole blood and tissue Mn levels by reclaiming Mn from bile, preventing deficiency. Furthermore, *ZIP8* deletion in mice has been shown to decrease Mn-dependent arginase or β-1,4-galactosyltransferase activity and impair protein N-glycosylation [24].

On the contrary, mutations in *SLC39A14* (*ZIP14*) and *SLC30A10* (*ZnT10*) showed different response patterns regarding Mn uptake and distribution. Mutations in *SLC39A14* have been found in patients with childhood-onset parkinsonism and dystonia potentially caused due to accumulation of systemic and brain Mn [43]. Further investigations in whole-body *Zip14* knockout mice also revealed impaired hepatic Mn uptake and intestinal Mn elimination compared to wild-type mice [21,44]. While it was initially assumed that this symptomatology was caused by a defective hepatobiliary Mn excretion, the knock-out of liver-specific *Zip14* in mice did not result in systemic Mn accumulation or motor deficits upon a normal diet [45]. However, these mice showed increased Mn levels in the brain and serum upon consuming a high Mn diet, but not in the liver [45].

According to the symptomatology caused due to mutations in *SLC39A14*, resemblance can be found in patients carrying mutations in *SLC30A10* (*ZnT10*). While the mutation in *ZIP14* does not directly affect hepatobiliary Mn excretion, Mn accumulation has been observed in liver tissue in individuals carrying a homozygous loss-of-function mutation in *ZnT10* [46]. Studies by Mercadante *et al.* have shown that ZnT10 is essential for Mn excretion, especially since it contributes to the export of Mn by the liver into bile. Whole-body *ZnT10*-deficient mice showed severe Mn in excess due to impaired systemic and biliary Mn excretion, which was not the case in mice with liver- or intestine-specific knockouts. However, the exact mechanisms and disease phenotypes are still under investigation but already highlight the importance of *ZIP14* and *ZnT10* in the liver and whole-body Mn homeostasis [45,47].

2.1.1.2. Biomarkers of Mn status

An indicator, which describes biological or pathogenic processes as well as responses to exposure is referred to as a biomarker. Hereby, biomarkers can be divided into three different classes namely biomarkers of exposure, effect, and susceptibility. In the following paragraph biomarkers of Mn exposure are described [48,49]. Adequate biomarkers for human Mn status are crucial for monitoring Mn homeostasis, micronutrient requirements, and also Mn risk

assessment. However, the choice of the best-suited biomarker is challenging, since all of them can be affected by a variety of factors such as short half-life, high variations, and external contamination [50]. Discussed biomarkers are Mn levels in serum, plasma, whole blood, urine, feces, or saliva, which are measured by atomic absorption spectrometry (AAS), inductively coupled plasma-optical emission spectrometry ICP-OES or ICP-tandem mass spectrometry (ICP-MS/MS). A study by Smith *et al.* (2007) evaluating the role of blood, plasma, and urine in Mn status suggests that the correlation of Mn exposure to blood, plasma, and urine Mn is limited. Since Mn is rapidly eliminated from plasma and only 1 % of absorbed Mn is excreted via urine, these two biomarkers do not reflect Mn status either in exposed or healthy individuals. Moreover, fecal Mn levels do include unabsorbed dietary Mn as well as excreted Mn via bile and are therefore less suitable for the assessment of Mn status. Whole blood appears to be more suitable after continuous Mn exposure but variation potentially due to dynamic exposure scenarios, intracellular Mn ion distribution, and probe handling (time of sampling, latency) limit the significance of a relationship between Mn exposure and measured Mn levels in blood [3,50-52]. Further Greger *et al.* attempted to determine inadequate Mn supply by combining serum Mn levels with MnSOD or blood arginase activity, however to date, there is no direct evidence of correlation of Mn depletion with the activity of Mn-dependent enzymes [3,53]. In the case of saliva, Wang *et al.* revealed, that results resemble those of serum, therefore not providing a more specific and precise biomarker [54]. Biomarkers using biological fluids also include cord blood as well as maternal blood Mn. Advantages and limitations equal those of blood Mn measurements, however, in consideration of Mn status during pregnancy, cord blood Mn levels do only reflect fetal Mn status in the last trimester, whereas maternal blood levels do not accurately reflect fetal tissue Mn levels as well as general fetal Mn status [55,56].

Other biomarkers like hair Mn, teeth Mn, and toenail Mn levels appear to be more promising. While all three biological matrices are easy to collect, they represent different exposure periods. Shed teeth from children are mainly used for investigating Mn exposure during fetal but also neonatal development. During mineralization, metals accumulate, forming a daily pattern, which can be compared to growth rings. Therefore, the measured dentin Mn levels reflect precise exposure information from the second trimester until 1 year of age [57]. However, distinct differences have been shown in healthy teeth and those already afflicted with caries [56]. One of the most controversial discussed biomarkers is hair Mn levels. Hair, which is sampled 2 cm close to the scalp reflects an exposure period of 2 – 4 months. While several studies found an association of hair Mn levels with occupational exposure, their

validity is striking. Hair in particular is susceptible to environmental contaminations, due to TEs binding to sulfhydryl groups, not representing initial Mn exposure. This makes using hair Mn level as a potential biomarker more difficult because hair samples have to be cleaned from contaminations strictly following established protocols for reliable assessment of Mn levels. Hereby, the amount of interior hair Mn, which may also be extracted during the washing procedures cannot be estimated [56,58]. Likewise, toenails do also cover longer exposure periods (7 – 12 months), since Mn is incorporated into the sulfur bonds of the keratin filament. It has been shown that toenail Mn levels in occupationally exposed individuals were distinguishable from non-exposed with high sensitivity and specificity. However, sample contamination and high variations have to be considered if using toenail Mn levels as a biomarker [59]. With 40 % of total body burden and a long half-life of about 8 – 9 years, measuring bone Mn levels has also been established as a potential long-term biomarker [50]. Hand bone Mn levels can be quantified using *in vivo* neutron activation analysis (IVNAA). The method is based on the measurement of gamma radiation, which is emitted during neutron interactions with Mn in the bone. Since studies have shown differences between exposed and non-exposed individuals even at low levels, providing a useful biomarker of Mn exposure. However, using irradiation for the assessment of Mn levels in the bone matrix is disadvantageous because several safety regulations have to be considered for the measurement [50,60].

While the majority of Mn exposure biomarkers are based on analytically determined metal content, Mn deposition can be assessed using MRI. MRI is a non-invasive imaging technique, which utilizes the paramagnetic properties of Mn(II)-ions. It has been shown that MRI signal intensities were higher in preferential Mn accumulation sites in the brain like the *globus pallidus*, which additionally correlate with Mn blood levels. Furthermore, studies have shown that Mn accumulation could be detected in Mn-exposed workers who have not exhibited clinical implications for Manganism. However, as signal intensities are declined after absence of Mn exposure this method is a useful tool to reveal Mn accumulation in the brain as observed in neurodegenerative disease or occupational Mn exposure, but not for individuals with long-term, low-dose Mn exposure [52,61,62].

In summary, the suitability of these biomarkers is controversially discussed in the literature since measured indicators can be affected by diet consumption, previous intake, or environmental pollution, independent of the underlying exposure (table 1). Additionally, biomarkers should not only represent the status of exposed individuals but also alterations in

the general population. To date, there are no sensitive, reliable, and validated biomarkers that meet these requirements [3].

Table 1: Overview and characteristics of Mn biomarker matrices (based on [3,50,51,56]).

Biomarker matrices and methods	Representative exposure duration	Advantages	Limitations
Hair [58]	2 – 4 months before sampling	• Non-invasive	• Large variations among individuals (sex-dependence) • External contamination • Pigmentation [56]
Bone [63]	8 – 9 years	• Non-invasive • Correlates well with exposure	• Neutron irradiation
Blood [64]	2 h – 40 days dependent on elimination pathway	• Less susceptible to contamination	• Short half-life • Dependent on the time of sampling • Does not correlate well with exposure
Feces [3]	Dietary intake	–	• Low specificity → Includes unabsorbed dietary Mn and excreted Mn levels in bile
Teeth [57]	13 – 16 weeks after gestation until 1 year of age	• Non-invasive • Precise exposure information • Prenatal and postnatal exposure are distinguishable	• Dependent on condition • Difficult to collect • Difficult to measure
Saliva and urine [54,65]	Not assessed	• Non-invasive • Easy to collect	• Does not correlate well with exposure • Large variation • Little Mn excretion via urine (1 % of absorbed Mn)

Continuation table 1

Toenail [59]	7 – 12 months before sampling	• Easy to collect, store and transport • Correlates well with exposure	• Large variations • Highly dependent on toenail amount • External contamination
MRI [61]	still under discussion	• Shows Mn accumulation sites in the brain • Correlates with blood Mn levels	• Not suitable for long-term, low-dose Mn exposure
Cord blood [66]	Last trimester of pregnancy	• Correlates well with dentine Mn	• Cannot be obtained in different stages of pregnancy
Maternal blood [66]	2 h – 40 days (elimination-dependent)	• Easy sampling	• Does not represent fetal tissue Mn

2.1.2. Iron

2.1.2.1. Occurrence, uptake, and distribution

Fe is the most abundant element on earth that occurs in the environment in the form of fine-sized Fe oxide particles. These are released from numerous industrial processes such as Fe ore mining, steel processing, welding, and pyrite production [67].

Fe is also known as an essential TE, important as a co-factor for oxygen transport by hemoglobin, in the Fe-S-clusters of the mitochondrial electron transport chain, and enzymes involved in DNA synthesis [68,69]. In contrast to other TEs, its physiological multifunctionality results from its ability to transition from the divalent to the trivalent oxidation state a process which is often referred to as the Fenton reaction. The Fenton reaction is defined as ferrous Fe (Fe(II)) reacting with hydrogen peroxide generating hydroxyl radical. Ferric Fe (Fe(III)) however, reacts with hydrogen peroxide forming a hydroperoxyl radical. The presence of this reaction and the ready transition of Fe(III) to Fe(II) highlights the redox potential of Fe [70]. In addition, Fe is also occurring physiologically bound to Tf, a glycoprotein, which consists of a polypeptide chain possessing two Fe(III) binding sites, heme, and ferritin. In plasma, 30 % of Tf

is saturated, while the rest is serving as a backup buffering system preventing the accumulation of redox-active Fe(II) or non-transferrin-bound-Fe (NTBI) [69,71].

One of the primary Fe exposure routes is dietary consumption. In food, Fe is apparent as heme-Fe, from meat or other animal-related sources, and non-heme, which includes ferritin Fe. Especially meat, fish but also cereals, nuts, and dark green vegetables are rich in Fe. While the Institute of Medicine of the US set a UL of 45 mg Fe/ day, the EFSA has renounced this UL, due to inadequate data resulting in non-reliable calculations of response curves considering intake, body burden, homeostatic adaptions, and adverse health effects. Therefore, the EFSA proposes an average requirement of 6 mg/ day and a Population Reference Intake (PRI) of 11 mg/day for men and 16 mg/day for premenopausal women [2].

In the gastrointestinal tract, duodenal enterocytes absorb about 1 – 2 mg Fe/ day. To get transported by DMT1, which is expressed on the apical membrane of the enterocyte, ferric Fe needs to be reduced to ferrous Fe by the duodenal cytochrome B (DcytB) [68]. Subsequently, ferrous Fe is transferred from the cytosol into the bloodstream via FPN, expressed on the basolateral enterocyte membrane [68,72]. According to Mn, it has been shown that ZIP8 and ZIP14 play also a role in intestinal Fe absorption and are expressed on the apical membrane of enterocytes [73-76]. For Fe uptake by apo-Tf (unbound Tf) in serum, it has to be oxidized to its ferric form. This is realized by hephaestin, a membrane-bound ferroxidase, which is coupled to the Fe exporter FPN. The oxidation can take place in the cytosol by the soluble ferroxidase ceruloplasmin [68,69]. Another form of transport is Fe bound to ferritin, a cytosolic protein, which is composed of 24 H- (heavy chain) and L- (light chain) subunits. Furthermore, excess intracellular Fe can also be stored in these ferritin subunits forming a shell-like structure, which can incorporate 4500 Fe(III) ions. As Fe is occurring in the divalent state in the cytosol, it has to be reduced to get stored in the ferritins. This can be done by ferritin itself since it possesses a ferroxidase activity [69]. However, as many other TEs are actively excreted via bile or urine, there are no direct excretion mechanisms for Fe. The main processes of Fe excretion are indirect via exfoliation of the skin, sloughing of the intestinal epithelium, and menstruation. Only very little is removed via urine or feces [68]. While in many other tissues and cells Fe transport is mainly mediated by TfR1 and the coupled endocytosis, it does not play a role in intestinal Fe absorption due to its localization on the basolateral membrane of enterocytes (fig. 2) [77]. Transporter involvement in Fe homeostasis has been discussed in more

detail in chapter 4 – Differences and Interactions in Placental Manganese and Iron Transfer across an *In Vitro* Model of Human Villous Trophoblasts.

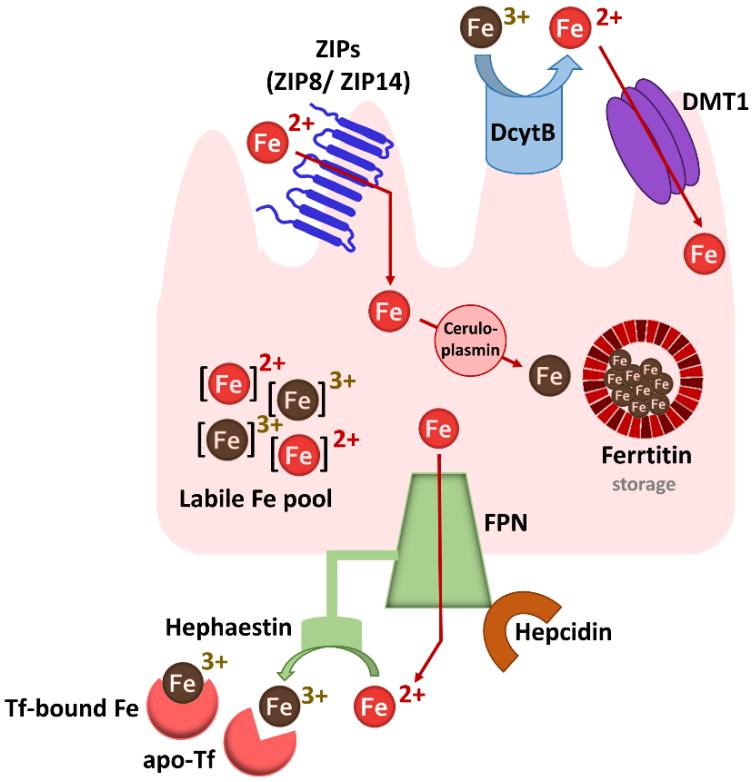

Figure 2: Intestinal Fe homeostasis (adapted and modified from [68]).

2.1.2.2. Homeostasis, deficiency, and overexposure

Since Fe cannot be actively excreted, maintaining Fe homeostasis is of central importance in avoiding Fe overexposure. The majority of Fe is used in the blood circulation for erythropoiesis, while the rest is distributed to other tissues like the liver. Within hepatocytes, Fe can be stored in cytosolic ferritins, which are highly variable in releasing if needed. Another compartment with the ability of rapid turnover are macrophages of the spleen, liver, and bone marrow since they can recycle Fe from degraded erythrocytes among others [78].

However, systemic Fe homeostasis is tightly regulated by the crosstalk of hepcidin and FPN. Hepcidin is a hepatic hormone, which is a 25 amino-acid-containing peptide. It is synthesized in hepatocytes and can be distributed to other tissues by secretion into the blood plasma. The negative feedback regulation of FPN by hepcidin can take place in two different ways, the occlusion and the endocytosis mechanisms. The occlusion mechanism means the conformational change of FPN by hepcidin, which leads to the occlusion of the binding site.

With decreasing hepcidin concentrations this process is reversible [78,79]. On the contrary, the endocytosis mechanism leads to the permanent removal of FPN from the cell surface due to ubiquitination after hepcidin-induced conformation change. The ubiquitylated units can then be a target for lysosomes and proteasomes initiating FPN degradation [78,80].

Besides regulation by hepcidin FPN, TfR1 and DMT1 can be regulated intracellularly. This is not only the case in Fe overexposure or deficiency, but also inflammatory stimuli can lead to alterations in mRNA levels. One of the main regulatory interfaces is the Fe-responsive element-Fe-responsive protein system (IRE-IRP system), which is involved in the translational processes of FPN, TfR1, and DMT1. Translation of these importers and the exporter is regulated by the 3' or 5' untranslated region IRE in the transporter-associated genes, which is targeted by the IRP1/2, inhibiting translation and therefore limiting Fe export but also import. In case of Fe deficiency, the hypoxia-inducible factor (HIF) machinery can be activated. HIF2α is able to positively affect the expression of Fe importers such as DcytB and DMT1 enhancing Fe absorption in the intestine [78,81,82]. Furthermore, FPN can also be positively regulated by Nrf2 (Nuclear Factor Erythroid 2-related Factor 2), a transcription factor often discussed in the context of the antioxidative defense [83]. Fe homeostasis has been discussed in further detail in chapter 4 – Differences and Interactions in Placental Manganese and Iron Transfer across an *In Vitro* Model of Human Villous Trophoblasts.

Even if Fe homeostasis is tightly regulated and several backup mechanisms exist, Fe homeostasis can also be disrupted potentially due to different disease phenotypes or interactions with other TEs, present in the environment [69].

Fe deficiency is a prevalent burden worldwide. It is most prevalent in young children (younger than 5 years), premenopausal women, and patients suffering from inflammation. In those cases, Fe stores are depleted due to inadequate Fe supply. While withholding of Fe from the plasma in patients with inflammation potentially results in Fe deficient erythropoiesis and anemia, a functional form of deficiency. Inherited hemoglobin disorders, often referred to as thalassemia also leads to Fe deficiency due to a defective hemoglobin synthesis [84,85]. Since Fe is important for many processes already described before, Fe deficiency can lead to detrimental health issues such as heart failure, ischemic heart disease, or hemodynamic instability and several symptoms like fatigue or reduced concentration [85]. Therapeutical interventions for Fe deficiency are oral Fe supplementation or parenteral Fe. However, thalassemia is treated with the

administration of blood transfusions, which is a common cause of Fe overexposure in these patients [85,86].

Fe overexposure and especially the accumulation of Fe in the brain has been observed in neurodegenerative disorders like Alzheimer's (AD) and PD. Fe accumulation in the brain is progress occurring during healthy aging. Most evident is this in brain regions already associated with neurodegenerative diseases such as the *substantia nigra*, *globus pallidus*, *caudate nucleus*, and *cortices*. In AD, several studies could show that Fe promotes the aggregation, oligomerization, and amyloidosis of amyloid β (Aβ) peptides, mostly due to its redox activity and the generation of free radicals leading to oxidative stress [87,88]. Additionally, translation of the amyloid precursor protein, involved in the formation of Aβ, is regulated by Fe by its IRE in the 5'-untranslated region mRNA [89,90]. PD studies have shown a correlation between Fe concentrations in the *substantia nigra* of Parkinson's patients with disease severity. Furthermore, Fe is involved in the induction of the conversion of α-synuclein leading to the formation of PD characteristic Lewy bodies, since the gene encoding α-synuclein possesses an IRE [89,91]. Another rather rare hallmark of brain disorders is the novel neurodegeneration with brain Fe accumulation. It is characterized by excessive Fe accumulation in the *basal ganglia*, *globus pallidus*, *substantia nigra*, and *cerebellar dentate nuclei*. This neurodegenerative syndrome is associated with mutations in the gene encoding IRP2 [92]. Mice lacking *Ireb2* (Fe-responsive element binding protein 2) had a disrupted Fe metabolism, which led to the development of an adult-onset progressive neurodegeneration concomitant with axonal degeneration and neuronal loss. These disease phenotypes were recapitulated in a reported case of a patient with biallelic loss-of-function variants in *IREB2*, which led to the complete absence of IRP2 [92-94].

Besides neurodegenerative disorders, hepcidin deficiency impairs Fe homeostasis leading to Fe overload and severe disease phenotypes. These phenotypes, often referred to as hereditary hemochromatosis have been observed in patients carrying hereditary mutations in genes involved in hepcidin and FPN metabolism. Discussed hallmarks of hereditary hemochromatosis are Fe overload because of uncontrolled Fe absorption and subsequent efflux into the blood, oversaturating of Tf, and increased accumulation of NTBI. Due to its high redox activity, NTBI can then induce oxidative damage in the liver, pancreas, and heart tissue. On the other hand, duodenal enterocytes and macrophages become Fe-deficient because of overexpressed FPN and reduced circulating hepcidin leading to an enhanced Fe efflux [71,95].

Hereditary hemochromatosis can occur in several forms differing in loss-of-function mutations in Fe metabolism-associated genes. The most prevalent form is autosomal-recessive HFE hemochromatosis [96]. Mutations in the *HFE* (homeostatic Fe regulator) gene have been shown to result in a low transduction signal for hepcidin synthesis, while serum ferritin and Tf saturation are increasing [95,97]. Patients carrying these mutations are often treated by phlebotomy, decreasing body Fe burden. However, to date, this therapy is not standardized and recommendations are rather empirical [95].

2.1.2.3. Biomarkers of Fe status

The assessment of Fe status in the human body is of central importance, to identify potential alterations in Fe uptake and utilization. However, as several biomarkers have been established, potentially reflecting body Fe status (table 2), the monitoring of Fe intake is not covered. This has to be realized by measuring the dietary intake [2,98]. Established Fe biomarkers can be divided into 3 categories, as they represent the utilization of Fe (hemoglobin synthesis), storage, and transport and supply to other tissues. Two of the widely used whole blood biomarkers for Fe status are hemoglobin and hematocrit values. The measurements only require small sample sizes and can be applied from fasted and non-fasted blood samples. Additionally, intra-individual hemoglobin variances are low. However, both markers have low specificity and sensitivity, especially for patients with high hemoglobin baseline but also due to many other phenotypes affecting hemoglobin levels such as dehydration or smoking. Even if the use of capillary blood is advantageous, inaccurate sampling can lead to highly variable results [2,99,100]. Measuring reticulocyte hemoglobin content from peripheral blood samples is often done for the diagnosis of Fe deficiency, but an increased mean corpuscular erythrocyte volume or thalassemia can lead to false normal values [2,99].

Among the hemoglobin-specific biomarkers, others rather represent nutritional Fe status. Similar to Mn, Fe levels can also be measured in serum via AAS, ICP-OES, or ICP-MS/MS. Besides serum Fe levels, Tf-saturation has controversially been discussed in the context of Fe status. However, both markers are limited by circadian variation and are highly affected by inflammation and dietary Fe intake [2,99]. Another way to assess Fe status by utilization of TfR is by measuring the soluble serum TfR (sTfR). Here, sTfR represents cellular Fe status, since it is dependent on erythrocyte precursors in the bone marrow and the number of TfRs within the cells. In comparison with TfR saturation, determining sTfR is less affected by inflammation. Nevertheless, it is a non-standardized method, also lacking specificity for Fe deficiency

[2,98,101]. Measuring ferritin, the Fe storage protein, as a biomarker has been recommended by the WHO (World Health Organization) [102]. It has been shown that serum ferritin is directly proportional to Fe stores of healthy individuals and can be used for the diagnosis of Fe deficiency anemia [99]. However, it is an acute-phase protein and is therefore not an accurate estimate of Fe stores, especially in patients suffering from chronic inflammation or infection [2,101]. Combining sTfR and serum ferritin levels can be used to assess total body Fe since the logarithmic function of this ratio correlates with the amount of Fe stores in Fe-replete patients and deficient Fe stores in tissue in Fe deficiency [99]. Additionally, following Fe supplementation, this biomarker is the most sensitive indicator [2]. Since all advantages and limitations of single sTfR and serum ferritin do also account for the ratio, it is not a more sensitive biomarker [99]. During heme synthesis in Fe deficiency, Zn is incorporated into the protoporphyrin ring. The ratio of Zn protoporphyrin with heme can then be measured from a drop of blood. It is a sensitive biomarker, especially for the diagnosis of Fe deficiency in adults but also children. This specificity is limited in the case of lead exposure, anemia, chronic diseases, and inflammation [99]. Among the non-invasive biomarkers, Fe status can also be assessed by the semiquantitative measurement of Fe in the stainable bone marrow, since it is one of the major storage sites of Fe. It has been an established gold standard method for the diagnosis of Fe deficiency. However, it is only applied in special circumstances, because it is highly invasive [101]. Recently, the role of hepcidin as a potential biomarker has been discussed. Since it is known as the master regulator of Fe homeostasis slight alterations result in rapid hepcidin response. Major advantages are the lack of confounding factors and the immediate overview of Fe requirement, which change can be indicated over time. To date, it is a non-standardized method and according to other biomarkers it is also affected by inflammation [101,103].

Table 2: Overview and characteristics of Fe biomarkers (based on [2,98,99,101,103]).

Biomarker	Advantages	Limitations
Hemoglobin/ hematocrit [101]	• Small sample sizes • Fasted and non-fasted blood samples	• Low specificity/ sensitivity • Interlaboratory differences
Reticulocyte hemoglobin [101]	• Differentiation between iron deficiency and other causes of anemia	• Affected by thalassemia and increased mean corpuscular erythrocyte volume
Serum Fe/ Tf saturation [99]	-	• Circadian variation • Affected by inflammation and dietary Fe intake → to date less applied
Soluble serum TfR (sTfR) [99]	• Less affected by inflammation	• Non-standardized • Less specific for Fe deficiency
Serum ferritin [99]	• Correlates with stainable Fe in the bone marrow • Well standardized	• Acute-phase protein • Affected by inflammation, chronic disease, and infection
Ratio sTfR to ferritin [99]	• Predicts bone marrow Fe • Sensitive indicator after Fe supplementation	• Affected by inflammation, chronic disease, and infection • No clear advantage compared to serum ferritin alone
Zinc protoporphyrin (ZPP) [101]	• A small sample size needed	• Affected by lead exposure, anemia, chronic diseases, and inflammation
Bone marrow biopsy [99]	• Well established	• invasive
Hepcidin [103]	• indicative over time • alight alterations result in rapid response	• non-standardized • affected by inflammation

2.1.3. Zinc

2.1.3.1. Occurrence, uptake, and distribution

Zn is the 23rd most abundant metal in the earth's crust and occurs mainly bound in ores as Zn sulfide. It appears ubiquitously in the environment through natural but also anthropogenic sources. Mining and galvanization processes are the main anthropogenic Zn entries. In the industry, Zn is commonly used in alloys protecting iron and steel products. Furthermore, since Zn possesses fungicide properties, it is often used in dental medicine but also cosmetics [104,105].

After Fe, Zn is the second most abundant TE. Its essentiality in humans has already been postulated in the early 1960s. To date, more than 300 enzymes are identified as Zn-dependent, which are regulated by more than 2000 transcription factors. In general, Zn is among others serving as a co-factor in mediating the cell cycle, cell proliferation, and differentiation, DNA replication, and reparation, apoptosis as well as lipid and carbohydrate metabolism [105,106]. Hereby, Zn-finger proteins are primarily involved in the regulation of these processes and implicated in translational regulation, ubiquitin-associated protein degradation, and signal transduction [107]. Zn is appearing in the divalent oxidation state and transition to other oxidation states does not play a role in Zn metabolism. The wide occurrence of Zn as a structural and signaling component is therefore established due to its redox-neutral characteristics. Furthermore, different from Mn and Fe, Zn has rather been discussed to be involved in antioxidant and anti-inflammatory processes and is also considered in the context of the regulation of redox homeostasis. There Zn(II) is potentially mediating oxidative protein modification by the interaction of the amino acid residues. As a structural component of the antioxidative enzyme CuZn superoxide dismutase (CuZnSOD) and its huge role in metallothionein (MT) synthesis, Nrf2 signaling, and NF-κB (nuclear factor kappa B), its antioxidative and anti-inflammatory role can further be highlighted.

To maintain homeostasis, adequate Zn supply is essential. This can be reached by dietary consumption of Zn-rich foods, which include meat, legumes, eggs, fish, grains, and grain-based products. It is also included in food supplements but also PN as essential TE [4,108]. Zn requirements for the general population have been assessed by EFSA by a two-factorial approach. Firstly, physiological requirements were estimated, which were additionally defined as the minimum amount of absorbed Zn to balance losses of endogenous Zn and also consider requirements needed for the growth of healthy infants and children, and pregnant and

lactating women. Secondly, the amount of dietary Zn has to be determined to meet all the requirements mentioned in part 1. Furthermore, the inhibitory effect on Zn absorption by phytate was also included. Therefore, EFSA proposed estimates average requirements of 6.2 – 10.2 mg Zn/ day for women and 7.5 – 12.7 mg Zn/ day for men and further derived PRI of 7.5 – 12.7 mg Zn/ day for women and 9.4 – 16.3 mg Zn/ day for men [4]. These reference intakes are in accordance with recently revised Zn reference intakes by the Nutrition Societies of Germany, Austria, and Switzerland (2020) of 7.0 – 10.0 mg Zn/ day for women and 11.0 - 16.0 mg Zn/ day for men [109].

Among other oral, inhalation, or dermal exposure routes, dietary consumption is the most prevalent one for the general population. Hereby, 16 – 50 % Zn are absorbed in the intestinal brush border membrane and transferred from the lumen to the epithelial enterocytes. The kinetics underlying these transport processes are unsaturated or saturated (carrier-mediated processes) (fig. 3). Carrier involved in Zn transport across the enterocytes include representatives of the conserved families of ZnT (solute carrier protein family 30 (SLC30)) transporters and ZIP (Zrt,- and Irt-like protein family (SLC39)) transporters [110-112]. While the 10 members of the ZnT family have been shown to play a role in the efflux and sequestration of Zn into organelles and vesicles, the 14 different transport proteins of the ZIP family rather mediate the transport of extracellular, organellar, or vesicular Zn into the cytoplasm [111,113]. Especially in intestinal Zn transport apical localized ZIP4 is discussed to import Zn into enterocytes, while basolateral localized ZnT-1 may serve as an exporter of Zn from the enterocyte into the portal blood. Moreover, ZIP5 and ZIP14 both localized on the basolateral membrane of the enterocyte have been shown to import Zn from the blood into the enterocytes potentially for the excretion into the lumen [111,114,115]. Initially, DMT1 was also discussed in intestinal Zn transport but shows low sensitivity. Therefore, the exact role of DMT1 in intestinal Zn transport is still discussed [115-117]. However, Zn is distributed to different organs and compartments, where skeletal muscle, bone, and liver are the organs with the highest Zn burden [106].

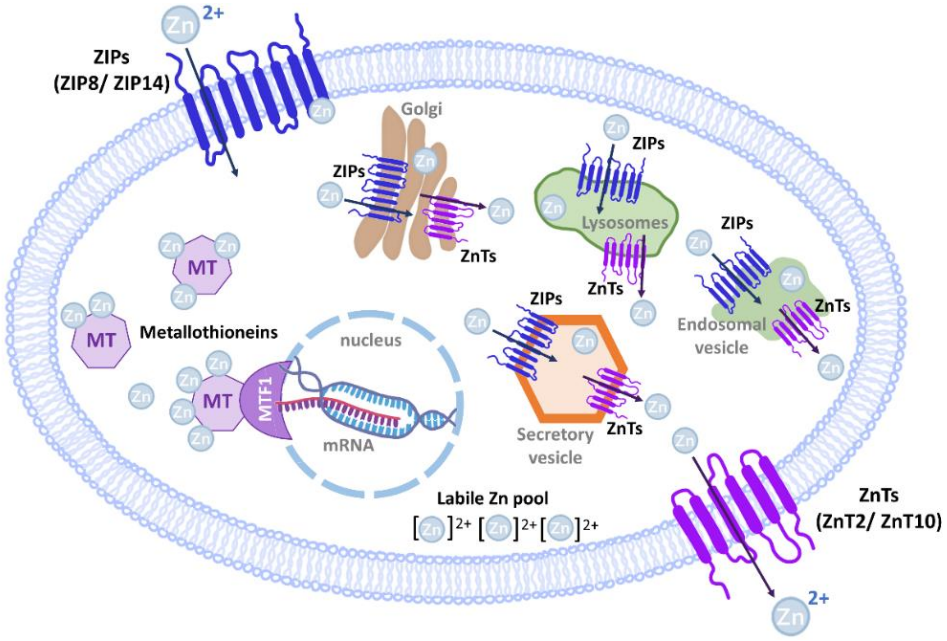

Figure 3: Cellular Zn homeostasis (adapted and modified from [106]).

2.1.3.2. Homeostasis, deficiency, and overexposure

Zn homeostasis in the human body is regulated by intestinal absorption. This is the case since there are no discrete Zn storage sites and endogenous renal or intestinal Zn losses have to be compensated by adequate dietary uptake [118]. Besides the intestine, the liver and the pancreas do also play a role in Zn homeostasis [112]. In general, the human body consists of 2 – 3 g Zn whereby plasma and serum Zn account for less than 1 % with a varying concentration of 12 – 16 µM Zn [119]. Since it is mainly bound to albumin or α-macroglobulin, only small amounts in the sub-nanomolar range occur unbound [115,120]. The huge variety of Zn im- and exporters and the existence of metalloproteins tightly regulated by cellular Zn levels highlight the importance of adequate Zn supply and distribution [113]. In 2017 Maret introduced a three-tiered system for the homeostasis of cellular Zn. He considers im- and export of Zn through the plasma membrane also including cytosolic proteins such as MT and the Zn sensor metal regulatory transcription factor 1 (MTF1), intracellular storage in vesicles often referred to as zincosomes, and release and generation of transient Zn and lastly Zn re-uptake [113]. Especially MT and MTF1 have been shown to play a main role in intercellular Zn homeostasis. MT are low molecular proteins, which are rich in cysteine residues. This makes them a good target scavenging ROS. In humans 11 functional isoforms are expressed in various organs and tissues and 5 – 15 % of the cytosolic Zn pool is bound to MT [106,121]. Moreover, within cells they serve to buffer excess intracellular Zn levels by chelation [122]. Furthermore, MTs are regulated by MTF1, a Zn finger transcription factor mainly involved in regulating metal-responsive gene

expression. It has been suggested that MTF1 has only a low intrinsic affinity for Zn ions, which is only increased in case of excess Zn, specifically if the Zn level reaches the nM to sub-µM range [122,123]. On the other hand, MTs can also be targeted by agents leading to Zn release, activation of MTF1, and subsequent induction of gene expression. In this case MT is serving as a signal transducer, using Zn signals in response to redox processes [113]. MTF1's role in Zn homeostasis can further be highlighted by mentioning its role as a Zn-responsive transcription factor involved in the regulation of several Zn transporters such as ZnT1 and ZnT2 [122].

However, a disturbed Zn homeostasis due to an imbalanced Zn status can result in detrimental health issues. With two billion people affected worldwide, Zn deficiency has been an emerging global health issue. It is highly prevalent in developing and poor countries. Moreover, vegans, vegetarians, and the elderly are also at increased risk for Zn deficiency [124-126]. In these people, deficiency is mainly initiated due to inadequate Zn supply caused by high dietary phytate content, malabsorption, or increased loss because of intestinal disorders. Deficiency can also be caused by inherited disorders such as *acrodermatitis enteropathica*, associated with a mutation in the intestinal ZIP4 transporter [115,126-128]. Nonetheless, the assessment of Zn deficiency is difficult due to the lack of adequate biomarkers and the wide range of symptoms from none to clinical manifestations such as growth retardation, systemic inflammation, skin changes, or mental lethargy [128,129].

Besides deficiency, Zn overexposure is a potential concern, especially in industrial and military settings. The widespread use of Zn oxide and Zn chloride in smoke bombs increases the risk of inhalative Zn overexposure for soldiers. Several clinical cases of adult respiratory distress syndrome have been reported, which were mainly associated with exposure to Zn chloride-containing smoke bombs [128,130]. Furthermore, the most known industrial disease of Zn overexposure is metal fume fever. The disease pathology is caused due to acute overexposure to Zn oxide-containing metal fumes, which has often been observed in welders and smelters. The symptoms include fever, painful muscles, nausea, chest pain, and cough. However, this syndrome is reversible within 4 days, without life-threatening consequences [131]. Dietary Zn overload has been discussed in the context of Zn-induced Cu deficiency. High dietary Zn induced the upregulation of MTs, which have a higher binding affinity to Cu. This in turn leads to an enhanced Cu excretion [119,128]. A disturbed Zn homeostasis in the brain has also been discussed in the pathology of neurodegenerative diseases such as AD and PD potentially due to high extracellular Zn levels and enhanced protein aggregation [5,132].

2.1.3.3. Biomarkers of Zn status

Especially for Zn, many biomarkers have been established. A review by Lowe *et al.* addresses 32 potential different markers discussed for the assessment of Zn status in humans [133]. While plasma, serum, and urinary Zn levels are responsive to nutritional Zn intake, other biomarkers are not well established and the lack of data limits their validity for the assessment of the clinical Zn status. Therefore, this paragraph will concentrate on the biomarkers widely established in the clinical setting but will also introduce novel biomarkers discussed in the last years (table 3).

The most applied biomarkers to determine Zn status in humans with well-established reference ranges are plasma or serum Zn levels, measured using AAS, ICP-OES, or ICP-MS/MS. In patients with a low or moderately low baseline, but also in adults (sex-independent), elderly, pregnant, and lactating women it is responsive to Zn supplementation but only in short periods due to the efficient homeostatic control maintaining plasma Zn concentrations [4,133,134]. Since plasma or serum Zn represents systemic Zn status it is affected by a variety of other factors such as inflammation, fasting, eating and pregnancy [133,135,136]. Furthermore, King *et al.* mention low sensitivity and a lack of specificity in disease pathologies resulting in or affected by more moderate Zn deficiency, and it does not unconditionally reflect individual Zn status [4,137,138]. Another limitation consists of the increased risk of external contamination from blood tubes as an example [135].

In healthy individuals, 15 % of daily Zn losses are attributed to urinary excretion. Both Zn supplementation and low dietary Zn intake are represented by the amount of Zn, excreted by urine [4,133]. However, this correlation is only reliable in patients with a moderate Zn status baseline. Additionally, the availability of data regarding urinary Zn is scarce, therefore its validity as an indicator for Zn status is still under discussion [135,139].

Stunting, a low height-for-age phenotype in children under 5 years of age has been postulated as an indirect biomarker of Zn deficiency in a specific population reflecting pre- and postnatal Zn supply. The WHO considered stunting prevalence greater than 20 % as a public health concern for Zn deficiency [135,140]. Additionally, epidemiological studies by Brown *et al.* have shown increased weight gain and linear growth in children, positively correlating with reduced stunting prevalence [140,141]. However, growth is not only affected by Zn deficiency, other factors contributing to decreased growth are inadequate supply of proteins and carbohydrates, and deficiencies in other micronutrients such as magnesium or phosphor [135].

Recently, other discussed Zn biomarkers include the determination of readily bioavailable labile Zn as well as MT and Zn transporter expression. Labile Zn can be determined in serum and intracellularly potentially reflecting the activity status of circulating Zn levels. This can be realized by using low molecular fluorescence probes [120,134,142]. Leukocyte-specific MT expression has also been assumed a reliable and sensitive indicator of Zn status. Studies have shown that MT expression is sensitive toward dietary Zn in a dose-dependent manner even if Zn levels are lower than the recommended dietary allowances. Due to the tightly controlled Zn homeostasis, plasma and serum Zn levels are insensitive toward small changes in Zn, which is not the case for MT expression [143]. However, the determination of labile Zn, as well as MT expression, is not well established and still needs to be validated. In 2021 Cheng *et al.* introduced the Zinc Status Index (ZSI), combining three different endpoints for the assessment of the Zn status. Due to the complexity of Zn homeostasis, a panel of biochemical assays are developed including the linolenic acid:dihomo-γ-linolenic acid ratio (LA:DGLA), mRNA gene expression of Zn-associated proteins, and fecal microbiome profiling. All three indices are affected by nutritional and clinical Zn status. Reed *et al.* have shown that the enterocyte-specific LA:DGLA ratio negatively correlates with dietary Zn, meaning the elevation of LA:DGLA ratio in the Zn-adequate group [144,145]. Additionally, while plasma Zn measurements did not find a correlation between nutritional Zn and Zn status, the LA:DGLA ratio was inversely correlated. This highlights the higher sensitivity of the LA:DGLA ratio compared to plasma Zn detecting early changes in physiological Zn status [144,145]. The second index, the mRNA expression of Zn-associated genes defines the investigation of changes in Zn transporter expression and also genes encoding other proteins of Zn metabolism such as hepatic Δ6-desaturase [144,145]. However, data on changes in mRNA expression are rather inconsistent, since Zn metabolism is tightly regulated [143]. Lastly, gut microbiome composition showed to be affected by dietary Zn status. This is in accordance with the increased production of short-chain fatty acids, which influence luminal pH. Furthermore, different bacterial biosynthetic pathways are affected in Zn deficient conditions such as cytochrome P450 activity, or bile acid production [145,146]. This is in turn another evidence for decreased Zn bioavailability and Zn status. However, more data has to be assessed to establish the ZSI as a more precise biomarker [145]. Currently, the assessment of the Zn status is limited by the lack of standardized methods, accepted guidelines specifying the best suitable biomarker but also data interpretation for diagnosis, which is often inconclusive [133,138,145].

Table 3: Overview and characteristics of Zn biomarkers (based on [4,133,135,136,140,143,145]).

Biomarker	Advantages	Limitations
Plasma Zn/ serum Zn [135]	• Responds to Zn supplementation	• Affected by inflammation, pregnancy, fasting, and eating • Lacks sensitivity and specificity in more moderate Zn deficiency • External contamination
Urinary Zn [135]	• Correlates with Zn uptake	• Correlates only in patients with moderate Zn baseline • Not validated so far due to limited data availability
Stunting [140]	• Non-invasive method • Require simple equipment	• Biomarker restricted to children • High individual errors due to unstandardized protocols
Labile Zn [142]	• Labile Zn = readily bioavailable Zn • Plasma labile Zn and intracellular labile Zn	• Not validated
MT expression [143]	• Expression changes dose-dependent • Responsive for small alterations in Zn status	• Not validated • Not established for adolescents and children • The expression is also affected by inflammation, free radicals

Continuation table 3

Zinc Status Index [145]	• LA:DGLA ratio detects early changes in Zn status • Mild Zn deficiency can affect Zn transporter gene expression and activity • Microbiome composition is altered according to dietary Zn intake	• Response of Zn transporter mRNA expression inconsistent across studies • Lack of data

2.1.4. Trace Element Interactions

Consequences of disturbed homeostasis have been widely investigated highlighting the importance of several regulatory processes within different tissues and cells. To date, the range of studies also considering potential alterations due to the presence of a variety of TEs in the environment has increased. Nevertheless, because of the dynamic nature of TE regulations in deficiency and overexposure, the identification of definite pathways and regulatory co-factors is still under discussion. Therefore, this paragraph will focus on interactions between the three TEs investigated in the context of this thesis.

2.1.4.1. Iron and Manganese

In the early 1990s, Finley and colleagues observed increased gastrointestinal Mn in women compared to men, which was associated with the Fe status and lower serum ferritin levels in men [147]. In recent years, substantial evidence has shown that Mn and Fe interactions predominantly rely on their similarities in uptake and transport mechanisms. This is feasible since they share physiological oxidation states and therefore are able to transition between the divalent and trivalent states. This makes a variety of proteins involved in Fe metabolism also a likely target for Mn. Regarding Fe uptake and distribution, studies have shown that both Fe(III) binding sites in Tf can be occupied by Mn (III) but the affinity is discussed to be higher for Fe than for Mn [148,149]. Furthermore, several im- and exporters like DMT1, TfR, and FPN have been discussed in Mn and Fe metabolism, which are differentially affected by either Mn or Fe exposure or in case of deficiency. DMT1 expression in the intestine has been observed to be upregulated during Fe deficiency resulting in increased basal Mn levels in several tissues

including the brain [27]. In the brain, Fe deficiency has been associated with increased Mn accumulation in the *caudate putamen* and *globus pallidus,* which may also be explained by increased *DMT1* expression [27,150]. In neuronal rat PC12 cells Mn exposure significantly increased the mRNA expression of *TfR* which was accompanied by elevated Fe levels [151]. This observation could be confirmed by a study in neuroblastoma SHSY5Y cells where it has been shown, that Tf-bound Mn was internalized into TfR to the same extent as Tf-bound Fe [152,153]. Therefore, DMT1 and TfR are affected by Mn altering systemic and tissue Fe levels. *In vivo* studies in a rat model of Mn-induced parkinsonism, Mn exposure resulted in increased DMT1 and decreased FPN expression leading to Fe overload in the *substantia nigra* [154]. Coupled with FPN expression increased hepcidin levels in liver tissue upon Mn treatment have been observed, which can be detrimental in an already Fe deficient state. Moreover, higher Mn levels in biosamples have been found in Fe deficient infants and occupational Mn exposed welders and smelters [155,156].

Besides transporter competition, Mn may also have an effect on the IRP/IRE machinery, involved in DMT1, TfR, and FPN regulation, leading to decreased Fe-binding affinity upon moderate Mn exposure and the opposite effect in case of Mn overexposure. It has been shown that translational regulation of FTH for example has been disturbed upon Mn treatment. It has been postulated that Mn may block the 5'-untranslated region of the FTH mRNA by increased binding of IRP1 to the IRE, which may result in the increased accumulation of Fe(II) able to generate ROS [153,157].

Nevertheless, comparing *in vitro*, *in vivo* and human studies still show controversial results considering Mn and Fe interactions in different tissues and cells, and further studies are needed to reveal the exact pathways of regulating combined Mn and Fe homeostasis [10].

2.1.4.2. Iron and Zinc

Considering pathologies of inadequate nutrient supply, Fe and Zn deficiency is most prevalent among populations. Interestingly, patients diagnosed with Fe deficiency or Fe deficiency anemia have also shown low serum Zn levels. This observation was one of the first indications that Zn status might be associated with Fe metabolism in clinical human studies. The same outcome could be observed in humans suffering from the inherited form of Zn deficiency, a*crodermatitis enteropathic*a, which concurrently developed Fe deficiency. Regarding intestinal Zn uptake, several studies have shown an inhibitory effect of Zn on Fe uptake and vice versa, which was only the case after administration of Fe and Zn-containing aqueous

solutions but not in complex food matrices [158,159]. Fe/Zn interactions have long been assumed to rely on competition on the DMT1 binding sites. To date, several studies could reveal that Zn is not transported by DMT1 due to the absence of protons, which are needed for the proton-coupled DMT1 metal transport [82,160]. However, mRNA and protein expression of DMT1 was increased in Zn-treated intestinal Caco-2 TC7 cells, which was accompanied by increased Fe absorption [161]. Zn has been shown to play a role in the regulation of DMT1 via the IRP2 pathway requiring activation of PI3K a phosphoinositide-3-kinase, which is mediated by MTF1 [9,138]. Contradictory to this Iyengar *et al.* described the involvement of the IRP/IRE machinery while Sharp *et al.* and Frazer *et al.* rather proposed post-translational regulation of DMT1 by Zn affecting Fe uptake. Therefore, data on DMT1 regulation is inconsistent and exact pathways need to be elucidated in further studies [82,162-164]. Alterations in Fe transporter regulation by Zn have also been discussed in Fe export by FPN. The study by Yamaji et al. additionally showed that *FPN1* mRNA expression was altered by Zn in human intestinal Caco-2 TC7 cells and Fe export increased potentially mediated by MTF1. On the contrary, Fe treatment did not lead to significant alterations in *FPN1* mRNA expression, even if FPN1 is the only known mammalian exporter of Fe [82,161]. At present, exact mechanisms regarding FPN1 regulation by Zn are still unclear. While it is discussed to be mainly regulated by hepcidin, it also possesses an IRE in the 5'-untranslated region and therefore a binding site for the IRP. Evidence suggests, that Zn is involved in the activation of an enzyme part of the BMP6/SMAD signaling pathway, which is particularly involved in hepcidin regulation [82,165,166]. Currently, several studies attempted to explain the cross-talk between Zn and intestinal absorption and utilization and mobilization of Fe. However, exact mechanisms regarding the influence of Zn status on Fe absorption, hepcidin levels, and therefore regulation of hepatic Fe metabolism by Zn are still unknown [167].

2.1.4.3. Manganese and Zinc

While Mn/Fe and Fe/Zn interactions have been investigated in more detail, interactions of Mn and Zn are rarely characterized. Transporters involved in either Mn and Zn uptake and distribution are ZIP8 and ZIP14. While both ZIPs were initially discussed to predominantly transport Zn, Liu *et al.* assumed that Mn is a likely physiological substrate for ZIP8 due to the underlying Michaelis-Menten constants [168]. This hypothesis could be supported by Kambe *et al.* reporting aspartic acid and asparagine residues in the ZIP binding sites as a preferential target for Mn-binding compared to Zn-binding [169]. This may also account for ZIP14 since

they are phylogenetically related [170]. Additionally, as already discussed for Fe, Zn may also affect gene and protein expression of TfR1 and DMT1, which in general are rather discussed in Mn homeostasis and do not play a role in Zn metabolism [82,160]. However, to which extent Zn is altering Mn transport by DMT1 and TfR1 is still unclear. Currently, underlying mechanisms can only be discussed based on evidence obtained from single TE studies, due to the lack of data regarding Mn and Zn interactions. Therefore, potential underlying mechanisms of Mn/Zn interactions are revisited in chapter 5 – The impact of Zinc on Manganese Bioavailability and Cytotoxicity in HepG2 cells.

2.2. The role of trace elements in the target organ liver

For all three TEs discussed in the context of this thesis, the liver serves as the main regulatory organ to maintain homeostasis. As the liver is also dependent on adequate TE supply for proper function, it is a presumed target for TE overexposure or deficiency. Therefore, disruption of either Mn, Zn, or Fe homeostasis may have different outcomes on hepatic function and TE metabolism. While Mn and Zn levels are regulated by hepatic distribution and partial hepatobiliary excretion, the liver is the main storage organ for Fe [8,171-173]. In a healthy individual's liver tissue TE amounts differ distinctly. Mn amounts in the liver range between 1.2 – 1.3 mg Mn/ kg wet weight, Zn amounts between 142 – 369 mg Zn/ kg dry weight, and Fe amounts between 200 – 2000 mg Fe/ kg dry weight. This is due to the fact, that the majority of liver Fe is occurring in form of heme Fe and Zn is widely allocated as a component of proteins and enzymes [105,174-177]. Among the many transport pathways discussed in Mn, Fe, and Zn homeostasis, carriers mediating intestinal absorption are also present in hepatic tissue. Expressed are several ZIPs, ZnTs but also DMT1 and the TfR. Different from intestinal Fe transport, Tf-bound Fe can also be taken up by hepatocytes via endocytosis. This process is mediated by the TfR and DMT1 since it has been shown that hepatic-specific inactivation of DMT1 led to a decrease in Fe uptake of 40 % [178]. However, TfR1-mediated Fe uptake is rather minimal since it is highly dependent on Fe status. Therefore, hepatic NTBI uptake by ZIP14 is regarded as the major pathway [179]. Apart from that Mn, Fe, and Zn uptake and distribution in hepatocytes follow the already discussed pathways whereas the role of ZIP8 and ZIP14 in Zn transport is higher in the liver compared to the intestine. The metalloprotein MT appears as apo-MT, the unbound protein with 7 Zn binding sites [106,180]. FPN, the predominant Mn and Fe exporter, plays also a role in hepatocytes since it has been shown that mice with hepatic-specific FPN deletion develop disruption of hepatic Fe mobilization and anemia [181]. The liver

is the predominant organ of hepcidin synthesis regulating the Fe storage in hepatocytes [177]. This regulation is perturbed in inherited hemochromatosis, a genetic disorder leading to increased FPN expression under low hepcidin levels in hepatocytes accompanied by NTBI accumulation. In case of inflammation, hepcidin is overexpressed resulting in Fe deficiency [177]. Rare genetic variants in ZIP14 and ZnT10, which have been discussed in the context of Mn homeostasis in the brain, have been shown to elevate several liver enzymes such as the alanine transaminase (ALT) potentially due to hepatic inflammation [182,183]. The same could be observed in blood samples of mine workers also including increased aspartate transaminase (AST) and acid phosphatase (ACP) levels. However, common hepatic disease pathologies associated with Mn exposure are hepatic encephalopathy and liver fibrosis in the cirrhotic liver [183]. Mn-induced hepatotoxic modes of action include among others inflammation, mitochondrial dysfunction by inhibiting complex I and IV of the respiratory chain, and calcium efflux, leading to enhanced oxidative stress and apoptosis [183]. For Zn, the liver is a fast-exchangeable Zn pool, which is not only important for Zn homeostasis [173]. While some tissue Zn levels remain unaffected in dietary Zn-deficient states, the liver is one of those showing decreased Zn levels also including decreased MT synthesis mediated by MTF1 [173,184]. Further, a reduction in Zn levels has been associated with impaired liver function including defective regeneration [185]. Regarding impaired liver function and *in vivo* animal studies indicating an influence on decreased hepatic and serum Zn levels in acute and chronic liver injury and hepatocellular carcinomas the role of Zn deficiency is not completely understood [173]. However, this highlights that disruption of TE homeostasis is not always the cause but the consequence of impaired liver function [173]. This can be underlined by the fact that alterations in transporter expression and regulatory proteins from single TEs discussed in this paragraph do not only have an impact on one element but on all those who are somehow related or affected by their regulation.

To investigate hepatic function and metabolism *in vitro*, 40 hepatic tumor cell lines have been established. Among others, HepG2 cells are commonly applied in scientific research as they exhibit key characteristics of hepatocytes, such as metabolic functions. HepG2 cells are derived from the liver tissue of a 15-year-old Caucasian boy, however, the histological liver tumor type is still under discussion. While HepG2 cells have been proposed to originate from hepatocarcinoma, López-Terrada *et al.* identified them as hepatoblastoma cells. In scientific research, HepG2 cells are utilized to study the effects of heavy metals, nanoparticles, and drugs. Additionally, many transporters involved in hepatic TE uptake and distribution are expressed

in HepG2 cells while the metalloprotein ceruloplasmin can only be determined in trace amounts. The role of TE transporters in HepG2 cells is discussed in further detail in chapter 5 – The Impact of Zinc on Manganese bioavailability and cytotoxicity in HepG2 cells [186-188].

2.3. The role of trace elements in the target organ brain

Maintaining homeostasis of Mn, Fe, and Zn is fundamental for proper brain function and adequate cellular brain TE supply. With inhalation as one of the major pathways of Mn, Fe, and Zn exposure, the brain is the initial target for TE-induced detriments, due to the bypass of the efficient regulation of the BBB typically avoiding excess TE supply. Disturbance of this homeostasis in the human brain has shown to induce damage in the central nervous system (CNS) in the form of neurodegeneration or neuroinflammation potentially leading to several pathologies referred to as neurodegenerative diseases [5,189].

The hallmarks of neurodegenerative diseases are continuous neuronal dysfunction and loss of neurons [190]. In the pathologies of PD and AD, these hallmarks are accompanied by the deposition of aggregated proteins. Discussed in this context are pathways including chronic exposure to excitotoxicants, which induce, among others, neuroinflammation, and autoimmunity but also the generation of increased RONS, which can be the cause or consequence of mitochondrial dysfunction [5]. Metal-induced neurotoxicity, which is associated with excessive metal accumulation may therefore initiate a cascade of compartment and protein detriments. Brain structures are more vulnerable to oxidative insults due to the high metabolic turnover and energy utilization. Therefore, a variety of enzymes are expressed in several organs of the human body balancing the redox homeostasis by maintaining antioxidative defense mechanisms such as superoxide dismutase (SOD), catalase (CAT), and glutathione. Since TEs like Mn and Zn are also important co-factors for the enzyme function of the SOD, disrupted metal homeostasis in both directions can lead to the opposite effect and the disturbance of the redox homeostasis [5,191,192].

In general, the brain is one of the organs with the highest Zn concentrations of about 150 µM [193]. Zn is essential for synaptic transmission and the modulation of post-synaptic receptors since it is released from the presynaptic vesicles of glutaminergic neurons. It is often associated with neuroprotection due to its involvement in the regulation of acute immune defense. Intracellularly, Zn occurs in different forms, protein-bound and free cytosolic Zn or extracellular in the vesicles. Studies have shown alterations in the CNS and its immune defense associated with changes in plasma Zn levels discussed in the context of multiple sclerosis.

While deficient but also excess cytosolic Zn has been implicated in the pathogenesis of AD [5,122,194]. Therefore, intracellular Zn levels are tightly regulated to avoid adverse effects [5]. Fe is important in the CNS for oxygen transportation, oxidative phosphorylation, and the synthesis and metabolism of neurotransmitters [195]. However, Fe-induced oxidative stress can result in Fe release from ferritin leading to interactions with macromolecules such as lipids and DNA which in turn may elicit neurodegeneration. On the other side, neurodegenerative diseases can be the cause of disturbed Fe homeostasis, especially of inadequate Fe distribution [5,196]. Mn predominantly maintains the function of the manganoprotein glutamine synthetase, pyruvate decarboxylase, serine/ threonine-protein phosphatase I, MnSOD, and arginase, which are important for neurotransmitter synthesis, metabolism, and neuronal function. In conditions of low brain Mn levels, the activity of the glutamate synthesis is decreased inducing excitotoxic effects as glutamate accumulation at the synapses. The transition of Mn(II) to Mn(III) triggers autoxidation of dopamine, which is one of the proposed mechanisms of Mn-induced neurotoxicity. Potential target brain regions are the *basal ganglia*, *globus pallidus*, *cerebellum*, and *thalamus*. Furthermore, the accumulation of Mn in mitochondria affects oxidative phosphorylation and ATP synthesis leading to mitochondrial dysfunction potentially due to an increase in oxidative stress and loss of mitochondrial membrane potential [5,27,35]. While physiological brain Mn concentrations range between 5.32 – 14.03 ng Mn/ mg protein, corresponding to 20.0 – 52.8 µM Mn, Mn concentrations in case of aberrant brain function are 3-fold higher with 14.96 – 42.09 ng Mn/ mg protein, corresponding to 60.1 – 158.4 µM Mn [197].

Mn, Fe, and Zn uptake take place across the BBB and B-CSF-B. The BBB separates interstitial brain fluid from the blood by a cellular structure, which is mainly composed of capillary endothelial cells. Contributing to the stability of the BBB are astrocytes, pericytes, and neuronal cells. The B-CSF-B is mainly composed of epithelial cells of the choroid plexus, accompanied by fenestrated capillaries, which separate blood from the CSF. Transporters involved in brain Mn, Fe, and Zn homeostasis are the same already discussed for the liver, and intestine with endocytosis via TfR, DMT1, ZIP8, ZIP14, and ZnT10. Additionally, the calcium-permeable AMPA channel ((α-amino-3-hydroxy-5-methyl-4-isoxazole-propionic acid)/ kainate channel) has been discussed to play a role in brain Zn homeostasis, while SPCA1 is important for brain Mn homeostasis [68,128,198-201]. Inherited mutations in the gene associated with ZnT10 already discussed in chapter 2.1 result in Mn accumulation in the brain. This can be explained by ZnT10 mRNA expression, which is generally high in brain tissue and shows a higher response to Mn than Zn [46].

As partly mentioned before, all three TEs have been discussed in the pathogenesis of AD and PD. Intracellular accumulation of Aβ, the main hallmark of AD, can be caused by increased oxidative stress and sequestration of Zn within the amyloid plaques. While intracellular Zn in the μM range has been shown to lead to the suppression of Aβ, higher Zn amounts enhanced Aβ formation and aggregation. The formation of these senile plaques was further associated with decreased mitochondrial MnSOD activity in the brains of AD patients. A similar phenotype has been observed for Fe, which may be able to accumulate in the amyloid plaques.

With symptoms similar to PD, manganism has been associated with Mn accumulation in the *basal ganglia*. However, as already mentioned, the pathologic phenotype is distinct from idiopathic PD. Regarding PD pathology, decreased Zn levels have been observed in PD patients compared to healthy individuals. Moreover, it has also been discussed to be involved in the formation of Lewy bodies and aggregation of α-synuclein [5,132,202,203].

To model PD *in vitro*, SH-SY5Y cells and PC12 cells have been proven to facilitate high-throughput screening due to simple culture procedures. However, their exact dopaminergic phenotype has been discussed until today. A cellular system ensuring physiological relevance is represented by the Lund human mesencephalic (LUHMES) cell line. They are derived from an embryonic human mesencephalon and are further immortalized by the introduction of a tetracyclin-responsive v-myc gene (TET-off). Differentiation with tetracyclin, cyclic AMP (cAMP), and glial-derived neurotrophic factor leads to the cell-cycle exit and development of dopaminergic-like neurons. These express dopaminergic-neuron-specific markers like tyrosin hydroxylase and β-tubulin and are able to develop an extensive neurite system, which offers several advantages regarding investigating the role of Mn, Fe, and Zn in dopaminergic neurotoxicity [204,205].

2.4. The role of trace elements in pregnancy

2.4.1. Formation and structure of the human placenta

The placenta is a transient, highly specialized organ promoting normal fetal development and growth. Alterations in placental developmental programming, including structure and function, have detrimental effects on fetal development, such as fetal growth restriction or preeclampsia or even miscarriage and stillbirth [206]. Not only the fetal development but the placental growth is a tightly regulated process of interactions between the maternal endometrium and fetal-derived cells of the implanting blastocyst [207].

The inception of placentation is taking place 5 – 6 days post-fertilization by the attachment of the blastocyst to the maternal endometrial epithelium [208]. For this, trophoblasts surrounding the blastocyst proliferate and invade the surface epithelium of the endometrium. Subsequently, the trophectoderm (trophoblasts) differentiates into an outer invasive syncytiotrophoblast mass and an inner cytotrophoblast layer immediately after the attachment (6 – 8 days post-fertilization) [207-209]. After the formation of a primary syncytium, syncytiotrophoblasts further invade the connective tissue of the endometrium forming the decidua [210,211]. Within the syncytial mass, fluid-filled areas termed lacunae, appear [210]. In this lacunae stage of placental development, lacunae coalesce to form the intervillous space, and syncytiotrophoblasts form columns, referred to as trabeculae, reaching from the maternal decidua to the embryonic part of the placenta [212]. Approximately 14 days post-fertilization, implantation is completed and the blastocyst is embedded in the decidua, surrounded by surface epithelium [207,210].

As placentation progresses, cytotrophoblasts of the inner cell mass penetrate the layer of syncytiotrophoblast trabeculae forming columns of extravillous cytotrophoblasts. These extravillous trophoblasts represent the primary villi of the villous tree (12 – 14 days post-fertilization) [207,208,212]. In case cytotrophoblasts penetrate the primary syncytium, they merge at the lateral side developing a cytotrophoblast shell to surround the conceptus. The cytotrophoblast shell is then in direct proximity to the endometrium, able to anchor the placenta to the decidua [208,210]. 17 – 18 days post-fertilization, extraembryonic mesenchymal cells invade the villous core, forming secondary villi. Within the core fetal capillaries develop, starting the progress of vascularization by the formation of tertiary villi [208,210]. By progressive branching, the villous tree extends from the chorionic plate multiplying into a complete system of villous trees. On the maternal-fetal interface, where the cytotrophoblast core meets the decidua, several cytotrophoblasts leave the shell and migrate into the decidua forming extravillous cytotrophoblasts. This process is resembling characteristics of epithelial-mesenchymal transition and is of central importance for later spiral artery transformation [208,210]. At the end of the first trimester with the formation of the extravillous cytotrophoblasts, the main structure of the placenta is specified and the process of placentation is finalized [210]. Despite the placental structure, the primary functions are developed by the second trimester [209]. However, as pregnancy progresses, the placenta develops further according to the increasing demands and metabolism of the fetus even until term [209]. This is realized especially by elaborating the complex structures of fetal vasculature and blood vessel

formation, facilitating the exchange of oxygen and nutrients across the maternal-fetal interface [207]. In that case, the mature placenta is separated into vascular units, represented by certain cotyledons. These cotyledons include the villous trees, which are separated from the maternal blood in the intervillous space by an epithelium-like layer often referred to as the placental barrier [213]. The formation of the human placenta from the implanting blastocyst to the definite placenta is depicted in the following fig. 4.

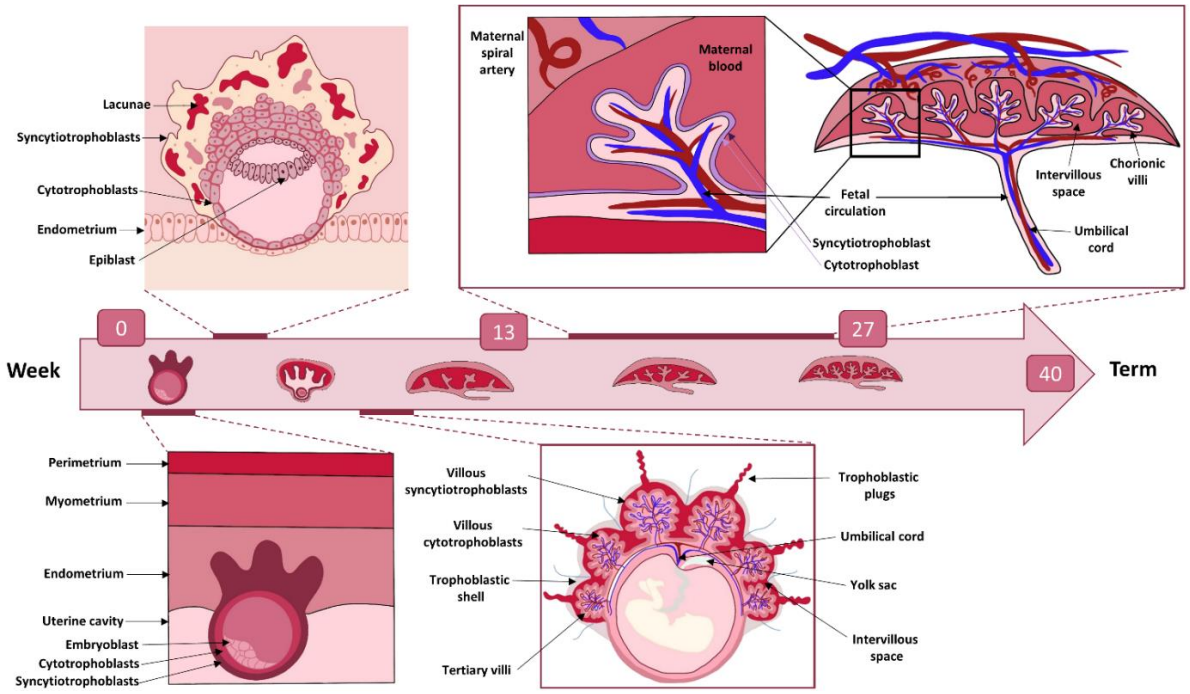

Figure 4: Formation of the placenta from implantation to the definite structure (adapted and modified from [209,214]).

2.4.2. The placental barrier

The placental barrier or blood-placental barrier is structured by four different cell types early in pregnancy (50 – 100 µm thickness), whereby the development occurs over the entire course of placentation [215,216]. Hereby, all cell types present in the placental barrier are derived from the blastocyst and are therefore of fetal origin [210]. Already three weeks post-fertilization, the surface of the recently developed villi is coated with two trophoblast layers (cytotrophoblasts, syncytiotrophoblasts), anchored to the basal lamina [213,217,218]. Under the trophoblast layer, extraembryonic mesenchyme (fibroblasts) can be found containing basic elements of vasculature like fetal vessels [217,218]. During the process of placentation, the layer of cytotrophoblasts becomes discontinuous, probably due to extensive proliferation and differentiation of the cytotrophoblasts resulting in the formation of multinuclear

syncytiotrophoblasts [215,217]. However, the total number and volume of the cytotrophoblast layer do not change, since they extend across the whole basal lamina [215,217]. It is assumed that asymmetrical cell division, differentiation, and fusion of the villous cytotrophoblast with the early syncytium is leading to the formation of the syncytiotrophoblast layer. By conversion of the syncytiotrophoblast to the syncytial state, the trophoblast phenotype is changing, resulting in the production of important pregnancy hormones like human chorionic gonadotropin (hCG) and placental lactogen, both of which are indispensable for placental development and maintenance of pregnancy [219-221]. Moreover, as pregnancy proceeds the syncytium is locally thinned, due to the rapid expansion of the surface area without the adaption of the cell volume. In this part of the so-called vasculo-syncytial membrane, the syncytium is in direct proximity to the fetal vessels [213,217]. At this stage of placental development, the placental barrier is composed of mainly syncytiotrophoblasts, a thin layer of cytotrophoblasts, and fetal endothelium of about 2 – 5 μm thickness [218,222,223]. At term, around 44 % of the basal lamina is covered by remaining cytotrophoblasts, however not affect nutrient transport across the syncytiotrophoblasts [215,222]. The structure of the human placental barrier is depicted in fig. 5.

One of the many functions of the placenta is the protection of the fetus against several xenobiotics or infections. Hereby, the placental barrier serves as the maternal-fetal interface regulating the passage of compounds negatively affecting fetal development. Besides the protection of the fetus as a gatekeeper, the placental barrier can also be a target of a compound- or xenobiotic-induced toxicity [213]. In the syncytiotrophoblasts isoforms of several phase I, and phase II enzymes of the xenobiotic metabolism are expressed (cytochrome P450, uridine diphosphate glucuronyltransferases, glutathione-S-transferases, and sulfotransferases among others) but also ABC (ATP binding cassette) transporters like breast cancer resistance protein, multidrug resistance-associated protein, and P-glycoprotein [221,224,225]. However further details on maternal-fetal drug metabolism exceed the scope of this thesis but are reviewed elsewhere [224,225].

To maintain fetal development, the placental barrier and especially the syncytiotrophoblasts are the key player in fetal nutrient supply. Nutrient transport processes across the syncytiotrophoblasts can be separated into three different groups such as transcellular, paracellular, and active modes of transport. Here the transport across the tight junctions of adjacent cells is referred to as paracellular transport, while transcellular transport includes

simple and facilitated diffusion [226,227]. Active modes of transport are primarily represented by transporter-mediated processes, which are accompanied by proton symport, transport against a concentration gradient, or ATP utilization [116,228-230]. The following paragraph 2.4.3 will give further information on maternal-fetal nutrient transfer mechanisms from early to late pregnancy including TE-assumed transport.

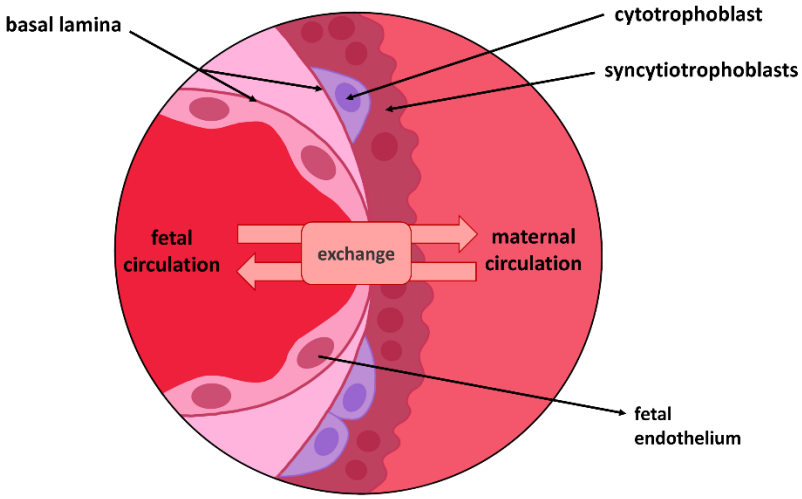

Figure 5: Structure of the human placental barrier (adapted and modified from [231]).

2.4.3. Transport of nutrients during gestation

During pregnancy, placental fetal nutrient supply is provided by villi bathing in maternal blood in the intervillous space. However, until 6 – 7 weeks of gestation, early spiral arterioles are plugged by endovascular cytotrophoblasts restricting maternal blood flow [207,219,232,233]. To maintain fetal development, the fetus is supplied with histotrophic nutrition [207,232]. Histotrophic nutrition means the phagocytosis of endometrial glandular secretions by the trophoblasts. Those secretions of the uterine gland are composed of glycogen, lipid droplets, and a variety of glycoproteins possibly transferred through the yolk sac [234]. During the first 9 weeks of pregnancy, anaerobic processes are important for proper organogenesis in the human embryo [235]. To satisfy the metabolic demands of the developing embryo, anaerobic glycolysis proceeds from glycogen, which accumulated in the syncytiotrophoblast [235]. Besides carbohydrates, proteins, and lipids, evidence suggests that the uterine secretions also contain glycodelin A, an enzyme, which is involved in immunosuppression, angiogenesis, and apoptosis but also cytokines, like TNF-α (tumor necrosis factor α), uteroglobin, epidermal growth factor, colony-stimulating factor and vascular endothelial growth factor. All of which are important for the proliferation and migration of trophoblasts *in vitro* [235-239].

Furthermore, after 10 – 12 weeks of gestation trophoblast plugs rupture, and maternal blood flows into the intervillous space begins [219,233]. Then maternal blood is in direct contact with the fetal villi resulting in nutrient transfer across the placental barrier, often referred to as hemotrophic nutrition [207,234]. In the syncytiotrophoblasts, the transporting endothelium of the placental barrier, nutrients have to cross two different polarized membranes until reaching fetal capillaries. While the microvillous plasma membrane is facing maternal blood, the basal plasma membrane is directed towards fetal capillaries [240]. Nutrient transport across those membranes is often referred to as vectorial transport, which means unidirectional from mother to child [241]. One of the many transport processes occurring in placental transport is diffusion, which is mostly driven by the concentration or electrochemical differences between maternal and fetal circulation [241]. Whereby diffusion is directly proportional to the exchange surface area but inversely proportional to the diffusion distance of the considered circulations (according to Fick's law) [241,242]. Despite the influence of placental structure, studies have shown electrical alternating gradients during gestation. While in mid-gestation a potential difference of -2.7 ± 0.4 mV has been determined, it is reduced to almost zero at term [242-244]. For small, hydrophobic molecules such as oxygen or carbon dioxide, transport proceeds rather across a concentration gradient than dependent on surface area or barrier thickness. Nevertheless, this concentration gradient is dependent on the rate of blood flow across the placental membranes and therefore oxygen and carbon dioxide supply are flow-limited [242]. However, this does not account for hydrophilic molecules since they are less affected by concentration gradients and do therefore not readily cross placental membranes [241,245]. It has been suggested that diffusion of these substances occurs through water-filled pores. Since the syncytiotrophoblast layer is a true syncytium, lateral intercellular pores are absent and the aqueous pores seem to be transcellular [246,247]. However, despite the controversy about placental structure, it has been suggested, that this yet rather paracellular route can potentially be formed during the denudation of the syncytiotrophoblasts [241,247,248]. Recently, 3D visualization of human syncytiotrophoblasts by Lewis *et al.* (2022) revealed non-selective trans-syncytial nanopores providing diffusion processes [249]. The structure of these nanopores is heterogeneous and those directed toward the basal lamina provide nutrients in the most direct way to the fetus [249,250]. However, the role of nanopores is still under discussion also in relation to nutrient transporters expressed on these foldings [249,250].

In order to provide fetal supply to hydrophilic or charged molecules, transporter proteins are expressed across the plasma and basal membrane. In general, the transport proteins share

several characteristics such as substrate specificity, saturation, or competitive inhibition [242]. A variety of proteins involved in macronutrient transport are expressed in the syncytiotrophoblasts like several isoforms of the GLUT family facilitating glucose transport or the energy-consuming active transport of amino acids by 20 different transport proteins like L-type transporters as an example [208,213,242]. Besides macronutrient transport, several trace metal-associated transporters are expressed in the placental tissue. According to the function of the respective transporter, they are localized on the plasma membrane or the basal membrane of the syncytiotrophoblasts [251]. Additionally, the role of other cell types like mesenchymal, Hofbauer, or endothelial cells in fetal TE supply across the placental barrier is still unknown [252]. Among the variety of metal-associated transporters, expression patterns of those involved in Fe transport are widely characterized. The Fe importer TFR1 is highly expressed in the human placenta and localized to the apical, maternal-facing side of the syncytiotrophoblasts, while DMT1 can be found intracellularly and at the basal membrane, facing fetal capillaries [251-255]. ZIP8 and ZIP14, both of which were initially assumed to be specific to transport Zn, are also expressed in the syncytiotrophoblasts [256]. However, ZIP8 mRNA expression is more abundant compared to ZIP14 mRNA expression [75,252]. Due to the pH dependence of the metal transport by DMT1, and ZIP8, it is assumed that both are expressed intracellularly on the membrane of endosomes [75,160,252,255,257]. Metal export is provided by FPN1, which can be found on the basal membrane, facing fetal capillaries [251].

Among the carrier-mediated transport, molecules like immunoglobulin G but also Fe are transferred across the syncytiotrophoblast via endocytosis. Endocytosis is defined as the regulated active transport mechanism of molecules incorporated into vesicles, which can be separated into clathrin-mediated, caveolae-mediated, or clathrin/caveolae-independent processes [258]. Furthermore, immunoelectron microscopy has shown that Tf and TfR1 are expressed on the membrane of intracellular vesicles and invaginations, which are also clathrin-coated [259,260]. These clathrin-coated pits can also be found on invaginations of the syncytiotrophoblast microvillous membrane highlighting the role of endocytosis in the context of Fe transfer [258,261].

2.4.4. Maternal-fetal micronutrient requirements and trace element interactions

Fetal but also placental development is dependent on adequate nutrient supply, which is ensured by maternal nutrition. During gestation, fetal micronutrient demands are rising, potentially increasing the risk of maternal micronutrient deficiency. Maternal malnutrition in

turn may also have an immense impact on fetal development by increasing the risk of diseases, among others related to congenital heart defects or neurodevelopment [262]. Additionally, the outcome of pregnancy can also be negatively affected, potentially leading to preterm labor or preeclampsia [263,264]. To avoid maternal micronutrient deficiency, several formulations of micronutrient supplements are commercially available, to increase nutrient supply which could not be ensured by balanced nutrition due to highly processed food or depleted TE amounts in soils [265]. Additionally, the micronutrient status of the majority of pregnant women is not monitored during gestation and the number of women using prenatal supplements is increasing. However, concerns are rising that the relation of an increased risk for adverse pregnancy outcomes such as preterm birth or small-for-gestational-age may be strongest for women regularly using supplementation [263,265]. Institutions like the DGE or EFSA revised data on micronutrient-related studies in order to assess recommendations for the general population but also sensitive populations like pregnant women [1-4]. However, data related to this is limited, since pregnant women are mainly excluded from nutrition studies, and data provided by animal models or *in vitro* data do not represent the complex structure of the human placenta *in vivo* or the process of pregnancy [7,266]. The Institute of Medicine from the United States on the contrary, also considers different body-related factors like the increase in body weight or hemoglobin mass as pregnancy progresses [267,268]. However, apart from the influence of maternal nutrient status in general, endocrine function and hormone metabolism of the mother and the fetus have an impact on fetal nutrient supply but exceeds the scope of this thesis (reviewed exemplarily in [269-271]). Despite the other micronutrients important for fetal development and placental homeostasis, the next paragraphs will focus on maternal-fetal micronutrient requirements of the three TEs Fe, Zn, and Mn.

Next to many functions within the metabolism of adults, Fe is also important for fetal development, serving as a co-factor in long-term neurodevelopment and erythropoiesis but also maintenance of placental homeostasis [272,273]. A total of 1040 mg of Fe are required for a healthy singleton pregnancy, with approximately 300 mg for the fetus, 50 mg for the placenta, 450 mg for the increasing maternal red cell mass, and 240 mg for basal iron losses. In consideration of sufficient iron stores, the net iron requirement in pregnancy is about 840 mg [2,274]. Since the mass of red blood cells is increasing immensely and fetal Fe supply is ensured only from the transfer across the placental barrier, women, in particular, are at risk for Fe deficiency with a prevalence of about 30 – 50 % affecting about 32 million pregnant women worldwide [264,272,275,276]. Severe Fe deficiency during gestation has been associated among

other pregnancy or disease-related outcomes with increased perinatal death, preterm birth, low birth weight, maternal mortality, impaired immune function, and long-term cognitive defects in newborns and infants [273,277,278]. Based on several studies showing that Fe supplementation alleviates the risk of Fe deficiency and resulting adverse pregnancy outcomes, the WHO recommends Fe supplementation of about 30 – 60 mg of elemental Fe for pregnant women [277,279]. In contrast to this, the Preventive Services Task Force of the United States stated, that data availability is insufficient to assess the balance between the benefits and harms of Fe supplementation during pregnancy [280,281]. Potential negative alterations of placental development and pregnancy in humans by Fe overexposure are still not well characterized [281]. However, it has been shown that especially preterm infants are more susceptible to oxidative stress induced by excess non-Tf-bound Fe due to their immature antioxidant system. Additionally, since Fe is not eliminated actively, ROS generated by the Fenton reaction may accumulate in the tissue leading to cytotoxicity [282]. This is particularly difficult in the developing immature brain, where antioxidative enzymes such as superoxide dismutase, catalase, and glutathione peroxidase have a decreased activity [283-285]. In pregnancies with higher risks of inflammation, placental cells are more sensitized by Fe-induced oxidative stress resulting in increased embryotoxicity [281]. Considering TE homeostasis of the developing placenta, Fe in excess may also interfere with Zn and Cu metabolism leading to an altered Zn and Cu availability and homeostasis [286]. Mn and Fe homeostasis in the placenta and across placental barrier-building cells is further discussed in chapter 4 – Differences and Interactions in Placental Manganese and Iron Transfer across an *In Vitro* Model of Human Villous Trophoblasts.

Since Zn is a component of a plethora of enzymes involved in human metabolism it plays an important role in several processes of fetal development. It is a determinant in chromatin biochemistry by affecting chromatin structure and function, which in turn may have an impact on gene expression of embryogenesis-associated genes [287,288]. Additionally, it has been shown that Zn deficiency during pregnancy may lead to reduced placental weight, trophoblast volume, and barrier thickness but also maternal blood pressure, potentially resulting in insufficient Zn supply to the fetus. It is affecting fetal programming of cardiovascular and renal diseases, which may result in an increased risk later in life [289-291]. Zn requirements during pregnancy were assessed by the EFSA in 2014. Considered data is based on the weight of tissue formed during gestation and their Zn concentration, which was measured by Widdowson and Dickerson *et al.* (1964) and added by calculations from Shaw *et al.* (1979) regarding Zn

accumulation by the growing, developing fetus. Regarding both studies, the total Zn requirement during pregnancy has been calculated to be about 100 mg, where 60 % accounts for the fetus and the rest for the placenta and other tissues. However, data regarding Zn requirements during pregnancy are inconsistent to modify those additional estimated daily increments. Therefore, the EFSA proposes a PRI of 1.6 mg Zn/ day including the additional physiological requirement of 0.4 mg/ day [4,292,293].

Due to placental Zn transport and Zn-binding MTs, the fetal Zn levels are higher compared to the maternal Zn levels [110]. Interestingly, an affinity for Zn and Zn uptake capacity in human placentae is affected by gestational age and low levels of maternal serum Zn even if both conditions do not alter [264,294,295]. Nonetheless, in case of insufficient Zn supply, maternal Zn deficiency affects placental and fetal development and has been associated with adverse pregnancy outcomes such as abortion, preterm delivery, stillbirth but also growth retardation and malformations like fetal neural tube defects [119,296]. Furthermore, the occurrence of other pathological conditions is affected by the Zn status in the first weeks of the neonate. Especially in the case of Zn deficiency, neonates have an increased risk for dermatitis, growth retardation, neurological damage (specifically in case of hypoxia), and infections [288]. Several studies have shown that Zn supplementation during pregnancy minimizes the risk of premature birth and has positive effects on fetal neurobehavioral development and birth length [119]. However, exceeding the required Zn amount by supplementation may have an impact on Cu homeostasis by increasing Cu excretion leading to Cu deficiency [119]. Additionally, it has been shown that combined exposure to Fe has a negative effect on Zn absorption. While a mass ratio of 1:1 Fe/Zn slightly reduces Zn absorption, increasing Fe amounts (2:1 or 3:1 Fe/Zn) limit Zn absorption, which in turn may lead to Zn deficiency [119,297].

According to Fe and Zn, Mn is also a co-factor critical for normal fetal neurodevelopment, growth, and cellular homeostasis and enzymes involved in carbohydrate metabolism and antioxidative defense [298,299]. Nonetheless, the availability of data on observed Mn intakes in pregnancy is limited mainly due to a lack of sensitive biomarkers of maternal/ fetal Mn status or Mn exposure despite some estimates based on blood concentrations [300]. While the Institute of Medicine from the USA proposed an AI of 2 mg/ day, which included the involvement of median weight gain during pregnancy, the EFSA derived an AI of 3 mg/ day, which is in accordance with the AI of non-pregnant women. Due to the homeostatic control of Mn, the EFSA did not include pregnancy-associated weight gain. However, Mn requirements in

pregnancy are still under discussion [3,267]. In comparison to other micronutrients, positive as well as negative effects of Mn on fetal development are not well characterized [301]. Few epidemiological studies exist where it has been shown that higher levels of Mn exposure *in utero* (measured as maternal blood and/ or cord blood concentrations) were inversely associated with neonatal neurodevelopment, including decreased psychomotor or mental development [66,302,303]. Since Mn crosses and accumulates in the placenta it is suggested, that enhanced Mn in placental tissue has a higher impact on fetal health than maternal Mn levels [304,305]. However, higher umbilical cord blood compared to maternal Mn levels have been positively correlated with intrauterine growth restriction and lower birth weight [306]. Moreover, Liu *et al.* suggested a dose-dependent correlation between higher Mn levels in placentas and the risk for neural tube defects, which is increased 4-fold [299]. In consideration of detrimental health issues later in life, an epigenetic approach by Maccani *et al.* provided first evidence on DNA methylation patterns in the placenta, which can be associated with prenatal Mn exposure. This may in turn contribute to neurodevelopmental problems during childhood and cancer later in life [305]. On the contrary, little is known about Mn deficiency in humans. Some animal studies have shown an association of Mn deficiency with impaired growth, skeletal defects, and abnormal glucose and lipid metabolism [301]. In contrast to Fe, the extent of fetal Mn exposure is not well understood, since Mn transfer across the syncytiotrophoblast is based on rodent data or measurements of maternal and umbilical cord blood [307]. An *in vitro* study in perfused placental lobules hinted at an active transport mechanism, however, as shown in chapter 4, Mn transfer may be more complex [306,308]. With regard to Fe and Zn, combined exposure of Mn with both TEs alters uptake, respectively, potentially due to the unspecificity of the transport systems [19,27,299].

Nevertheless, there is a lack of knowledge about the exact modes of transport and interactions of Mn, Fe, and Zn across placental tissue, which are urgently needed to also understand the homeostatic control of combined TEs. In general, studies focusing on health effects due to micronutrient supplementation do not include pregnant women. In a recently published research article by Smith *et al.*, the lack of data regarding micronutrient requirements during pregnancy is addressed, highlighting the difficulty of micronutrient requirement assessment [7].

2.4.5. Modeling the placental barrier – advantages and limitations

Understanding the structure and functionality of the placenta and the placental barrier is important for investigating fetal nutrient supply. For this several studies focused on suitable models recapitulating most of the functions *in vivo*. These studies include *ex vivo* placental perfusion, animal models as well as *in vitro* cell culture approaches [208].

Ex vivo placental perfusion has been an established gold standard method in regarding nutrient transfer studies. It was first implemented by Panigel *et al.* in 1962 and further developed by Schneider *et al.* and Miller *et al.* [309-311]. To date, lots of progress has been made in optimizing perfusion conditions and methods also regarding the experimental outcome. Perfusion methods used today can be separated into non-circulating (open/ single-pass) or recirculating (closed) perfusion systems [312]. They are realized mainly on term placentae, independent if delivered by vaginal birth or cesarean section [313]. However, methods used for the perfusion of placentas collected directly after delivery, are not standardized and differ across laboratories [312]. Nevertheless, perfusion experiments represent the complexity of the placenta as a whole organ also including placental metabolism [312,314]. On the other hand, since the placenta is not only highly species-specific but also shows high donor-to-donor variations, reproducibility is difficult to obtain. Furthermore, shortly after delivery, placental tissue starts to degenerate, limiting perfusion duration and is therefore disadvantageous regarding experimental throughput and success rate [220,222,315,316].

The utilization of animal models represents pregnancy in a whole organism, including fertilization, implantation of the blastocyst, and placental and fetal development [317,318]. Due to large litter sizes and short gestation periods, they have been demonstrated as a useful tool with relatively low costs in housing and maintenance [317]. Nevertheless, many studies highlighted distinct differences between the stages of pregnancy, formation of the placenta, and underlying placental tissue, making it difficult to extrapolate results to potential outcomes in humans [266,319]. In general, humans and mice develop the same type of placenta, the haemochorial type, where fetal villi are bathing in maternal blood [320]. However, the placental structure in mice is organized in a junctional and a labyrinthine zone, with the labyrinthine zone as the maternal-fetal exchange layer [234,266]. On the contrary, the human placenta has a more villi-like structure. One major difference regarding maternal-fetal nutrient transfer is the composition of the placental barrier. While the mouse placental barrier is hemotrichorial (consisting of three different trophoblast layers) the human placental barrier is

hemomonochorial, meaning the occurrence of one syncytiotrophoblast layer [266,317]. These interspecies differences are disadvantageous regarding substance-specific effects in human pregnancy. However, according to the 3R principle (Refinement, Reduction, Replacement), the choice of animal models should be refined, reduced, or replaced. Therefore, many *in vitro* approaches were established trying to represent the complex structure of the placental barrier but also models of early stages of pregnancy like early blastocyst implantation and trophoblast invasion [209,266,318,319,321].

Starting from trophoblast invasion lots of progress has been made in combining organoids of first trimester trophoblasts and the endometrium. Here, cells for those organoids are derived from unused blastocysts of *in vitro* fertilization, first trimester placentae, or the endometrium of non-pregnant women [321-324]. These isolated multipotent trophoblast stem cells or first trimester trophoblasts can further differentiate from villous cytotrophoblasts into syncytiotrophoblasts and extravillous trophoblasts. It has been proven, that organoids differentiated to syncytiotrophoblasts are able to release hCG and among other syncytiotrophoblast-specific markers express CD46 and CD71 (integrin α-IIb and TfR) [324]. Furthermore, they can be cultivated for up to 6 months with continuous passaging and can also be cryopreserved, convenient for the establishment of biobanks [318,321-324]. These models highly promote trophoblast research. However, since first trimester placentae are obtained from elective pregnancy terminations, tissue availability is limited and studies need to be justified from an ethical point of view and approved by the local ethics committees [321,324].

Next to investigations of the early stages of placental development, a variety of *in vitro* model systems focused on the maternal-fetal interface, the placental barrier. To represent the villous and extravillous structure of the placental barrier, cells derived from gestational choriocarcinoma or immobilized trophoblasts are applied. Depending on the stage of pregnancy and the underlying cellular structure of the placental barrier, a variety of cell lines are well established. Among the widely used BeWo subclone b30, other cell lines include Jeg-3, JAR, ACH-3P, HTR-8/Svneo, and Swan-71. Hereby, BeWo b30, Jeg-3, and JAR cells are derived from the gestational choriocarcinoma, while ACH-3, HTR-8/Svneo, and Swan-71 cells are virus-transfected primary trophoblasts derived from villous explants or fused with a choriocarcinoma cell line (ACH-3P) [325-328]. Using trophoblast cell lines is beneficial regarding handling, availability, and long-term culture since they are highly proliferative [222,329,330]. However, due to their malignancy, they have an abnormal number of chromosomes, and not

all of them showed syncytiotrophoblast-, or barrier-like characteristics, and proliferate without transfection or subcloning [318,331,332]. Additionally, gene expression or metabolic processes may be altered because of their tumor characteristics [329]. To overcome these limitations, primary trophoblasts are used, which can be applied to investigating early trophoblast invasion if isolated from first-trimester placentae [219]. Using primary trophoblasts, which rather resemble *in vivo* conditions (compared to cell lines) is also challenging, since isolated first-trimester trophoblasts either exit the cell cycle, differentiate to syncytiotrophoblasts, or degenerate because of the induction of apoptosis, limiting the lifespan immensely [326,333,334]. In addition, contaminating maternal epithelial, and fetal mesenchymal cells, which are not separated carefully, can outgrow the freshly isolated trophoblast population [210,324]. However, spontaneous syncytiotrophoblast formation of primary cytotrophoblasts can be advantageous regarding investigations on syncytialization [219,329].

Especially trophoblast cell lines are often cultured on semipermeable membranes, facilitating the investigation of the transfer of nutrients, environmental pollutants, toxicants, or hormone secretion due to a compartmentalized approach [209]. In order to get primary indications on substance-specific transfer and the role of the trophoblast, monolayer models are applied. Despite their simplicity, this model allows an efficient analysis and high throughput of experiments focusing on mechanisms and properties of the trophoblast layer of the placental barrier. However, the monolayer insufficiently represents the complex structure and microenvironment of the placental barrier [209]. Furthermore, the microporous membrane interferes with cellular crosstalk of villous and extravillous trophoblasts and does not allow the investigation of gene programming involved in the formation of complex cellular structures such as trophoblast vesicles [329,335]. The absence of physiological complexity can be addressed by including components of the cellular microenvironment like fibroblasts and endothelial cells. Kreuder *et al.* applied a bioprinted methacrylated gelatin membrane mimicking features of extracellular matrix but also villous stroma by including primary placental fibroblasts [336]. Furthermore, BeWo b30 trophoblasts and primary human endothelial cells can be cultured on either side, additionally increasing the complexity of this model [336]. Moreover, the Transwell® system can also be upgraded by seeding laminin- and collagen-coated trophoblasts (BeWo or primary cytotrophoblasts) onto self-assembled capillary networks from human umbilical vein endothelial cells (HUVEC) in a fibrin hydrogel, which have also been shown to interact, even if the vessels modelled were not perfused [209,337].

Another advanced model of the placental barrier is the "placenta-on-a-chip". This technique includes a co-culture of trophoblast (BeWo b30) and human placental vascular endothelial cells (HPVEC) or HUVECs. According to the model established by Blundell *et al.* cells are seeded on a polydimethylsiloxane device with two channels, separated by a thin porous membrane. Cells are then constantly perfused, increasing fluid flow, mimicking the hemodynamic shear stress in maternal and fetal compartments. Furthermore, trophoblast syncytialization can be induced in BeWo b30 cells, which have already formed a monolayer on the surface of the microchannel. Contrary to the Transwell® system, which models nutrient transfer in a static condition, applied fluid flow leads to the formation of cellular phenotypes, the trophoblast microvilli [338,339]. Especially in the case of maternal-fetal glucose transport, the mainly involved GLUT1 transporter is expressed in higher abundance on the apical microvillous membrane, directed to the maternal intervillous space *in vivo* [340]. Additionally, transfer rates of glucose are comparable to *ex vivo* placental perfusion. Therefore, this system is a useful model for recapitulating the microenvironment of the placental barrier, fluid flow, and nutrient transporter expression patterns, which can be compared to the *in vivo* conditions. Nevertheless, as BeWo b30 cells are used as trophoblast cells in this model, limitations regarding cancer cell lines have also to be considered in this context [339].

2.4.6. BeWo b30 as a model system for nutrient transfer

Regarding studies on nutrient transfer across the placental barrier, BeWo b30 cells are commonly used, since they resemble most trophoblast characteristics and are a suitable *in vitro* model of trophoblast metabolism. Early studies in the primordial cell line BeWo have identified that 96 – 99 % of cells consist of cytotrophoblast-like cells, while the rest of the population recapitulates mononuclear syncytiotrophoblast-like characteristics [341]. However, it is unclear which stage of pregnancy is represented by the BeWo b30 trophoblasts, and whether the molecular mechanism of cell fusion and differentiation is altered compared to villous trophoblasts *in vivo* [329]. Treatment with forskolin, a potent activator of adenylate cyclase, has been shown to induce the differentiation of BeWo b30 cells to multinuclear syncytiotrophoblasts via the cyclic AMP pathway [342,343]. While it has been postulated that among BeWo cells, Jeg-3 and JAR cells are able to form a syncytium, a study by Borges *et al.* has shown, that only BeWo cells can fuse among forskolin treatment [344]. As BeWo cells were first isolated and duplicated by Hertz *et al.* in 1959, their widespread use led to the development of several strains, which were formed due to genetic drifts. Therefore, especially regarding

fusion efficiencies of syncytium formation, varying results were obtained by different laboratories [329,330,345]. However, investigating syncytialization in the context of nutrient transfer is important, since trophoblast differentiation has also been shown to impact nutrient transporter mRNA expression in the BeWo trophoblast and primary cytotrophoblasts [346]. Those studies have highlighted, that the majority of nutrient transporters are altered in similar expression patterns comparing BeWo cells and primary cytotrophoblasts. Thus, prior to the investigation of nutrient transfer across the syncytium, the suitability of BeWo cells should be considered regarding altered expression patterns compared to primary cytotrophoblasts [346,347].

As semipermeable inserts are mainly used for the investigation of a unidirectional transfer of nutrients *in vitro*, using primary cytotrophoblasts is disadvantageous, since they are not able to form a tight-junctioned monolayer. They rather form aggregates including large intercellular spaces. Therefore, using the BeWo b30 cell lines compares the advantage of the formation of a confluent monolayer and the ability of trophoblast fusion [331]. Additionally, the morphology of BeWo cells is similar compared to primary trophoblast cultures, including close cell-cell contacts and the development of the microvillous structure [331,348]. Furthermore, BeWo cells appear polarized, which has been shown by the expression of apical and basolateral marker enzymes and transporters, also in agreement with the patterns in primary trophoblasts [331,349]. These features cover transcellular processes, but also endocytic and transcytotic pathways like TfR-mediated endocytosis are conserved in BeWo b30 cells [217,350]. Also important for transfer studies is that the relative transfer rate of small molecules of the BeWo monolayer is consistent with transfer rates in *ex vivo* placental perfusions [226,351].

Besides the many advantages of using BeWo b30 cells for the investigation of nutrient transfer across the trophoblast layer, one of the main limitations is represented by the malignancy of the cancer cell line. As already mentioned, the malignancy of those cells results in an abnormal chromosome amount and therefore, gene expression patterns and responses may be altered [209,318,329]. Additionally, since BeWo b30 cells are subcloned, they are not contact inhibited, which is another challenge regarding the establishment of the *in vitro* system and further discussed in chapter 3 [352]. Contact inhibition is a process involved in fundamental tissue physiology in epithelial cells, which is equivalent to the inhibition of cell proliferation due to a decrease in mitotic rate and cell mobility in conditions of high cell density [353]. Nevertheless,

the simplicity of the cultivation of BeWo b30 cells and their rapid cell cycle facilitated the efficient high-throughput screening of substances and nutrient transfer [222].

Abstract

The placenta is a transient organ, which is responsible for nutrient and oxygen supply for the developing fetus. For this, maternal and fetal circulations are connected by a thin cellular structure referred to as the placental barrier. On one hand, the placental barrier is serving as the main regulatory interface but on the other hand, it may be also the target of several chemicals and xenobiotics. While effects of xenobiotics are partly characterized, exact pathways underlying micronutrient supply in pregnancy are rarely clarified. However, studies are needed for an adequate assessment of micronutrient requirements in pregnancy, which are nowadays rather based on data extrapolation.

To date, established testing strategies are standardized for mouse models. However, lots of progress has been made to develop *in vitro* and *in vivo* alternatives. One of the *in vitro* systems includes the BeWo b30 Transwell® system, which is also developed in the present study to investigate maternal-fetal nutrient transfer. This model represents the transfer across the trophoblast layer of the placental barrier in a compartmentalized approach since the apical and basolateral compartments are separated.

For the model development, optimal culture conditions and seeding cell count of the BeWo b30 trophoblasts were determined. Barrier tightness was monitored by measuring the transepithelial electrical resistance using the cellZscope® device and barrier integrity was verified by sodium fluorescein exclusion and immunocytochemical staining of the tight junction proteins γ-catenin and tubulin.

The BeWo b30 cell layer has been shown to form a confluent monolayer after cultivating 85,000 – 150,000 cells/ insert in EC medium for three days. However, BeWo b30 cell proliferation patterns have to be considered and monitored to avoid the formation of a multilayer. This is of central importance since the multilayer does not represent the physiological structure of the placental barrier *in vivo* and is therefore disadvantageous for micronutrient transfer studies.

Chapter 3 – Development of an *in vitro* model of human placental villous trophoblasts

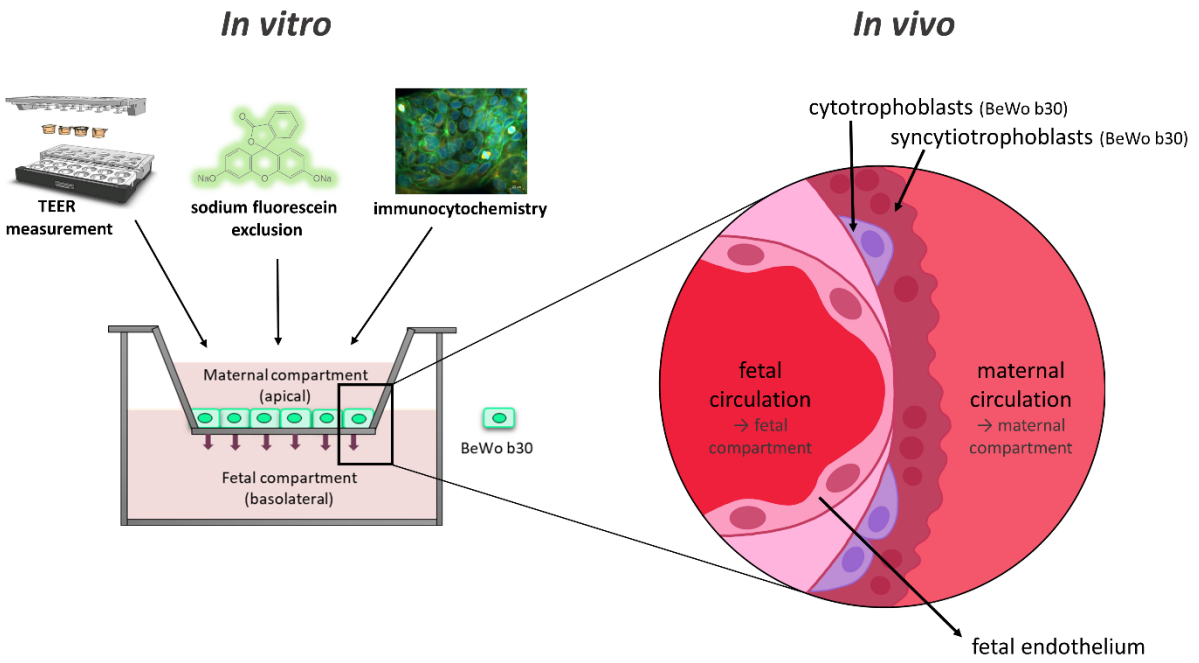

Figure 6: Graphical Abstract: Development of an *in vitro* model of human placental villous trophoblasts (adapted and modified from [231]).

3.1. Introduction

The placenta is a highly species-specific organ, which mediates fetal oxygen and nutrient supply and is involved in fetal metabolism. Nutrients or oxygen available in the maternal blood can reach the fetus by crossing a thin cellular structure of 2 – 4 µm thickness, called the placental barrier. It separates maternal and fetal circulation and is located at the branching villi, which extend into maternal blood in the ambient intervillous space [207]. In the early stages of pregnancy, the placental barrier comprises four different cell structures. While cytotrophoblasts and syncytiotrophoblasts are assigned to the maternal side, fetal stroma and fetal endothelial cells belong to the fetal side [226]. During pregnancy, precursor cytotrophoblast cells exit the cell cycle and differentiate into multinuclear syncytiotrophoblasts, which leads to the formation of a thinner structure referred to as syncytium [218]. The thinning of the syncytium allows a higher permeability for nutrients and oxygen needed to satisfy the increasing demands of the developing fetus [207,224]. Besides nutrient supply, the placental barrier is also serving as a protective interface preventing fetal exposure to xenobiotics such as environmental pollutants or drugs but it is not completely impenetrable for certain substances, which was emphasized by the thalidomide debacle in the 1960s. Since then research on maternal-fetal drug transfer has been augmented to identify potential harms to the developing fetus. Therefore, in basic chemical and pharmaceutical

testing harmonized guidelines for Developmental and Reproductive Toxicity (DART) were established by the Organization for Economic Co-operation and Development (OECD) [222,230,354].

Established testing strategies of DART rely on rodent models with large numbers of animals as parent and offspring populations have to be considered [266,355]. The application of rodent models like mouse models is advantageous since they develop the same type of placenta compared to humans – the hemochorial type (fetal-derived cells are in direct contact with maternal blood). However, the placental morphology and the structure of the placental barrier differ distinctly [266]. One of the main differences between mice and humans is the formation of a second placental structure, namely the choriovitelline placenta. The choriovitelline placenta, also called inverted yolk sac placenta, is essential in mouse pregnancy and therefore rather the target of many chemicals and pharmaceuticals [266]. Since it is not formed during human pregnancy, extrapolating adverse effects observed in mouse toxicity tests to humans may lead to false-positive outcomes [266,319]. Additionally, the mouse placenta is constituted in two different zones with the labyrinth zone as a comparable maternal-fetal exchange layer [234,266]. It is composed of three layers of trophoblasts with the syncytium in the middle, while the human placenta is organized in villi with only one syncytial trophoblast layer [317].

To date, lots of progress has been made to support the humane and ethical use of animals in scientific research. To refine or reduce animal studies (according to the Refinement, Reduction, and Replacement (3R) principle first described in 1959 [356]) but also due to evolutionary species differences, various studies focused on the development of a model of the human placental barrier *in vitro* [209,355]. For this, models using microporous inserts were applied [209,222]. The placenta and also the placental barrier are developing on morphological as well as functional levels throughout pregnancy [220]. Thereby defining the stage of placentation and gestation by the choice of cell lines or primary cells is of central importance. While in early gestation, the trophoblast layer of the placental barrier is mainly composed of cytotrophoblasts, in late gestation, the majority of trophoblasts occur as syncytiotrophoblasts [219]. Both of which can be modeled *in vitro*.

To investigate placental function and trophoblast biology, several trophoblast cell lines were applied. Widely used are those derived from choriocarcinoma, which includes BeWo, Jeg-3, and JAR cells [331]. Besides cancer cell lines, where it has to be considered that they are highly malignant and contain abnormal chromosome complements. Modified isolated primary

trophoblasts are also used to investigate placental function [318]. These include ACH-3P cells, which are established by fusion of first-trimester trophoblasts, and the choriocarcinoma cell line AC1-1 or HTR-8/Svneo, which are simian virus 40 large T antigen transfected cells isolated from the chorionic villi of first-trimester placentae [326,327]. Since transfection in HTR-8/Svneo cells has shown to induce abnormal phenotype and karyotype, Swan-71 cells were immortalized by human telomerase reverse transcriptase transfection showing characteristics of first-trimester trophoblasts even after subculture [328]. Regarding the cellular and physiological complexity of the placenta, primary cells isolated from first-trimester or term placentae rather represent *in vivo* conditions [209]. However, it has to be considered, that primary cytotrophoblasts, originating from first-trimester placentae are not able to divide, and spontaneously exit the mitotic cell cycle and fuse to syncytiotrophoblasts, modeling late and not early gestation [327,334]. Furthermore, the availability of tissue from first-trimester placentae is limited due to ethical reasons, because they can only be obtained in case of early termination of pregnancy [220,357,358]. On the other hand, primary cells of term placentae are mainly used to investigate the formation of syncytiotrophoblasts, since processes involved in trophoblast invasion are reduced [219].

The widely used *in vitro* system for xenobiotic and chemical transfer across the placental trophoblasts is the BeWo b30 Transwell® model. After subcloning, the cancer cell line BeWo develops barrier-like functions, such as the formation of a polarized confluent monolayer (BeWo b30 cells) [331]. Additionally, they resemble the morphology of third-trimester trophoblasts and express a variety of transporters involved in macro- as well as micronutrient metabolism in expression patterns resembling late gestation [341,359]. In this model, transfer rates of small reference substances like antipyrine but also caffeine and benzoic acid are comparable to *ex vivo* placental perfusion experiments, the "gold standard" method for placental transport, established by Panigel *et al.* [226,310,351,360,361]. Since perfusion of human placentae, collected shortly after delivery, is challenging due to quick tissue degeneration and high biological variations, using *in vitro* translocation models is beneficial regarding handling and experimental throughput [220,222]. Nevertheless, it has to be considered, that cancer cell lines of placental trophoblast do not fully share the physiological structure of trophoblasts present in the placental barrier *in vivo* [222].

Xenobiotic testing is well-established due to its importance for pregnancy maintenance and outcome. However, the investigation of the fundamentals of micronutrient transport and

potential negative outcomes of disrupted micronutrient homeostasis is needed, since the mother and fetus are exposed to micronutrients every day by dietary consumption. Nutrients like TEs are rather discussed due to their essentiality and the regulation of several micronutrient supplementations recommended for pregnant women is not well established [362,363]. Therefore, investigating the effects of several food components is critical since inadequate nutrition may have an adverse impact on fetal development [269]. For this, understanding the mechanisms involved in the nutrient transfer is crucial for the assessment of micronutrient requirements during pregnancy to preserve a healthy life for the unborn child [7]. Various studies already focused on the transport of individual macro- and micronutrients but data on the complex mixture of nutrients as they occur in food is scarce [252,308,364,365]. In order to protect the fetus from potential negative outcomes, pregnant women are excluded from nutrition studies [7]. Therefore, developing a model of the maternal-fetal interface *in vitro* may reveal the fundamentals of combined micronutrient transport but also important processes involved in fetal nutrient supply.

3.2. Materials and Methods

3.2.1. Cultivation of BeWo b30 cells and cell seeding

The human choriocarcinoma cell line BeWo b30 was cultured as described in [308]. Briefly, BeWo b30 cells were cultured in Ham's F-12K medium (Gibco, Thermo Fisher Scientific, Waltham, USA) supplemented with 10 % fetal calf serum (FCS; Biochrom GmbH, Berlin. Germany), 1 % penicillin/streptomycin and 2 mM L-glutamine (Sigma Aldrich, Steinheim, Germany) in a humidified incubator at 37°C and 5 % CO_2 with a medium change every two days. During sub-culturing, cells were detached using 0.05 % trypsin-EDTA (Sigma Aldrich). For transfer experiments, the cell medium was changed to the endothelial growth medium (EC) supplemented with 1 vial SupplementMix (PromoCell, Heidelberg, Germany) and 1 % penicillin/streptomycin according to the manufacturer's protocol. For an optimal attachment of 2 x 10^4 – 1.5 x 10^5 cells on microporous inserts (Transwell® with a polycarbonate membrane, 0.4 µM pore size, 1.12 cm^2 growth area (Corning Life Sciences, Amsterdam, Netherlands)), inserts were coated before cell seeding using a solution of 50 µg/mL human placental collagen (Sigma Aldrich) in phosphate-buffered saline (PBS) for 1 h at 37°C. The established workflow for the BeWo b30 in vitro system is depicted in fig. 7.

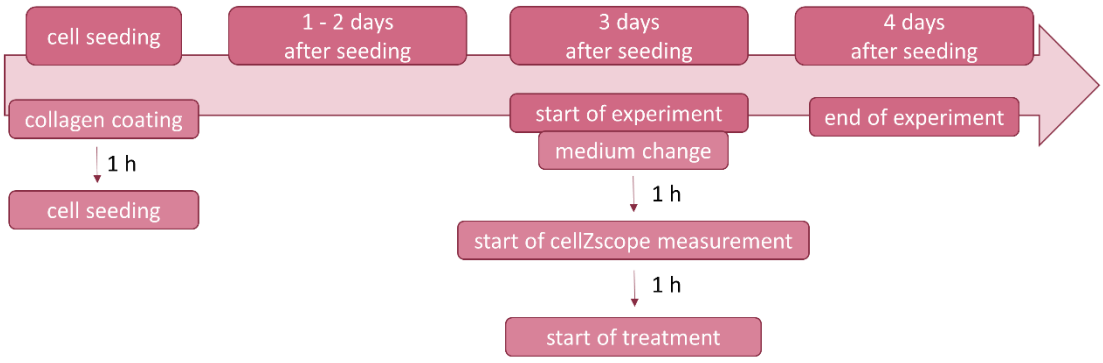

Figure 7: Workflow from cell seeding until treatment of the BeWo b30 *in vitro* system.

3.2.2. Transepithelial electrical resistance measurement

Barrier integrity was monitored by measuring the transepithelial electrical resistance (TEER), which describes the ionic conductivity of the tight junctions present in the cellular monolayer following Ohm's law [366]. For this, the cellZscope® device (nanoAnalytics, Münster, Germany) was used, whose measurement principle is based on impedance spectroscopy [367].

3.2.3. Sodium fluorescein exclusion assay

For barrier permeability studies, exclusion of sodium fluorescein (NaFlu) was determined in cells 3 days after seeding as described by Aengenheister *et al.* [222]. Therefore 0.5 mL of 5 µM NaFlu (Sigma Aldrich) diluted in phenol red-free Roswell Park Memorial Institute (RPMI) 1640 medium (Sigma Aldrich) supplemented with 10 % FCS and 1 % penicillin/streptomycin was added to the apical and 1.5 mL of RPMI 1640 without NaFlu on the basolateral compartment of the insert. 3 h after incubation, samples of each chamber were transferred into a 96-well plate. Fluorescence was measured using a Tecan® plate reader (Tecan® Infinite Pro M200, Tecan®, Crailsheim, Germany) at an excitation of 490 nm and an emission of 530 nm. The NaFlu amount was determined using an external calibration and calculated as a ratio to the starting concentration.

3.2.4. Immunocytochemical staining of BeWo b30 cells

The immunocytochemical staining of tight junction and microtubule proteins was performed as described in Aengenheister *et al.* [222]. For this, cells were fixed using 4 % PFA and 0.2 % Triton™ X-100 for 10 min at room temperature (RT). After washing with PBS, inserts were blocked with 5 % goat serum in PBS (Invitrogen, Thermo Fisher Scientific) for 30 min at 37°C. Afterward, a 1:1000 dilution of rat anti-tubulin (Abcam, Cambridge, United Kingdom) in 0.5 % BSA/PBS and a 1:500 dilution of mouse anti-(γ)-catenin (BD Biosciences, Heidelberg, Germany) in 0.5 % BSA/PBS was applied for 1 h at RT. A 488 goat anti-mouse and A 555 goat anti-rat (Invitrogen, Thermo Fisher Scientific) antibody diluted 1:400 in 0.5 % BSA/PBS were used for 2nd antibody staining for 1 h at RT. Before mounting, the nucleus was stained using 1 % Bisbenzimide H 33258 (Hoechst, Calbiochem, Sigma Aldrich) in methanol for 30 s at RT. To ensure an even surface, whole insert membranes were embedded in Mowiol 4-88 (Sigma Aldrich) at 40°C over night. Immunocytochemical analysis was performed with inserts 1, 2, and 3 days after seeding as well as for different cell densities. Immunostaining was captured with a Leica DMB6 fluorescence microscope (Leica Camera AG, Wetzlar, Germany) using an overlay of L5 (Ex: 460 – 500 nm; Em: 512 – 542 nm), 405 (Ex: 375 – 435 nm; Em: 450 – 490 nm), and TxR (Ex: 540 – 580 nm; Em: 592 – 668 nm) filters and 20- or 60-fold magnification objects. Images were processed using the Leica Thunder to extract overlaying fluorescence intensity from the mounting medium.

3.3. Results and Discussion of the Method Development

3.3.1 BeWo b30 barrier formation is dependent on culture medium

In order to develop the *in vitro* system of human villous trophoblasts, various BeWo b30 cell numbers (45,000 cells/ insert – 150,000 cells/ insert) were seeded on the apical side of the placental collagen-coated inserts. 24 h after seeding, inserts were placed in the cellZscope® device to monitor the formation of a confluent monolayer. The choice of culture medium was thereby supported by literature, which suggested the cultivation of BeWo b30 cells in either Ham's F-12K medium or a mixture of F-12K and high glucose Dulbecco's Modified Eagle's Medium (DMEM) [222,352]. In the following, starting conditions of the TEER measurement are defined as the first measured TEER value of the experiment.

TEER values were decreased in all tested conditions (alternating cell numbers), which might be explained by cells habituating to their new environment and the applied voltage. Afterward, TEER values of 100,000 cells cultivated on inserts, decreased independent of the culture medium. Additionally, seeding higher cell numbers (125,000 – 150,000 cells/ insert) resulted in a marginal increase, in the same range as the starting condition. However, about 35 h after seeding TEER values reached a constant level, although not clear if cells formed a tight barrier or if TEER values were not increasing due to reduced cell proliferation (fig. 8A, B). In contrast to other cell lines used for barrier studies [199,368], BeWo b30 cell proliferation is not inhibited by cell contact, and cell differentiation is not necessary for barrier formation. Therefore, obtaining reproducible and intact cell layers is more difficult, and more precise monitoring is required [352].

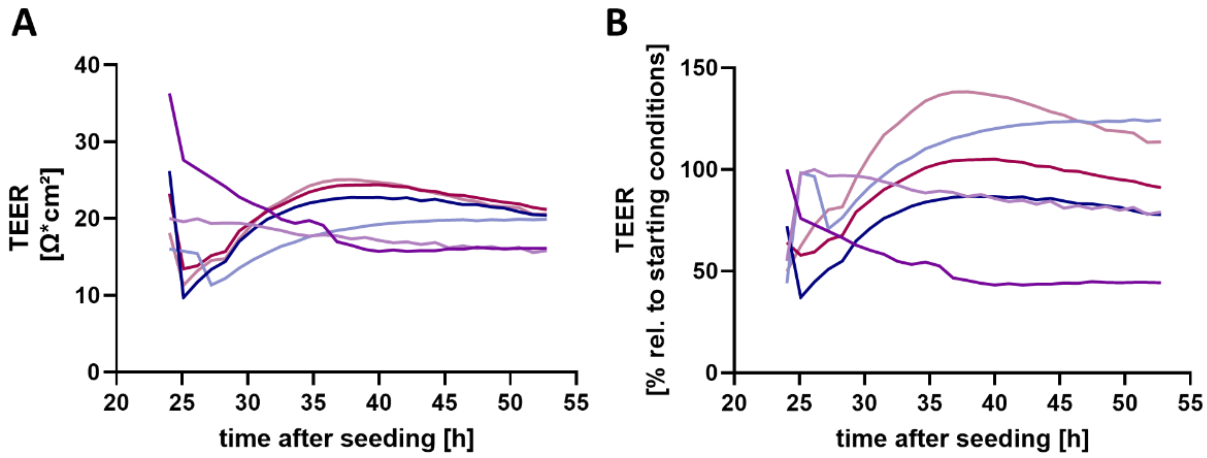

Figure 8: TEER values of the BeWo b30 cell layer cultivated in two different culture medium compositions (F-12K/ F-12K + DMEM (50:50)) on the apical side of the Transwell® insert 24 h after seeding. Shown is the progression of the TEER values for about 48 h in (A) Ω*cm² and (B) relative to starting conditions of one representative experiment. Starting conditions are defined as the first measured TEER value. Graphs are assigned to the following: (▬) 100,000 cells/ insert (F-12K), (▬) 100,000 cells/ insert (F-12K/DMEM), (▬) 125,000 cells/ insert (F-12K), (▬) 125,000 cells/ insert (F-12K/DMEM), (▬) 150,000 cells/ insert (F-12K), (▬) 150,000 cells/ insert (F-12K/DMEM).

To investigate if TEER values determined are low due to an insufficient cell number, inserts with cell numbers ranging from 45,000 cells/ insert - 90,000 cells/ insert were applied. Due to the fact, that BeWo b30 cells do not develop well in high glucose DMEM (fig. S1), also observed by Crowe *et al.* using the BeWo subclone b24, cells were cultivated using F-12K [369]. However, TEER values obtained were indistinguishable compared to higher cell counts, which hints that the barrier formation was not successful (fig. 9A, B).

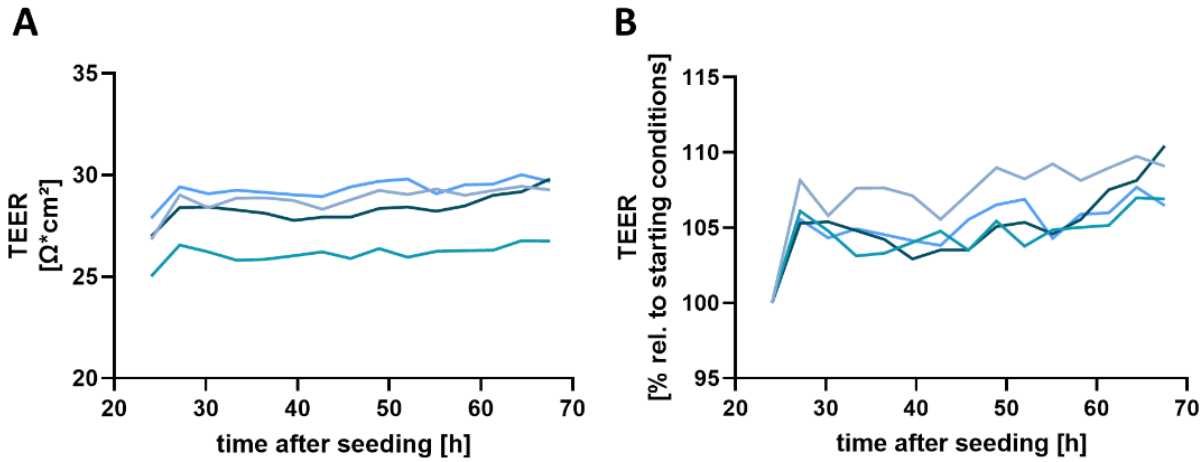

Figure 9: TEER values of the BeWo b30 cell layer cultivated in F-12K on the apical side of the Transwell® insert 24 h after seeding. Shown is the progression of the TEER values for about 70 h in (A) Ω*cm² and (B) relative to starting conditions of one representative experiment. Starting conditions are defined as the first measured TEER value. Graphs are assigned to the following: (▬) 45,000 cells/ insert (F-12K), (▬) 60,000 cells/ insert (F-12K), (▬) 75,000 cells/ insert (F-12K), (▬) 90,000 cells/ insert (F-12K).

In consideration of this, TEER measurement of inserts without cells revealed that the intrinsic resistance was not exceeding 30 Ω*cm², verifying that cells seeded on inserts did not form a barrier-like cell layer. Furthermore, seeding cells in barrier-like conditions in 12-well culture dishes showed that in case of immense vibration or movement during cultivation, floating adherent cells cluster in the middle of the culture dish (data not shown). This phenomenon was described by Szaraz *et al.* as secondary flow, which is associated with uneven sedimentation and adherence, negatively affecting cell culture quality [370]. Therefore, after cell seeding, inserts were moved as little as possible and TEER measurements were not conducted until cells reached a confluent monolayer. For this, cell numbers, as well as the time post-seeding, were defined according to protocols of already published BeWo b30 *in vitro* systems. Optimal cell concentrations described in the literature suggested cell numbers of 1.0×10^5 – 1.5×10^5 cells/ insert with a cultivation time of 3 days post-seeding before performing transfer studies [222,314,371].

Using the Transwell® system offers the opportunity to not only investigate the transfer of substances across a monolayer but allows a co-culture of different cell lines. In the case of the placental barrier, many studies combined the epithelial BeWo b30 cells with macrovascular cells like HUVEC or microvascular human venous endothelial cells (HPEC-A2) [222,372]. In order to establish adequate culture conditions for both cell lines, the right type of culture medium needs to be selected. As described by Aengenheister *et al.*, BeWo b30 cells can also be cultivated in EC medium, initially used for the cultivation of endothelial cells [222]. Nevertheless, the cultivation of BeWo b30 cells in the EC medium resulted in a strong increase of the TEER values of about 80 – 300 Ω*cm² (fig. 10), possibly due to the growth factors added to the supplement mix of the EC medium. According to the manufacturer's protocol, the supplement mix is composed of FCS, endothelial cell growth supplement, epidermal growth factor, basic fibroblast growth factor, insulin-like growth factor, vascular endothelial growth factor 165, ascorbic acid, heparin and hydrocortisone [373]. Especially, the insulin-like growth factor is involved in cytotrophoblast proliferation, and the epidermal growth factor has shown to induce cell proliferation of BeWo b24 cells without enhanced aggregation, leading to the hypothesis that barrier formation is ameliorated in EC medium compared to F-12K medium [369,374].

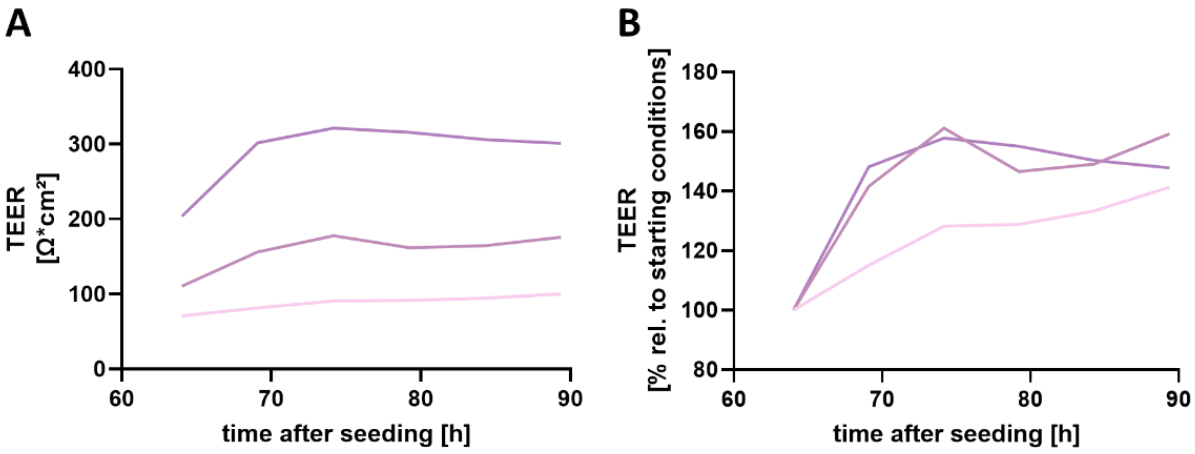

Figure 10: TEER values of the BeWo b30 cell layer cultivated in EC medium on the apical side of the Transwell® insert 3 days after seeding. Shown is the progression of the TEER values for an additional 24 h in (A) Ω*cm² and (B) relative to starting conditions of one representative experiment. Starting conditions are defined as the first measured TEER value. Graphs are assigned to the following: (▬) 115,000 cells/ insert (EC), (▬) 125,000 cells/ insert (EC), (▬) 150,000 cells/ insert (EC).

3.3.2 Verification of barrier integrity using sodium fluorescein exclusion assay and immunocytochemistry

To investigate the integrity of the BeWo b30 cell layer, NaFlu exclusion and the staining of the adherens and tight junction proteins γ-catenin or zonula occludens-1 (ZO-1), and the microtubule protein tubulin via immunocytochemistry was used. In order to get first indications of the BeWo b30 cell proliferation behavior during barrier formation, inserts with 115,000 or 125,000 cells were stained 1, 2, or 3 days after seeding. As depicted in fig. 11 and 12 BeWo b30 cells have grown from the edge to the middle of the insert, closing the remaining holes in the cell layer until day 3.

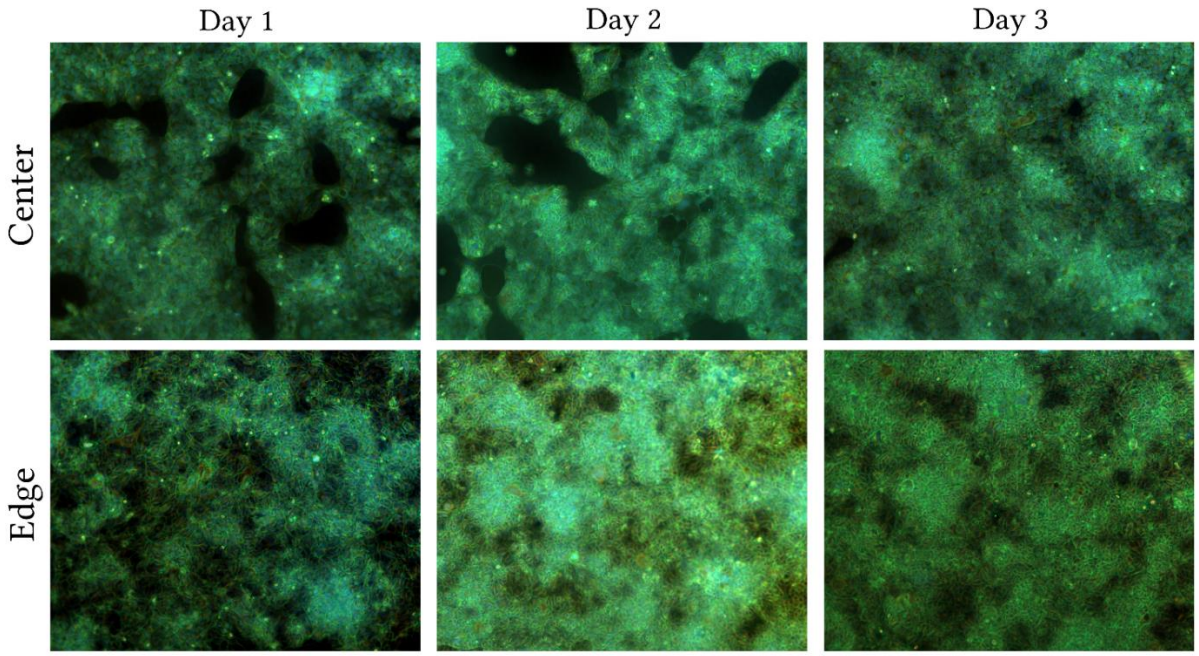

Figure 11: Staining of the tight junction protein γ-catenin (green), the microtubule protein tubulin (red), and the nucleus using Hoechst staining (blue) via immunocytochemistry. Shown are the pictures of a proliferation timeline of 115,00 cells/ inserts 1, 2, and 3 days after seeding depicted as overlays of the respective filter of one representative section of the membrane at a 20-fold magnification.

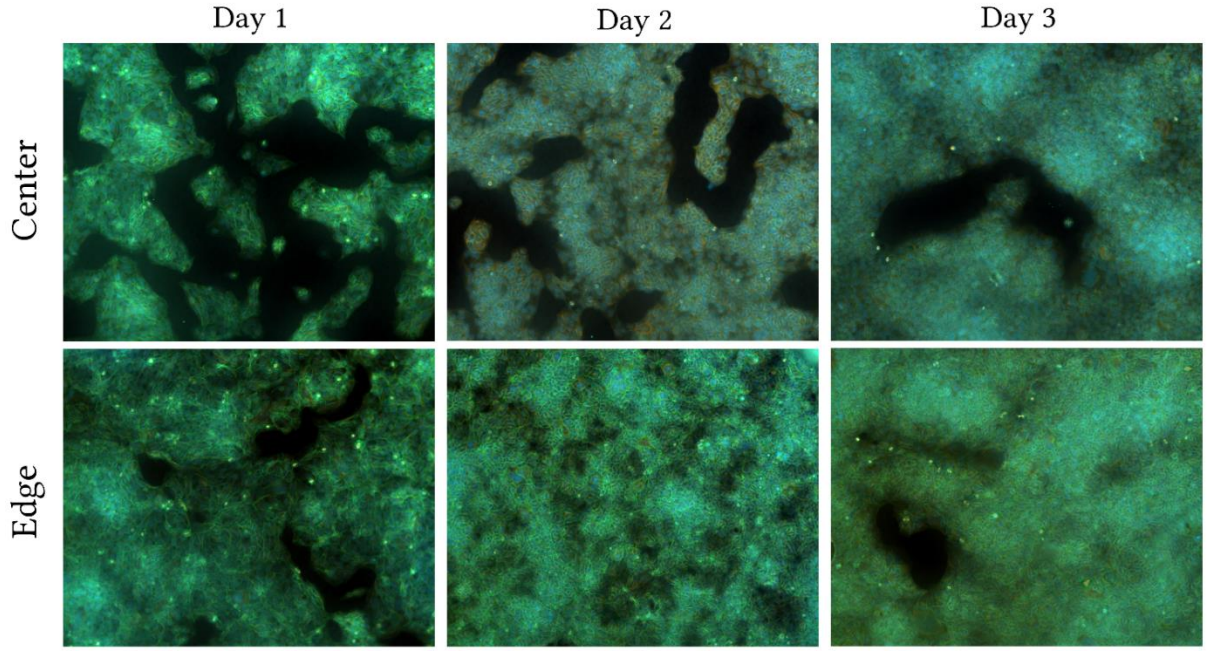

Figure 12: Staining of the tight junction protein γ-catenin (green), the microtubule protein tubulin (red), and the nucleus using Hoechst staining (blue) via immunocytochemistry. Shown are the pictures of a proliferation timeline of 125,000 cells/ inserts 1, 2, and 3 days after seeding depicted as overlays of the respective filter of one representative section of the membrane at a 20-fold magnification.

Additionally, after 3 days of culture, the basolateral NaFlu amounts ranged between 6.5 % (seeding 115,000 cells) and 15.2 % (seeding 125,000 cells), indicative of an apparent confluent

cell layer (fig. 13). In contrast to this, staining of the tight junctions revealed remaining holes, which showed clearly that NaFlu retention of 93.5 % and 84.8 % is too low for defining a confluent cell layer. Furthermore, contradictory to expectations, an increase in cell number resulted in an increase in NaFlu permeability, which could not be explained yet, but possibly emphasizes that reproducibility of confluent cell layer formation is more challenging due to the secondary flow mentioned before [370].

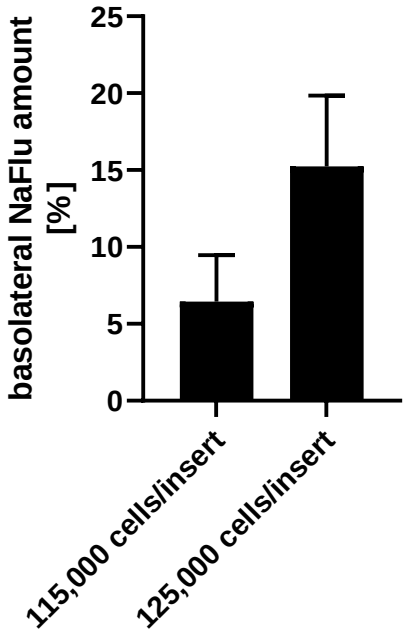

Figure 13: Basolateral NaFlu amount [%] of 115,000 and 125,000 cells/ insert 3 days after seeding. Shown are the means + SD of one representative experiment with two technical replicates.

In order to avoid the secondary flow in microporous inserts, 115,000; 125,000; and 150,000 cells were seeded for 3 days before the performance of the NaFlu exclusion assay and immunocytochemistry. Staining of the tight junction proteins revealed that the cell layer could be considered confluent if cultivating 150,000 cells/ insert for 3 days (fig. 14). Different from the barrier formation observed before, the number of holes across the cell layer was lower with higher cell numbers (fig. 11, 12, 14).

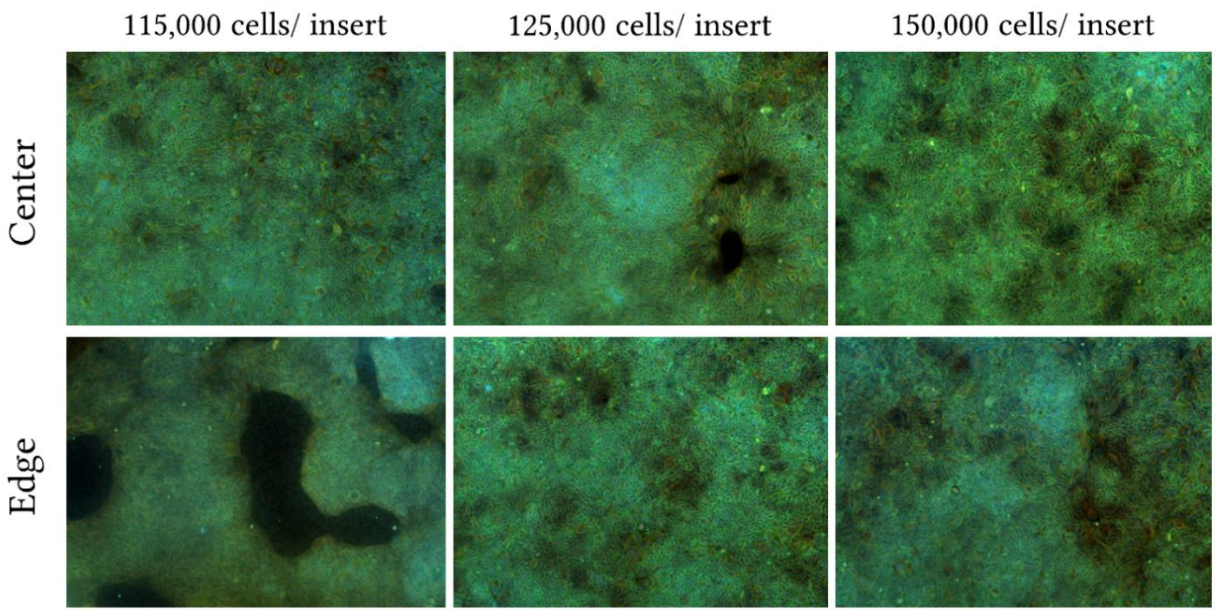

Figure 14: Staining of the tight junction protein ɣ-catenin (green), the microtubule protein tubulin (red), and the nucleus using Hoechst staining (blue) via immunocytochemistry. Shown are the pictures of cell layers of 115,000; 125,000; and 150,000 cells/ insert 3 days after seeding. Depicted are overlays of the respective filter of one representative section of the membrane at a 20-fold magnification.

Furthermore, seeding higher cell numbers on inserts led to decreased NaFlu permeability with basolateral NaFlu amounts ranging from 5 % (115,000 cells/ insert) to 1.5 % (150,000 cells/ insert) (fig. 15). This observation was in accordance with the staining of the tight junction protein ɣ-catenin. In consideration of the TEER measurement, the cell layer can be considered confluent at TEER values higher than 100 Ω*cm² (fig. 10).

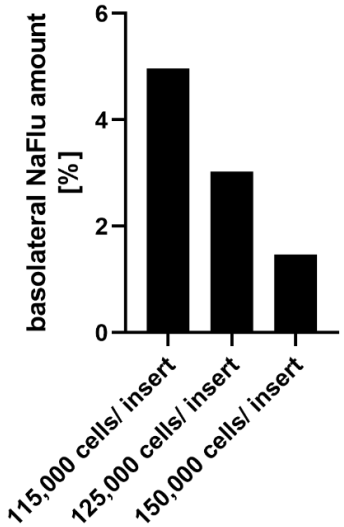

Figure 15: Basolateral NaFlu amount [%] of 115,000; 125,000; and 150,000 cells/ insert 3 days after seeding. Shown are the means of one representative experiment.

Adequate barrier formation could therefore be reached by seeding 150,000 cells/ insert in EC medium for 3 days before treatment with TEER values higher than 100 Ω*cm². Regarding current literature, the culture conditions of the BeWo b30 cell layer are diverse in terms of culture medium, cell densities, and times post-seeding. The model has therefore to be optimized according to the respective application and laboratory environment [222,352,371]. While the results obtained from the integrity assays are individually different, the dimensions are comparable. One example is the study by Cartwright *et al.*, which used a cell density of 100,000 cells/ insert, cultivated in a mixture of DMEM and F-12K. NaFlu exclusion was minimal 5 days post-seeding with about 6 % regarding the initial dose [371]. In the present study, immunocytochemistry revealed remaining holes in the cell layer, although only 6.5 % of the initial NaFlu dose reached the basolateral compartment (fig. 11, 13). In order to increase experimental throughput due to shorter cultivation times, Aengenheister *et al.* applied a slightly increased cell number of 1.5 x 10^6 b30 cells/ insert cultivated in EC medium for 3 days until reaching adequate barrier-like morphology [222]. This corroborates the results obtained in the present study.

Besides γ-catenin as a marker for adherens junctions [222], ZO-1 was also postulated as a marker for tight junctions in epithelial cells and is expressed in the BeWo b30 cell line [220,375]. BeWo b30 cells developed sharp cell boundaries, ZO-1 expression was evenly distributed across the cell layer, and the subsequent visualization of the cell nuclei showed the formation of a consistent barrier (fig. 16).

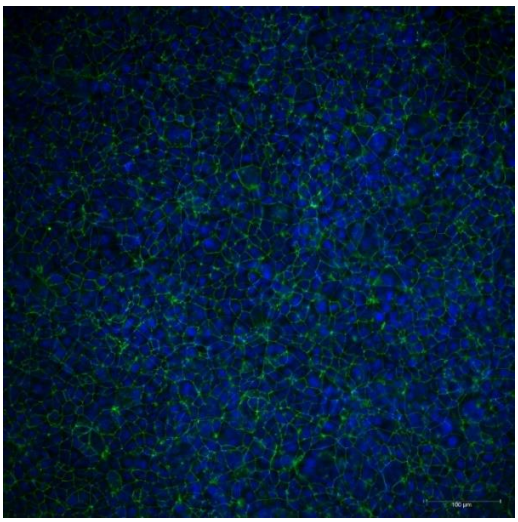

Figure 16: Staining of the tight junction protein ZO-1 (green), and the nucleus using Hoechst staining (blue) via immunocytochemistry. Shown is a picture of the cell layer after seeding 150,000 cells/ insert for 3 days. Depicted is the overlay of the respective filter of one representative section of the membrane at a 20-fold magnification. The picture was processed by a Leica Thunder imager extracting the fluorescence of the mounting medium.

The application of the developed BeWo b30 Transwell® model for nutrient transfer revealed further difficulties in reproducibility. TE transfer was compromised if TEER values of cell layers, formed after seeding 150,000 cells/ insert, exceeded 330 Ω*cm². This indicated the formation of a BeWo b30 multilayer, which cannot be avoided due to the absence of contact inhibition (see chapter 4 – Differences and Interactions in Placental Manganese and Iron Transfer across an *In Vitro* Model of Human Villous Trophoblasts). Under physiological conditions *in vivo*, this cell layer is composed of only one layer, whereby the formation of the monolayer is crucial for relevant study results [314]. Nevertheless, a few studies were deliberately done on a BeWo multilayer, in order to avoid adverse effects of barrier leakage caused by cytotoxicity [376] or because cells formed a multilayer before they reached confluence [352]. However, this was not the intention of this study but highlighted that growing consistent and intact BeWo monolayers is challenging [352,376]. To overcome the difficulties of cell seeding, barrier formation was monitored from cell numbers ranging from 20,000 to 150,000 cells 3 days post-seeding. Subsequently, TEER values and NaFlu exclusion were measured, and the presence of tight junctions was investigated. For this TEER values were measured daily until 3 days post-seeding. They demonstrated that seeding 85,000 cells/ insert is sufficient to reach comparable TEER values in regard to those obtained during method development in general. Furthermore, cell densities of 20,000 and 45,000 cells/ inserts were too low, because TEER values did not exceed the intrinsic resistance of the insert (fig. 17).

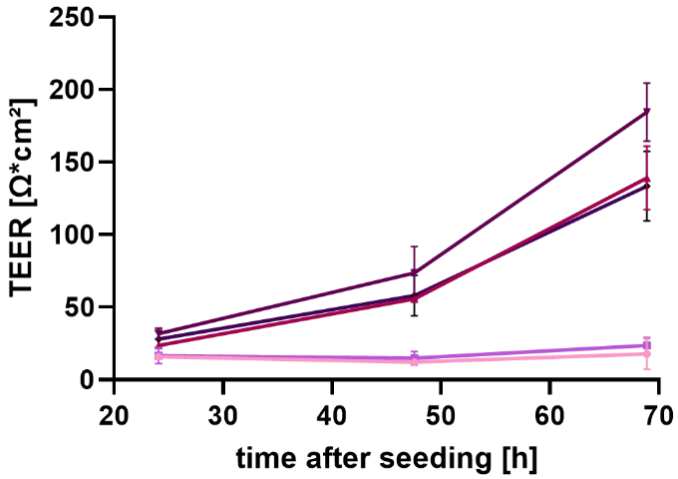

Figure 17: TEER values of the BeWo b30 cell layer cultivated in EC medium on the apical side of the Transwell® insert. Shown is the progression of the TEER values [Ω*cm²] ± SD for 1, 2, and 3 days after seeding of one representative experiment with 4 technical replicates. Graphs are assigned to the following: ( ) 20,000 cells/ insert (EC), ( ) 45,000 cells/ insert (EC), ( ) 85,000 cells/ insert (EC), ( ) 120,000 cells/ insert (EC), ( ) 150,000 cells/ insert (EC).

The staining of the tight junction proteins corroborated this hypothesis since the cultivation of 85,000 cells/ inserts led to the formation of an even cell layer with an adequate distribution of cell-cell boundaries (fig. 18). Additionally, also seeding of 150,000 cells/ insert resulted in the formation of a consistent BeWo b30 barrier.

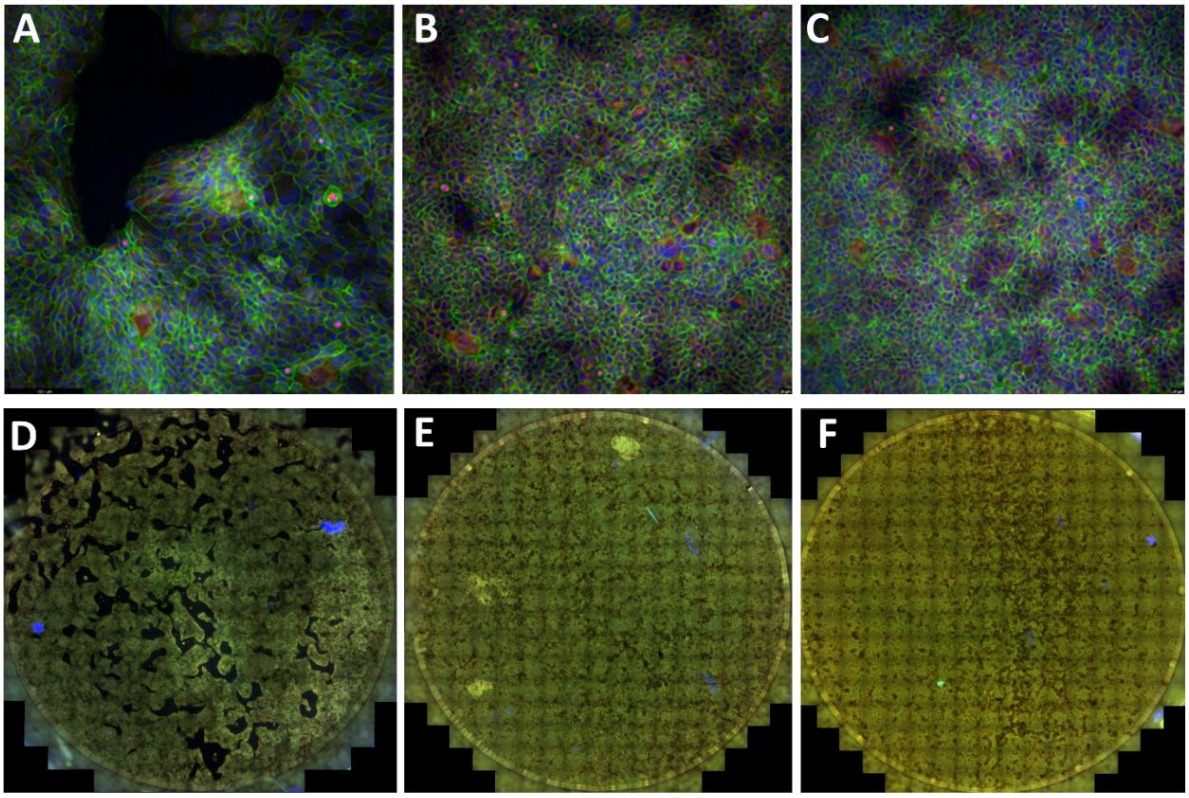

Figure 18: Staining of the tight junction protein γ-catenin (green), the microtubule protein tubulin (red), and the nucleus using Hoechst staining (blue) via immunocytochemistry. Shown are pictures of one representative segment (A – C) and the whole cell layer (D – F) after seeding 45,000 cells; 85,000 cells, and 150,000 cells/ insert for 3 days, respectively. Depicted is the overlay of three filters at a 20-fold magnification. The pictures were processed by a Leica Thunder imager extracting the fluorescence of the mounting medium.

According to the immunohistochemistry and measurement of the TEER values, also NaFlu exclusion was minimal after seeding 85,000 and 150,000 cells/ insert. Additionally, basolateral NaFlu amount was indistinguishable between those cell densities (fig. 19).

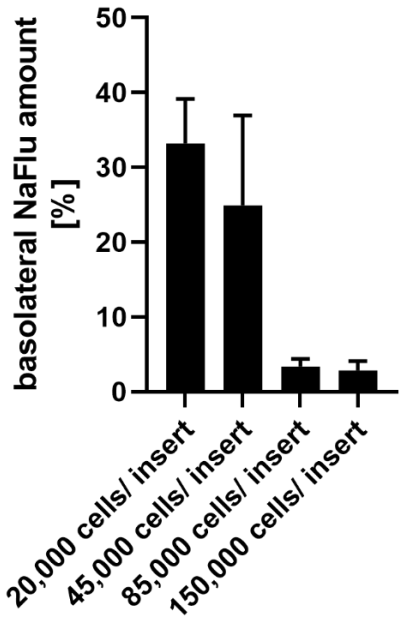

Figure 19: Basolateral NaFlu amount [%] of 20,000; 45,000; 85,000 and 150,000 cells/insert 3 days after seeding. Shown are the means + SD of at least one representative experiment with two technical replicates.

Different from the optimized culture conditions postulated before, seeding 85,000 cells/ insert was already sufficient to reach barrier-like morphology and adequate barrier integrity. However, due to the fact, that inserts of 150,000 cells/ insert showed comparable barrier integrity, it can be defined that seeding cells ranging between 85,000 cells/ insert to 150,000 cells/ insert led to the formation of a BeWo b30 cell layer with adequate integrity. Nevertheless, it is not clear why the cells show different proliferation behavior. One possible explanation may be the lot dependence of the FCS, which is included in the supplement mix of the EC medium, possibly leading to compromised or enhanced proliferation behavior. However, the exact reason remains to be elucidated in future studies, and barrier formation needs to be monitored precisely before treatment.

3.4. Limitations and future opportunities

The BeWo b30 Transwell® model is an adequate tool to model trophoblasts of the placental barrier *in vitro.* They resemble most of the functions of trophoblasts and express a variety of transporters involved in nutrient transfer. Different from cell lines used for the investigation of other physiological barriers, BeWo b30 cells are not contact inhibited and do not need to be differentiated to form a confluent cell layer. This behavior makes it difficult to obtain a reproducible and consistent model system. Therefore, the development of the culture conditions has to be done precisely and has to be adapted to each desired application.

As BeWo b30 cells are derived from choriocarcinoma, they represent a specific differentiation pattern of trophoblasts and may show a different response to several stimuli compared to *in vivo* conditions [209]. Instead of cancer cell lines, primary trophoblasts can be isolated from first-trimester or term placentae without changing their morphology and function *in vitro*. However, using primary cells for long-term experiments is limited due to the induction of senescence processes leading to reduced proliferation or complete cell cycle arrest [209]. To overcome this limitation, human embryonic or human pluripotent stem cells can be applied. Furthermore, stem cells can be differentiated into either extravillous as well as villous trophoblasts, also resembling *in vivo* conditions of placental function and structure [209].

The model established in this study represents one single cell layer of the placental barrier. The Transwell® insert system allows the combination of several cell lines and their compartmentalization (apical or basolateral affinity) due to polarization [339]. By applying the BeWo b30 cells on the apical compartment of the insert, the maternal facing side of the placental barrier is covered. However, this monolayer does not represent the complex microstructure and heterogeneity of cell layers of the placental barrier. Furthermore, as pregnancy progresses, the fetal endothelium is gaining more importance due to increased angiogenesis and vascularization. Fetal programming and regulation will then be adopted by fetal endothelial cells, which also affect the regulation of fetal nutrient supply [231,377]. Additionally, since the formation of the vascular system is dependent on trophoblast signaling, interactions of epithelial (trophoblasts) and endothelial cells are important to consider. Therefore, the development of an *in vitro* co-culture system would facilitate the investigation of nutrient transfer across associated cell layers not only in regard to maternal and fetal circulations [378].

In order to model fetal endothelium, several studies used HUVECs [379-381]. They can be isolated from the umbilical vein directly after delivery but are also commercially available [372,382]. In consideration of the underlying cell type, HUVECs represent macrovascular cells, while the majority of endothelial cells, present in the human placenta, are microvascular cells (HPMECs). They can be isolated from fetal chorionic arteries of term placentae [372]. In addition, HPMECs can also be transfected by simian virus 40 to facilitate cultivation (HPEC-A2 cells). However, HUVECs, as well as HPMECs differ regarding phenotype (morphology) and physiological function [222,372,378]. Studies have shown distinct differences in the expression of several homeobox genes (important in embryogenesis), as well as the release of vasoactive substances and endothelial mitogen response [372,378]. Due to the heterogeneity of fetal endothelial cells, effects obtained in macrovascular cells cannot be extrapolated to microvascular cells. The choice of fetal endothelial cells for the *in vitro* system has, therefore to be made in regard to the desired point of view since fetal microvascular cells are in direct proximity and part of the placental barrier, while macrovascular cells of the umbilical vein are involved after nutrients have reached fetal capillaries [222,372,383].

Besides the choice of cell lines used for Transwell® experiments, progress has been made to substitute the polycarbonate membrane by bioprinting a methacrylated gelatin membrane modeling extracellular matrix. In order to additionally mimic fetal stroma, primary fetal fibroblasts are included. In combination with trophoblasts (BeWo) and fetal endothelium (primary cells), this system represents a more complex model of the placental barrier [336]. Furthermore, Nishiguchi *et al.* had a similar approach to a 3D culture system. They seeded laminin- and collagen-coated trophoblasts on a layer of the capillary network, which was formed in advance from primary fibroblasts and HUVECs in a hydrogel containing fibrin, therefore covering the trophoblast layer, connective tissue, and vascular endothelium of the placental barrier [337].

Using the BeWo b30 monolayer, however, is a useful tool for the investigation of nutrient transfer across the villous trophoblasts. The simplicity of the monolayer facilitates experimental throughput in order to gain first insights into fetal nutrient supply and underlying mechanisms, which have to be elucidated in future studies. Extending the *in vitro* system by adding fetal endothelium and extracellular matrix will represent a more complex model of the placental barrier and will cover alterations due to interactions of maternal trophoblasts and fetal endothelium.

Abstract

Manganese (Mn), as well as iron (Fe), are essential trace elements (TE) important for the maintenance of physiological functions including fetal development. However, in the case of Mn, evidence suggests that excess levels of intrauterine Mn are associated with adverse pregnancy outcomes. Although Mn is known to cross the placenta, the fundamentals of Mn transfer kinetics and mechanisms are largely unknown. Moreover, exposure to combinations of TEs should be considered in mechanistic transfer studies, in particular for TEs expected to share similar transfer pathways. Here, we performed a mechanistic *in vitro* study on the placental transfer of Mn across a BeWo b30 trophoblast layer. Our data revealed distinct differences in the placental transfer of Mn and Fe. While placental permeability to Fe showed a clear inverse dose-dependency, Mn transfer was largely independent of the applied doses. Concurrent exposure of Mn and Fe revealed transfer interactions of Fe and Mn, indicating that they share common transfer mechanisms. In general, mRNA and protein expression of discussed transporters like DMT1, TfR, or FPN were only marginally altered in BeWo cells despite the different exposure scenarios highlighting that Mn transfer across the trophoblast layer likely involves a combination of active and passive transport processes.

Chapter 4 – Differences and Interactions in Placental Manganese and Iron Transfer across an *In Vitro* Model of Human Villous Trophoblasts

Based on:

Vivien Michaelis, Leonie Aengenheister, Max Tuchtenhagen, Jörg Rinklebe, Franziska Ebert, Tanja Schwerdtle, Tina Buerki-Thurnherr and Julia Bornhorst.

Published in: International Journal of Molecular Sciences, Special Issue: "Homeostasis: Metals and Cellular Redox and Immunity Status"

DOI: 10.3390/ijms23063296

Keywords: manganese, iron, placental transfer, TE interactions, BeWo b30 trophoblasts

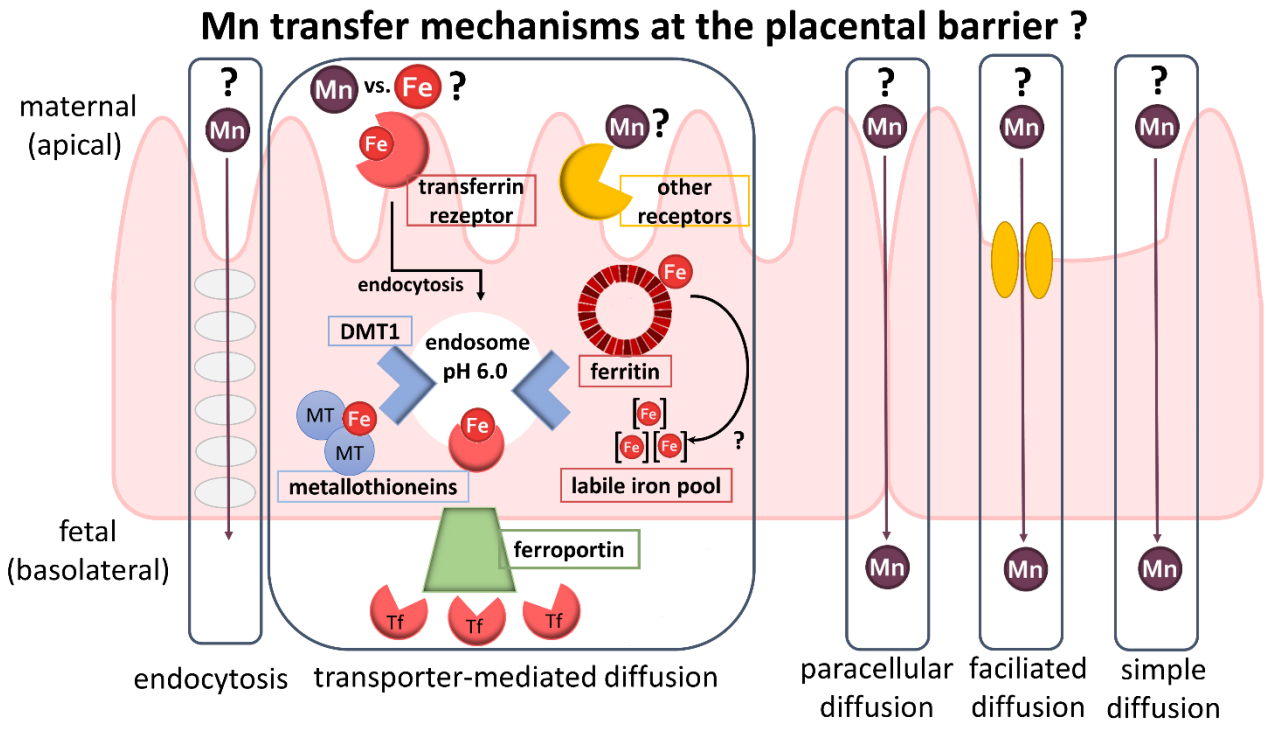

Figure 20: Graphical Abstract: Differences and Interactions in Placental Manganese and Iron Transfer across an *In Vitro* Model of Human Villous Trophoblasts.

4.1. Introduction

Although trace elements (TE) like manganese (Mn) and iron (Fe) are essential to sustain physiological processes, many studies have shown that excessive metal uptake could lead to health issues such as neurodegenerative diseases with metal-induced oxidative stress as a potential underlying pathway [5,384]. Mn and Fe may cause oxidative stress directly induced by Fenton and Fenton-like reactions or indirectly by inhibition of mitochondrial respiratory chain complexes [70,385]. This adverse outcome of excessive Mn and Fe exposure is presently established for adults, but may be of particular concern for sensitive populations like expecting mothers and their unborn children. In early stages of neurodevelopment, the neuronal network is highly susceptible to oxidative damage due to a not fully developed antioxidant system and a high oxygen consumption rate [386]. Therefore, an efficient TE homeostasis has to be maintained to avoid accumulation of metal species or reactive oxygen species (ROS) and ensure optimal fetal (neuro)development [387]. Maternal-fetal TE transfer is tightly regulated by the placenta, a highly species-specific organ performing a variety of essential functions including the exchange of nutrients in order to sustain fetal development. Among the many cell types forming the placental barrier, the syncytiotrophoblast facing the maternal blood stream is the key barrier layer, which performs most pregnancy-relevant functions and expresses a wealth

of enzymes and transporters. Early in pregnancy, cytotrophoblast precursor cells expand and differentiate from a bilayer to a thin multinuclear syncytiotrophoblast (2 – 4 µm thickness), which leads to an increased placental permeability in later stages of pregnancy [207,224]. While the transfer of Fe across placental barrier building cells has already been addressed in numerous studies (reviewed in [252,261]), little is known about the transfer of Mn.

Mn is involved in several processes of fetal development like growth, bone formation, immune function, or neurodevelopment [8,388]. Since Mn appears ubiquitously in nutrition (e.g. nuts, grains, rice, and tea) but also in the environment through anthropogenic pollution of air or drinking water, Mn deficiency has not been observed in humans so far [3,28]. However, excess levels of Mn *in utero* (measured as maternal blood and/ or cord blood concentrations) have been associated with adverse pregnancy outcomes such as a higher risk for intrauterine growth restriction or neural tube defects, lower birth weight, or an altered neurodevelopment in terms of psychomotor and mental skills [66,299,302,306]. The underlying toxicity mechanisms are still unknown [389,390]. For adults including pregnant or lactating women, the European Food Safety Authority (EFSA) proposed an adequate Mn intake (AI) of 3 mg/ day (2013), which relies on extrapolated data from the Institute of Medicine, Panel on Micronutrients on weight gain during pregnancy (2001) [3,267]. Nonetheless, Mn requirement in pregnancy is still under discussion.

To identify possible placental TE transfer mechanisms, Duck *et al.* reviewed Fe transfer across different physiological barriers including the placenta [68]. Different from Fe transfer in the gut, placental Fe transfer is described as a unidirectional (from mother to child only) transferrin (Tf) mediated endocytosis including active transport mechanisms. In more detail, Tf-bound trivalent Fe(III) (Tf-Fe) is transported to the endosome where it is pH-dependently released and subsequently transported into the cytosol through the divalent metal transporter 1 (DMT1). Once in the cytosol, it can be stored in the storage proteins ferritin light and heavy chain (FTL, FTH) or exported to the fetal side through ferroportin (FPN) [68]. The limited data available on placental Mn transfer suggest that Mn is transported actively since the Mn amount was significantly higher in umbilical cord blood than in maternal serum [307]. In addition, the Mn transfer rate across a perfused human placental lobule was reduced compared to the passive diffusion marker antipyrine [306]. Nevertheless, further mechanistic studies on placental Mn transfer and safety, including transfer kinetics as well as underlying translocation and toxicity mechanisms are urgently needed to understand micronutrient requirements in pregnancy [7].

Therefore, we investigated placental Mn transfer and cytotoxicity at the villous trophoblast barrier using an *in vitro* BeWo b30 transfer model. In particular, we focused on elucidating Mn transfer kinetics and underlying translocation pathways like the involvement of relevant transporters (DMT1, TfR, and FPN) and regulatory proteins (metallothioneins (MT), FTH, FTL). As previously described for other tissues, Mn and Fe might share the same transport mechanisms because they both occur in two physiological relevant species ((+II) and (+III)) [19,27]. Hence, we included Fe in our study for comparison. This study helps to fill the knowledge gaps in the transfer of single TEs but also emphasizes the importance of TE interactions in order to maintain a balanced TE homeostasis.

4.2. Materials and Methods

4.2.1. Cultivation of BeWo b30 cells

The human placental choriocarcinoma cell line BeWo subclone b30 was cultivated as described previously [222]. Briefly BeWo b30 cells were cultured using Ham's F-12K medium (Thermo Fisher Scientific (Gibco), Schwerte, Germany) supplemented with 1 % fetal calf serum (FCS; Biochrom GmbH, Berlin, Germany), 1% penicillin/ streptomycin and 2 mM L-glutamine (Sigma Aldrich, Steinheim, Germany). Cells were sub-cultured twice a week using 0.05 % trypsin-EDTA solution (Sigma Aldrich, Steinheim, Germany) with a medium change every two days and cultured in a humidified incubator at 37°C with 5 % CO_2.

4.2.2. Cytotoxicity Testing for Dosage Regimen

Stock solutions of $MnCl_2$ ($MnCl_2{\cdot}4H_2O$, 99.9 % trace element basis, Honeywell™, Morristown, NJ, USA) and $FeCl_2$ ($FeCl_2{\cdot}4H_2O$, 99.9 % trace element basis, Merck Millipore, Darmstadt, Germany) were prepared freshly before the experiment using sterile purified water (18 MΩ). The abbreviations Mn and Fe used in this study refer to both metals in the divalent form (Mn(II) and Fe(II)). For cytotoxicity testing via Hoechst Assay, 31,000 cells/cm² were seeded in 96-well plates in order to reach confluency after three days [222]. One hour after medium change, cells were incubated with different concentrations of $MnCl_2$ and $FeCl_2$ ranging from 100 – 1000 µM for up to 24 h. In short, Hoechst assay was carried out by fixing cells using 4% formaldehyde followed by a permeabilization step with Triton™ X-100 (Sigma Aldrich, Steinheim, Germany) to allow Hoechst staining (Bisbenzimide H 33258, Calbiochem, Sigma Aldrich, Steinheim, Germany) to interact with the DNA of living cells [391].

4.2.3. Mn and Fe Transfer across the BeWo b30 cell Layer

For transfer experiments, 8.5 x 10^4 cells were seeded in endothelial growth medium MV (EC) supplemented with 1 vial SupplementMix according to the manufacture's manual (PromoCell, Heidelberg, Germany) and 1 % penicillin/ streptomycin on the apical side of microporous inserts (Transwells® with a polycarbonate membrane, 0.4 µm pore size, 1.12 cm^2 growth area, Corning Life Sciences, Amsterdam, Netherlands). Before cell seeding, inserts were coated using a 50 µg/mL solution of human placental collagen for 1 h at 37°C (Sigma Aldrich, Steinheim, Germany). Three days after seeding, the medium was changed 2 h before TE treatment. Barrier tightness was monitored right before and during an experiment by measuring transepithelial electrical resistance (TEER) using the cellZscope® device (nanoAnalytics, Münster, Germany). Additionally, barrier integrity was proven by sodium fluorescein translocation and staining of the tight junction and microtubule proteins γ-catenin and tubulin as described elsewhere [222]. For transfer studies, cells were treated with non-cytotoxic concentrations of $MnCl_2$ (100 – 1000 µM) and $FeCl_2$ (10 – 500 µM) on the apical side. Samples were taken from the apical and basolateral compartment 6, 24, and 48 h after treatment. Permeability coefficients were calculated as followed:

$$P = \frac{\Delta Q\ [\mu g]}{A\ [cm^2] * \ c_0 \left[\frac{\mu g}{cm^{-3}}\right] * \Delta t\ [s]} \quad (1)$$

with the permeability (P; cm s^{-1}) determined as the quotient of the basolateral amount (ΔQ; µg; normalized to sample volume) and the product of the area of the microporous insert (A; cm^2), the apical concentration at the start of the incubation (c_0; µg cm^{-3}) and the respective time point (t; s)

To quantify the TE content in cells grown on inserts, the membrane was cut out with a scalpel and washed in ice-cold PBS to remove remaining medium. Cells were stored at 20°C until lysis. For cell lysis, cells were digested using a lysis buffer consisting of 1 mM TRIS (Roth, Karlsruhe, Germany), 0.1 M NaCl (Roth, Karlsruhe, Germany), 1 mM EDTA disodium salt (VWR, Darmstadt, Germany) and 0.1 % Triton™ X-100. Lysates diluted in 2 % HNO_3 were measured using an inductively coupled plasma-optical emission spectrometer (ICP-OES; Spectro, Krefeld, Germany) or Agilent ICP-MS/MS Triple Quad system (ICP-QQQ-MS 8800, Agilent, Waldbronn, Germany). Measurement parameters can be found in the supplementary information (table S3,

S4). TE amounts were validated by measuring acid-assisted digested certified reference material BCR®-274 (Single Cell Protein, Institute for Reference Materials and Measurement of the European Comission, Geel, Belgium) and SRM®-1640a (Trace Elements in Natural Water, National Institute of Standards & Technology, Gaithersburg, MD, USA). The cellular TE concentration was normalized to the protein amount determined by BCA-assay.

4.2.4. Transporter Inhibition Study

Transporter inhibition was determined according to single or combined TE incubation as described in 4.2.3. Furthermore, Hepcidin/ LEAP-1 (Human) (Axxora-Enzo Life Sciences, Lörrach, Germany) was incubated 1 h before and Ferristatin II (NSC 8679, NCI Developmental Therapeutic Program) simultaneously in combination with $MnCl_2$ or $FeCl_2$ on the apical side of the microporous insert. After 6 and 24 h samples were taken from the apical as well as basolateral compartment and quantified using ICP-OES. Cellular Mn and Fe uptake was also assessed after cell lysis.

4.2.5. Quantitative Real-time PCR Analysis

Expression of human metal transport- and storage-associated genes was investigated from TE-exposed cells cultivated on microporous insert. Total RNA was isolated using NucleoSpin® extraction kit (Marcherey-Nagel GmbH & Co. KG, Düren, Germany) and RNA yield was determined with Nano Drop One Spectrometer (Thermo Fisher Scientific, Waltham, USA). RNA with absorption ratios A260/A280 and A260/A230 between 1.8 – 2.2 were considered as pure. For cDNA synthesis, 1 µg RNA was transcribed with High-Capacity cDNA Reverse Transcription Kit (Applied Biosystems™, Thermo Fischer Scientific, Waltham, MA, USA) according to the manufacturer's protocol. Prior to RT-qPCR analysis with iQ™ SYBR® Green Supermix (Bio-Rad Laboratories Inc., Hercules, CA, USA) as fluorescence probe, primer efficiency was validated by a cDNA concentration curve and primer concentrations ranging from 0.2 – 0.6 µM and product purity was verified by gel electrophoresis. Only primers with an efficiency between 90 % – 120 % were used (table S5). The applied temperature program carried out on the AriaMx Real-Time PCR System (Agilent, Waldbronn, Germany) included a polymerase activation step at 95°C for 3 min, DNA denaturation at 95°C for 30 s, primer annealing at 56°C for 1 min, and extension phase at 72°C for 15 s. The cycle from DNA denaturation to extension was repeated 37 times. After each extension phase, fluorescence intensity was measured. For melting curve analysis DNA was denaturized at 95°C for 1 min with a subsequent increment from 60 – 95°C within a minute.

values determined were normalized to β-actin as the housekeeping gene and evaluated in consideration of the primer efficiency.

4.2.6. Western Blot Analysis

For Western Blot analysis cell pellets, pelletized from culture dishes, were lysed in ice-cold RIPA buffer in combination with sonification using an ultrasonic probe (6 s, amplitude: 100 %, cycle 0.5). Protein amounts from 10 – 30 µg denaturated with 5x Laemmli buffer (12.5 % β-mercaptoethanol (v/v), 10 % SDS (w/v), 50 % Glycerol (v/v), 0.2 M Tris (pH 6.8), 0.625 % Bromphenol blue) were applied for SDS-PAGE. Protein transfer on a nitrocellulose blotting membrane (0.2 µm pore size, Amersham™ Protran™, Merck, Darmstadt, Germany) via tank blotting (Bio-Rad Laboratories Inc., Hercules, CA, USA) was verified using 0.2 % Ponceau staining. After blocking membranes in 3 % (w/v) non-fat dry milk in 1x Tris buffered saline containing 0.1 % (v/v) Tween® 20 (T-TBS) for 1 h at RT, primary antibodies diluted in blocking solution were incubated at 4°C over night. Recombinant anti-β-actin (1:2500, ab115777, Abcam, Cambridge, United Kingdom), anti-Metallothionein (1:500, UC1Mt, Invitrogen, Thermo Fischer Scientific, Waltham, MA, USA), anti-DMT1 (1:500, ab55735, Abcam, Cambridge, United Kingdom), anti TFRC (1:1000, D7G9X, Cell Signalling, Danvers, US), anti-FTH1 (1:500, D1D4, Cell Signalling, Danvers, US) and anti-FTL (1:500, ab69090, Abcam, Cambridge, United Kingdom) were used as primary antibodies. Horseradish peroxidase (HRP)-conjugated goat anti-mouse or goat anti-rabbit antibodies (1:10000, Bio-Rad Laboratories Inc., Hercules, CA, USA) were incubated as secondary antibodies for 1 h at RT. Since the primary anti-bodies against TfR, FTH and FTL are very potent and belong to the same species as the first antibody against β-actin, the secondary HRP goat anti-rabbit antibody was diluted 1:2500. Chemiluminescence detected with Amersham Imager 600 (GE Healthcare, Chicago, IL, USA) was achieved by incubation of immunoblots with Clarity™ Western ECL Substrate (Bio-Rad Laboratories Inc., Hercules, CA, USA). Protein bands were quantified using ImageJ software and normalized to β-actin as loading control.

4.2.7. Statistical Analysis

Statistical analysis was performed using GraphPad Prism 9 Software (GraphPad Software, La Jolla, CA, USA). Unless otherwise stated data are shown as mean ± SD and significance values are depicted as * $p< 0.05$, ** $p< 0.01$, and *** $p<0.005$ compared to untreated control.

4.3. Results

4.3.1. Mn and Fe Cytotoxicity in Confluent BeWo b30 Cells

The cytotoxicity of $MnCl_2$ and $FeCl_2$ was assessed in confluent BeWo b30 cells to determine nontoxic concentration ranges for transfer experiments. Indirect determination of the cell number via Hoechst assay after 24 h showed no effect for concentrations up to 1000 µM of either $MnCl_2$ or $FeCl_2$ (fig. S2). Therefore, concentrations between 100 – 1000 µM $MnCl_2$ or 10 – 500 µM $FeCl_2$ were applied for single element transfer and 100 µM $MnCl_2$ and 10 – 100 µM $FeCl_2$ for combination studies.

4.3.2. Mn and Fe Transfer across the BeWo b30 Cell Layer

Growing BeWo b30 cells to a confluent and polarized layer on microporous inserts allows the investigation of Mn and Fe transfer across two chambers where the apical chamber refers to the maternal side and the basolateral chamber to the fetal side of the placental barrier.

BeWo barrier integrity and tightness was verified by measuring the transepithelial electrical resistance (TEER), sodium fluorescein exclusion and immunocytochemical staining of adherence junction (γ-catenin) and microtubule proteins (tubulin) as described in Aengenheister *et al.* [222]. TEER reached values of 300 ± 30 Ω*cm² and capacitance values of 2.8 ± 1.1 µF/cm² after 3 days of cultivation on inserts and remained at this level throughout the duration of the transfer experiment. Transwells® with TEER values exceeding 330 Ω*cm² were not used for transfer experiments since BeWo b30 cells do not undergo contact inhibition of growth and formed a multilayer already within the 24 h of TE exposure, which led to a compromised TE transfer (data not shown) [352].

Applying Mn to the apical side and quantifying the basolateral Mn amount revealed a time- and concentration-dependent Mn transfer across the BeWo b30 cell layer (fig. 21A, C). Interestingly, normalization to the applied dose (fig. 21A) showed that Mn transfer amounts are comparable in all applied doses in the range of 8 % ± 3 % after 6 h and 21 % ± 5 % after 24 h. However, applying Fe to the apical side, the basolateral Fe amount normalized to the applied dose (fig. 21B) decreased from 24 % ± 5 % (10 µM $FeCl_2$, 24 h) to 4 % ± 2 % (500 µM $FeCl_2$, 24 h) with increasing $FeCl_2$ incubation concentration. Concentrations higher than 100 µM lead to a plateau with only 4 % ± 1 % of applied $FeCl_2$, indicating a different transfer mechanism compared to Mn.

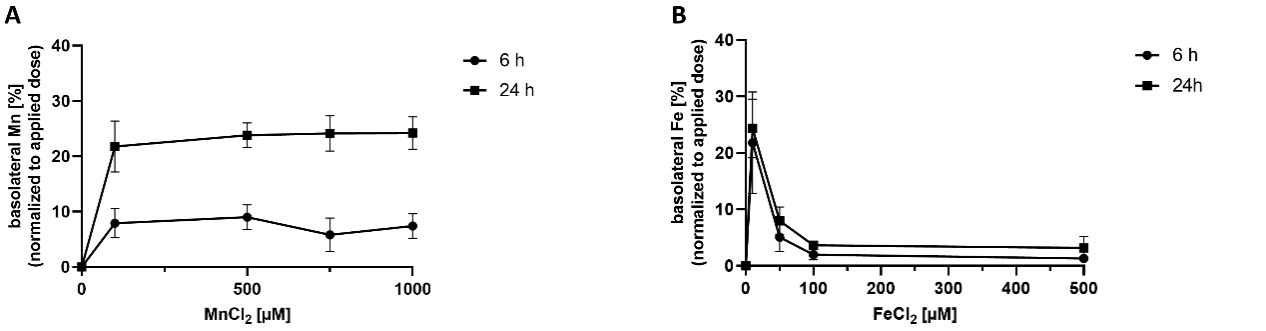

C

Starting conditions (apical) [µM]	Mn amount (basolateral) [µM] 24 h
100	20.0 ± 4.5
500	109.8 ± 13.8
750	161.5 ± 26.5
1000	213.5 ± 33.2

D

Starting conditions (apical) [µM]	Fe amount (basolateral) [µM] 24 h
10	3.2 ± 0.9
50	3.7 ± 1.2
100	3.5 ± 0.7
500	16.6 ± 8.4

Figure 21: Basolateral Mn and Fe amounts 6 h and 24 h after $MnCl_2$ or $FeCl_2$ treatment of confluent BeWo b30 cells. Data are presented as mean ± SD of three independent experiments with two replicates each. Figures (A, B) show the basolateral Mn and Fe amount [%] normalized to the applied dose after 6 h and 24 h. Tables (C, D) show the respective basolateral amount [µM] exemplarily after 24 h.

To get a better understanding of the underlying transfer kinetics, the permeability of Mn as well as Fe was determined. The permeability coefficient allows comparing Mn and Fe transfer to other marker substances such as antipyrine as carried out by Aengenheister *et al.* [222] or other *in vitro* and *ex vivo* models [351]. Incubating 100 µM $MnCl_2$ for 24 h on the apical side resulted in a total crossover of 21.4 % ± 4.6 % to the basolateral side with a defined permeability of $1.2 \times 10^{6} \pm 3.8 \times 10^{-7}$ cm/s. Since percental Mn crossover was concentration independent (fig. 21A), similar permeability coefficients were obtained for all applied Mn concentrations (fig. 22A). Incubating 100 µM $FeCl_2$ resulted in a crossover to the basolateral side of only 3.7 % ± 0.8 % and a permeability of $9.5 \times 10^{-8} \pm 7.4 \times 10^{-8}$ cm/s (fig. 22C), which is less compared to Mn transfer rates. In comparison, $FeCl_2$ permeability was higher for the incubation of lower concentrations like 50 µM $FeCl_2$ ($1.3 \times 10^{-6} \pm 6.7 \times 10^{-7}$) and lower at higher $FeCl_2$ concentrations like 500 µM $FeCl_2$ ($3.0 \times 10^{-7} \pm 1.1 \times 10^{-7}$) (fig. 22B).

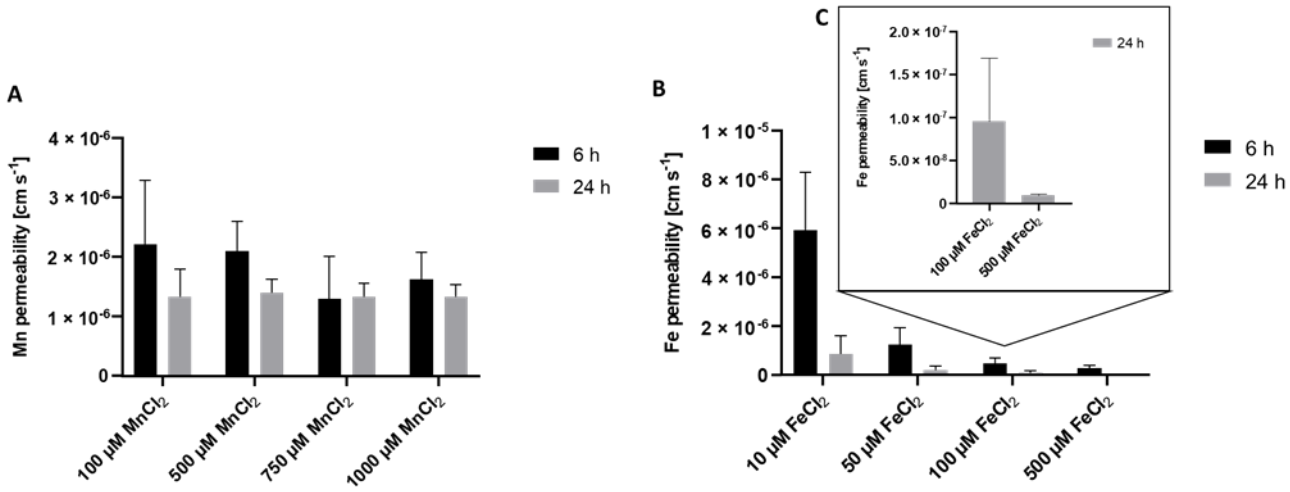

Figure 22: Mn and Fe permeability coefficients across the confluent BeWo b30 cell layer. Permeability was determined in regards to apical Mn or Fe treatment after 6 h and 24 h. Shown is the mean + SD of at least three replicates each. (A) Mn permeability, (B) Fe permeability, (C) enlarged section of permeability coefficients of 100 µM $FeCl_2$ and 500 µM $FeCl_2$ after 24 h.

4.3.3. Mn and Fe Transfer Interactions

To further characterize Mn transfer in terms of transporter involvement and a potential competition with Fe, Mn and Fe were concurrently incubated on the apical side of the BeWo b30 layer for 24 h. Therefore, the concentration of $MnCl_2$ was set to 100 µM while various $FeCl_2$ concentrations ranging from 10 µM – 500 µM were applied. Simultaneous incubation with 100 µM $MnCl_2$ and 10 µM $FeCl_2$ for 24 h significantly decreased Mn transfer. While without Fe, the basolateral Mn amount was 21.4 % ± 4.6 % normalized to the applied dose; only 14.2 % ± 1.9 % were transferred to the basolateral side in combination with 10 µM $FeCl_2$ (fig. 23A). However, co-exposing BeWo b30 cells with either 50 µM $FeCl_2$ or 100 µM $FeCl_2$ and 100 µM $MnCl_2$ showed no impact on the transferred Mn amounts.

Mn transfer and also Fe transfer were both altered by combined Mn and Fe exposure. Incubating 50 µM $FeCl_2$ or 100 µM $FeCl_2$ with 100 µM $MnCl_2$ resulted in a significantly increased Fe transfer of 18.6 % ± 11.1 % vs. 8.0 % ± 2.4 % (Fe only) and 11.1 % ± 7.2 % vs. 3.7 % ± 0.8 % (Fe only), respectively (fig. 23B). Since Fe exhibited an impact on Mn transfer and also Mn affected the Fe transfer, it could be assumed that they share similar transport systems in trophoblast cells.

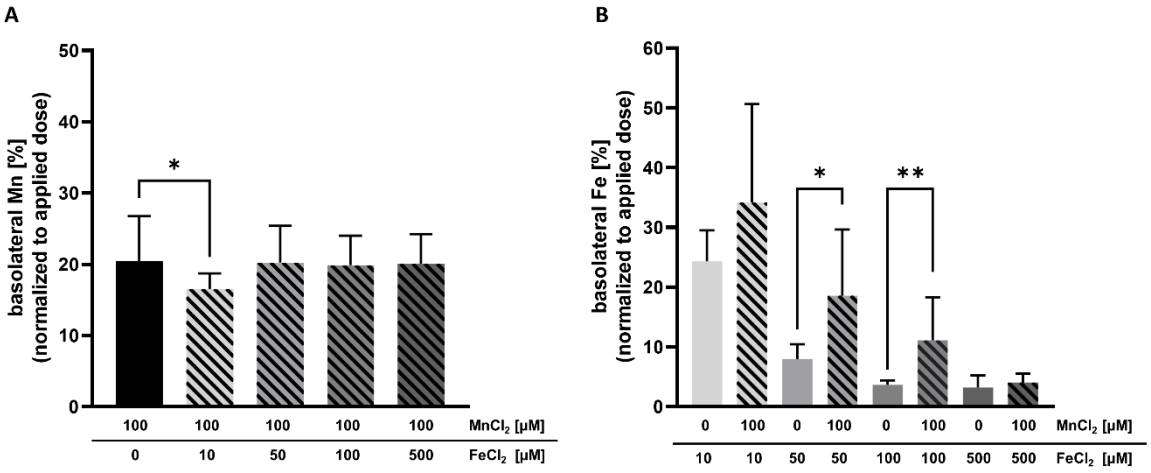

Figure 23: Basolateral Mn and Fe amounts after concurrent treatment after 24 h. Shown is the mean + SD of at least three independent experiments with two replicates each. (A) Basolateral Mn amount [%] normalized to the applied dose. (B) Basolateral Fe amount [%] normalized to the applied dose. Statistical analysis is based on an unpaired t test with Welch's correction compared to single TE treatment. Statistical analysis is indicated as followed: *: compared to single TE treatment.

4.3.4. Cellular Amount of Mn and Fe

Alongside the transferred amounts of Mn and Fe, we quantified the cellular amount of these TEs in the BeWo b30 cells. Single exposure to $MnCl_2$ or $FeCl_2$ resulted in an increased cellular content indicating that Mn and Fe are taken up by the cells (fig 24A, B). Cellular Mn levels were not considerably altered by combinational incubation with $FeCl_2$. However, the trend of a slight decrease in the cellular Mn content was observed at all $FeCl_2$ concentrations, which may be a first indication that Mn bioavailability could be compromised in the presence of high Fe levels (fig. 24A). In contrast, Fe uptake was significantly increased in cells treated with 100 µM $FeCl_2$ + 100 µM $MnCl_2$ compared to single Fe treatment (fig. 24B) but in the other combinations the cellular concentrations were indistinguishable from single Fe exposure.

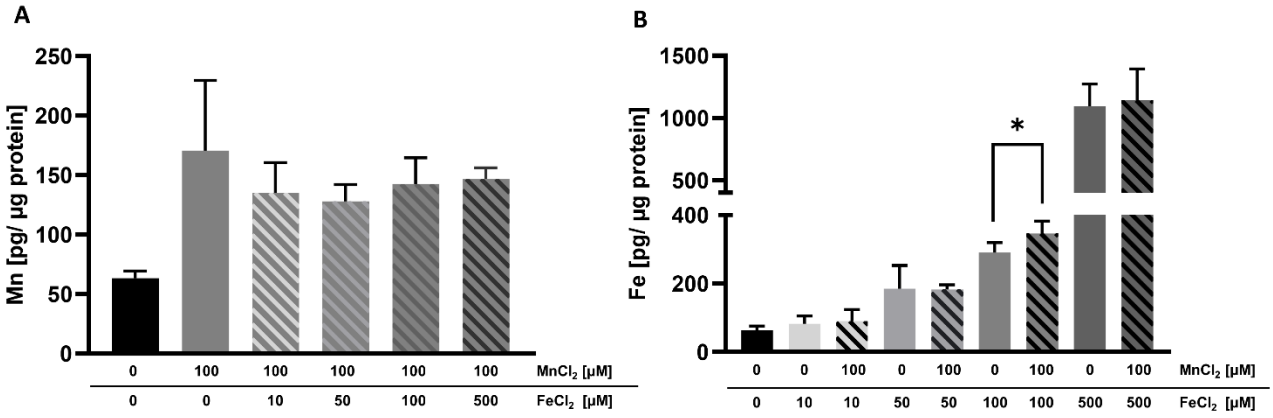

Figure 24: Mn and Fe bioavailability in BeWo b30 cells grown on inserts. BeWo b30 cells were incubated with $MnCl_2$ and/ or $FeCl_2$ for 48 h respectively. Total Mn or Fe amount was determined analytically using ICP-OES or ICP-MS/MS. (A) Mn amount [pg Mn/ µg protein], (B) Fe amount [pg Fe/ µg protein]. Shown is the mean + SD of three independent experiments with two replicates each. Statistical analysis which is based on an unpaired t test is indicated as followed: *: compared to single TE treatment.

4.3.5. mRNA and Protein Expression of Mn and Fe Associated Genes and Related Proteins

mRNA as well as protein expression was determined in BeWo b30 cells after 24 h of TE exposure to specify which Mn and Fe transporters may be involved in single placental Mn and Fe transfer and in case of combined exposure (fig. 25). Considered transporters in this study were TfR, DMT1, ZIP14, and FPN and the transport and storage proteins MT isoforms 1A and 2A (MT1A, MT2A), FTH, and FTL. These are all discussed to be involved in Mn as well as Fe transfer and expressed in placental tissue [251,346,392,393]. For reasons of clarity and comprehensibility, *FTH*, *FTL,* and *ZIP14* gene expression is shown in the supplementary information (fig. S3) since they were not regulated on the transcriptional level by Mn and/ or Fe treatment in this study, as well as *MT1A* gene expression, which showed the same trend as *MT2A*.

Relative gene expression of *DMT1* and *FPN1* as well as FTL protein expression was significantly downregulated by 100 µM $MnCl_2$ exposure of BeWo b30 cells for 24 h (fig. 25C, 25F and 25I). All other transporter-associated genes and proteins were not affected by $MnCl_2$ incubation. $FeCl_2$ exposure of BeWo b30 cells resulted in a significant downregulation of TfR on a transcriptional (100 µM $FeCl_2$) and translational level (10 µM and 100 µM $FeCl_2$) (fig. 25A and 25B) and *DMT1* gene expression was also downregulated after incubation with 100 µM $FeCl_2$ (fig. 25C). Relative mRNA expression of *MT2A* was significantly upregulated by 100 µM $FeCl_2$ (fig. 25G) and *FPN1* expression was significantly downregulated after 10 and 100 µM $FeCl_2$ exposure (fig. 25I). As opposed to relative gene expression levels translational regulation

of FTH and FTL was strongly affected by Fe treatment. FTH and FTL protein expression was significantly increased 24 h after treatment with 10 µM or 100 µM $FeCl_2$. Interestingly, the combination of 10 µM $FeCl_2$ or 100 µM $FeCl_2$ with 100 µM $MnCl_2$ reduced FTH and FTL protein levels compared to single $FeCl_2$ treatment (fig. 25E and 25F). Concurrent incubation of $MnCl_2$ and $FeCl_2$ also resulted in a significant downregulation of TfR on mRNA level (100 µM $FeCl_2$ + 100 µM $MnCl_2$) and protein level (10 µM $FeCl_2$ + 100 µM $MnCl_2$) as well as in *DMT1* mRNA expression (100 µM $FeCl_2$ + 100 µM $MnCl_2$) (fig. 25A, 25B and 25C). DMT1 protein expression showed a similar trend of downregulation for exposures to the combinations of both TEs (10 or 100 µM $FeCl_2$ + 100 µM $MnCl_2$) (fig. 25D). Additionally, protein expression of MT1/2 (fig. 25H) was significantly reduced by exposure to 100 µM $FeCl_2$ + 100 µM $MnCl_2$ while *MT2A* gene expression for 100 µM $FeCl_2$ + 100 µM $MnCl_2$ was significantly less affected compared to single Fe treatment (fig. 25G). *FPN1* mRNA expression (fig. 25I) was altered by 100 µM $FeCl_2$ + 100 µM $MnCl_2$ showing a significant downregulation compared to untreated cells. Compared to single $FeCl_2$ treatment, TfR protein expression was significantly less affected by incubating 10 µM $FeCl_2$ + 100 µM $MnCl_2$ (fig. 25B). The same effect was observed in *MT2A* gene expression, where the combination of 100 µM $FeCl_2$ + 100 µM $MnCl_2$ resulted in a significantly lower upregulation compared to single $FeCl_2$ treatment (fig. 25G).

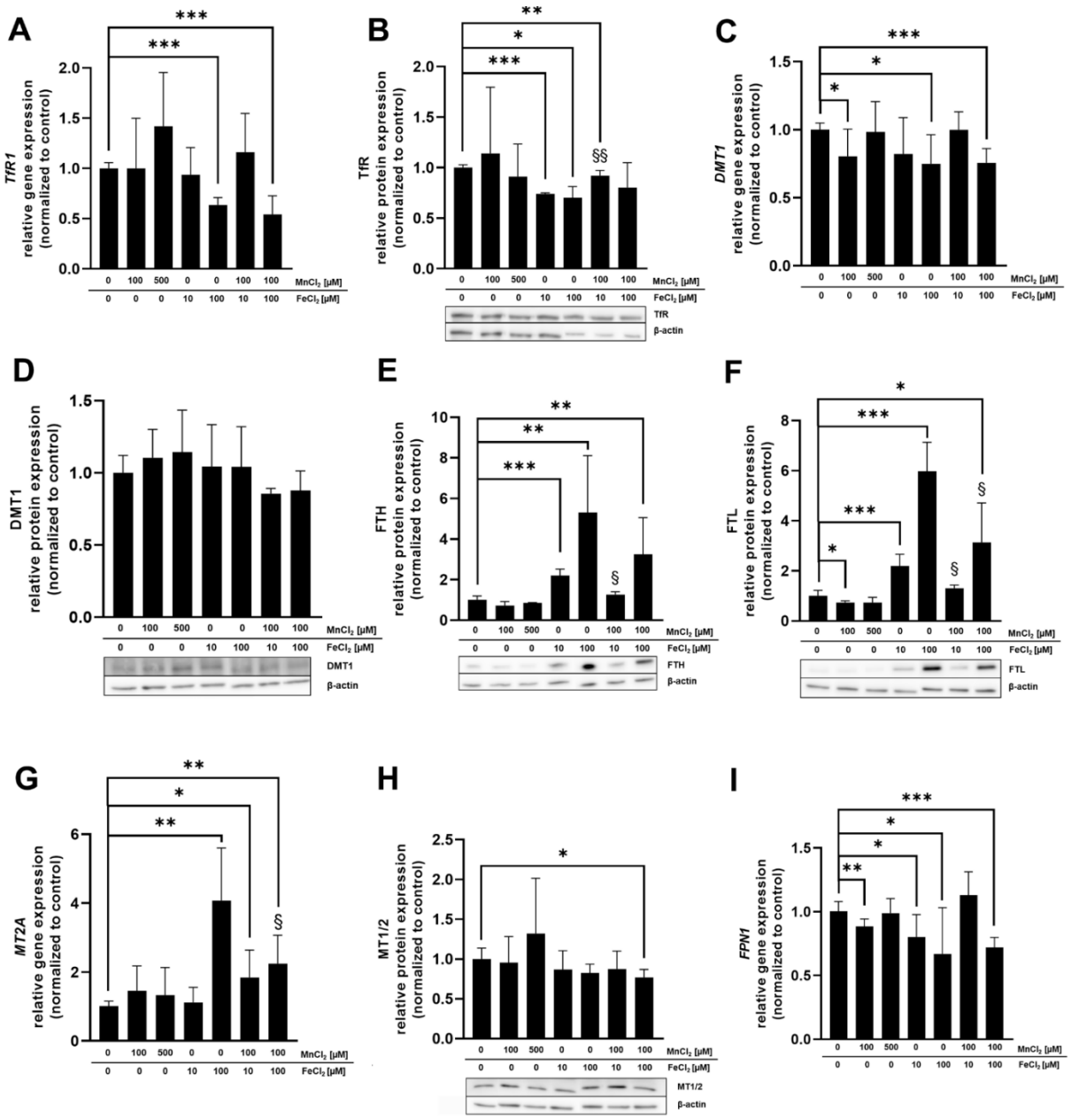

Figure 25: Relative mRNA and protein levels of Mn and Fe transport- and storage-associated genes and their respective proteins. (A) *TfR1* relative gene expression, (B) TfR relative protein expression, (C) *DMT1* relative gene expression, (D) DMT1 relative protein expression, (E) FTH relative protein expression, (F) FTL relative protein expression, (G) *MT2A* relative gene expression, (H) MT1/2 relative protein expression, (I) *FPN1* relative gene expression. Confluent BeWo b30 cells were incubated with $MnCl_2$ and/ or $FeCl_2$ for 24 h. Relative gene expression was determined using RT-qPCR and normalized to *ACTB* (β-actin) as the housekeeping gene. Protein quantification via Western Blot was realized after β-actin normalization of determined protein levels. Bars are assigned to (left to right): untreated control, 100 µM $MnCl_2$, 500 µM $MnCl_2$, 10 µM $FeCl_2$, 100 µM $FeCl_2$, 10 µM $FeCl_2$ + 100 µM $MnCl_2$, 100 µM $FeCl_2$ + 100 µM $FeCl_2$. Shown is the mean + SD of at least three biological replicates. Statistical analysis was performed via unpaired t test with Welch's correction and indicated as followed: *: compared to untreated control, §: compared to single Fe treatment.

4.4. Discussion

While Mn is known to be essential for fetal development, concerns are rising about consequences for the developing fetus in the case of Mn overexposure *in utero*. Although it is known that Mn is able to cross the placenta and excess intrauterine Mn may lead to adverse pregnancy outcomes, it is surprising that underlying mechanisms of Mn transfer in placental barrier-building cells have not been established yet. This key gap was addressed in this study using human BeWo b30 cells. BeWo b30 cells cultivated on microporous inserts are widely used as a model for the placental barrier because they form a confluent polarized monolayer resembling the structure and function of trophoblast cells *in vivo* [222,394]. Additionally, the relative transfer rates of small substances determined in the BeWo b30 monolayer correlate well with transfer indices from *ex vivo* placenta perfusions. BeWo cells further exhibit transcellular transport processes which are involved in placental nutrient transfer [226,348,395]. While data regarding Mn transfer across the placental barrier are rare, Mn translocation across the blood-brain, the blood-cerebrospinal fluid (blood-CSF) or the intestinal barrier has already been elucidated in several studies [199,396]. It appears that multiple transfer pathways are involved, including facilitated diffusion and active transfer processes. The intestinal but also blood-brain barrier studies highlight an involvement of DMT1 and TfR in metal import and FPN for metal export [396,397]. Additionally, they have shown a competition for metal binding sites in metal transporters with Fe [199,396,398]. Therefore, we hypothesized that these transport pathways as well as competitive uptake between Mn and Fe would also occur in placental tissue. Fe transfer kinetics across the placental barrier and placental Fe homeostasis is already clarified in more detail in literature [251,392,393].

Fe is transported through TfR-mediated endocytosis which is only unidirectional from mother to child. Once in the endosome, Fe is released from the Tf-Fe complex and subsequently transported into the cytosol from DMT1. If not stored in FTH or FTL it can be transported to the fetus through FPN [68]. For placental Mn transfer, active transport mechanisms have been suggested mainly based on extrapolations from other TE transport or from rodent data [399] but a distinct proof of active transport and the involved transporters in humans is still lacking. Therefore, the comparison of Mn and Fe transfer and transfer interactions further help to clarify Mn transfer across the human villous trophoblast layer.

First data presented in this work showed that the barrier integrity of the BeWo b30 cell layer was not perturbed by $MnCl_2$ and $FeCl_2$ treatment for up to 1000 µM since TEER values as well

as capacitance values were not affected by TE treatment. In contrast, Bornhorst *et al.* showed that barrier building cells of the blood-CSF barrier for example are more susceptible to $MnCl_2$ treatment with 200 µM $MnCl_2$ being sufficient to cause barrier leakage [199]. Similarly, incubation of differentiated Caco-2 with 15 – 50 µM Fe(II)/ascorbate lead to disruption of the barrier after 2 h [400]. Barrier leakage or complete disruption was not reached in BeWo b30 cells with either $MnCl_2$ or $FeCl_2$ treatment, which hints that BeWo b30 trophoblasts may have adapted to relatively high levels of metal exposure. Since the placenta possesses lots of mitochondria, ROS accumulation is a constant condition which increases during gestation. Therefore, the placenta is provided with a high antioxidant capacity which allows efficient retention of metal-induced ROS [401,402]. The ability of BeWo b30 cells to survive high metal yields facilitates screening the transfer across a wide concentration range to show possible alterations in case cells are overexposed and to reveal a potential risk of an impaired fetal development because of high metal amounts reaching the fetal circulation. However, it has to be considered that concentrations from 100 µM $MnCl_2$ applied in this study are not obtained under physiological relevant conditions in maternal serum or umbilical cord blood but in placental tissue with Mn amounts ranging from 62 ng/ g to 89 ng/ g dry weight [403-407].

In food but also in food supplements, the most important oxidation state of Mn is the divalent form. According to the Directive 2002/46/EC of the European Parliament relating to food supplements, $MnCl_2$ is one of the used species for supplementation [408]. Since pregnant women are mainly exposed to divalent Mn through nutrition and drinking water, Fe was also applied in its divalent form in order to compare transfer mechanisms.

Transfer experiments conducted in this study pointed out distinct crossover kinetics for Mn or Fe, respectively (fig. 21). Expressing the data as percent of the applied dose revealed a constant Mn transfer that was independent of the applied concentrations but showed a time dependency with a higher transfer for longer exposure duration. A previous study on Mn transfer conducted in a perfused human placental lobule observed a restricted Mn transfer presumably following an active transport mechanism [306]. This mechanism was also proposed for other physiological barriers like the blood-brain or blood-CSF barrier [199,409]. However, Bornhorst *et al.* concluded that DMT1 is not the only involved transporter for Mn transfer at the blood-CSF barrier since incubation with a DMT1 inhibitor did not result in a restricted transfer [199]. In addition, previous rodent data or measurement of maternal serum or cord blood further corroborated the hypothesis of an active transfer of Mn across biological barriers [307,399,410].

However, for the placental trophoblast barrier, our data did not support a transport exclusively based on active pathways since no transfer restriction or concentration-dependency could be observed. Consequently, transcellular or paracellular transport mechanisms involving passive diffusion or transfer across the tight junctions should be considered as well in this context [348]. For first indications of transporter-mediated Mn transfer we also incubated inhibitors for DMT1 and TfR (Ferristatin II) and FPN (Hepcidin) in combination with Mn [78,411,412]. Mn transfer and Mn bioavailability were not affected by inhibitor treatment (fig. S4A, B) and in general mRNA and protein expression of TfR1, DMT1, and FPN1 was only slightly altered by Mn treatment. This is also underlining the hypothesis that Mn transfer is not only transporter-mediated but likely involves a combination of active, transcellular and paracellular transfer mechanisms, which needs to be further elucidated in future studies.

This can also be confirmed focusing on Mn bioavailability. Cellular Mn concentration does not increase over time, indicating that Mn homeostasis is maintained through effective import and export mechanisms within the cells. However, while the BeWo b30 trophoblast transfer model is recapitulating the most relevant barrier layer for nutrient transfer to the fetus, further studies should be performed using a co-culture model of trophoblasts and endothelial cells to understand the contribution of the endothelial barrier to maternal-fetal Mn transfer [222,306,413].

Interestingly, different from Mn transfer, Fe transport was highly concentration-dependent until reaching a plateau at 100 µM $FeCl_2$. The 100 µM $FeCl_2$ might be a critical concentration above which the Fe transfer is more tightly regulated to maintain Fe homeostasis and avoid toxicity from excess metal exposure. Additionally, cellular Fe uptake was affected by inhibitor treatment, leading to a significant decreased Fe uptake after inhibition of TfR1 and DMT1 by Ferristatin II and also a trend for a slight increase in cellular Fe in combination of 100 µM $FeCl_2$ with hepcidin, which is involved in FPN regulation (fig. S4C, D) [78]. This is well in line with previous work showing that Fe transfer is a tightly regulated transporter-mediated process in many cells and tissues [81,414]. Heaton *et al.* proposed a passive diffusion for non-transferrin-bound Fe in BeWo b30 cells. Since passive diffusion is limited by molecular size, only unbound Fe can be transferred. It is therefore likely that in our study, Fe was also bound to Tf present in the cell culture medium to restrict the transfer across the BeWo b30 layer at high $FeCl_2$ exposure concentrations but this has to be verified by further studies focusing on Fe speciation [352,415].

Instead of focusing on isolated TEs, the more realistic exposure scenario for the population is the consumption of mixtures of TEs in the normal diet where Mn occurs mainly in cereal-based products or nuts, which are also rich in Fe [2,3]. This underlines the necessity to consider the entirety of all dietary ingredients. Additionally, Mn and Fe are typically added as micronutrients to food and supplements. Especially food supplements are taken in pregnancy in order to preserve a healthy future for the fetus and the pregnant woman [363] and it has also been postulated that dietary Mn absorption rate is also affected by Fe [416]. Therefore, combinations of different TEs and their effect on BeWo b30 trophoblasts were elucidated in this study.

Concurrent Mn and Fe exposure of BeWo b30 cells showed that Mn and Fe transfer is influenced by the respective other TE. 10 µM $FeCl_2$ significantly decreased transfer of 100 µM $MnCl_2$ while 100 µM $MnCl_2$ significantly increased Fe transfer (50 µM and 100 µM $FeCl_2$). To understand if shared use of transporters is one possible mechanisms of transfer interaction, we determined mRNA and protein expression of different transporter-, transport proteins- and storage-associated proteins involved in TE transfer and homeostasis. In general, incubation of either Mn or Fe or the combination of both, affected mRNA and protein expression only marginally except for protein expression of FTH and FTL. TfR protein expression was significantly downregulated by all tested single Fe conditions and adding 10 µM $FeCl_2$ to 100 µM $MnCl_2$ led to a decreased TfR downregulation compared to the single TE treatments. The same trend was also seen for *DMT1* mRNA expression, which was decreased in all conditions except 500 µM $MnCl_2$ and the combination of 10 µM $FeCl_2$ + 100 µM $MnCl_2$. Together, these results indicate that BeWo cells responded to the increased Fe and Mn exposure in order to prevent intracellular accumulation of excess TE. However, quantifying the cellular amount, the cellular Fe concentration following 100 µM $FeCl_2$ was significantly increased in combination with 100 µM $MnCl_2$ (fig. 24). This observation can be explained by the decreased *FPN1* gene expression leading to a decreased Fe export. However, downregulation of *FPN1* gene expression was not distinguishable from single Fe treatment. It could be assumed that translational FPN1 regulation plays a bigger role, but data conducted in this study do not allow a clear explanation of the underlying mechanisms yet, since mRNA as well as protein expression of importers were not altered by concurrent Mn and Fe treatment compared to single Fe treatment as well. The cellular Mn content was slightly decreased in combination with 10 and 50 µM $FeCl_2$, which indicates that Mn uptake is slightly compromised in combination with Fe. This is consistent with mRNA and protein expression data, which

showed TfR1 and DMT1 downregulation for the combination but also for certain single TE treatments. Therefore, Mn import was restricted in combination with low Fe concentrations. Crucial for this observation may be the lower binding affinity of Mn to Tf which is not as high compared to the competing Fe present in the medium and therefore inhibiting Mn transfer by the TfR [148]. It is still unclear why this effect was not observed with higher Fe concentrations investigated in this study.

Several studies have shown that in case of high metal exposure, importers like *DMT1* and *TfR1* are downregulated and the export by *FPN1* is upregulated on mRNA level in order to avoid metal accumulation [417,418]. However, in this study, mRNA expression of the exporter *FPN1* was downregulated by Fe treatment which is observed in other studies in case of Fe deficiency [419]. Li *et al.* also observed *FPN1* downregulation in BeWo cells after treatment with human holo-transferrin but the underlying mechanism cannot be explained yet [420]. One possible hypothesis may be that trophoblast cells are preventing an influx of excess metal to avoid oxidative stress, but simultaneously decrease export to store Fe which is left in the cell to prevent Fe deficiency and maintain proper cell function. On the other hand, it could also be that the export is reduced to avoid overexposure of the sensitive developing fetus. FPN1 downregulation was previously observed in studies from Sangkhae *et al.* which showed that under severe maternal Fe deficiency the placenta downregulates Fe export to maintain Fe homeostasis and to ensure fetal development [277]. Since Fe transfer was enhanced in the presence of Mn while *FPN1* mRNA expression was downregulated, it can be suggested that Fe transfer across the trophoblast layer is not exclusively mediated by Fe exporters but involves other mechanism like passive diffusion.

Focusing on Fe treatment, FTH and FTL protein expression was strongly upregulated in both Fe conditions which additionally indicates that Fe is incorporated into FTH and FTL subunits to prevent Fe accumulation [421,422]. On the contrary, FTL protein expression was significantly decreased after treatment with 100 µM $MnCl_2$. In comparison with single Fe treatment, FTH and FTL protein expression was less affected in combination with Mn. However, it is not obvious if Fe storage is decreased due to the presence of Mn or if Fe is released from FTH/FTL through lysosomal degradation [421]. Fe is stored in FTH or FTL by Fe binding to the iron regulatory protein (IRP), resulting in a release from the 5' untranslated region (5'-UTR) from *FTH/FTL* mRNA [414]. Venkataramani *et al.* observed FTH downregulation in neuronal SH-SY5Y cells after Mn treatment which is in line with the results in this study [157]. The authors

concluded that the 5'-UTR of the *FTH* mRNA transcript was blocked by Mn, thereby inhibiting FTH protein expression [157]. Tai *et al.* also revealed that low Mn doses were sufficient to increase autophagic ferritin degradation and free Fe pool in SH-SY5Y cells, which in turn might lead to increased ROS formation [153,423,424]. This supports also the higher Fe bioavailability in the trophoblasts measured in this study. Interestingly, *MT2A* gene expression is highly induced after treatment with 100 µM $FeCl_2$ but not in the presence of Mn. Since MTs are metal-binding proteins able to scavenge ROS, because they are rich in cysteine, it could be assumed that incubating two TEs would cause a higher induction because there is a higher potential for ROS formation [121]. However, there was no clear evidence why *MT2A* gene expression was less affected in the presence of Mn.

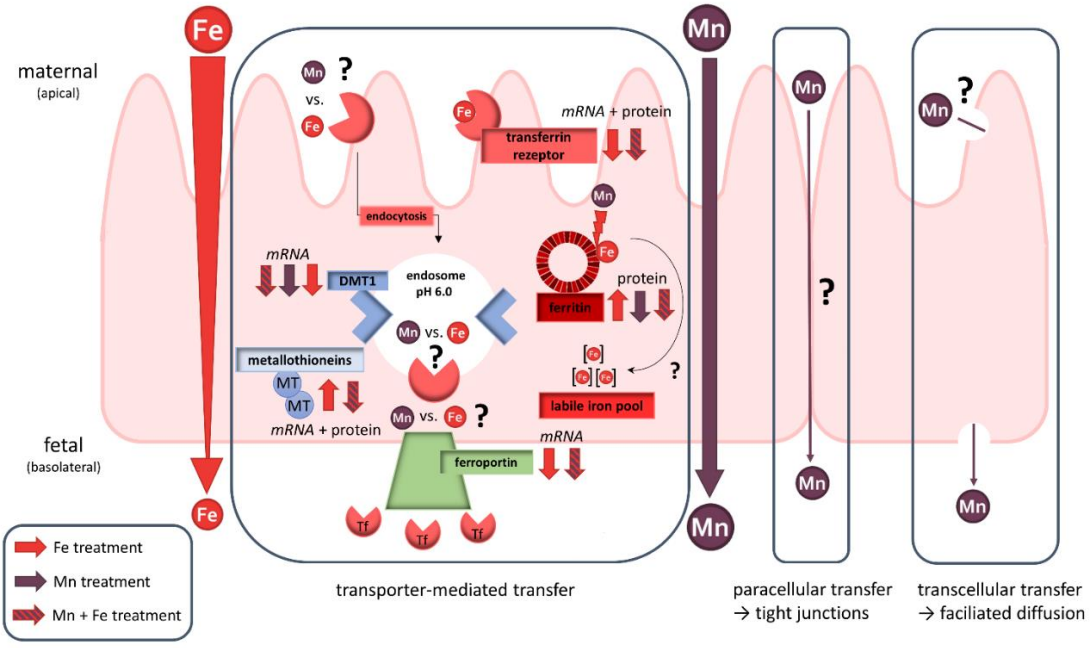

Figure 26: Schematic overview of placental transfer processes of Mn and/or Fe and their effect on transporter expression in the BeWo b30 trophoblast. While Fe seems to be transferred transporter-mediated, Mn transfer appears to follow several transfer mechanisms like paracellular, transcellular, and transporter-mediated pathways.

4.5. Conclusions and Outlook

Although many studies already discussed Mn and Fe transfer across physiological barriers this study is to our knowledge the first to investigate Mn transfer in comparison to the already clarified Fe transfer in human trophoblasts. Since interaction of these TEs in regard of shared transport systems has been elucidated in different tissues and cell types before, this study highlighted the role of Mn and Fe transfer interactions in BeWo b30 cells as well. By applying the widely used BeWo b30 Transwell® model, we were able to show that Mn transfer differs

from Fe since it is not a restricted, concentration-dependent mechanism. Analysis of mRNA as well as protein expression of discussed transporters and storage proteins did not reveal one single mechanism that contributes to Mn transfer across the trophoblast. However, we found that placental Mn transfer involves a combination of transcellular, paracellular and active transport mechanisms including metal transporters (fig. 26). Since we focused on active transfer mechanisms in BeWo b30 cells, transcellular and paracellular processes should be the focus of future transfer studies as well as Mn and Fe speciation analysis and further mechanistic studies on adverse effects. Additionally, we could show that Mn and Fe interactions are also taking place in trophoblast cells which is a crucial observation highlighting that it is important to consider not only one single TE. This can also be underlined by our single TE transfer studies which put an emphasis on the fact that not every TE is transferred the same way and extrapolation of mechanisms from single TE on other TEs should be avoided. Since placental Mn transfer data are scarce putting Fe transfer in relation was necessary to get ideas for possible mechanisms and also revealed important interactional processes. TE interactions in pregnancy should be a major part of future research studies to understand homeostatic alterations caused by TE mixtures in order to improve the assessment of micronutrient requirements during pregnancy.

4.6. Acknowledgments

We thank Alan L. Schwartz (Washington University School of Medicine, Washington, MO, USA) for the permission to use BeWo subclone b30. Additionally, we would like to thank Claus-Werner Vandenhirtz and Kail Matuszak (Institute of Foundation Engineering, Water- and Waste-Management, University of Wuppertal) for their support in single ICP-OES measurements.

4.7. Author contribution

V.M. and J.B. designed the study and prepared the manuscript. V.M. conducted the experiments and analyzed the data. M.T. did the ICP-MS/MS measurements. L.A. assisted in applying the *in vitro* model with helpful tips in handling. F.E. supported in RT-qPCR and Western Blot development and realization. T.B.-T. and L.A. contributed with ideas for the experimental setup and additionally with T.S. and J.R. with important intellectual input. All authors were involved in manuscript preparation and approved the final version. J.B. rendered this work possible. All authors have read and agreed to the published version of the manuscript.

Further work – Metal-induced oxidative stress in BeWo b30 cells

4.8. Introduction

The process of pregnancy is predestined to oxidative stress due to the high metabolic turnover to satisfy the metabolic needs of the mother, the developing fetus, and the placenta [425]. However, due to restricted maternal blood flow by trophoblast plugs early in pregnancy, the fetal nutrient supply is provided by histotrophic nutrition and oxygen is reaching the embryo only through small intercellular pores leading to a low oxygen environment (~ 20 mmHg, equivalent to ~ 2.5 % O_2) [426,427]. This is important to protect the developing fetus from oxidative stress, resulting from oxygen radicals present in the placenta, which can negatively affect organogenesis, the formation of the cytotrophoblast shell, and the villous tree [208,428,429]. However, this is not a hypoxic period, since there are no differences in the ATP/ADP ratio, levels of ADP, NAD+, lactate, or glucose as gestation progresses showing that the placenta is not energetically compromised in the first trimester [208]. By 10 – 12 weeks of gestation and beginning hemotrophic nutrition, oxygen-rich maternal blood is flooding the villous trees resulting in a strong increase of oxidative stress in placental tissue [430]. O_2 tension is then rising to 60 mmHg (equivalent to ~ 8.5 % O_2) however promoting trophoblast differentiation and maturation [427].

In the syncytiotrophoblast, accompanied by rising nutrient demands, increased oxygen levels lead to the stimulation of the mitochondrial metabolic activity, which in turn may generate RONS. Since syncytiotrophoblasts have abundant unsaturated fatty acids in their plasma membrane these are preferably targeted by RONS compared to cytotrophoblasts. In addition, concentrations of antioxidative enzymes such as MnSOD are decreased [431,432]. In case syncytiotrophoblasts degenerate due to an imbalance in RONS and the antioxidative enzymes and proteins, underlying cytotrophoblasts differentiate and fuse to a new generation of syncytiotrophoblasts, which are morphologically equivalent [430]. However, controlled production of RONS is also important for signaling transduction, the activation of proangiogenic genes, promotion of vasodilation, and anti-inflammatory processes [433,434]. Furthermore, redox-sensitive transcription factors and protein kinases are activated. The redox-sensitive transcription factors like p53, nuclear factor kappa-light-chain-enhancer of activated B cells (NF-κB) or activator protein 1 (AP-1) are then available for regulating pro-inflammatory cytokines, cell differentiation, and apoptosis [433]. In the placenta, several antioxidative enzymes are expressed providing an adequate RONS balance. These enzymes

include CuZnSOD (SOD1), MnSOD (SOD2), and CAT. Furthermore, the RONS detoxifying GSH/GSSG redox cycling machinery can also be found in placental tissue. Involved are enzymes of the glutathione-S-transferase family (highest prevalence of isoenzymes pi and T2-2) and glutathione peroxidases, where 80 % of placental GPx activity can be attributed to GPx1, while GPx3 and GPx4 are also expressed [431,435-437]. Placental antioxidant status is also maintained by the abundance of RONS scavengers and metal chelators among others, MTs, ceruloplasmin, albumin, and ferritin [431,438,439].

Oxidative stress has been shown to play a main role in the pathogenesis of preeclampsia (PE), a hypertensive gestational disease, and fetal growth restriction (FGR) often caused by PE [440]. Among the many sources of RONS, studies have shown an association between mitochondrial-derived RONS in PE pathology due to increased oxidative stress markers like isoprostanes, or decreased SOD activity in mitochondria of PE placentas [441-443]. Excessive RONS formation in the mitochondria results from placental implantation defects and the impaired remodeling of the maternal spiral arteries by the extravillous trophoblasts. Then placental perfusion is insufficient leading to irregular arterial blood flow, oxidative stress, and inflammation [431,440,444]. FGR is a common consequence of PE. As a result of placental insufficiency, impaired blood flow, and intrauterine hypoxia, fetal nutrient and oxygen supply is compromised leading to decreased fetal growth [434]. In consideration of maternal TE status, studies have shown decreased levels of Fe, Zn, Mn, and Cu in the serum of women with preeclamptic pregnancies. However, to date, it is not clear if decreased levels result from insufficient nutrient supply or other circumstances [445,446].

In comparison to Fe deficiency, the role of Fe-induced oxidative stress during pregnancy is widely under-investigated. While several studies exist discussing adverse pregnancy outcomes in case of deficiency, data on effects upon overexposure are limited. However, the availability of free Fe can be increased due to alterations in TfR1 and ferritin expression and ferritinophagy, a process that leads to the release of lysosomal Fe(II) and enhanced lysosomal RONS. Excess Fe can also be absorbed due to unnecessary Fe supplementation in Fe-replete mothers. This may enhance the formation of RONS, which can result in lipid peroxidation or DNA damage in placental cells [6,401]. Potential events of increased risk for Fe overexposure are high Fe content, hypoxia, or reperfusion. These events are naturally occurring in placental physiology and can trigger oxidative stress in susceptible trophoblasts [447]. Increased clinical markers for Fe such as serum Fe, ferritin, or Tf saturation are higher in placental tissue of PE pregnancies, which is may be attributed to downregulation of FPN1, highlighting the role of metal

homeostasis in the redox machinery. Involved in placental stress signaling are the Nrf2 and the MAPK (mitogen-activated protein kinase) signaling pathways, which are also involved in villous trophoblast differentiation and associated with the pathology of PE. Therefore, impaired regulation of these pathways might contribute to severe pregnancy complications due to dysfunction in proliferation, differentiation, inflammation, and apoptosis. Moreover, data on Mn-induced oxidative stress in the placenta and during pregnancy is lacking but several studies indicate a role in the activation of the MAPK and Nrf2 pathway [6,448-452]. Thus, this study aims to elucidate cellular alterations in oxidative stress-related pathways upon single Mn, single Fe, and combined Mn and Fe exposure to reveal if oxidative stress induced by either Mn, Fe, or the combination of both is a potential concern in BeWo b30 trophoblasts.

4.9. Materials and Methods

4.9.1. qPCR analysis of oxidative stress-associated genes

The qPCR analysis was conducted as described in 4.2.5 Quantitative Real-time PCR Analysis [308].

4.9.2. Carboxy-DCFH-DA measurement for RONS analysis

RONS measurement with 5-(&6)-carboxy-2',7'-dichloro-dihydrofluorescein-diacetate (carboxy-DCFH-DA) was carried out as described in [453]. Briefly, cells were seeded in a 96-well plate and incubated with $MnCl_2$ for 24 h after reaching confluency 3 days after seeding. Post-incubation cells were treated with a solution of 25 µM carboxy-DCFH-DA in EC (37 °C) and incubated for an additional 20 min (37°C, 5 % CO_2). To investigate long-term effects on RONS generation by Mn, 24 h treated cells were continuously incubated with Mn in the respective concentration scenarios and hydrogen peroxide (H_2O_2, 200 µM) as a positive control. For short-term RONS measurement, untreated cells were incubated with the dye and subsequently treated with $MnCl_2$ or H_2O_2. Afterward, fluorescence was measured every hour with a microplate reader (Tecan®, Ex: 485 nm, Em: 520 nm).

4.10. Results and Discussion

While several studies are focusing on the effects of TE deficient mothers and potential outcomes for the developing focus, the role of Mn- and/ or Fe-induced oxidative stress upon overexposure is under-investigated. Nevertheless, various studies have shown that Mn- and/ or Fe-induced oxidative stress may lead to mitochondrial dysfunction, impaired lipid membranes, and DNA damage up to the induction of cell death pathways in other tissues and cells [6,41]. Therefore, this study aims to elucidate first indications on the capability of Mn- and/or Fe-induced oxidative stress and transcriptional oxidative stress response in the BeWo b30 trophoblasts. Determination of RONS by the Carboxy-DCFH-DA is based on the hydrolysis of the dye by intracellular esterases and the subsequent reaction of the remaining DCHF with RONS [454]. The reliability of the test system was verified by 200 µM H_2O_2 as a positive control, which showed significant induction of RONS compared to control (fig. 27A, B). Short-term as well as long-term exposure to a wide range of $MnCl_2$ concentrations did not result in the induction of RONS in BeWo b30 cells (fig. 27A, B). While various studies on Mn in the context of placental development or several pregnancy outcomes are based on maternal and cord blood measurements or epidemiological studies, data could not be related to the direct effects of Mn on placental cells [66,299,389]. In an astrocyte cell line, Bornhorst *et al.* have observed a significant but moderate induction of RONS, due to incubation with 10 µM $MnCl_2$ after 24 h of preincubation and an additional 4 h post-treatment. Compared to this, porcine brain capillary endothelial cells (PBCEC) were more sensitive toward Mn-induced oxidative stress, with a significant induction after 30 min post-treatment with 0.5 µM $MnCl_2$. The incubation with 500 µM $MnCl_2$ led to a decreased RONS induction, which could be explained by cytotoxicity [453]. Nevertheless, $MnCl_2$ treatment up to 1500 µM did not show any cytotoxic effects in BeWo b30 cells (fig. S2).

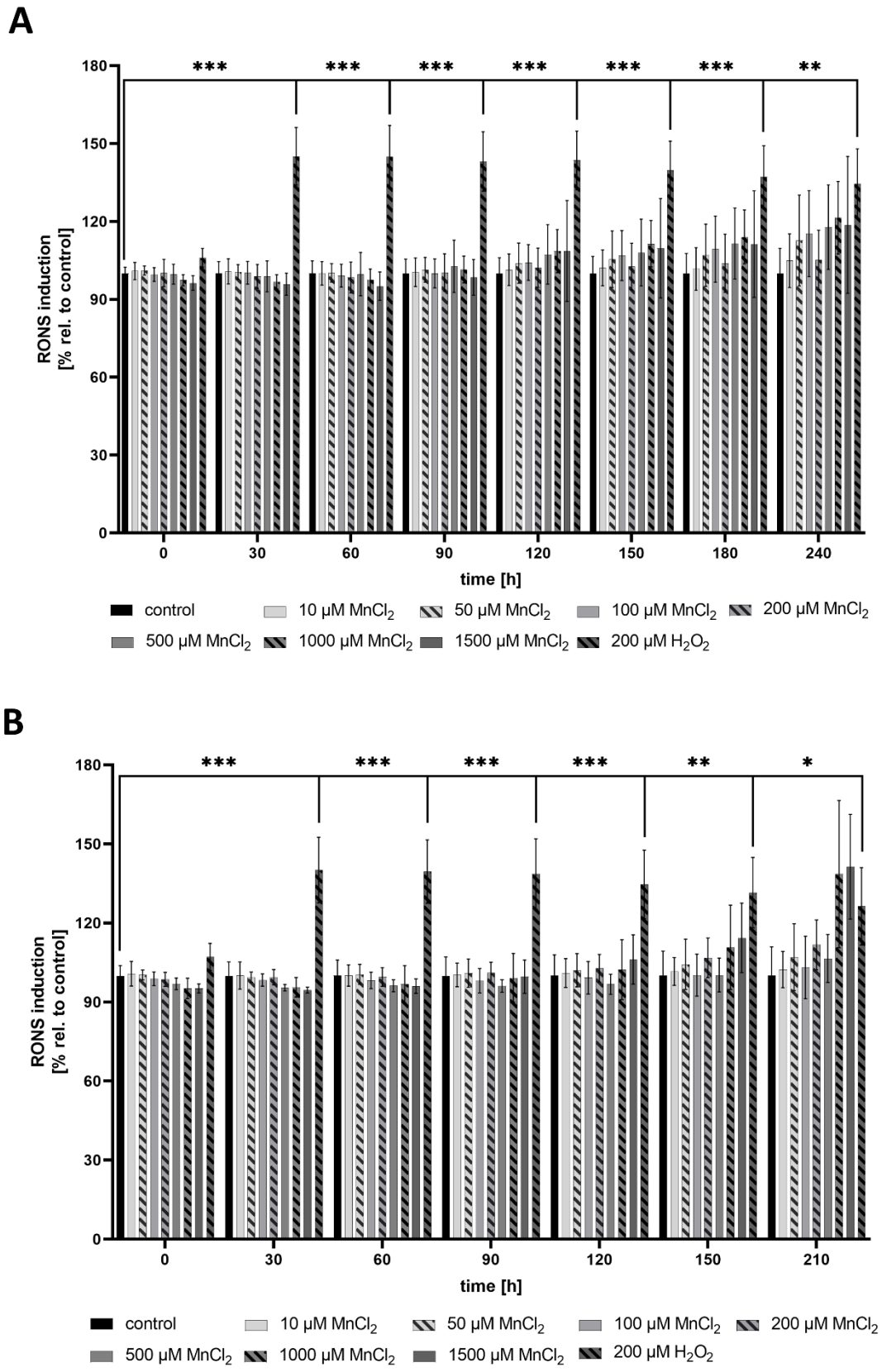

Figure 27: RONS induction after (A) short-term and (B) long-term $MnCl_2$ treatment. BeWo b30 cells were (A) treated with $MnCl_2$ after dye treatment and (B) incubated with $MnCl_2$ for 24 h, which was continued after dye treatment. H_2O_2 was implemented as the positive control. Shown is the mean ± SD of one representative experiment. Statistical analysis is based on an unpaired t test with Welch's correction and indicated as followed: * $p < 0.05$, ** $p < 0.01$, *** $p < 0.001$, compared to untreated control.

Since RONS induction by Mn could not be observed in BeWo b30 trophoblasts, the investigation of oxidative stress-associated genes potentially reveals transcriptional activation of the oxidative stress response, which would further indicate if RONS are already detoxified by the antioxidative defense. Due to the fact that metal homeostasis and the antioxidative defense are strongly related, potential alterations may also explain changes in transporter expression discussed in 4.4.

In general, gene expression of those genes investigated in this study was altered marginally from single $MnCl_2$, single $FeCl_2$, and combined $MnCl_2$ and $FeCl_2$ treatment. While *GSTP1* expression was significantly reduced after treatment with 500 µM $MnCl_2$, *GSTA1* gene expression was unaffected (fig. 28A, B). However, the standard deviation of *GSTA1* gene expression had a wide range, and the data obtained was less reliable compared to *GSTP1* gene expression (fig. 28B). Generally, *GSTA1* is expressed in placental tissue but to a lesser extent compared to other GST isoforms like *GST Theta 1* (*GSTT1*) [455,456]. This may also be verified by the C_q values, which were only slightly below the no-template control (data not shown). The no-template control serves as a quality control to detect potential contamination of cDNA and genomic DNA in the individual reaction components. Alterations in *GSTP1* gene expression may be explained by DNA methylation, which has shown to be involved in *GSTP1* downregulation. DNA methylation changes in the placenta in turn have been associated with fetal Mn exposure. This may hint at potential DNA methylation changes in BeWo b30 cells upon Mn exposure [305,457-459].

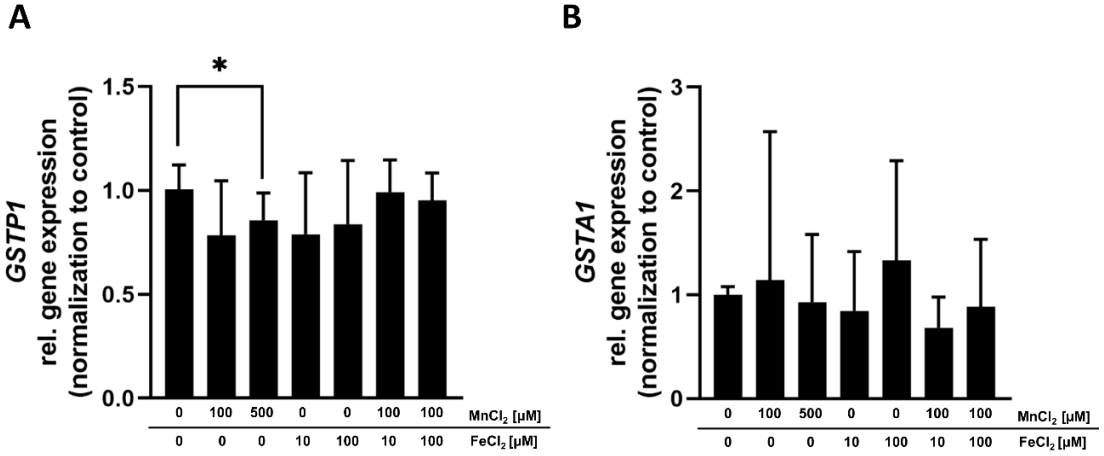

Figure 28: Relative mRNA expression of oxidative stress-associated genes (A) *GSTP1*, (B) *GSTA1*. Confluent BeWo b30 cells were incubated with $MnCl_2$ and/or $FeCl_2$ for 24 h. Relative mRNA expression was determined using RT-qPCR and normalized to ACTB (β-actin) as the housekeeping gene. Bars are assigned to (left to right): untreated control, 100 µM $MnCl_2$, 500 µM $MnCl_2$, 10 µM $FeCl_2$, 100 µM $FeCl_2$, 10 µM $FeCl_2$ + 100 µM $MnCl_2$, 100 µM $FeCl_2$ + 100 µM $MnCl_2$. Shown is the mean + SD of at least three biological replicates. Statistical analysis was performed via unpaired t test with Welch's correction and indicates as followed: *p< 0.05 compared to untreated control.

Moreover, mRNA expression of the *CuZn-dependent SOD* (*SOD1*) was significantly downregulated by treatment with 100 µM $FeCl_2$, which was not the case after incubation with 10 µM $FeCl_2$ for 24 h (fig. 29A). A study by Lim *et al.* has identified a conformational and dynamic change in the Zn(II)-binding site of CuZnSOD by Fe(II). Due to the incorporation of Fe instead of Zn, Cu loading and formation of the disulfide bridge, which is crucial for proper enzyme function is impaired. This may lead to the complete disruption of the SOD system leading to downregulation, which has also been observed in case of cellular apoptosis. Furthermore, Danzeisen *et al.* have reported that decreased *SOD1* mRNA expression is correlating with decreased *TfR1* mRNA expression, which verifies the data obtained in our study. However, underlying mechanisms are still under discussion. Milczarek *et al.* assume the involvement of IRP in this regulatory process [460-463]. Surprisingly *Mn-dependent SOD* (*SOD2*) expression was not altered by Mn treatment (fig. 29B). A study by Lee *et al.* has shown intraperitoneal Mn supplementation in wild-type mice led to increased MnSOD activity without an increase in MnSOD protein level. This was potentially achieved due to the higher metalation of MnSOD. In a previous study, it was shown, that cytosolic Fe levels negatively affected MnSOD activity because of altered mitochondrial Mn availability in a mouse model of hemochromatosis (disturbed Fe homeostasis) [464,465]. However, in the present study, neither single Mn, single Fe nor combined Mn and Fe exposure led to alterations in transcriptional *MnSOD* expression. In this context, it has to be highlighted, that the relationship between transcriptional regulation and enzyme activity is very complex since the response can be triggered by several cellular pathways [466]. It has been shown that p53 is involved in transcriptional *MnSOD* expression in a bidirectional manner. Low p53 levels increased MnSOD protein expression, while p53 overexpression results in increased MnSOD protein expression. The same pattern could be observed on the transcriptional level. The authors suggest, that this bi-directional regulation may be the adaption to the stress levels and execution of cell death mechanisms in case of excess stress [467]. The role of p53 has also been discussed in the context of Mn-induced neurotoxicity with increased p53 expression in Mn-exposed brain regions, which would, combining these two studies, lead to decreased *MnSOD* expression and induction of cell death. Due to the absence of cytotoxicity and unaffected mRNA expression in *SOD2*, this may not be the case in the BeWo b30 trophoblasts [467,468]. Additionally, p53 is also involved in *ZIP14* expression, but it was also not affected by single Mn, Fe, and combined Mn and Fe exposure in BeWo b30 cells (fig. S3) [469].

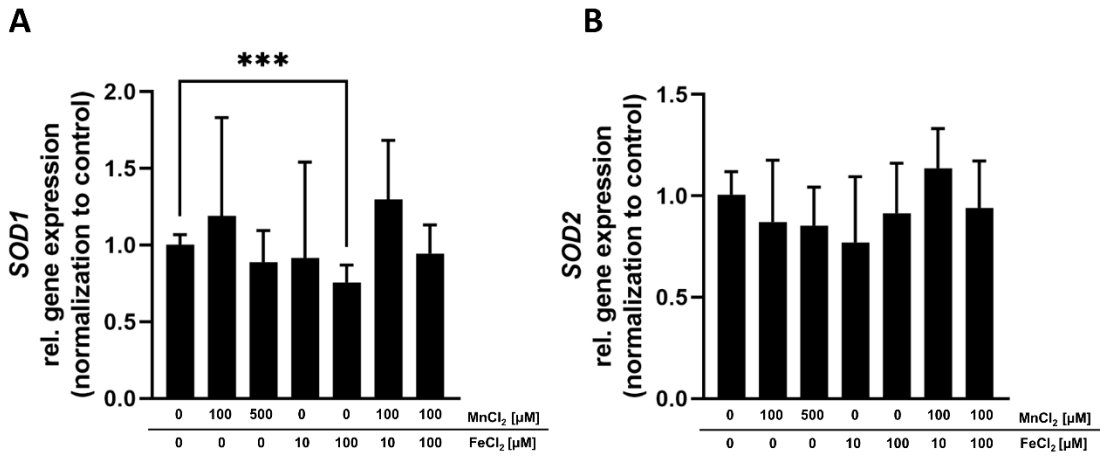

Figure 29: Relative mRNA expression of oxidative stress-associated genes (A) *SOD1 (CuZnSOD)*, (B) *SOD2 (MnSOD).* Confluent BeWo b30 cells were incubated with $MnCl_2$ and/or $FeCl_2$ for 24 h. Relative mRNA expression was determined using RT-qPCR and normalized to *ACTB* (β-actin) as the housekeeping gene. Bars are assigned to (left to right): untreated control, 100 µM $MnCl_2$, 500 µM $MnCl_2$, 10 µM $FeCl_2$, 100 µM $FeCl_2$, 10 µM $FeCl_2$ + 100 µM $MnCl_2$, 100 µM $FeCl_2$ + 100 µM $FeCl_2$. Shown is the mean + SD of at least three biological replicates. Statistical analysis was performed via unpaired t test with Welch's correction and indicates as followed: ***p<0.001 compared to untreated control.

Several isoforms of SOD and GST are downstream targets of the transcription factor Nrf2 (encoded by *NFE2L2*). Besides its role in the transcriptional regulation of these antioxidative defense enzymes, it is also maintaining intracellular Fe homeostasis by interfering in transcriptional *FTH*, *FTL*, and *FPN* regulation [470-472]. Nrf2 regulation is dependent on the Kelch-like ECH-associated protein 1-nuclear factor (KEAP1). In case of oxidative stress, the conformation of the KEAP1 binding site is changed and KEAP1 is not able to interact with Nrf2, leading to Nrf2 activation. In Fe homeostasis, Nrf2 activation may result in transcriptional upregulation of *FTH* and *FTL,* decreasing the labile Fe pool. It is assumed that the underlying mechanism includes the binding of Nrf2 to the ARE (antioxidant response element) present in the *FTH* and *FTL* mRNA [471]. Additionally, Nrf2 is also involved in the modulation of the labile Fe pool by interfering in Fe efflux processes. Hereby, Nrf2 is able to bind to the ARE region in the mRNA of *FPN*, promoting its transcription. In our study, single Fe and combined Mn and Fe exposure did not result in an induction of *Nrf2*, *FTH*, and *FTL* mRNA (fig. 30A, S3A, S3B). Therefore, FTH and FTL are rather regulated translationally by Fe than by Nrf2. *FPN1* mRNA was significantly reduced after exposure to 10 µM Fe, however, it has been shown that Nrf2 rather targets *FPN1* upregulation (fig. 25I). Thus, discussed *FPN1* downregulation in 4.4 cannot be explained by *Nrf2* activation because of metal-induced oxidative stress [471,473]. It is also possible that the labile Fe pool is still under homeostatic control and therefore Nrf2 is not activated. Regarding Mn, studies have shown that Nrf2 protein expression was increased in the cytoplasm and the nucleus of Mn exposed neuronal PC12 cells, which was inhibited by

pretreatment of N-acetyl cysteine (NAC) a precursor needed for glutathione synthesis. However, this is not comparable in the context of our study, since we only investigated *Nrf2* mRNA but not protein expression or translocation. Nguyen *et al.* reported, that *Nrf2* mRNA was also not affected by the treatment of HepG2 cells with *tert*-butylhydroquinone, which is known to induce oxidative stress. Authors suggest that Nrf2 regulation may rather rely on post-transcriptional processes. In general, Nrf2 is regulated post-transcriptionally by the mRNA binding protein HuR. However, data on the role of Mn and Fe in post-transcriptional regulation by HuR is lacking [448,474-476].

Another target of ARE-dependent Nrf2 activation of transcription is heme oxidase 1 (HMOX1). In the human body, HMOX1 catalyzes the decomposition of heme molecules, releasing divalent Fe ions, which are under homeostatic control and utilized for heme production. In states of enhanced oxidative stress, *HMOX1* is transcriptionally upregulated by Nrf2, which in turn can prevent proteasomal degradation of Nrf2. This allows Nrf2 to induce other phase II detoxifying enzymes [477]. *HMOX1* mRNA expression was slightly but significantly upregulated by combined Mn and Fe exposure in BeWo b30 cells (fig. 30B), which may be attributed to increased oxidative stress due to high amounts of metal present in the cell culture medium. Li *et al.* have shown an Nrf2-dependent upregulation in *HMOX1* gene expression in PC12 cells, which they also attributed to increased Mn-induced oxidative stress rather mediated by the ubiquitin-proteasome pathway than Nrf2 phosphorylation by MAPK [448]. The role of HMOX1 in Fe metabolism has been investigated for heme-bound Fe(III) where it has been shown, that induction of *HMOX1* expression by hemin resulted in ferroptosis. Ferroptosis is a form of necrotic cell death associated with the accumulation of membrane lipid peroxides due to Fe accumulation. Increased HMOX1 protein expression after hemin treatment was also observed in colonocytes. Interestingly, they also found out that this effect was not present after treatment with inorganic Fe(III) species. These in turn were also not able to induce RONS, which was assessed by flow cytometry. However, these studies are only partly comparable with this study, since there are differences in incubated Fe species and *HMOX1* expression was only investigated at the transcriptional and not translational level [478-480]. Therefore, further studies are needed to explain, why *HMOX1* mRNA expression was induced transcriptionally by combined Mn and Fe exposure in BeWo b30 cells.

Despite the Nrf2-associated pathway, c-Jun (Jun proto-oncogene) is an important protein involved in the signaling cascade of the JNK (c-Jun terminal kinase) and ERK (extracellular signal-regulated kinase), part of the MAPK pathway often associated in the context of

inflammation [481,482]. Hereby, c-Jun is a subunit of the transcription factor AP-1, involved in apoptotic processes [481]. Several studies have also shown a contribution of c-Jun in the regulation of Fe homeostasis since hepcidin and FTH expression can be altered potentially by promotor transactivation [483,484]. Hepcidin in turn is involved in the regulation of FPN. In our study we observed a significant decrease in *FPN1* mRNA expression, after incubation of 100 µM $MnCl_2$, 10 µM, and 100 µM $FeCl_2$, but not in *JUN* (encoding c-Jun) mRNA expression (fig. 25I, 30C). The influence of c-Jun on *HAMP* mRNA expression (*HAMP* encoding human hepcidin) has only been associated with an increase in c-Jun protein expression. Therefore, the role of c-Jun in the downregulation of FPN after Mn and Fe treatment cannot be ruled out completely, since Hirata *et al.* also revealed an increased c-Jun protein expression in Mn-exposed neuronal PC12 cells [450].

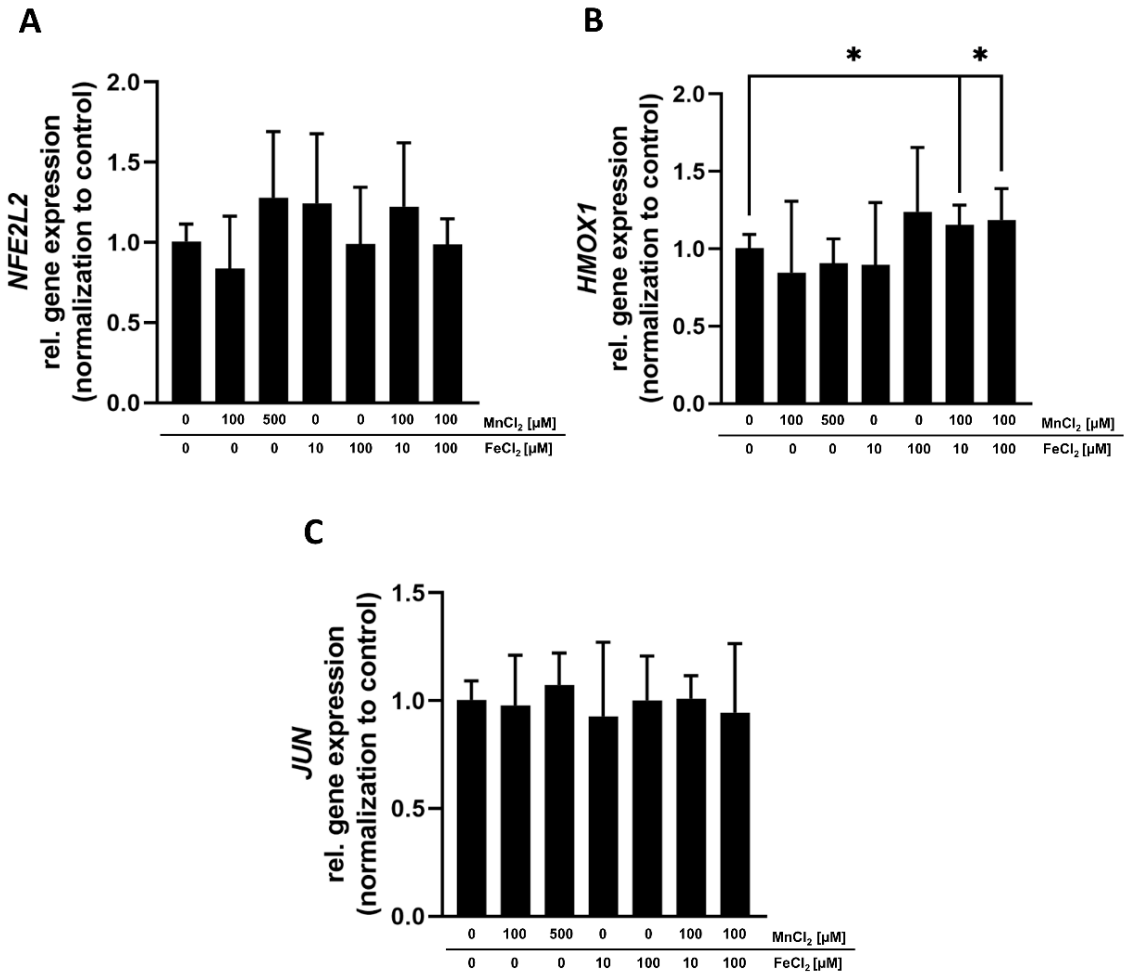

Figure 30: Relative mRNA expression of oxidative stress-associated genes (A) *NFE2L2 (Nrf2)*, (B) *HMOX1*, (C) *JUN*. Confluent BeWo b30 cells were incubated with $MnCl_2$ and/or $FeCl_2$ for 24 h. Relative mRNA expression was determined using RT-qPCR and normalized to *ACTB (β-actin)* as the housekeeping gene. Bars are assigned to (left to right): untreated control, 100 µM $MnCl_2$, 500 µM $MnCl_2$, 10 µM $FeCl_2$, 100 µM $FeCl_2$, 10 µM $FeCl_2$ + 100 µM $MnCl_2$, 100 µM $FeCl_2$ + 100 µM $FeCl_2$. Shown is the mean + SD of at least three biological replicates. Statistical analysis was performed via unpaired t test with Welch's correction and indicates as followed: *p< 0.05 compared to untreated control.

4.11. Conclusion and future directions

Due to their redox activity, Mn and Fe have often been shown to induce oxidative stress in case of overexposure. Due to the high metabolic turnover in the placenta oxidative stress is a present concern in placental tissue, shown to result in impaired placental function and adverse pregnancy outcomes. However, data on the role of Mn- and/or Fe-induced oxidative stress in pregnancy and potential effects on placental tissue and cells of the placental barrier is lacking. Therefore, this study should help to elucidate alterations of metal-induced oxidative stress and potential activation of the oxidative stress response in BeWo b30 cells. Single Mn, single Fe, and combined Mn and Fe exposure showed no clear evidence for increased RONS in BeWo b30 trophoblasts. Either short- or long-term exposure to a variety of $MnCl_2$ concentrations did not induce RONS, and gene expression of oxidative stress-associated genes was only altered marginally. Slightly, but significant alterations in *GSTP1*, *SOD1*, and *HMOX1* gene expression could be observed. This may hint at an apparent stress response to both metals present in the medium. However, data on potential mechanisms is inconsistent. It is not clear to which extent oxidative stress is occurring in BeWo b30 cells and which pathways are either activated or repressed. Therefore, future studies should focus on the investigation of alterations in the GSH/GSSH ratio, revealing a potential role of the GSTs and antioxidative capacity, or endpoints regarding inflammatory insults and subunits of the MAPK pathway. Furthermore, as Nrf2 translocates and accumulates in the nucleus of oxidatively stressed cells, leading to the activation of inducible Nrf2 target genes, determining Nrf2 expression in the nucleus would be another interesting oxidative stress response marker. Regarding oxidative stress-associated genes evaluated in this study, the assessment of the protein expression would also contribute to a better understanding of the role of Mn- and/or Fe- induced oxidative stress in BeWo b30 trophoblasts.

Abstract

Manganese (Mn) and zinc (Zn) are essential trace elements involved in a plethora of metabolic processes. The general population is adequately supplied with balanced nutrition. However, a substantial number of people tend to add supplements to their diets. Although essential, several studies have shown that either Mn or Zn overexposure might lead to detrimental health effects. Both rely on similar transport systems and yet the role of Zn in Mn transfer and toxicity is still unknown.

Total cellular Mn and Zn amounts were determined analytically using inductively coupled plasma-based spectrometry and labile Zn was assessed using the fluorescent probe FluoZin™-3. mRNA expression of genes involved in metal homeostasis and potential underlying mechanistic endpoints in terms of Mn cytotoxicity and cell death mechanism are addressed in this study. Data suggest that Zn has an impact on Mn-induced cytotoxicity and Mn bioavailability in HepG2 cells including a decreased activation of caspase-3 as well as lactate dehydrogenase (LDH) release.

Zn protects against Mn cytotoxicity in HepG2 cells possibly due to decreased Mn bioavailability in the presence of Zn. Additionally, the mRNA expression of metal homeostasis-related genes indicates possible underlying pathways that need to be focused on in future studies.

Chapter 5 – The Impact of Zinc on Manganese Bioavailability and Cytotoxicity in HepG2 cells

Based on:

Vivien Michaelis, Silja Kasper, Lisa Naperkowski, Jan Pusse, Alicia Thiel, Franziska Ebert, Tanja Schwerdtle, Hajo Haase and Julia Bornhorst

Submitted to: Molecular Nutrition and Food Research (under revision)

Keywords: HepG2, manganese, trace element homeostasis, trace element transport, zinc

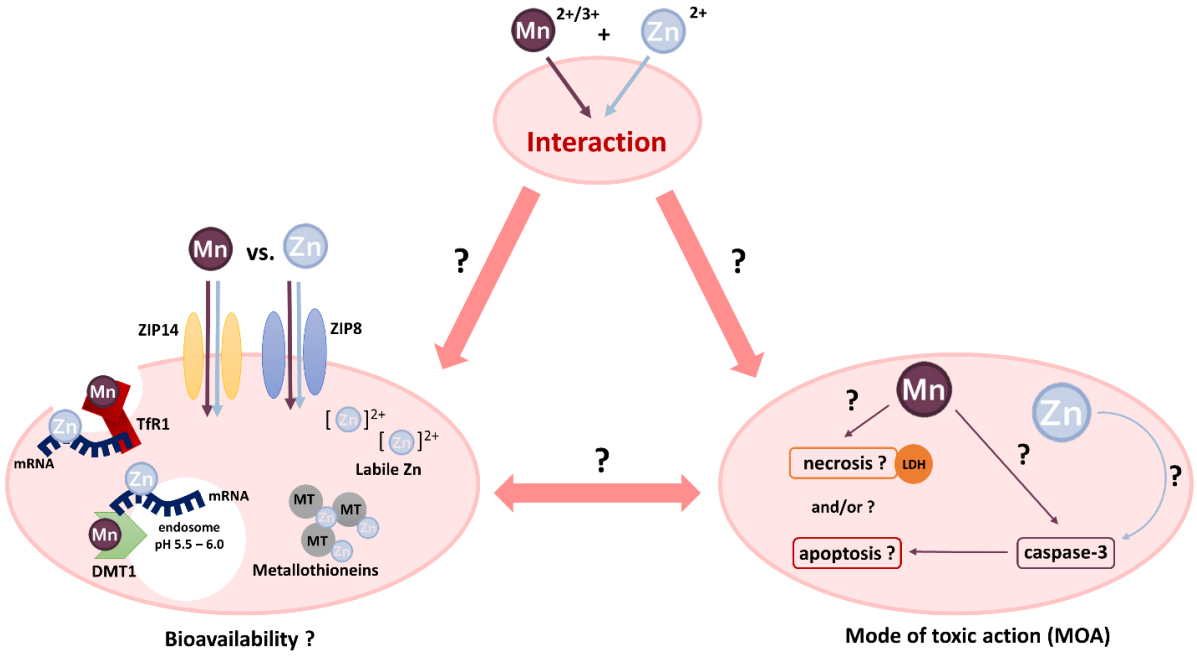

Figure 31: Graphical Abstract: The Impact of Zinc and Manganese Bioavailability and Cytotoxicity in HepG2 cells.

5.1. Introduction

A balanced diet is substantial in order to preserve a healthy life while aging. Although intake recommendations for trace elements (TE) that are proposed by different authorities like the German Nutrition Society (DGE) or the European Food Safety Authority (EFSA) can be reached through balanced nutrition, a substantial number of people tend to add supplements to their diets in order to optimize TE supply [485]. Despite the essentiality of the TEs manganese (Mn) and zinc (Zn), overexposure may also lead to detrimental health issues, among others, caused by unbalanced metal homeostasis [486,487].

In general, Mn is involved in several physiological processes in the human body such as antioxidative defense or carbohydrate metabolism [8]. The EFSA proposed in 2013 an adequate intake of 3 mg/ day for adults, which can easily be attained by drinking water and diet, for example by consuming rice, grains, or tea [3]. Due to its plentiful dietary sources, Mn deficiency is rarely observed in humans [28]. However, studies could show that exceeding the homeostatic range to a great extent may lead to adverse effects. Cellular and molecular modes of action of Mn-induced toxicity include, among others, mitochondrial dysfunction, induction of protein aggregation, glutamate excitotoxicity, disturbed DNA repair, and impaired homeostasis of other TEs. Additionally, especially oxidative stress has been identified as a sensitive endpoint

of Mn toxicity with the formation of reactive oxygen species (ROS), either formed by Fenton chemistry or inhibition of complexes of the mitochondrial respiratory chain [8,28].

In contrast, Zn, which is involved in cell cycle regulation, DNA replication, and apoptosis, is a redox-inert TE with antioxidative, anti-inflammatory, and anti-apoptotic functions [105]. However, the antioxidative characteristics of Zn are dependent on certain dynamic conditions of the amount of labile and protein-bound Zn present in the cells [106,488]. Nevertheless, Zn intake drastically exceeding or falling below the reference intake values of 7.0 – 10.0 mg Zn/ day for women and 11.0 – 16.0 mg Zn/ day for men, (recently revised by the Nutrition Societies of Germany, Austria, and Switzerland (2020) in regard of absorbed, excreted and phytate-bound Zn [106,109,488]) has an impact on metal homeostasis and maintenance of the cellular metabolism [128,489]. For example, high dietary Zn intake may result in copper (Cu) deficiency, because metallothioneins (MT), primarily Zn-binding proteins, have a higher binding affinity compared to Zn leading to enhanced Cu binding with subsequent excretion [490]. On the other hand, it has been shown that Zn deficiency may result in oxidative stress or induction of apoptosis by disrupting ERK and AKT, two kinases involved in growth factor signaling [491]. Therefore, maintaining Mn as well as Zn homeostasis is needed to sustain health.

The liver is centrally involved in Mn and Zn metabolism of the human body. It tightly regulates Mn and Zn distribution to other tissues as well as hepatobiliary excretion of Mn [8,172]. Compared to other tissues and organs, the highest Mn amounts of 1.2 – 1.3 mg/ kg wet weight [174] can be found in the liver while it contains about 142 – 369 mg Zn/ kg dry weight [175]. On the cellular level, transporters involved in Mn and Zn transport into hepatocytes are, among others, the divalent metal transporter 1 (DMT1) and transporters of the ZRT/IRT-like protein (ZIP) family, namely ZIP8 and ZIP14, but also Zn-binding proteins like MTs [23,492-494]. Transport mechanisms and distribution are well understood for single TEs [8,106]. However, TE interactions and homeostatic alterations caused by metal mixtures are rarely characterized. Studies revealed an influence of Mn on Fe uptake because both TEs compete for metal binding sites of the transporters mentioned before, but also for the transferrin-bound transport by the transferrin receptor (TfR) [27,149,495]. Additionally, Zn is affecting the regulation of Fe homeostasis mainly during deficiency since Zn increases *DMT1* as well as *ferroportin* (*FPN*) mRNA expression leading to enhanced Fe efflux [10,82,162]. Those studies show that TE transport is highly dependent on metal homeostasis, which may be altered by the induction of

regulatory processes caused by other TEs taken up from the environment. Therefore, this study aims to elucidate further mechanisms of metal homeostasis focusing on Mn and Zn in HepG2 cells in order to reveal alterations that may have an influence on metal intake and distribution in human hepatocytes.

5.2. Materials and Methods

5.2.1. Cultivation of HepG2 cells

The human hepatoma cell line HepG2 was cultivated as described previously [496]. Briefly, HepG2 cells were cultured in Eagle's Minimum Essential Medium (MEM; Sigma Aldrich, Steinheim, Germany) supplemented with 10 % fetal calf serum (FCS; Biochrom GmbH, Berlin, Germany), 2 % (v/v) penicillin/ streptomycin (Sigma Aldrich, Steinheim, Germany) and 1 % (v/v) non-essential amino acid solution (NEA; Sigma Aldrich) in a humidified incubator at 37°C with 5 % CO_2. Cells were sub-cultured every second day using a 0.25 % trypsin-EDTA solution (Sigma Aldrich, Steinheim, Germany).

5.2.2. Exposure scenarios and dosage regimen

Unless otherwise stated, the abbreviations Mn and Zn refer to both metals in the divalent form (Mn(II) and Zn(II)). To investigate the effect of short- and long-term Zn exposure on Mn transfer and cytotoxicity in HepG2 cells two scenarios were applied. For short-term exposure, cells were preincubated with 50 µM or 100 µM $ZnSO_4$ for 2 h (24 h after seeding) followed by 24 h incubation with $MnCl_2$. For long-term exposure, cells were preincubated with 50 µM or 100 µM $ZnSO_4$ for 24 h (24 h after seeding) followed by a 24 h incubation with $MnCl_2$. In consideration of the cell cycle of HepG2 cells, single $MnCl_2$ treatment was carried out for 26 h (corresponding to 2 h Zn preincubation) and 48 h (corresponding to 24 h Zn preincubation) after seeding. Accordingly, single Zn treatment was realized for 26 h of incubation (corresponding to 2 h pretreatment + 24 h $MnCl_2$ treatment) and 48 h (corresponding to 24 h pretreatment + 24 h $MnCl_2$ treatment).

5.2.3. Cytotoxicity testing

Stock solutions of $MnCl_2$ ($MnCl_2 \cdot 4H_2O$, 99.9 % trace element basis, Honeywell™, Morristown, NJ, USA) and $ZnSO_4$ ($ZnSO_4 \cdot 7H_2O$, 99.9 % trace element basis, Sigma Aldrich, Steinheim, Germany) were prepared freshly before the experiment in sterile purified water (18 MΩ). For the assessment of the cytotoxicity 15,000 cells/cm² were seeded in 96-well plates. The

cytotoxicity of $MnCl_2$ and $ZnSO_4$ was determined after 24 h and 48 h of incubation and for the combined exposures described in 5.2.2.

5.2.3.1.Hoechst Assay

For the indirect determination of the cell number by Hoechst staining, cells were fixed using 4 % formaldehyde in PBS followed by permeabilization of the membrane using a solution of 0.2 % Triton™ X-100 in PBS (Sigma Aldrich, Steinheim, Germany). After permeabilization, Hoechst dye (Bisbenzimide H 33258, Calbiochem, Sigma Aldrich, Steinheim, Germany) interacted with the DNA of living cells [391]. Subsequently, fluorescence was detected using a microplate reader (Tecan® Infinite Pro M200, Tecan, Crailsheim, Germany; Ex: 355 nm; Em: 460 nm).

5.2.4. Mn and Zn bioavailability

For the determination of Mn and Zn bioavailability cells were seeded in 6 cm diameter cell culture dishes (growth area 22.1 cm^2) and incubated with Mn and/ or Zn, respectively (see 5.2.2). After incubation, cells were pelletized by detaching from the culture dish using 0.25 % trypsin-EDTA (Sigma Aldrich, Steinheim, Germany) and washing with ice-cold PBS containing 5 % FCS (Biochrom GmbH). The cell suspension was centrifuged at 340 x g, 4°C for 5 min. The supernatant was removed and the cell pellet was resuspended in ice-cold PBS to remove the remaining FCS. After another centrifugation (3750 x g, 4°C, 5 min) and removal of the supernatant, cell pellets were stored at -20°C until further analysis. For the preparation of the TE measurement, cells were digested using a mixture of 65 % HNO_3 (Suprapur®, VWR, Darmstadt, Germany) and 30 % hydrogen peroxide (Sigma Aldrich, Steinheim, Germany) at 95°C over night. Ashes diluted in 2 % HNO_3 were measured using an inductively coupled plasma-optical emission spectrometer (ICP-OES; Spectro, Krefeld, Germany) or Agilent ICP-MS/MS Triple Quad system (ICP-QQQ-MS 8800, Agilent, Waldbronn, Germany). Measurement parameters can be found in the supplementary information (table S6, S7). ICP measurements were validated using certified reference material BCR® (single cell protein, Institute for Reference Materials and Measurement of the European Commission, Geel, Belgium), which was digested according to the protocol for cells. The cellular TE amount was normalized to cell volume, which was determined using an automated cell counter (CASY®TTC, OMNI Life Science GmbH, Bremen, Germany).

5.2.5. Determination of labile Zinc [Zn^{2+}] using FluoZin™-3

Labile Zn was determined using the FluoZin™-3 AM dye (Invitrogen, Thermo Fischer Scientific, Waltham, USA). In brief, cells seeded in a 96-well plate were incubated with Mn and/ or Zn, respectively (see 5.2.2). After the incubation period, the cell medium was replaced by a solution of 2.5 µM FluoZin™-3 in incubation buffer (IB), consisting of measurement buffer (MB; 120 mM NaCl, 5.4 mM KCl, 5 mM glucose, 1 mM $MgCl_2$, 1 mM NaH_2PO_4, 10 mM HEPES, pH 7.35) and 0.3 % bovine serum albumin for 30 min at 37°C. Subsequently, the dye solution was removed and cells were washed twice with MB. The determination of labile Zn is based on an equilibrium reaction depending on the maximal (F_{max}) and minimal fluorescence (F_{min}) [497]. In order to reach maximal fluorescence, a combination of 0.5 mM $ZnSO_4$ + 50 µM sodium pyrithione (Sigma Aldrich), serving as an ionophore, was incubated. 50 µM TPEN (N,N,N',N'-tetrakis(2-pyridinylmethyl)-1,2-ethanediamine) were applied as a Zn chelator, yielding the minimal fluorescence. To determine the fluorescence of labile Zn in cells (F), cells were treated with MB and incubated for 2 h at 37°C before fluorescence measurement using a microplate reader (Tecan® Infinite Pro M200, Tecan, Crailsheim, Germany; Ex: 490 nm, Em: 525 nm) every 30 min until the equilibrium is reached. Labile Zn concentration [nM] was calculated as follows with a K_D value of 8.9 nM [498]:

$$[Zn^{2+}]\,[nM] = K_D * \frac{(F - F_{min})}{(F_{max} - F)} \quad (1)$$

5.2.6. Caspase-3 activity and Lactate Dehydrogenase Assay

Both caspase-3 activity, as well as the measurement of lactate dehydrogenase (LDH) release, are assays serving as an endpoint for the cell death mechanism. While caspase-3 is activated during apoptosis, LDH is released in case of necrotic cell death [499,500].

5.2.6.1.Caspase-3 activity

Caspase-3 activity was determined by cleavage of the substrate N-acetyl-asp-glu-val-asp-7-amino-4-trifluoromethylcoumarin (Ac-DEVD-AFC) into the fluorescent residue 7-amino-4-trifluoromethylcoumarin (AFC). For this, 18,000 cells/cm² were seeded in a 24-well plate and incubated according to the exposure scenarios (see 5.2.2). After incubation, cells were washed with PBS to remove the remaining medium. Afterward, cells were lysed using a lysis buffer (1 mM Tris, 0.1 M NaCl, 1 mM EDTA disodium salt, and 0.1 % Triton™ X-100) for 15 min on

ice. Cells were scraped from the culture dish and transferred into a reaction tube. The cell suspension was centrifuged for 10 min at 16,000 x g, and 4°C. An aliquot of the supernatant was transferred into a black 96-well plate. The substrate AFC (7.3 µM) was added to the supernatant, diluted in a reaction buffer consisting of caspase buffer (41 mM PIPES, 10 mM EDTA disodium salt, 8 mM CHAPS, pH 7.4) and 1 mM dithiothreitol and the solution was incubated at 37°C for 1 h. Subsequently, fluorescence intensity was measured every hour using a microplate reader (Tecan® Infinite Pro M200, Tecan, Crailsheim, Germany; Ex: 405 nm, Em: 510 nm). AFC content was quantified via external calibration and normalized to protein amount determined by BCA assay. Additionally, the assay was validated beforehand using staurosporine as a positive control [501].

5.2.6.2.Lactate Dehydrogenase Assay

In case of necrotic cell death, LDH is released into the cell culture medium because of an impaired cell membrane. For the assessment of released LDH, the conversion of pyruvic acid to lactate was used. Available LDH reduces NADH to NAD^+, resulting in a measurable change in absorption [502]. After incubation (see 5.2.2) an aliquot of the cell culture medium was transferred into a black 96-well plate. Cells were lysed as described in 5.2.6.1 and the resulting supernatant was transferred as well. The LDH reaction buffer consisting of 0.2 mM NADH disodium salt (Roth, Karlsruhe, Germany), 10 mM pyruvic acid (Roth, Karlsruhe, Germany), and LDH buffer (100 mM HEPES buffer, pH 7.0) was added to start the reaction. Absorption at 355 nm was measured every 54 s for 50 cycles with a microplate reader (Tecan® Infinite Pro M200, Tecan, Crailsheim, Germany). LDH release was normalized to the protein amount determined by the BCA assay.

5.2.6.3.Determination of the protein amount via BCA assay

The determination of the protein amount is based on the formation of a colored chromophore after the complexation of Cu(I)-ions with bicinchoninic acid (BCA) in the presence of protein [503]. Briefly, after cell rupture, the supernatant was mixed with a solution of BCA (Sigma Aldrich, Steinheim, Germany) and Cu(II)sulfate (Sigma Aldrich, Steinheim, Germany) in a 1:50 ratio and incubated at 37°C for 30 minutes. Thereafter, the mixture was further incubated for 1 h at RT, and absorbance was measured at 560 nm using a microplate reader (Tecan® Infinite Pro M200, Tecan, Crailsheim, Germany).

5.2.7. RT-qPCR analysis of transport-associated genes

For the determination of the mRNA expression of metal transport-associated genes, HepG2 cells were pelletized from culture dishes according to 5.2.4. RNA isolation was achieved using the NucleoSpin® extraction kit (Marcherey-Nagel GmbH & Co. KG, Düren, Germany) and the RNA amount was quantified using a NanoDrop One Spectrometer (Thermo Fischer Scientific, Waltham, MA, USA). RNA with absorption ratios higher than 2.0 (A260/A280; A260/A230) were used for cDNA transcription using the High-Capacity cDNA Reverse Transcription Kit (Applied Biosystems™, Thermo Fischer Scientific) according to the manufacturer's protocol. RT-qPCR analysis was realized by the SYBR green method using iQ™ SYBR® Green Supermix (Bio-Rad Laboratories Inc., Hercules, California, USA) as the fluorescent probe. Before analysis, primer efficiencies were determined and product purity was verified via gel electrophoresis. Primers with efficiencies ranging from 100 – 120 % were used (table S8). The temperature program with polymerase activation at 95°C for 3 min, DNA denaturation at 95°C for 30 s, primer annealing at 56°C for 1 min, and extension at 72°C for 15 s (repeated 37 times) was carried out on the Agilent AriaMx Real-time PCR System (Agilent, Waldbronn, Germany). For *MTF1* gene expression analysis, the annealing temperature was adjusted to 54°C. For every measurement, a melting curve analysis was performed with a DNA denaturation at 95°C for 1 min and a subsequent increment from 60°C – 95°C within one minute. Relative gene expression was normalized to the housekeeping gene *ACTB* (*β-actin*) and was calculated in consideration of the primer efficiency.

5.2.8. Statistical analysis

Statistical analysis was performed using GraphPad Prism 9 Software (GraphPad Software, La Jolla, CA, USA). Data are shown as means ± SD and significance values are depicted as * $p < 0.05$, ** $p < 0.01$, and *** $p < 0.005$ compared to untreated control unless otherwise stated.

5.3. Results

5.3.1. Zn preincubation results in reduced Mn cytotoxicity

In order to investigate the impact of a combined incubation with Zn on Mn cytotoxicity, single Mn cytotoxicity in HepG2 cells (also shown in comparison to Zn alone in fig. S5, S6) was compared to the incubation with Mn and Zn in combination after Zn pretreatment. While cell survival was significantly affected after treatment with 200 µM Mn and higher for 24 h (79.1 ± 9.5 % of cell number relative to untreated control) neither a preincubation with 50 µM $ZnSO_4$ for 2 h nor 24 h led to a decrease in cytotoxicity compared to Mn treatment alone (fig. 32A). Increasing the concentration of $ZnSO_4$ to 100 µM showed significant alleviation of Mn cytotoxicity from 75 µM – 1000 µM $MnCl_2$ after 24 h pretreatment, but not for 2 h pretreatment (65.7 ± 11.5 % rel. to untreated control for 500 µM $MnCl_2$ vs. 94.2 ± 10.5 % rel. to untreated control for the combination of 100 µM $ZnSO_4$ (24 h) + 500 µM $MnCl_2$ (24 h)) (fig. 32B).

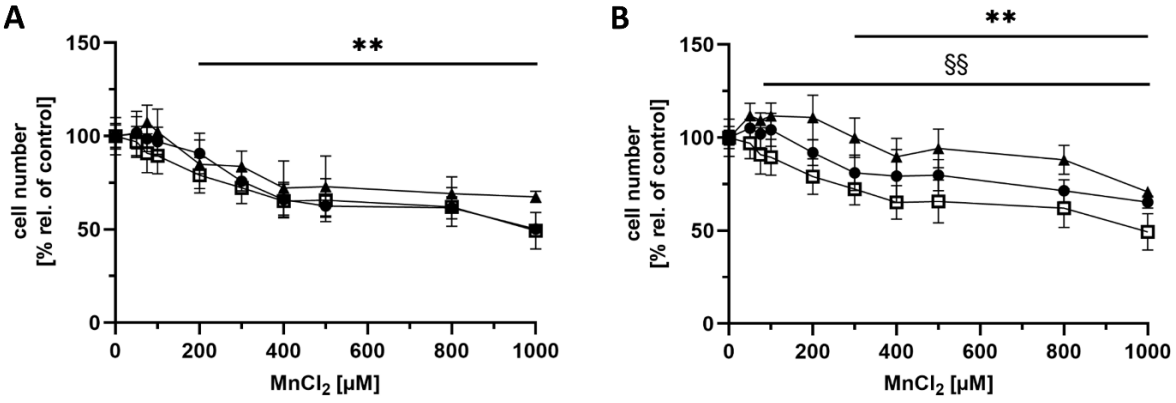

Figure 32: Mn cytotoxicity and the effect of Zn on Mn cytotoxicity in HepG2 cells. Cytotoxicity was determined after 2 h or 24 h Zn preincubation and subsequent Mn treatment for 24 h in comparison with Mn treatment alone for 24 h via Hoechst assay with (A) time-dependent comparison of 50 µM Zn (2 h (–●–) or 24 h (–▲–)) + Mn (24 h) with Mn treatment alone (–□–) (B) time-dependent comparison of 100 µM Zn (2 h (–●–) or 24 h (–▲–)) + Mn (24 h) with Mn treatment alone (–□–). Shown are the means ± SD of at least three independent experiments. Significance is depicted as $^{**}p< 0.01$: Mn treatment alone compared to untreated control (unpaired t-test), $^{§§}p< 0.01$: Combination of preincubation of 100 µM $ZnSO_4$ for 24 h and $MnCl_2$ treatment for additional 24 h compared to Mn treatment alone (two-way ANOVA (Šidák's multiple comparisons)).

5.3.2. Zn preincubation influences protein amount, caspase-3 activity, and LDH release induced by Mn

Additional to cytotoxicity testing via Hoechst assay, caspase-3 activity, LDH release, and protein amount was measured to get further insights into possible cytotoxicity pathways and mechanisms. Therefore, HepG2 cells were treated with 200 µM $MnCl_2$ (start of the cytotoxic range), 400 µM $MnCl_2$ (cytotoxic), and 800 µM $MnCl_2$ (cytotoxic) alone or in combination with 2 h or 24 h pretreatment with 100 µM $ZnSO_4$. Single Mn treatment (200 µM – 800 µM) resulted in significantly reduced protein amounts compared to untreated control 24 h (fig. 33A) as well as 48 h after seeding (fig. 33B). In contrast, $ZnSO_4$ treatment alone led to a significantly increased protein amount (modulating 2 h of pretreatment) (fig. 33A) and additionally in the combination with 200 µM and 400 µM $MnCl_2$ after 24 h of pretreatment (fig. 33B). Caspase-3 activity was significantly decreased in the combinations of 100 µM $ZnSO_4$ + 400 µM or 800 µM $MnCl_2$ for 2 h of pretreatment compared to untreated control (fig. 33C). In comparison, caspase-3 activity was induced by incubation with 400 µM and 800 µM $MnCl_2$, which was reversed by pretreatment of 100 µM $ZnSO_4$ for 24 h (fig. 33D). Furthermore, LDH release was significantly increased incubating 400 µM and 800 µM $MnCl_2$ 24 h after seeding (fig. 33E) and even significant for 200 µM $MnCl_2$ 48 h after seeding (fig. 33F). Concurrent incubation of 200 µM and 400 µM $MnCl_2$ with 100 µM $ZnSO_4$ (2 h pretreatment) resulted in a significantly decreased LDH release compared to untreated control and single Mn treatment (fig. 33E). The same could be observed after 24 h pretreatment with 100 µM $ZnSO_4$ in combination with 400 µM $MnCl_2$ (fig. 33F).

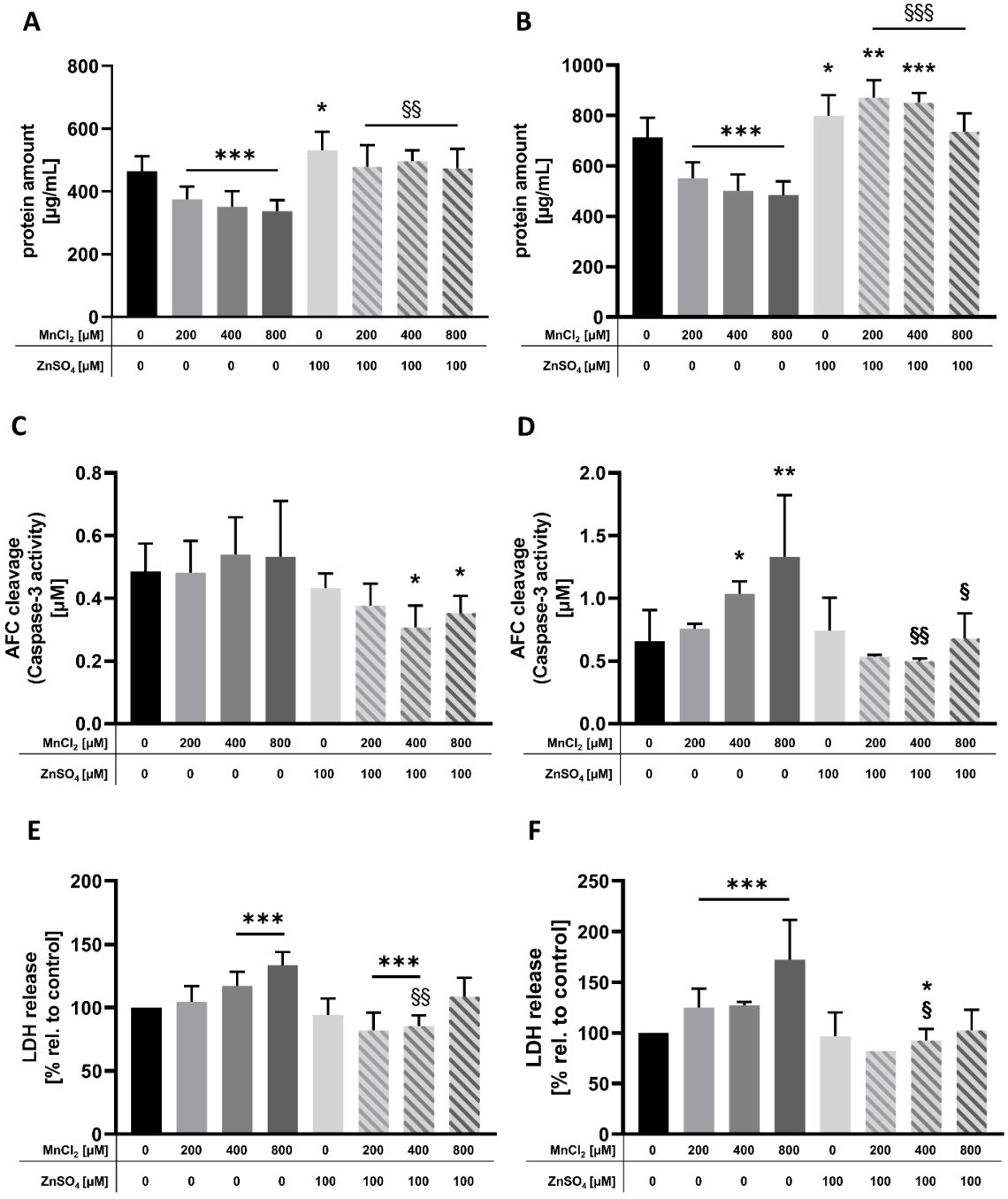

Figure 33: The effects of Zn and/or Mn treatment on protein amount, caspase-3 activity (AFC cleavage), and LDH release after 2 h or 24 h preincubation of 100 µM $ZnSO_4$ and subsequent Mn treatment for additional 24 h. Shown are the means + SD of at least two independent experiments of (A) protein amount [µg/mL] of cells treated with 2 h $ZnSO_4$ before 24 h $MnCl_2$ treatment, (B) protein amount [µg/mL] of cells treated with 24 h $ZnSO_4$ before 24 h $MnCl_2$ treatment, (C) AFC cleavage [µM] of cells treated with 2 h $ZnSO_4$ before 24 h $MnCl_2$ treatment, (D) AFC cleavage [µM] of cells treated with 24 h $ZnSO_4$ before 24 h $MnCl_2$ treatment, (E) LDH release of cells treated with 2 h $ZnSO_4$ before 24 h $MnCl_2$ treatment, (F) LDH release [µM] of cells treated with 24 h $ZnSO_4$ before 24 h $MnCl_2$ treatment. Significance provided by an unpaired t-test with Welch's correction is depicted as *p< 0.05, **p< 0.01, ***p< 0.005: compared to untreated control, §p< 0.05 §§p<0.01: compared to Mn treatment alone.

5.3.3. Effect of Mn and Zn on TE bioavailability

To investigate if altered uptake of Mn, as well as Zn, is one possible mechanism of attenuated Mn cytotoxicity in HepG2 cells, cellular Mn as well as Zn amounts were measured using ICP-OES or -MS/MS and normalized to cell volume in order to compare incubated concentrations with resulting cellular concentrations. Untreated control cells contained 20.5 µM ± 9.2 µM Mn and 286.3 µM ± 83.7 µM Zn. Overall, single $MnCl_2$ treatment resulted in an increased Mn concentration between 664.2 µM ± 323.2 µM (200 µM $MnCl_2$) and 3,388.1 µM ± 987.0 µM Mn (800 µM $MnCl_2$) in HepG2 cells regardless if cells were treated 24 h or 48 h after seeding (fig. 34A, B). The combined exposure to 800 µM $MnCl_2$ together with 50 µM or 100 µM $ZnSO_4$ significantly decreased Mn uptake after 2 h preincubation and also the uptake of 400 µM and 800 µM $MnCl_2$ after 24 h preincubation with $ZnSO_4$ (fig. 34A, B). Similar to $MnCl_2$ treatment alone, application of $ZnSO_4$ in the absence of Mn resulted in a concentration-dependent significant increase of the Zn concentration compared to untreated cells (fig. 34C, D). In combination, adding 200 µM, 400 µM, and 800 µM $MnCl_2$ 2 h after $ZnSO_4$ treatment for additional 24 h showed a significant decrease of cellular Zn compared to 50 µM $ZnSO_4$ treatment alone and also for 100 µM $ZnSO_4$ + 800 µM $MnCl_2$ (fig. 34C). 24 h of $ZnSO_4$ preincubation further significantly influenced Zn uptake in the combination of 100 µM $ZnSO_4$ + 400 µM $MnCl_2$ and 100 µM $ZnSO_4$ + 800 µM $MnCl_2$. However, all other dose combinations showed a slight trend for decreased Zn uptake (fig. 34C, D).

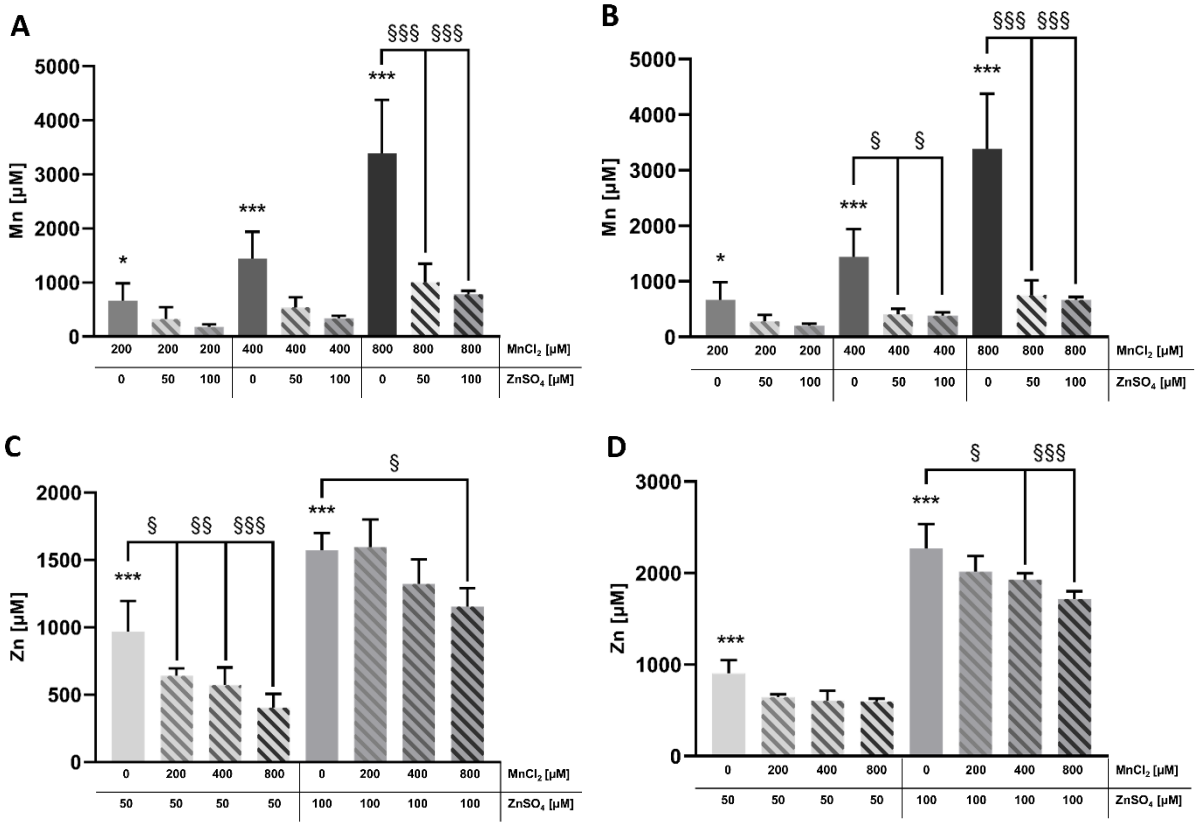

Figure 34: Mn and Zn bioavailability in HepG2 cells. HepG2 cells were preincubated with either 2 h or 24 h $ZnSO_4$ and subsequently incubated with $MnCl_2$ for additional 24 h.Total Mn and Zn amounts were measured with ICP-MS/MS or ICP-OES and normalized to cell volume. Shown are the means + SD of at least 3 independent experiments from Mn concentration [µM] of cells (A) preincubated with Zn for 2 h and/ or Mn treatment for 24 h, (B) preincubated with Zn for 24 h and or Mn treatment for 24 h, and Zn concentration [µM] of cells (C) preincubated with Zn for 2 h and/ or Mn treatment for 24 h, (D) preincubated with Zn for 24 h and/ or Mn treatment for 24 h. Significance provided by one-way ANOVA with Tukey's multiple comparison is depicted as *p< 0.05, ***p< 0.005: compared to untreated control, §p< 0.05, §§p< 0.01, §§§p< 0.005: compared to single TE treatment respectively.

5.3.4. Labile Zinc [Zn^{2+}] Measurement

In order to specify the amount of labile Zn, which is crucial for Zn activity in HepG2 cells [504], the FluoZin™-3 dye was used. Incubation with 100 µM $ZnSO_4$ showed a strong increase of labile Zn with concentrations up to 46.4 nM and 30.5 nM according to 2 h and 24 h of preincubation, respectively (fig. 35A, B). On the contrary single Mn treatment significantly decreased labile Zn compared to untreated control independent of preincubation time (fig. 35A, B). Concurrent incubation of 100 µM $ZnSO_4$ together with either 200 µM or 400 µM $MnCl_2$, had no additional effect on labile Zn compared to Zn treatment alone (fig. 35A, B).

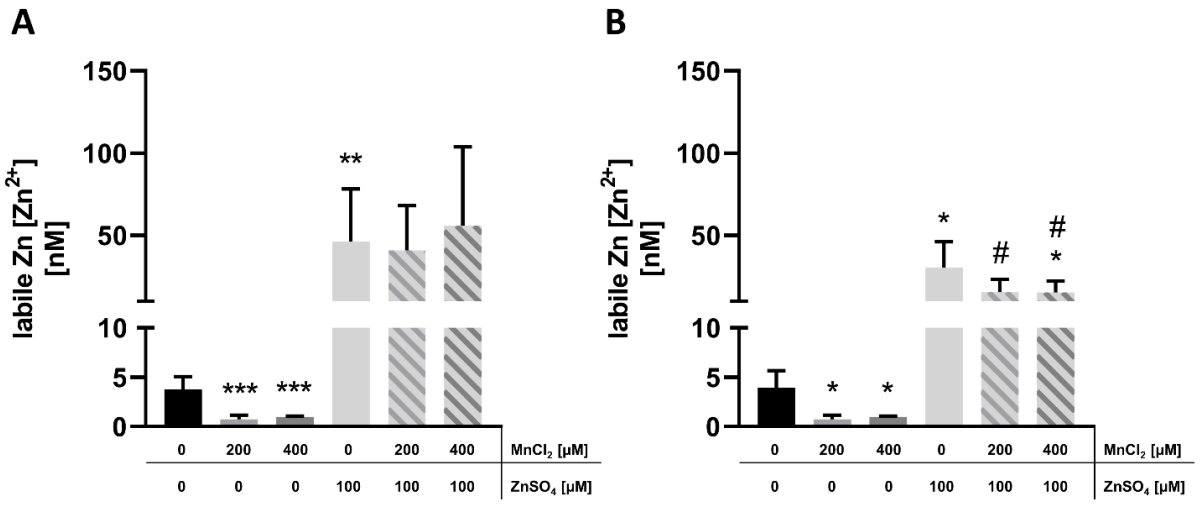

Figure 35: Labile Zn [Zn^{2+}] [nM] measurement via FluoZin™-3 dye. HepG2 cells were preincubated with either (A) 2 h or (B) 24 h $ZnSO_4$ and subsequently incubated with $MnCl_2$ for additional 24 h. Labile Zn amount was determined after reaching the equilibrium. Shown are the means + SD of at least 3 independent experiments. Significance provided by unpaired t-test with Welch's correction is depicted as *p< 0.05, **p< 0.01, ***p< 0.005: compared to untreated control, #p< 0.05: compared to Mn treatment alone.

5.3.5. qPCR analysis of transporter-associated and transport protein-related genes involved in Mn and Zn transport

Since Mn and Zn uptake was decreased after combined incubation with $ZnSO_4$ and $MnCl_2$ in all exposure scenarios, the RT-qPCR analysis of transporters involved in Mn and Zn transport should give an insight into possible affected transport mechanisms. $MnCl_2$ treatment alone resulted in decreased mRNA expression of *DMT1, ZIP8,* and *ZIP14,* while *MT1A, MT2A*, and also *TfR1* (for 400 µM $MnCl_2$) gene expression was significantly increased (fig. 36A-F). While $ZnSO_4$ treatment alone significantly decreased *ZIP14* mRNA expression, *ZIP8* gene expression was significantly upregulated in all exposure scenarios and additionally showed strong induction of *MT1A* and *MT2A* gene expression up to 45-fold compared to the untreated control (fig. 36C, D, 37E, F). According to single TE treatment *DMT1* mRNA expression was significantly downregulated in combination of 100 µM $ZnSO_4$ + 200 µM $MnCl_2$ (after 2 h and 24 h preincubation) and 100 µM $ZnSO_4$ + 400 µM $MnCl_2$ (after 2 h preincubation) compared to untreated control. In comparison to single Mn treatment, *DMT1* mRNA expression was significantly less affected in both combinations with 100 µM $ZnSO_4$ with a preincubation time of 2 h (fig. 36A). *TfR1* and *ZIP14* gene expression were significantly downregulated in the combinations as well, whereas preincubation with 100 µM $ZnSO_4$ for either 2 h or 24 h ameliorated the decrease of *ZIP14* mRNA expression compared to treatment with $MnCl_2$ alone

(fig. 36B, D). Interestingly, *MT1A* and *MT2A* gene expressions were also strongly upregulated in the respective combinations independent from preincubation time, but in comparison to $ZnSO_4$ treatment alone, the effect of a time-dependent higher induction of *MT1A* gene expression (24 h preincubation) was completely counterbalanced in combination with 400 µM $MnCl_2$ (fig. 37E, F). The mRNA expression of *metal regulatory transcription factor 1 (MTF1)*, which is involved in MT regulation, was significantly upregulated by incubation with 400 µM $MnCl_2$ alone and significantly downregulated in combination with 100 µM $ZnSO_4$ with a preincubation time of 24 h (fig. 37G).

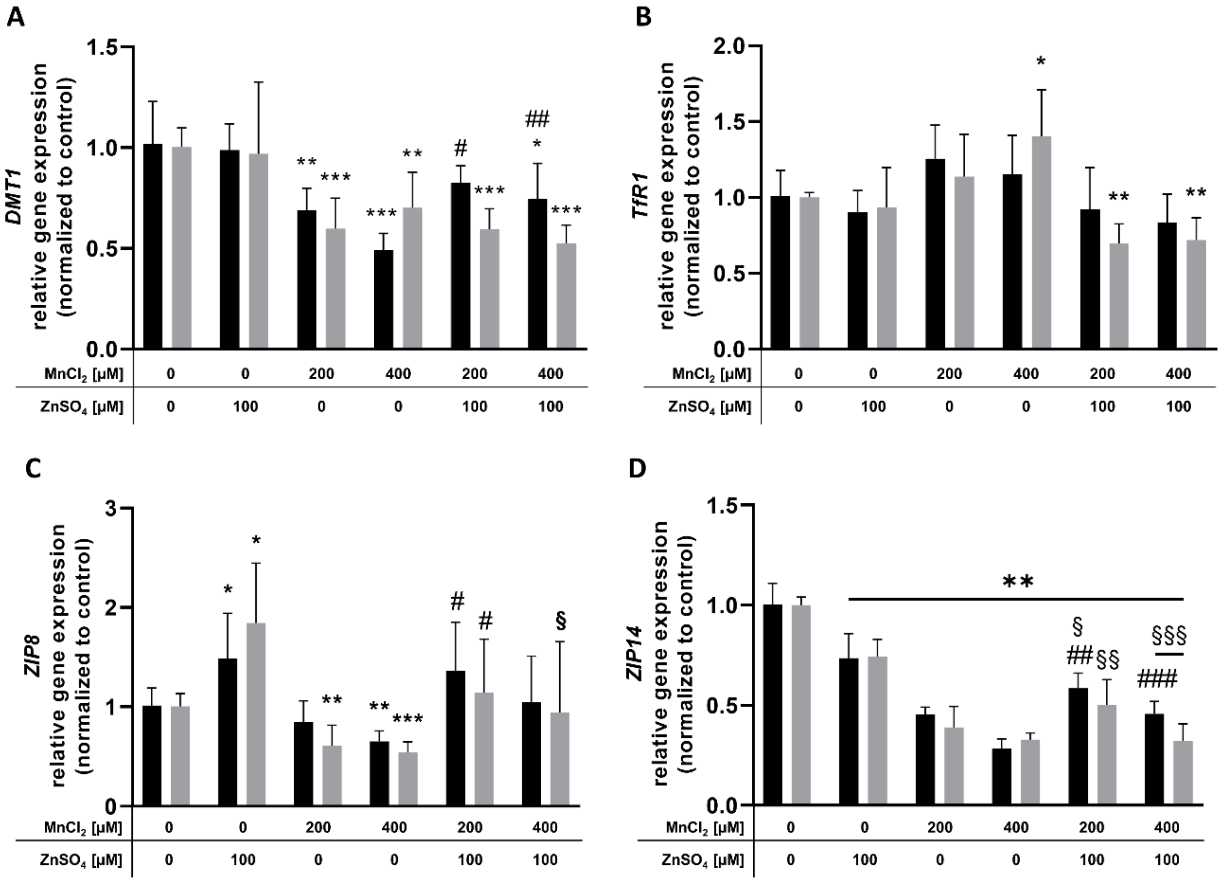

Figure 36 A – D: Relative mRNA expression of Zn and Mn transporters and transport proteins in HepG2 cells preincubated with 100 µM $ZnSO_4$ for either 2 h (▬) or 24 h (■) following 24 h $MnCl_2$ treatment. Relative mRNA expression was assessed using RT-qPCR and normalized to *ACTB* (β-actin) as the housekeeping gene. Shown are the means + SD of at least three independent experiments with two technical replicates each for (A) *DMT1*, (B) *TfR1*, (C) *ZIP8*, (D) *ZIP14*, respectively. Significance provided by an unpaired t-test with Welch's correction is depicted as $^{*}p< 0.05$, $^{**}p< 0.01$, $^{***}p< 0.005$: compared to untreated control, $^{§}p< 0.05$, $^{§§}p< 0.01$, $^{§§§}p< 0.05$: compared to Zn treatment alone, $^{\#}p< 0.05$, $^{\#\#}p< 0.01$, $^{\#\#\#}p< 0.05$: compared to Mn treatment alone.

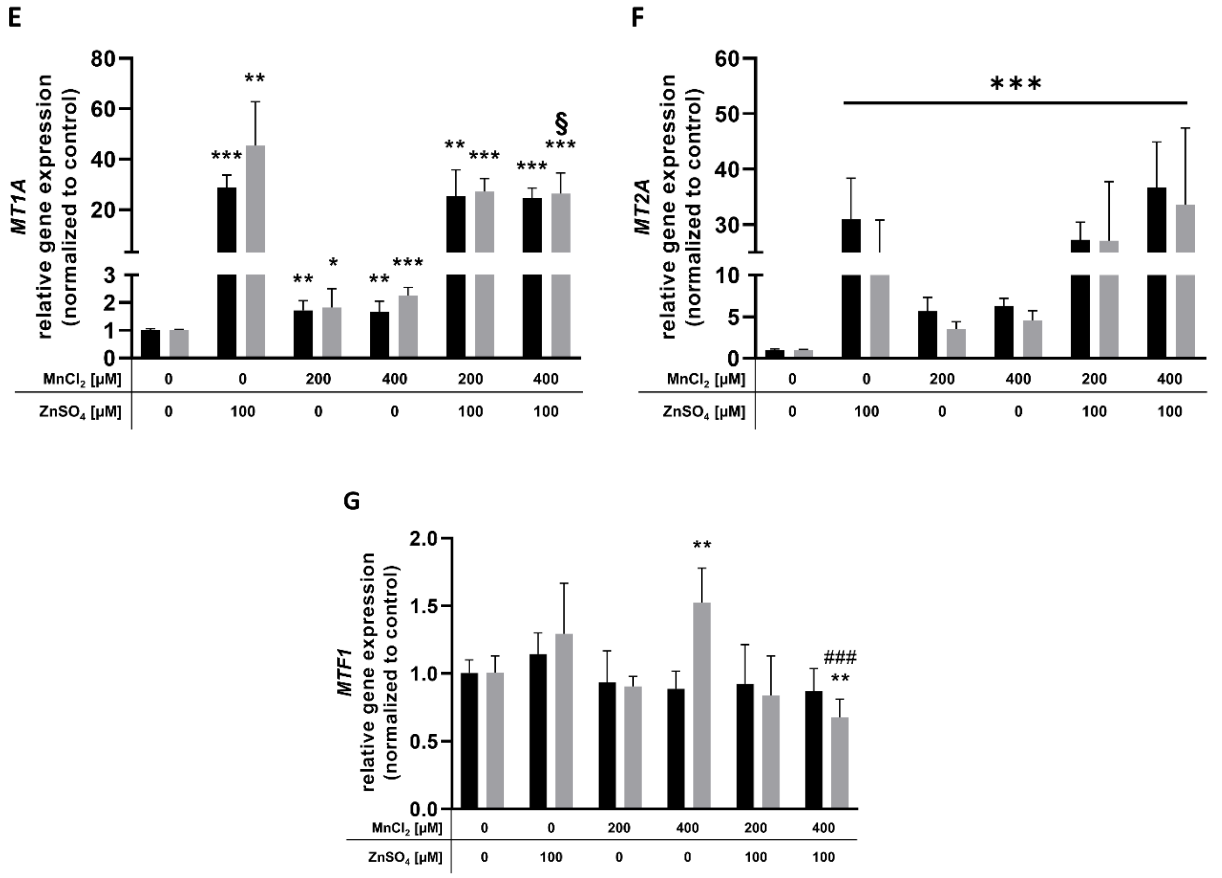

Figure 37 E – G: Relative mRNA expression of Zn and Mn transporters and transport proteins in HepG2 cells preincubated with 100 µM $ZnSO_4$ for either 2 h (▬) or 24 h (■) following 24 h $MnCl_2$ treatment. Relative mRNA expression was assessed using RT-qPCR and normalized to *ACTB* (β-actin) as the housekeeping gene. Shown are the means + SD of at least three independent experiments with two technical replicates each for (E) *MT1A*, (F) *MT2A*, and (G) *MTF1* respectively. Significance provided by an unpaired t-test with Welch's correction is depicted as $^{*}p< 0.05$, $^{**}p< 0.01$, $^{***}p< 0.005$: compared to untreated control, $^{§}p< 0.05$, $^{§§}p< 0.01$, $^{§§§}p< 0.05$: compared to Zn treatment alone, $^{\#}p< 0.05$, $^{\#\#}p< 0.01$, $^{\#\#\#}p< 0.05$: compared to Mn treatment alone.

5.4. Discussion

Mn and Zn are indispensable for a plethora of processes involved in human metabolism to sustain health [8,105]. In order to optimize TE supply, a substantial number of people tend to resort to supplements even if they are adequately supplied by nutrition [485]. While many studies already focused on the effects of either Mn or Zn overexposure, data on Mn and Zn interactions is limited [28,128]. However, this is a more realistic exposure scenario, because nutrition is composed of more than one micronutrient. For example, grain-based products are rich in Mn and Zn, as well as supplements often contain both [3,4,485]. Physiological TE resorption is tightly regulated in the intestine [505]. However, patients with liver dysfunctions or in case of administration of total parenteral nutrition (PN) are more vulnerable to metal

overdosing, because Mn and Zn are not excreted properly, or the efficient homeostasis of the intestine is bypassed and high amounts of Mn and Zn reach the liver due to bioavailability of almost 100 % [8,34].

This study addresses the gap of knowledge regarding Mn and Zn interactions upon overdosing using the human hepatoma cell line HepG2, which is widely used in pharmaco-toxicological research resembling most functions of hepatocytes [188]. Furthermore, HepG2 cells express a variety of metal transporters also involved in Mn and Zn transport such as DMT1, TfR, ZIP8, and ZIP14 as well as several MT isoforms [494,506-508]. Recently, studies have shown that ZIP8 and ZIP14, initially associated with Zn transport, are also playing an essential role in systemic Mn homeostasis [509]. Even though the Mn and Zn concentrations applied in this study are not physiologically relevant because they cannot result in serum from dietary Mn and Zn intake, administration of PN, as well as liver dysfunction may lead to Mn and Zn accumulation in liver tissue [34,510].

With a focus on cytotoxicity, incubation with 200 µM $MnCl_2$ was sufficient to significantly reduce the cell viability of HepG2 cells after 24 h of incubation. Investigation of the cell death mechanism revealed induction of either caspase-3 as well as LDH release, however, dependent on seeding time. Surprisingly, a significant induction of caspase-3 activity was only observed in cells incubated with $MnCl_2$ 48 h after seeding (corresponding to the scenario of 24 h preincubation with $ZnSO_4$) while LDH release was constantly present independent of seeding time. Mn cytotoxicity has often been associated with apoptosis (reviewed in [40]), which is in line with enhanced caspase-3 activity observed in this study. Simultaneous induction of LDH release, however, may also hint at a combination of apoptosis and necrosis, defined as regulated necrosis or parthanatos, which has already been postulated by Porte Alcon *et al.* in the context of Mn-induced murine microglial cell death [511]. Additionally, the absence of caspase-3 activation in cells incubated 24 h after seeding with Mn might be indicative of the initiation of cellular senescence and subsequent cell cycle arrest, which is associated in the literature with Mn-induced DNA damage and dysregulated DNA repair [468,512,513]. Interestingly, preincubation with 100 µM $ZnSO_4$ 24 h before Mn treatment for additional 24 h decreased caspase-3 activation and LDH release, which results in increased cell survival of HepG2 cells in comparison to single Mn treatment. However, it is not obvious if Zn is preventing the induction of oxidative stress, which in turn would lead, among others, to decreased induction of cell death, or if it is interfering by regulating factors involved in anti-

apoptotic or anti-necrotic pathways [514]. Zn is involved in the regulation of apoptotic as well as anti-apoptotic factors such as Bax and Bcl-2. A study conducted in HepG2 cells exposed to 10 µg/ mL aflatoxin B1 (AFB1) showed that concurrent incubation with 50 µM $ZnSO_4$ lead to decreased Bax and increased Bcl-2 induction, therefore, alleviating AFB1-induced apoptosis [515]. The exact role and mechanism behind Zn-induced HepG2 cell survival after $MnCl_2$ treatment needs to be elucidated in further studies focusing on oxidative stress endpoints including gene and protein expression of senescence, oxidative stress, and DNA damage-associated genes.

Nevertheless, alleviation of Mn-induced cytotoxicity by Zn may also be explained by focusing on Mn and Zn bioavailability and alterations in gene expression of transport-associated genes. Quantifying the cellular TE concentrations in this study revealed that Zn is strongly affecting Mn uptake in HepG2 cells, leading to a prominent decrease in cellular Mn upon exposure in combination with Zn. Furthermore, the effect of Mn on Zn uptake is not as strong, but with an apparent Mn dose-dependency (fig. 34C, D). This effect was not observed in the study by Liu *et al.*, which investigated the protective effect of Zn in cultured rat primary hepatocytes in comparable dose regimes [516]. Since Mn uptake is significantly decreased by the combination of 50 µM and 100 µM $ZnSO_4$ + 400 µM $MnCl_2$ within 24 h of preincubation, but not after 2 h of preincubation, an impact of Zn on transport regulation on a translational level seems plausible. Fujishiro *et al.* revealed that after inhibition of ZIP8 and ZIP14 using siRNA transfection in mouse cells of the proximal tubule, Mn uptake was reduced to about 70 % and 50 % respectively [517]. Xin *et al.* corroborated this hypothesis by investigating Mn homeostasis in hepatocyte-specific ZIP14-knockout mice. Upon consuming a high Mn diet these mice had increased Mn levels in the brain and pancreas, but not in the liver [45]. Lately, several studies have focused on the metal binding affinity of ZIP8 and ZIP14 both involved in either Mn or Zn transport. They have shown that divalent metal transport by ZIP8 and ZIP14 can be described by Michaelis-Menten kinetics with V_{max} factors of 2.0 µM for Mn(II) in HepG2 cells [492] and 0.26 µM for Zn(II) determined in Xenopus oocytes, leading to the hypothesis that Mn may be one of the physiological substrates for ZIP8 [168]. This could be explained by studies by Kambe *et al.* investigating the amino acid composition in the active site of various ZIPs. Higher affinity of Mn(II) to ZIPs in comparison to Zn(II) is attributed to the preferential binding of Mn(II) to aspartic acid and asparagine residues prevalent in the ZIP metal-binding site [169]. Regarding metal transporters present in cells, transport by ZIPs may not be the main pathway involved in Mn and Zn transport. DMT1, as well as TfR1, are also discussed mainly for Mn but not Zn

transport, due to the physiologically relevant trivalent oxidation state (relevant for metal transport via TfR) and pH dependency during uptake, important for divalent metal transport by DMT1 [27,518]. Although Zn is involved in mRNA regulation of both DMT1 and TfR1 with the iron responsible element (IRE) as a possible target [519]. Therefore, focusing on alterations in gene expression of involved transporters may clarify their role in Mn and Zn interactions.

In general, *DMT1*, *ZIP8*, and *ZIP14* mRNA expression were downregulated by single Mn treatment. In the case of Mn overexposure, metal importers are downregulated in order to avoid the accumulation of metal species that might otherwise lead to the formation of ROS [520]. One exception is the increased mRNA expression of *TfR1* in the scenario according to 24 h of preincubation, after exposure to 400 µM $MnCl_2$ (fig. 36B). Upregulation of metal importers is often associated with TE requirements in case of deficiency [27]. However, TfR1 upregulation may rather be associated with impaired Fe homeostasis. A study by Herbison *et al.* has shown that *TfR1* gene expression was upregulated in order to compensate reduced Fe uptake in presence of transferrin-bound Mn, but is not the focus of this study [521].

Interestingly, although ZIP8 and ZIP14 are phylogenetically related but distinct from the other 12 ZIPs [170], *ZIP8* and *ZIP14* mRNA expression showed a different response to single Zn treatment. While *ZIP8* was significantly upregulated after exposure to 100 µM $ZnSO_4$, *ZIP14* gene expression was downregulated, independent of the exposure duration. Especially in the case of ZIP8 and ZIP14, it is not obvious if altered mRNA expression is the cause or consequence of excess metal in cultured HepG2 cells. Transcriptional *ZIP8* upregulation has recently been shown as part of the anti-inflammatory pathway involving NF-κB [522]. In case of inflammation, ZIP8 provides a NF-κB binding site, increasing the sequestration of cytosolic Zn. In turn, cytosolic Zn, negatively regulates NF-κB activation by inhibition of the IκB kinase, leading to decreased induction of inflammation [522]. This hypothesis may be underlined by a study from Foligne *et al.* showing a Zn-dependent inhibition of intestinal inflammation caused by experimentally induced mouse models of colitis. They postulated an induction of *Mt1* and *Mt2* gene expression in the colon of healthy mice after administration of a dietary high-dose Zn supplementation as a possible reason for preventing gut inflammation [523]. The same effect might be observed in the present study because treatment with 100 µM $ZnSO_4$ also led to increased *ZIP8* and *MT1A* and *MT2A* mRNA expression. In addition, treatment with 200 µM and 400 µM $MnCl_2$ in the absence of $ZnSO_4$ also increased *MT1A* and *MT2A* gene expression in HepG2 cells, however not as strong as Zn treatment alone. Since MTs themselves do not

bind Mn, as shown by Waalkes *et al.* and others, MTs induced by Mn treatment are binding Zn ions, which is in line with the decreased labile Zn amounts in HepG2 cells after Mn treatment alone observed in our study [524,525]. Furthermore, Kobayashi *et al.* associated a dose-dependent MT induction by Mn administration in ICR mice liver with a rapid increase in interleukin-6 in the serum of these mice which would also contribute to inflammation [525]. Contrary to our study, they observed an upregulation in *ZIP14* mRNA [525]. Mn treatment alone leads to a decrease in *ZIP14* mRNA in HepG2 cells. On the one hand, this could be the response to excess Mn present in the medium in order to avoid metal accumulation, on the other hand a study by Zhao *et al.* has shown a contribution of p53 in *ZIP14* mRNA regulation that also underlines the hypothesis discussed regarding Mn cytotoxicity and the induction of cellular senescence [469]. Additionally, in the case of cellular senescence NF-κB is also involved as a master regulator for the immune survival of senescent cells, therefore also contributing to the hypotheses postulated before [526].

To summarize, data obtained in this study showed that Zn is alleviating Mn cytotoxicity, possibly due to decreased Mn bioavailability in the presence of Zn. However, underlying mechanisms cannot yet be explained by the mRNA expression of assumed transporters involved in both Mn and Zn uptake. In addition, the mechanisms proposed in this study remain to be elucidated in further studies to reveal the exact mechanisms of Zn and Mn interactions in HepG2 cells. Nevertheless, this study provides a closer look at the combined exposure of Zn and Mn and emphasizes that Zn as well as Mn homeostasis, and corresponding regulatory processes are dependent on the respective other TE taken up from the environment. To date, mechanisms involved in metal homeostasis are not completely understood and need to be focused on in future studies.

5.5. Acknowledgments

This work was supported by the DFG Research Unit TraceAge (FOR 2558, BO4103/4-2, HA 4318/4-2).

5.6. Author contributions

V.M and J.B. conceptualized the study and wrote the manuscript. S.K. conducted the RT-qPCR experiments and realized labile Zn measurements. J.P. applied the caspase-3, LDH, and BCA assay. L.N. did the cytotoxicity measurement and with S.K. the bioavailability experiments. F.E. assisted with helpful tips in the handling of the *in vitro* system and established the protocols

of the caspase-3 and LDH assay beforehand. H.H. and A.T. supported the experimental design and together with T.S. with important intellectual input. All authors were involved in manuscript preparation and approved the final version. J.B. rendered this work possible.

Abstract

Manganese (Mn) is an essential trace element, but overexposure is associated with toxicity and neurological dysfunction. Accumulation of Mn can be observed in dopamine-rich regions of the brain *in vivo* and Mn-induced oxidative stress has been discussed extensively. Nevertheless, Mn-induced DNA damage, adverse effects of DNA repair, and possible resulting consequences for the neurite network are not yet characterized. For this, LUHMES cells were used, as they differentiate into dopaminergic-like neurons and form extensive neurite networks. Experiments were conducted to analyze Mn bioavailability and cytotoxicity of $MnCl_2$, indicating a dose-dependent uptake and substantial cytotoxic effects. DNA damage, analyzed by means of 8-oxo-7,8-dihydro-2′-guanine (8oxodG) and single DNA strand break formation, showed significant dose- and time-dependent increases of DNA damage upon 48 h Mn exposure. Furthermore, the DNA damage response was increased which was assessed by analytical quantification of poly(ADP-ribosyl)ation (PARylation). Gene expression of the respective DNA repair genes was not significantly affected. Degradation of the neuronal network is significantly altered by 48 h Mn exposure. Altogether, this study contributes to the characterization of Mn-induced neurotoxicity, by analyzing the adverse effects of Mn on genome integrity in dopaminergic-like neurons and respective outcomes.

Chapter 6 – Mechanistic studies on the adverse effects of manganese overexposure in differentiated LUHMES cells

Based on: Merle M. Nicolai, Barbara Witt, Sharleen Friese, **Vivien Michaelis**, Lisa Hölzl-Armstrong, Maximilian Martin, Franziska Ebert, Tanja Schwerdtle and Julia Bornhorst.

Published in: Food and Chemical Toxicology

DOI: 10.1016/j.fct.2022.112822

Keywords: Manganese, dopaminergic neurons, DNA integrity, DNA repair, neurodegeneration, oxidative stress, genotoxicity

Highlights:

- Manganese decreases the DNA integrity of differentiated LUHMES cells
- Degradation of the neurite network is induced by manganese overexposure
- Analytical measurement of 8oxodG allows semi-quantitative analysis *in vitro*

6.1. Introduction

Manganese (Mn) is an essential trace element required as a co-factor for many cellular systems involved in growth, metabolism, neuronal functions, and cellular homeostasis [8,527]. The ubiquitous divalent metal is naturally occurring in food (nuts, grains, vegetables) and drinking water in varying concentrations and a deficiency in humans has therefore not been observed [416,528]. Due to the increasing industrial use of Mn and its mining, environmental exposure has been rising immensely in some regions, causing risks of adverse health effects to exposed humans. Countries with a high environmental Mn burden include Brazil, South Africa, Russia, Gabon and Australia [529]. Chronic Mn overexposure is associated with neurodegeneration, and epidemiological studies link the overexposure of the trace element to various neurological effects in children and adults all over the world [530,531] and reviewed by Bjørklund *et al.* [532]. Recent results from Michalke *et al.* 2021 indicate, that the neural barriers in general strictly control the passage of transition metals into the cerebrospinal fluid, but less so for Mn [533]. This finding elevates the problematic nature of rising environmental Mn levels. Physiological concentrations of Mn in the human brain are estimated to be between 5.32 – 14.03 ng Mn/ mg protein (corresponding to 20.0 – 52.8 µM Mn) [197], but bioavailability studies showed that Mn can accumulate strongly upon overexposure. Concentrations vary greatly between different brain regions, whereby the accumulation is especially high in mitochondria of the dopamine-rich region of the *basal ganglia*, particularly the *substantia nigra* [534-536]. The primary target cells in Mn-induced neurotoxicity are discussed to be astrocytes and neuronal cells [537-539]. While the association between Mn and neurodegeneration is avowed, little is known about the mechanistic pathways behind the adverse effects of Mn on movement, cognition, emotion, and behavioral responses, with severe neurological dysfunctions similar to Parkinson's disease [540-542]. A better understanding of the neurotoxic mechanism is therefore of highest importance. Mn, as a transition metal, can induce increased formation of reactive oxygen and nitrogen species (RONS), either directly by Fenton-like reactions or indirectly by inhibiting the respiratory chain in mitochondria [453,543]. Especially neurons are enriched in mitochondria and possess a rather high metabolic turn-over [192]. Increased RONS in turn might increasingly interact with macromolecules, such as proteins, lipids, and DNA; potentially causing DNA damage and/ or impairment of the DNA damage response [544-546]. It has been shown before, that Mn overexposure causes oxidative stress *in vitro* and *in vivo* and an increase of DNA damage and disturbed DNA damage response under high Mn conditions [541,547,548]. Nevertheless, results regarding the genotoxic potential are inchoate and the fate of neurotoxic

endpoints is still unclear. Especially to safeguard the cellular genome from (oxidative) damage in post-mitotic neurons which incur DNA damage, the DNA damage response is of central importance [549]. Therefore, we decided to focus the investigations on Mn-induced DNA damage and cellular DNA damage response in neuronal cells and the consequences on the neuronal network. For that reason, the Lund human mesencephalic (LUHMES) cell line was chosen for experimental investigations. Once differentiated, which is achieved by treatment of the neurons with tetracycline, cyclic AMP (cAMP), and glial-derived neurotrophic factor (GDNF), the cells exit the cell cycle and develop into dopaminergic-like neurons within one week. At this point, they express dopaminergic neuron-specific biochemical markers and develop an extensive neurite network [204,205]. LUHMES are TET-off immortalized cells and are derived from embryonic human mesencephalons. This cellular system offers a high physiological relevance, acceptable culture procedures, and a large culture scale, needed for efficient and meaningful investigations of the mechanisms underlying Mn-induced neurotoxicity.

6.2. Materials and Methods

6.2.1. Cell culture of human neurons

LUHMES were cultivated and differentiated as described previously [550,551]. In short, undifferentiated LUHMES cells were seeded on pre-coated dishes (50 µg/ mL poly-L-ornithine hydrobromide (Sigma Aldrich, USA), 1 µg/ mL fibronectin from bovine plasma (Sigma Aldrich)). For proliferation medium, advanced DMEM/F12 (Life Technologies GmbH, USA) was supplemented with N2 supplement (Life Technologies GmbH), 2 mM L-glutamine (Biochrom, Germany), and 40 ng/ mL recombinant human basic fibroblast growth factor (FGF, R&D Systems, USA). The differentiation process was initiated after 24 h of cultivation by changing the proliferation medium to differentiation medium (Advanced DMEM/F12, supplemented with N2, 2 mM L glutamine, tetracycline (Sigma Aldrich), dibutyryl cyclic adenosine monophosphate sodium salt (cAMP, Sigma Aldrich), recombinant human cell-derived neurotrophic factor (GDNF, R&D Systems)). Two days later, cells were seeded on pre-coated culture dishes with a defined cell density of 150,000 cells/cm^2. The medium was replaced 48 h after seeding. Cells are completely differentiated and qualified for treatment after six days.

6.2.2. Incubation with $MnCl_2$, preparation of the stock solution, dosage information/regimen

Cells were exposed to $MnCl_2$ for 24 h or 48 h with 10 – 1000 µM $MnCl_2$ for cytotoxicity assays and bioavailability studies were performed at 25 – 300 µM $MnCl_2$, as this concentration span proved to be most relevant for cytotoxicity. The genotoxic potential of Mn was assessed after 48 h at various sub-toxic concentrations (around the most sensitive effective concentration of 30% (EC_{30}) in cytotoxicity assessment) or in a time-dependent manner.

Stock solutions of $MnCl_2$ (> 99.9 % purity, Sigma Aldrich) were prepared in sterile dH_2O, filtered and diluted shortly before the experiment.

6.2.3. Bioavailability of Mn, and other trace elements

For assessment of the bioavailability of Mn, copper (Cu), magnesium (Mg), calcium (Ca), iron (Fe), zinc (Zn), and selenium (Se) cells were differentiated and seeded in pre-coated 24-well cell culture plates. After Mn exposure, cells were pelletized on ice using RIPA (NaCl, Tris (pH 7.6), EDTA (pH 7.6), sodium-deoxycholate (Sigma Aldrich), Triton™ X-100, and 10 % sodium dodecyl sulfate (Roth, Germany)). To ensure complete cell rupture, cells were sonicated (UP100H ultrasonic processor (Hielscher, Germany), 6 sec, 100 % amplitude, cycle 0.5) and centrifuged at 15,500 x g for 20 min at 4°C. The protein level of the supernatant was measured via the Bradford assay (Bio-Rad Laboratories, USA) for normalization. For acid-assisted digestion, the cell suspensions were firstly dried overnight at 60°C. Afterward, 500 µL digestion solution (35 % H_2O_2, 65 % HNO_3, 1:1) were added to the cell pellets, mixed well and finally digested overnight at 95°C. For analysis, digested pellets were resuspended in 1 mL 10 % HNO_3 and 10 µg/L Rhodium as internal standard and mixed well before diluting the analytes 1:1 in 10 % HNO_3.

The analytical quantification was conducted by inductively-coupled plasma coupled to tandem mass spectrometry (ICP-MS/MS, Agilent ICP-QQQ 8800 system, Agilent, Germany) using the following parameters: plasma RF power 1550 W, plasma gas flow 15 L/ min, auxiliary gas flow: 0.9 L/ min, nebulizer gas (argon) flow 4.3 mL/ min, and collision cell gas (helium) type MicroMist®. The certified reference material NIST Trace Elements in Natural Water 1640A (LGC Standards GmbH, UK) were used for internal quality control. The following mass to charge (m/z) ratios were used for trace element and internal standard (IS) identification and

quantification: Mn *m/z* 55 → 55, Fe *m/z* 56 → 56, Cu *m/z* 63 → 63, Zn *m/z* 66 → 66, and rhodium *m/z* 103 → 103.

For comparison of Mn uptake to other cell lines described in literature, results of cellular Mn content were related to the cell volume and number, respectively, to calculate the molar Mn concentration. The cellular volume was determined by the cell number per well (300,000 cells) and the peak volume of LUHMES (690.6 fL) estimated from the measurements by using an automatic cell counter (CASY®TTC, OMNI Life Science GmbH, Bremen, Germany).

6.2.4. Cytotoxicity testing

Cytotoxicity was assessed by investigating the dehydrogenase activity, mitochondrial membrane potential, and cell number. For this, cells were differentiated and seeded in pre-coated 96-well cell culture plates.

6.2.4.1. Dehydrogenase activity

Dehydrogenase activity was measured by the resazurin reduction assay as described before [550]. The method is based on the reduction of the blue non-fluorescent redox dye resazurin to the pink fluorescent resorufin by intracellular dehydrogenases. NADH is used as the co-factor. After incubation with $MnCl_2$, the medium was replaced with a 5 µg/ mL resazurin solution (7-hydroxy-3H-phenoxazin-3-one-10-oxide sodium salt (Sigma Aldrich), differentiation medium). Incubation lasted for 3 h at 37°C before measuring the fluorescence (Tecan® Infinite Pro M200, Tecan, Switzerland) with excitation: 530 nm and emission: 590 nm.

6.2.4.2. Mitochondrial membrane potential normalized to cell number

Mitochondrial membrane potential and cell number were determined simultaneously using MitoTracker®Orange CMTMRos (Invitrogen, USA) [552,553] and Hoechst 33258 (Merck, Germany) staining [554]. After incubation with $MnCl_2$, the medium was replaced with 300 nM MitoTracker®Orange CMTMRos in assay buffer (80 mM NaCl, 75 mM KCl, 25 mM D-glucose, 25 mM HEPES pH 7.4) for 30 min at 37°C. After incubation, cells were fixed with 3.7 % formaldehyde in assay buffer for 10 min at 37°C. After replacing the formaldehyde with assay buffer, fluorescence was measured at excitation: 544 nm and emission: 590 nm. Thereupon, cell membranes were permeabilized using 2.2 % Triton™ X-100 (Sigma Aldrich) for 10 min at 37°C to allow Hoechst 33258 staining. For this, 6 µM Hoechst 33258 in PBS was incubated at 37°C for 30 min, before replacing the solution once again with assay buffer. Fluorescence was

measured with the fluorescence plate reader (ex: 355 nm, em: 460 nm). The mitochondrial membrane potential was calculated and normalized to the cell number.

6.2.5. Detection of 8oxodG using HPLC-MS/MS

The oxidative DNA damage 8-oxo-7,8-dihydro-2´-guanine (8oxodG) was quantified analytically by high-performance liquid chromatography coupled to tandem-mass spectrometry (HPLC-MS/MS). For this, cells were differentiated and seeded into 25 cm^2 flasks and incubated with $MnCl_2$. Cells were pelletized and the DNA was isolated using the Qiagen Tissue and Blood DNA extraction kit (Qiagen, Germany), following the manufacturer's instructions. After vacuum drying the DNA samples, enzymatic hydrolysis was used to obtain mononucleotides, which is based on methods by Greer *et al.* and Finke *et al.* [555,556]. Dried DNA samples were dissolved in 10 µL dH_2O and 6.5 mM butylated hydroxytoluene (BHT) was added to each sample. Then, dsDNA was separated into single DNA strands by incubating all samples for 3 min at 100°C while shaking. Immediate cooling on ice for another 2 min allows the DNA to re-form double helixes, but more loosely than before. At this point, isotope-labeled internal standards (IS) for 8oxodG and deoxycytidine (dC) were added to each analyte for later normalization. 5 µL sodium-succinate/ $CaCl_2$ (100 mmol/ 50mmol/l, pH 6) buffer were added before pipetting 1.6 µL 0.556 U/µL micrococcus nuclease to each sample. The mixture was vortexed thoroughly before adding 2.5 µL 0.001 U/µL phosphodiesterase. All samples were vortexed thoroughly for enzyme incubation overnight at 37°C. Afterward, 2 µL 1U/µL alkaline phosphatase were added for an incubation of 2 h at 37°C. All enzymes were obtained from Sigma-Aldrich. Lastly, samples were filtered using a 10 kDa cut-off filter (Nanosep 10K, Pall, USA), and samples were centrifuged for 20 min at 13,000 rpm at RT. HPLC-MS/MS was conducted using an Agilent HPLC system (Agilent 1260 Infinity II) coupled to a Sciex triple quadrupole-mass spectrometer (Sciex QTrap 6500+, Sciex, USA). Separation was conducted using a YMC Triart-PFP column (reversed-phase; hybrid silica material modified with pentafluorophenyl propyl; 3 x 150 mm; 3 µm; 120 Å, YMC, Japan) and a corresponding pre-column of the same material. Samples were separated at a flow rate of 0.3 mL/min, using a 15 min mobile phase gradient with 5 mM ammonium formate in dH_2O (pH 4.2) and 5 mM ammonium formate in MeOH as eluents. Electrospray ionization in positive ion mode (ESI+) was used for ionization. Quantifier mass transition of 8oxodG (m/z 284⟶168) was used in relation to the mass transition of 8-oxo-dG-^{13}C,-$^{15}N_2$ (m/z 287⟶171). For normalization, dC was measured in samples diluted 1:200 in dH_2O. All analyzed mass m/z transitions (table S9),

MS parameter (table S10), and the LC mobile phase gradient (table S11) can be found in the supplementary.

6.2.6. Determination of DNA single-strand breaks by alkaline unwinding

Quantification of DNA strand breaks was realized by alkaline unwinding, a method described before [557,558], and adapted for LUHMES cells. Briefly, cells were incubated with $MnCl_2$ in 12-well cell culture plates and washed with ice-cold PBS. An alkaline solution (0.03 M NaOH, 0.02 M Na_2HPO_4, and 0.9 M NaCl) was added to each sample and incubated in the dark for 30 min. After neutralizing, transfer of the cell pellets into glass tubes, sonification of the cell mixtures, and addition of sodium dodecyl sulfate (SDS), single- and double-stranded DNA (ssDNA/ dsDNA) were separated using 60°C tempered hydroxyapatite columns. The ssDNA and dsDNA were eluted using 0.15 M and 0.35 M potassium phosphate buffers, respectively. By adding Hoechst dye to the obtained DNA solutions and measuring the fluorescence using a microplate fluorescence reader (Tecan®, SPECTRA Fluor), relative DNA fractions can be determined. The calculation of DNA strand breaks is based on calibrations with X-ray irradiations as described by Hartwig *et al.* [559].

6.2.7. Quantification of poly(ADP-ribosyl)ation (PAR) levels

For analysis of PAR levels, an isotope-diluted LC-MS/MS method was adapted from a previously published method [547,560,561]. Cells were differentiated and seeded in 12-well cell culture plates. After Mn exposure cells were washed with 1.5 mL ice-cold PBS before adding 1.5 mL of ice-cold 20 % (w/v) TCA for cell lysis and precipitation of macromolecules. Afterward, cells were placed on ice and acid-insoluble materials were scraped from the cell culture dish using a cell scraper before transferring the cell suspension into a 2 mL reaction tube. Cell culture dishes were washed with another 0.5 mL ice-cold 20 % (w/v) TCA to ensure complete transferal. The samples were centrifuged (3000 x g at 4°C for 5 min) and pellets were washed twice with 500 µL ice-cold 70 % EtOH. After the last washing step, samples were air-dried at 37°C. The alkaline treatment was initiated by adding 255 µL 0.5 M KOH to detach protein-bound PAR. Pellets were resolved at 37°C while shaking (600 U/min) constantly until no pellet was visible. This may take up to 70 min (depending on cell number used) and vortexing was done for 30 s every 20 min. When the solution was clear, 50 µL 4.8 M MOPS were added and mixed in for neutralization. 30 µL of the solution were stored at -80°C for determination of DNA concentration by the Hoechst method [547].

2.5 pmol of ^{13}C,^{15}N labeled-PAR were added to each sample, before adding 6.25 µL 2 M $MgCl_2$, 2.5 µL 100 mM $CaCl_2$, 15.5 µL 2 mg/mL DNAse (Qiagen) and 2.5 µL 10 mg/mL RNAse (ThermoFisher Scientific, USA) for nucleic acid digestion. The mixture was incubated at 37°C on a shaker (400 U/min). After a 3 h incubation, 1.25 mL 40 mg/mL protein kinase K were added, mixed well, and samples were further incubated overnight. To enrich samples for PAR, a High Pure miRNA kit (Roche, Switzerland) was used. 624 µL binding buffer were added to each sample before adding 400 µL binding enhancer. The solutions were resuspended until completely clear and 700 µL were transferred onto a high pure column and centrifuged at 15,700 x g for 30 s. The flow-through was discarded and the last centrifugation step was repeated until the entire mixture was filtered. The filter was washed with 200 µL washing buffer (15,700 x g for 30 s) and dried by centrifuging at 15,700 x g for 1 min. The columns were placed into new reaction tubes and 100 µL dH_2O were added for another centrifugation step (15,700 x g for 1 min). Columns were discarded and the digestion of the purified PAR was initiated by adding 342 µL of digestion master mix (60 µL 10 mM MgAc, 60 µL 250 mM NH_4Ac, 220 µL dH_2O, 1 µL 10 U/ µL alkaline phosphatase, 1 µL 0.5 U/ µL PDE). Samples were vortexed and incubated for 3 h at 37°C while shaking (400 U/ min). After incubation, samples were transferred to Nanosep Omega 10K filter and filtered at 13,000 x g for 10 min to remove the enzymes. Samples were then vacuum-dried and pellets resuspended in 25 µL Millipore dH_2O for HPLC-MS/MS measurements. Quantification of PAR was conducted using an Agilent 1260 Infinity LC system coupled with an Agilent 6490 triple quadrupole-mass spectrometer (LC-MS/MS) (both Agilent) interfaced with an electron-ion source operating in the positive ion mode (ESI+) which is described in detail by Neumann *et al.* [547].

6.2.8. Gene expression screening of DNA repair-associated genes

Relative mRNA expressions of genes involved in the relevant repair pathways were analyzed using the qPCR-based method. Cells were differentiated and seeded in 25 cm^2 cell culture flasks. After Mn exposure (20 µM, 48 h (EC_{30})) cells were trypsinized, centrifuged, washed with ice-cold PBS, and pellets were stored at −20°C. Using the "NucleoSpin RNA II kit" (Machery-Nagel, Germany), RNA was isolated and the concentration was measured using a Nanodrop (ThermoFisher Scientific). 1 µg RNA was used for reverse-transcribed to cDNA by using the "qScript Kit" (Quanta Biosciences, USA). Primer sequences and efficiencies, thermal cycling programs and calculations of relative gene expressions for the 96-well based RT-qPCR method were described in Ebert *et al.* 2016 [562]. Actin serves as the housekeeping gene.

6.2.9. Assessment of neurite toxicity via tubulin staining

For the assessment of Mn toxicity on the neurite network, immunofluorescence staining of the neuronal cytoskeleton protein βIII-tubulin was conducted, followed by a semi-automatic quantification of the neurite mass as described by Witt *et al.* 2017 [563]. Briefly, differentiated LUHMES cells were seeded on pre-coated 18 mm glass coverslips and cells were incubated with $MnCl_2$ for 48 h. Afterward, cells were fixed with PBS containing 1 % formaldehyde (Roth), washed with PBS containing 0.05 % Tween® 20 solution, permeabilized with PBS containing 0.2 % Triton™ X-100, washed again, and incubated with 1 % bovine albumin in PBS for 30 min at RT. The primary antibody (anti-tubulin β3 [TUBB3], Clone: Tuj1, BioLegend GmbH, USA) was incubated overnight at 4°C before incubating the secondary antibody (Alexa Fluor® 488 goat anti-mouse IgG, Invitrogen, USA) for 1 h at RT, both in blocking buffer (PBS, 1 % bovine albumin). For low background signaling, several washing steps with washing buffer were carried out after each antibody incubation. Lastly, cells were mounted in Vectashield mounting medium containing DAPI (Vector Laboratories, USA), and the neuronal network was assessed on a Leica DM6 B wide-field fluorescence microscope, equipped with a microscope lens HC Plan APO 10X and 20X/0.70, a CTR6 LED lamp and a cooled Leica DFC 365 FX CCD camera (Leica, Germany). For quantification of the neurite mass, the LAS X Core 2D Analyse imaging software (Leica) was used. The relative fluorescence of the intensity of neuronal network surrounding the nuclei (identification via DAPI staining), was measured. A minimum of 20 images per sample was evaluated for neurite mass.

6.3. Statistical analysis

Statistical analyses were performed using GraphPad Prism 9 (GraphPad Software, USA). If not otherwise stated, one- or two-way ANOVA with Dunnett's post-hoc test for group comparison have been used. Statistical tests performed are listed in the respective figure captions and significance is depicted as *: $p<0.05$, **: $p<0.01$, and ***: $p<0.005$ compared to respective untreated control.

6.4. Results and Discussion

6.4.1. Cellular bioavailability, cytotoxicity, and adverse effects of Mn on the mitochondrial membrane potential

For investigations of Mn uptake by neurons, differentiated LUHMES cells were incubated with $MnCl_2$ for 24 h and 48 h with various concentrations of up to 300 µM $MnCl_2$, and 50 µM $MnCl_2$ respectively. The cellular Mn concentrations increased in a dose- and time-dependent manner in both incubation periods (fig. 38A, B) for up to the highest tested concentrations each. Cells incubated with 300 µM $MnCl_2$ for 24 h showed a total Mn content of ~0.56 µg Mn/ mg protein. A 48 h incubation with 50 µM $MnCl_2$ resulted in a total Mn concentration of ~0.12 µg Mn/ mg protein. The same concentration of $MnCl_2$ after only 24 h incubation caused an increase of the cellular concentration to 0.078 µg Mn/ mg protein, indicating that the Mn uptake is almost directly proportional to the incubation time. This effect is less distinct when looking at 25 µM $MnCl_2$. Here the uptake after 48 h is only slightly higher compared to a 24 h exposure. Currently, we cannot explain the observed data and clarification of the underlying transport mechanisms are needed. A linear uptake of Mn after 24 h and 48 h incubations has not been observed in earlier studies using different human cell lines (CCF-STTG1 (CCL-185™), A549 or HeLa cells) [453,557,564]. Studies by Bornhorst *et al.* 2012 for example show that astrocytes do not show significant differences in Mn uptake after either 24 h or 48 h exposure to the same $MnCl_2$ concentration. In addition, comparing the cellular Mn concentrations of astrocytes and neurons, Mn bioavailability is 15 – 20 times higher in LUHMES cells [564]. The effect of excessive Mn uptake on the status of other trace elements was also investigated in LUHMES, as other studies suggest an interrelation of other trace elements in uptake and homeostases [565]. Analysis of Cu, Mg, Ca, Fe, Zn, and Se indicated that the overexposure of differentiated LUHMES cells with up to 40 µM Mn for 48 h does not significantly affect the homeostasis of these trace elements (fig S7). The cytotoxicity assessment was likewise conducted for cells exposed to $MnCl_2$ for 24 h and 48 h. The metabolic activity was determined using the resazurin assay, which measures the dehydrogenase activity. Concentrations of ≥ 50 µM $MnCl_2$ caused a highly significant decrease of the metabolic activity for both incubation times (fig. 39A, B), which is dose- and time-dependent. The EC_{30} is estimated to be ~150 µM $MnCl_2$ and 40 µM $MnCl_2$ after a 24 h incubation and 48 h, respectively (fig. 39C). The decrease of the cell number yielded more sensitive cytotoxic concentrations of $MnCl_2$ in the differentiated neurons compared to the resazurin assay. Highly significant decreases of cell numbers after 24 h and

48 h incubation were reached at concentrations of ≥ 25 µM $MnCl_2$. The approximated EC_{30} values are at 58 µM $MnCl_2$ for 24 h Mn exposure and > 25 µM $MnCl_2$ after 48 h Mn exposure. These results indicate that neurons are a highly important target for Mn-induced toxicity as they are much more sensitive than other brain-associated cell lines. Astrocytes incipient cytotoxic effects at incubation concentrations of 1000 µM for 24 h [564].

Measuring the mitochondrial membrane potential using MitoTracker® Orange allowed us to draw conclusions regarding the effect of Mn on mitochondrial function. Excessive levels of free radicals can disturb the mitochondrial integrity, which in turn can cause further formation of RONS. Additionally, Mn ions showed to induce H_2O_2 generation at the binding site of the complex II of the respiratory chain in mitochondria [566]. Mitochondrial membrane potential is therefore a likely target of Mn-induced oxidative stress. Exposing differentiated LUHMES cells for 24 h affected the potential already at low concentrations (≤ 50 µM $MnCl_2$) and a 50% reduction can be seen at 75 µM $MnCl_2$ (fig 40A). Even higher concentrations (≥ 200 µM $MnCl_2$) lead to a constant low level of ~ 15% compared to non-exposed cells. Incubation with Mn for 48 h showed an EC_{30} of 25 µM $MnCl_2$ (fig 40B), which is, likewise to the 24 h incubation, marginally under the EC_{30} cytotoxicity values. The disturbance of the membrane potential by Mn shown in this study can correlate with oxidative stress, as the endpoint is both, an indicator for a cause and consequence of increases in RONS. This is in line with previous studies (*in vitro* and *in vivo*) that have shown before that Mn causes an increase in oxidative stress [547,548,557]. The analyzed cytotoxicity endpoints showed different sensitivities towards Mn-induced effects/toxicity. The deviating sensitivities (time- and dose-dependency) might be explained by the underlying cellular toxic mode of action and cellular mechanisms (e.g. saturation processes, counter regulations, target organelles), that need to be investigated further. Both metabolic activity and mitochondrial membrane potential are strongly linked to mitochondrial function which is further involved in oxidative stress and induction of ROS. Consequences of oxidative stress, especially in neurons, are of great concern, due to the inability of self-replenishment of post-mitotic cells. On account of the almost linear cellular bioavailability and estimated EC_{30} values, we decided to conduct all following mechanistic studies after a 48 h Mn exposure with 0 µM, 20 µM, and 40 µM $MnCl_2$. This allowed the investigation of genotoxic endpoints at concentrations of sub-toxic (10 µM and 20 µM $MnCl_2$) and toxic concentrations (40 µM $MnCl_2$).

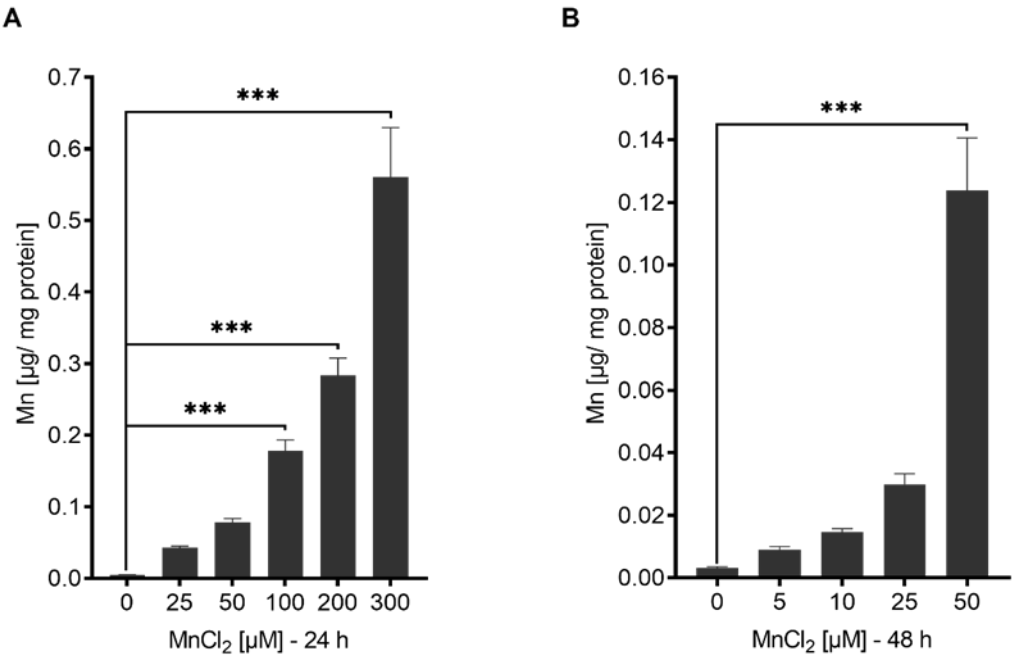

Figure 38: Mn bioavailability in LUHMES cells after Mn overexposure. Results show dose- and time-depended Mn uptake [µg Mn/ mg protein] in differentiated LUHMES cells following a (A) 24 h and (B) 48 h incubation. Bioavailability was measured analytically via ICP-MS/MS. Data are expressed as means ± SD of at least six independent experiments. For statistical analysis, the one-way ANOVA with Dunnett´s multiple comparisons test was performed.

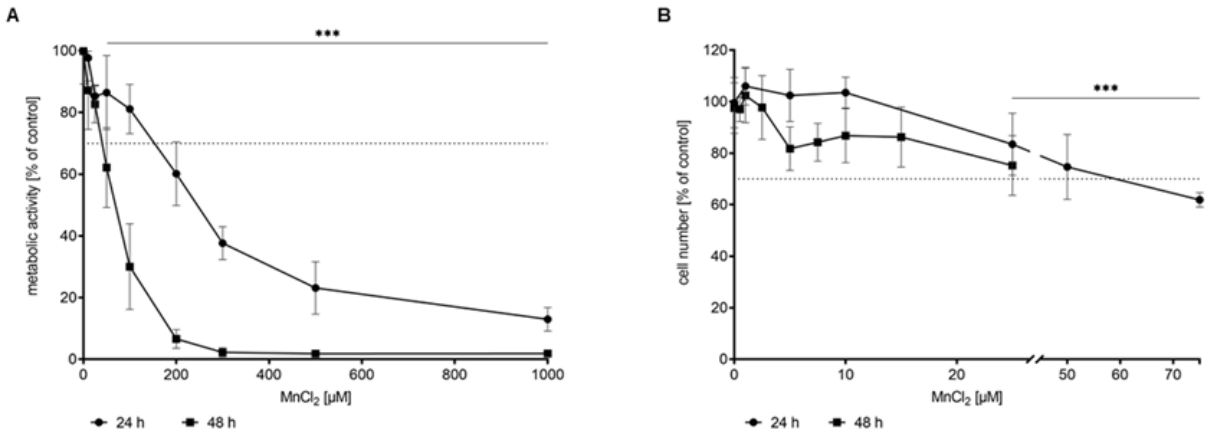

C

EC_{30} [µM]		
	Resazurin (metabolic activity)	Hoechst (cell number)
24 h	150	58
48 h	40	> 25

Figure 39: Cytotoxicity assessment of LUHMES cells after 24 h and 48 h Mn overexposure. (A) The metabolic activity measured via the resazurin reduction assay decreases dose- and time-dependently after $MnCl_2$ incubation. (B) Measurement of the cell number via the Hoechst assay indicates a decrease of cell number that is concentration-, but not time-dependent. (C) Comparison of the EC_{30} levels of the different endpoints. Data are expressed as means ± SD of at least six independent experiments. For statistical analysis, the 2way ANOVA with Dunnett´s multiple comparisons test was performed.

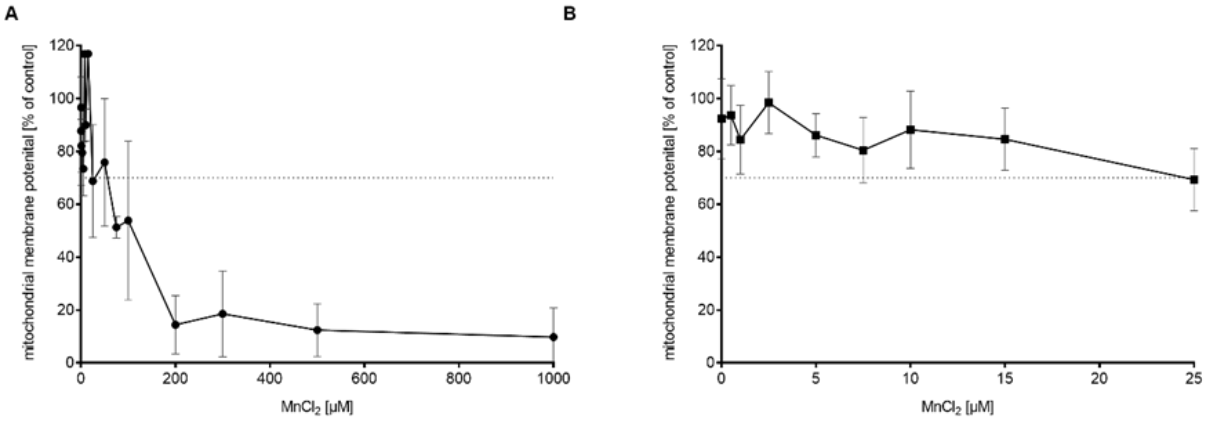

Figure 40: Measurement of mitochondrial membrane potential using MitoTracker® Orange. Results show a dose-dependent decrease of the mitochondrial membrane potential after (A) 24 h and (B) 48 h $MnCl_2$ incubation of differentiated LUHMES cells. Data are expressed as means ± SD of at least six independent experiments.

6.4.2. Mn overexposure reduces the DNA integrity of post-mitotic neurons

Oxidative DNA damage is a major adverse outcome of oxidative stress, causing genomic integrity to be in jeopardy. An imbalance of antioxidant systems and oxidative stress can induce increased interactions of RONS with macromolecules such as DNA, causing DNA damage [567,568]. While genomic stability is immensely important in cells that still undergo mitosis and meiosis (e. g. germline cells), it is equally important in post-mitotic cells, which are irreversibly withdrawn from the cell cycle [549,569]. DNA damage can occur in the nuclei and even more in mitochondrial DNA. The latter is especially important for neuronal cells, due to their high mitochondrial mass and great energy dependence [570,571]. A slow build-up of DNA damage in the genome causes loss of information that transfers from DNA to proteins. This could increase the transcription of defective proteins, their accumulation, cell death, and eventually neurodegeneration and disease [570,572]. For this study, we decided to investigate DNA damage in the entirety of the neurons, not only mitochondrial DNA modifications, to elucidate the effect of Mn on the DNA integrity of the whole post-mitotic cell. For this, differentiated LUHMES cells were again exposed to Mn for 48 h at sub-toxic and toxic concentrations. First, 8oxodG was analytically quantified by HPLC-MS/MS, after isolating and hydrolyzing the DNA of $MnCl_2$ incubated cells. The simultaneous quantification of the cytosine content allowed normalization to the respective hydrolysis rate as well as the actual DNA content. 8oxodG is the most investigated and likely the most frequently occurring oxidative DNA base modification, due to the low oxidation potential of guanine [573]. The interaction of singlet oxygen with guanine leads to the formation of 8oxodG and

8-hydroxyguanosine (8OHdG), which are in equilibrium with each other and are equally used as biomarkers in both *in vitro* and *in vivo* studies [574-576]. The results of the analytical quantification show that exposure of differentiated LUHMES cells to Mn caused a linear increase of the DNA damage, which is significantly different at 40 µM $MnCl_2$ compared to non-incubated cells (fig 41). At this concentration, the level of oxidative DNA damage is three times higher as compared to control cells. If repaired, 8oxodG, and other oxidative DNA modifications, are repaired mainly via base excision repair (BER), which causes single-strand breaks as repair intermediates [577]. The damaged bases are excised by glycosylases, leaving apurinic/ apyrimidinic (AP) sites, which are then processed further by endonucleases to DNA single-strand breaks before being repaired by further BER repair enzymes [578-580]. Apart from DNA repair, strand breaks can be caused directly by exogenous or endogenous sources and can lead to loss of information and mutations, DNA-protein crosslinks, and alterations of the secondary DNA structure [581-583]. Quantifying the percentage of double-stranded DNA (dsDNA) and thereby strand breaks per cell using the alkaline unwinding assay allows us to draw conclusions regarding the overall genomic integrity. In Mn-incubated cells, again for 48 h, a high increase of DNA strand breaks is detectable compared to control cells, already starting at 10 µM $MnCl_2$ (fig 42A). Exposure to 20 µM $MnCl_2$ caused a further increase to 4 x 10^3 strand breaks per cell. Doubling the incubation concentration does not further increase the damage and a plateau is reached with 50 % dsDNA. When looking at the time-dependent effect of Mn exposure, a coherence is visible between the amount of strand breaks and exposure time. The neurons were incubated with 20 µM $MnCl_2$ for 0 h, 2 h, 4 h, 8 h, 24 h, or 48 h and the data suggest a consistent increase of DNA strand breaks and decrease of dsDNA (fig 42B). The results of both genotoxicity endpoints indicate significant induction of DNA strand breaks and oxidative DNA damage 8oxodG. These results are in line with other *in vitro* [41,548,549] and *in vivo* [584] studies that investigated DNA damage (DNA strand breaks and DNA base modifications) after Mn exposure, employing the alkaline COMET assay or analytical and immunohistochemical analysis of oxidative base modification.

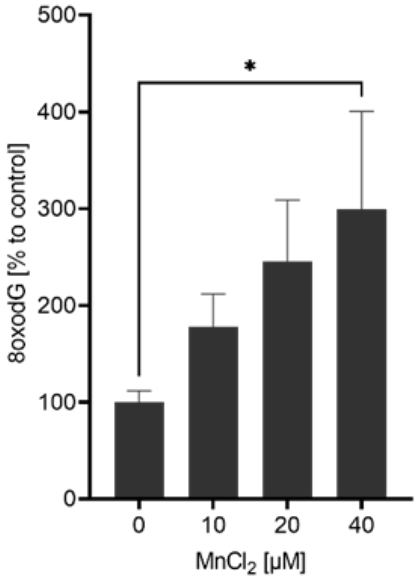

Figure 41: Induction of 8oxodG formation in LUHMES cells after 48 h Mn exposure. The increased formation of 8oxodG was measured analytically via HPLC-MS/MS. Sub-toxic (10 µM – 20 µM $MnCl_2$) and toxic (40 µM $MnCl_2$) concentrations of Mn cause a dose-depend increase of oxidative DNA damage that is significantly higher at 40 µM $MnCl_2$ compared to control cells. Data are expressed as means + SD of at least six independent experiments. For statistical analysis, the ordinary one-way ANOVA with Dunnett´s multiple comparisons test was performed.

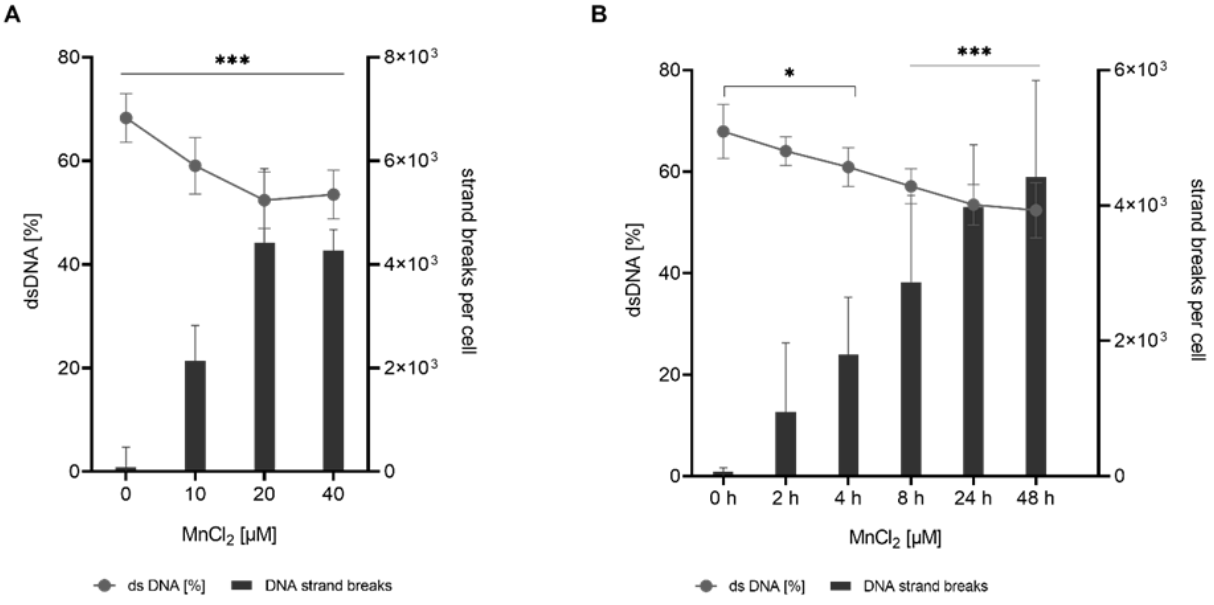

Figure 42: Measurement of dsDNA [%] and strand breaks per cell using the alkaline unwinding assay as marker for genomic integrity. (A) Differentiated LUHMES cells were exposed to 0 µM, 10 µM, 20 µM, and 40 µM $MnCl_2$ for 48 h. (B) Differentiated LUHMES cells were incubated with 20 µM $MnCl_2$ for different exposure times (0 h, 2 h, 4 h, 8 h, 24 h, and 48 h). Data are expressed as means ± SD of at least nine independent experiments. For statistical analysis, the 2way ANOVA with Dunnett´s multiple comparisons test was performed.

6.4.3. Induction of the DNA damage response and increased DNA repair gene expression are results of Mn overexposure

Unrepaired DNA damage may trigger cell death, making an effective DNA repair crucial for neuronal survival. The DNA damage response involves different pathways and genes responsible for sensing and responding to DNA damage and therefore initializing DNA repair, apoptosis, and in case of proliferating cells cell cycle regulation [585]. Poly(ADP-ribose) (PAR) signaling is one of the first activated pathways upon DNA damage and is needed to ensure access of repair protein to the DNA lesion in the otherwise tightly packed DNA double-helix [586,587]. The PAR polymerase (mainly PARP1) recognizes and binds to DNA lesions, and then catalyzes the formation of PAR chains on close-by histones and itself [588-590]. These PAR chains can act as binding platforms for downstream pathway proteins, e.g. XRCC1, which initializes the DNA repair [591]. Relative PAR levels can be analytically quantified as a measure of the onset of the early DNA damage response. Results of this study showed that PARylation in 10 µM and 40 µM $MnCl_2$-treated differentiated LUHMES cells were significantly higher compared to non-incubated cells, indicating a response to DNA damage (fig 43A). PARylation has also been identified as a sensitive endpoint in other brain cells. Previous studies in astrocytes identified an efficient disturbance of PARylation upon Mn exposure [453]. Gene expression studies allow the conclusion that the increased levels of PARylation in Mn-exposed LUHMES might be regulated by enzyme activity or protein translation; not on RNA level. The gene expression analysis of *PARP1* and genes involved in base and nucleotide excision repair showed no significant changes in Mn-exposed cells compared to controls (fig 43B). A slight increase in gene expression can be detected for *OGG1*, which encodes for the bifunctional 8-oxoguanine DNA glycosylase. This glycosylase removes 8oxodG and initializes the base excision repair by nicking the DNA backbone [592]. There is evidence that OGG1 is involved in the repair of oxidative damage in neurons and high gene expression levels were found in the *substantia nigra* of patients suffering from neurodegenerative diseases [593]. The results of this study indicate that Mn does not have a strong effect on *OGG1* but further studies are needed to confirm the results on a protein and enzyme activity level.

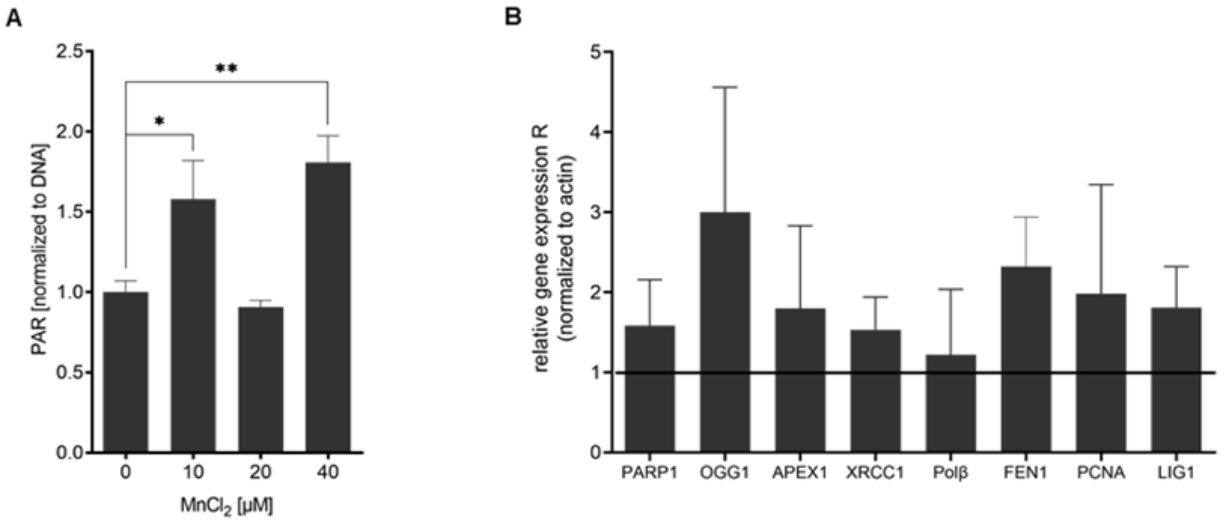

Figure 43: Analysis of DNA damage response and DNA repair in differentiated LUHMES cells upon Mn exposure. (A) Analytical measurement of relative PAR induction after 48 h $MnCl_2$ (10 µM – 40 µM) exposure via HPLC-MS/MS. (B) Measurement of relative gene expression of DNA damage response and BER-involved genes after 48 h incubation with 20 µM $MnCl_2$. Data are expressed as means + SD of at least four (A) or three (B) independent experiments. For statistical analysis, the unpaired t-test was performed.

6.4.4. Decreased tubulin expression indicates Mn caused neurodegeneration

Immunofluorescence staining of the neuronal cytoskeleton protein βIII-tubulin was used to investigate the adverse effects of Mn on the neurite network. Maintenance of the long intercellular synaptic connections is required for the propagation of electrochemical signals across vast cellular distances [594]. Changes in the synaptic morphology are linked to neurodegeneration and adverse changes can be observed in patients with Parkinson´s disease [595,596]. Differentiated LUHMES cells are well suitable for neurite toxicity testing, as they form extensive dendrite outgrowth and neuronal networks [204,205]. The immunofluorescence staining of cells incubated with 20 µM or 40 µM $MnCl_2$ for 48 h showed a significant decrease compared to non-incubated cells (fig 44A). Both concentrations caused a relative decrease of around 20%. The degradation of the neurite network is also visible in the exemplary microscopic pictures shown in fig 44B. The results indicate an adverse effect of Mn on the tubulin expression and therefore neuronal network. These results are in line with observations by Stanwood *et al.* that showed that acute Mn exposure induces early and profound changes in neurite length and integrity of primary mesencephalic culture cells at sub-toxic Mn concentrations (100 µM $MnCl_2$) [597].

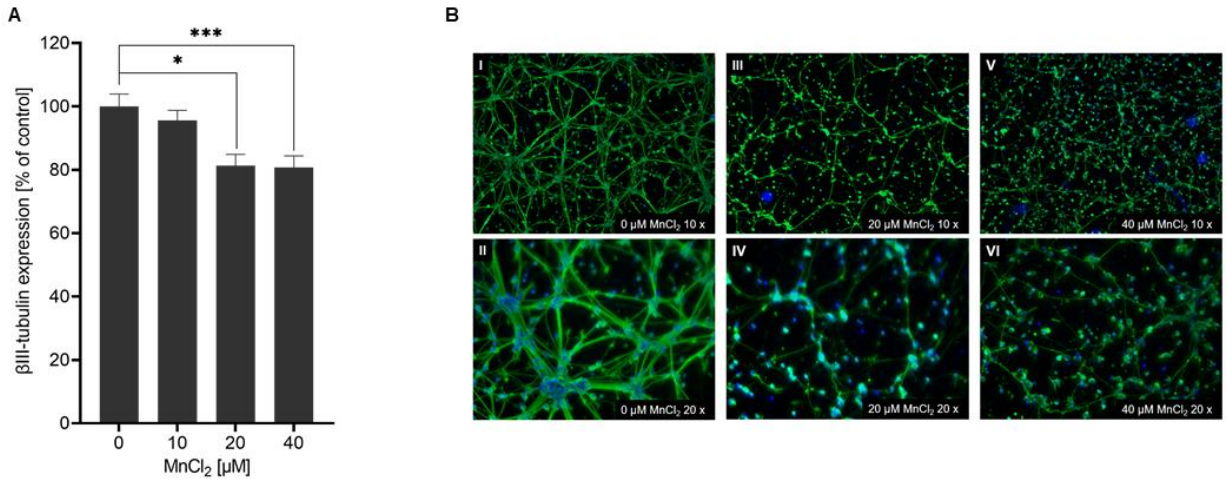

Figure 44: Immunofluorescence staining of βIII-tubulin for assessment of neurite mass. (A) Semi-automatic measurement of the relative βIII-tubulin expression in immunofluorescence-stained differentiated cells. LUHMES were incubated for 48 h with 0 µM, 10 µM 20 µM or 40 µM $MnCl_2$. Data are expressed as means + SD of at least 2 independent experiments. For statistical analysis, the ordinary one-way ANOVA with Dunnett´s multiple comparisons test was performed. (B) Representative microscopic images of the neuronal network of LUHMES cells after 48 h Mn exposure with 0 µM (I + II), 20 µM (III + IV), and 40 µM (V + VI) $MnCl_2$. βIII-tubulin was stained with TUBB3 and Alexa Fluor® 488 (portrayed in green) and nuclei using DAPI (portrayed in blue). 10 x and 20 x objectives were used.

6.5. Conclusion

Mn is a ubiquitous trace element and due to increased industrial use, rising exposure to the transition metal is unavoidable. While Mn overexposure has been linked to neurodegeneration before, understanding the underlying neurotoxic mechanisms is imperative. Utilizing the LUHMES cell line allowed us to investigate the adverse effects of Mn on dopaminergic-like neurons. Determination of bioavailability and cytotoxicity of $MnCl_2$ allowed us to find the right dosing regimen for investigations of Mn-induced DNA damage and DNA damage response/ DNA repair. Additionally, the results indicate that mitochondria function is disturbed, which can be both a consequence and cause of RONS. An increase of 8oxodG and a decrease of the dsDNA in Mn-exposed cells indicate a loss of genomic integrity. While the DNA damage response was triggered by Mn exposure, gene expression studies revealed only minor alterations in BER-involved genes. The neurite network, assessed via immunofluorescence staining of tubulin, on the other hand, showed significant adverse changes induced by Mn. Altogether, the results of this study are shedding more light on the underlying mechanisms of Mn-induced neurotoxicity. The outcome of the investigations confirms the hypothesis that Mn at high exposure leads to increased genomic instability. Future studies of specific endpoints of oxidative stress could help to understand the nature of Mn-induced RONS. For a deeper insight, studies of repair enzyme expression and activity levels are required. Especially the link between genomic instability and the degradation of the neurite network is of high interest and

will be the focus of follow-up repair studies to understand the persistence and consequences of DNA damage in more detail.

6.6. Acknowledgments and Funding

We thank Prof. Dr. Marcel Leist (University of Konstanz) and Prof. Dr. Stefan Schildknecht (Albstadt-Sigmaringen University) for providing the LUHMES cells and tips and tricks on their handling. This work was supported by the DFG Research Unit TraceAge (FOR 2558, BO4103/4-2). Additional funding was obtained from the DFG project BO4103/2-1.

6.7. Author contributions

Experiments were designed by J.B. and B.W. and mostly performed by B.W., S.F., and MM.N. M.M and L.HA. conducted the experiments regarding bioavailability and PARylation. F.E. performed the gene expression studies. Data analysis and interpretation were done by MM.N. J.B. and MM.N conceptualized the study and wrote the manuscript. V.M. and T.S. contributed to data interpretation, helped with ideas for experimental setup, and revised the manuscript critically for important intellectual content. All authors were involved in compiling the manuscript and approved the final version. J.B rendered this work possible.

Chapter 7 – Final discussion and Outlook

7.1. Final discussion and Outlook

Mn, Fe and Zn are essential for a plethora of metabolic processes sustaining human health. To ensure adequate TE supply in the general population several institutions like the EFSA and DGE estimated AI amounts based on TE uptake, distribution, excretion, and food constituents. Even if the minimum adequate amounts are easily attained by balanced nutrition, an increasing number of individuals use TE supplementation to improve TE supply in order to preserve health. However, people excessively consuming supplements and patients receiving PN are at increased risk of Mn, Fe, and Zn overexposure, which has been discussed to play a role in impaired liver function and neurodegeneration. This concern does not only account for the general population but also sensitive populations like pregnant women since the developing fetus is highly susceptible and fetal development vulnerable to metal overexposure [1-4,34,485]. Since all three TEs share similar cellular transport routes for uptake, distribution, and excretion, interrelations in their respective metal homeostasis are likely. However, a shift in these interrelations and metal homeostasis may result in adverse effects, which can consequently lead to insufficient nutrient supply and complete disruption of metal homeostasis in the three pivotal organs the placenta, the liver, and the brain. Nevertheless, exact pathways of placental TE transfer, competition on transporter binding sites, regulatory interferences, and effects on the integrity of the organs and the developing fetus are rarely characterized [10].

Therefore, studies conducted in this thesis have focused on the fundamentals of TE transport and Mn/Fe interactions across the trophoblast layer of the placental barrier, which is mainly involved in the nutrient transfer to the fetus. With Fe as one of the most investigated TEs in pregnancy, comparing Fe transfer kinetics with the rarely characterized Mn transfer facilitated the choice of an underlying pathway of nutrient transfer across the placental trophoblasts. For this, the BeWo b30 Transwell® model was applied, which allows investigating nutrient transfer in a compartmentalized approach modeling maternal- and fetal-facing side, as well as cellular uptake in the BeWo b30 trophoblasts. This model was established beforehand to achieve adequate culture conditions as closest as possible to physiological barrier function. Aside from metal transfer and bioavailability in the BeWo b30 cells, transporter expression on the transcriptional and translational levels was investigated. This was further focused on HepG2 cells revealing the role of Zn in liver Mn homeostasis and vice versa, which is largely unknown by now. In a more mechanistic approach, adverse effects of Mn exposure in human

mesencephalon cells (LUHMES) were investigated, focusing on the role of Mn-induced alterations in neuronal genomic integrity and neural outgrowth.

7.2. Establishing a model of the placental barrier for nutrient transfer studies

With the placental barrier as the main regulatory interface between maternal and fetal circulation, the trophoblast layer (one of the many underlying cellular structures) acts as the key player in oxygen, nutrient, and xenobiotic transfer. Within the range of already established *in vivo*, *ex vivo*, and *in vitro* approaches to model nutrient transfer across the placental barrier, the BeWo b30 monolayer Transwell® system has been proven to allow transfer studies with high experimental throughput due to simplified handling [222]. BeWo b30 cells are widely used since subcloning of the parent cell line BeWo enabled the formation of the confluent and polarized monolayer, sharing the coarse physiological structure of trophoblast *in vivo* [331]. Additionally, BeWo b30 cells resemble the morphology of third-trimester trophoblasts and express a variety of transporters involved in micronutrient metabolism, in expression patterns of late gestation [341,359]. Due to their polarized behavior, transporters are located according to their function as in- and exporters [331]. In comparison to *ex vivo* placental perfusion experiments, BeWo b30 cells showed similar transfer rates of small reference substances like antipyrine, caffeine, and benzoic acid making them a useful tool for the investigation of the fundamentals of micronutrient transfer [226,310,351,360,361]. Seeding BeWo b30 cells on Transwell® inserts facilitates the investigation of maternal-fetal micronutrient transfer in a compartmentalized approach, and additionally allows BeWo b30 cells to follow their polarized phenotype. However, different from other barrier building cells like PBCECs (BBB) and Caco-2 (intestinal barrier), BeWo b30 cells do not have to be differentiated to achieve barrier function [9,199,209]. This is beneficial since the time of differentiation has not to be considered in the general culture time of the *in vitro* system. Therefore, short culture times until reaching confluency is one advantage regarding experimental throughput.

On the contrary, the absence of contact inhibition in BeWo b30 cells leads to the quick formation of a multilayer, which does not represent *in vivo* conditions. While Heaton *et al.* deliberately use the BeWo b30 cells in multilayers, as they observed a multilayered structure before the formation of a confluent monolayer, we tried to establish a monolayer model nearest to *in vivo* conditions [314,352]. For this, barrier properties have to be monitored precisely in every experiment to detect potential alterations in the proliferation behavior of BeWo b30 cells. Even if optimal culture conditions were developed beforehand, using the system for nutrient

studies revealed, that these conditions can potentially be altered due to the use of different FCS batches or dependent on environmental influences such as vibrations, or increased incubator use, discussed in 3.3.1 [370]. To overcome these difficulties in reproducibility results from studies using the BeWo b30 Transwell® system have to be monitored and documented accurately to recognize alterations in trophoblast transfer. In our studies, we observed decreased micronutrient transfer rates, which were found in cell layers exceeding TEER values of 330 Ω*cm². In case of this test substance-independent effect, culture conditions had to be evaluated again to adjust these according to the proliferation behavior. Besides the simplicity of the monolayer, established in the BeWo b30 *in vitro* system, it sparsely represents the complete physiology and structure of the placental barrier *in vivo*. During gestation, endothelial cells of fetal vessels are gaining more importance since they are also playing an important role in maternal-fetal nutrient transfer as the villous trees are developed sufficiently. Moreover, the formation of the vascular system is dependent on trophoblast signaling highlighting the importance of interactions between epithelial trophoblasts with endothelial vascular cells [378]. By applying the Transwell® system, epithelial and endothelial cells can be co-cultured in the same insert allowing the investigation of vectorial micronutrient transfer across both cellular structures. However, as the same medium has to be used, culture conditions have to be adjusted to the needs of both cell types. Since BeWo b30 cells in the established *in vitro* system are already cultured in the endothelial growth medium, developing a co-culture with endothelial HUVECs, for example, can be implemented without further studies on medium suitability [598]. Another interesting approach would be a co-culture with pericytes (located between the syncytiotrophoblasts and fetal endothelium), which are among stabilization of the blood vessels, and trophoblast differentiation involved in nutrient transfer [599]. To further enhance the *in vitro* model according to the microenvironment of the placental barrier *in vivo*, Kreuder *et al.* developed a co-culture model of BeWo b30 trophoblasts and endothelial HPVEC cells, which are cultivated on a bioprinted methacrylated gelatin matrix including fetal fibroblasts simulating extracellular matrix and villous stroma. This is a clear advantage since an artificial polycarbonate membrane, as it is implemented in the Transwells®, can be avoided [336]. Moreover, with the Transwell® system, BeWo b30 cells are cultivated under static conditions, which does not represent the *in vivo* situation. Among other cell types present in the placental barrier, trophoblasts are able to sense fluid sheer stress induced by continuous blood flow through mechanotransduction. One possible adaption to this is the formation of the trophoblast microvilli, which is crucial to model physiological transporter

localization [339,600]. This in turn can influence metabolic turnover immensely since studies could already show increased glucose uptake in BeWo b30 cells due to increased *GLUT1* mRNA expression under constant flow conditions [338,600]. Besides investigations under fluid flow combining these with a low oxygen environment, another critical parameter in the regulation of trophoblast and placenta development would also consider first-trimester conditions [337,600]. Nevertheless, alterations in Mn, Fe, and Zn transport due to fluid flow or the involvement of other placental barrier-building cells was not investigated so far offering new opportunities for future studies to fill the lack of knowledge in fetal nutrient supply.

7.3. Investigation of single Mn, single Fe, and combined Mn and Fe transfer across an *in vitro* model of human villous trophoblasts (BeWo b30)

Adequate Mn and Fe supply are crucial for fetal development in terms of fetal growth, neurodevelopment, erythropoiesis, and cellular and placental homeostasis due to their involvement as co-factors needed for proper enzyme function in human metabolism and maintenance of pregnancy [272,273,298,299]. Since women, in particular, are more susceptible to Fe deficiency, the role of Fe supply during pregnancy and the transfer of Fe across the placental barrier is extensively investigated and reviewed elsewhere [68,85]. Furthermore, several studies in other tissues and cells have reported effects of Mn on Fe homeostasis and vice versa due to their similar physiological appearance in the divalent or trivalent oxidation state and therefore, the potential competition on transporter binding sites [19,27]. However, data on Mn transport across the placental barrier is mainly based on rodent data, studies in a perfused placental lobule, and modeling approaches where all of which are proposing an active mode of transport. Exact Mn transport pathways have not been elucidated so far and additionally, active transport was not verified by further investigations on transporter involvement and ATP utilization but extrapolated from Fe transfer [306,307,410]. Therefore, the studies conducted in this thesis should concentrate on mechanistic investigations on Mn transfer across the placental barrier-building trophoblasts, and potentially highlight similarities or differences compared to Fe transfer. For this, the already developed BeWo b30 Transwell® system was used, allowing for a simplified investigation of Mn and/or Fe transfer across the trophoblast layer getting primary insights on direct effects on the trophoblast cells. Contrary to expectations and general underlying data, this study clearly showed that Mn transfer across the BeWo b30 trophoblasts is more complex and does not only include active modes of transport. Mn transfer normalized to the applied dose was independent of the incubated $MnCl_2$ concentrations but showed a time-dependency,

suggesting that Mn transfer across the trophoblast layer is constant. In our study active transport was investigated by the applied mRNA and protein expression analysis of metal transporters expressed in placental tissue. Transporter involvement could be verified since mRNA and protein expression of the main discussed in- and exporters like DMT1, TfR1, ZIP8, ZIP14, and FPN showed a slight response to Mn treatment. On the contrary, Mn transfer was not affected by treatment with Ferristatin II or hepcidin, postulated to inhibit DMT1, TfR1, or FPN, respectively, in combination with Mn [78,411,412]. Thus, Mn transport may be facilitated by other routes such as tight junctional transport or diffusion processes. In comparison, treatment of BeWo b30 cells with $FeCl_2$ showed concentration-dependent decreased transfer kinetics (normalized to the applied dose) with 100 µM $FeCl_2$ as critical concentration lowering Fe transfer to 2 – 6 %. This may hint at a more restricted Fe transfer across the BeWo b30 trophoblast layer. This could also be supported by significant alterations in TfR1 protein expression, decreased transfer amounts, and enhanced cellular Fe after concurrent treatment with the DMT1, TfR1, and FPN inhibitors. In accordance with studies in other tissues and cells, Mn and Fe transport were altered by combined $MnCl_2$ and $FeCl_2$ exposure revealing potential interactions of Mn and Fe on their respective homeostasis, especially in the regulation of protein expression of the Fe storage proteins FTH and FTL [27,157]. This observation is important to consider to ensure adequate Mn and Fe supply to the fetus to maintain fetal development.

Nevertheless, the applied *in vitro* model has several limitations, which have to be contemplated in the context of Mn and Fe nutrient supply across the trophoblast layer. Among the limitations of static culture in the Transwell® system and the limited modulation of the placental barrier microenvironment and complex cellular structure discussed in 7.2, using the cancer cell line BeWo b30 limits the comparability to trophoblasts *in vivo*. Kallol *et al.* have performed an analysis of expression patterns of different nutrient-associated genes and showed that differentiated and undifferentiated BeWo b30 cells show different patterns compared to differentiated and undifferentiated primary human trophoblasts. Especially alterations in lipid metabolism have been observed, which was assumed due to their effect on cell membrane composition and syncytialization [346]. Furthermore, in regard to different metal species, we only investigated the role of divalent Fe in placental transfer, however not clarified in which oxidation state Fe is occurring in the cell culture medium upon incubation. Therefore, Fe speciation measurements via capillary electrophoresis coupled to inductively coupled plasma mass spectrometry (CE-ICP-MS) or size exclusion chromatography-inductively coupled

plasma-dynamic reaction cell-mass spectrometry (SEC-DRC-ICP-MS) will potentially reveal the species predominantly taken up by BeWo b30 cells but will also give an overview of the Fe(II)/Fe(III) ratio, as well as Fe, bound to ferritins, which will additionally hint at potential oxidative stress potential within BeWo b30 cells [415,533]. In summary, this study highlighted that every TE has to be evaluated individually and the effects of one TE cannot be extrapolated to the other even if they share many similarities. Additionally, results obtained in this study revealed the complexity of Mn and/ or Fe transfer, but exact underlying pathways and regulatory targets have still to be elucidated.

Aside from transcriptional and translational regulation, over 100,000 post-translational modifications have been identified in the human proteome leading to a subsequent response to cellular and systemic signals to maintain homeostatic regulation. In case of Mn and Fe transport ubiquitination has shown to be the predominant form involved in the degradation of TE transporters [601]. Therefore, the assessment of transporter ubiquitination will potentially reveal further alterations in Mn and/or Fe transport across the BeWo b30 cell layer. Furthermore, the involvement of tight junction-associated transport in Mn and/or Fe transfer can be investigated among others by measuring tight junction conductance, the flux of molecular tracers, or via protein expression of tight junction proteins like different claudin isoforms, which are mainly involved in tight junctional ion permeability [602]. We investigated immunocytochemical staining of tight junction and microtubule proteins described in 3.2.4 in Mn and/or Fe exposed cells (data not shown). However, there were no alterations in either γ-catenin, tubulin, or Hoechst staining upon Mn and/or Fe treatment such as cleaved cell-cell boundaries. An interesting approach would be the analysis of the fluorescence intensity of the tight junction proteins, which can also be analyzed and quantified by use of the analysis tool of the microscope software, after establishing an adequate protocol. Additionally, protein expression analysis of the tight junction protein claudin, for example, may also indicate if tight junction integrity is perturbed by Mn and/or Fe treatment even if cytotoxicity testing and measurement of the BeWo b30 barrier integrity via TEER did not show any effects (fig. S2 and also discussed in 4.4). Decreased expression of tight junction proteins upon Mn overexposure has been discussed in the context of enterocyte toxicity leading to increased permeability [603]. Expression of claudins 1, 3, and 5 was also diminished in placentas from preeclamptic pregnancies, hinting at more leaky tight junctions due to decreased vessel perfusion [604].

Moreover, Karahoda *et al.* have shown that trophoblast differentiation positively affects the protein expression and activity of TfR1. Therefore, it would be interesting if the differentiation of BeWo b30 cells with forskolin results in altered transfer kinetics compared to undifferentiated BeWo b30 cells [342,343,347]. Forskolin is a potent activator of adenylate cyclase, activating the cyclic AMP pathway and leading to the differentiation of BeWo b30 cells to multinuclear syncytiotrophoblasts. However, forskolin treatment has to be established beforehand in consideration of the fact that differentiation efficiency has great variability ranging from 10 – 80 % comparing several laboratories. This may be attributed to the variety of BeWo b30 strains, which were developed due to their wide and long-term use since they were isolated in 1959 [330,345].

Since it has been postulated that inherited mutations in *ZIP8, ZIP14*, and *ZnT10* may lead to a perturbed Mn homeostasis, it would be of particular interest to investigate changes in maternal-fetal Mn transfer and interactions across placental-barrier forming trophoblasts with *ZIP8*, *ZIP14*, and *ZnT10* dysfunction. While adverse effects caused by these mutations are already discussed in the context of Mn-induced neurotoxicity and the pathologies of neurodegenerative diseases, the role in pregnancy is largely unknown [42,43,46]. This could be realized by inhibition experiments using siRNA transfection in BeWo b30 cells. Additionally, after collecting several specimens from mothers carrying these mutations such as maternal blood, cord blood as well as placental and umbilical cord tissue, investigating altered TE levels as well as mRNA and protein expression patterns of different potentially affected metal transporters would be important to reveal alterations in TE homeostasis. Furthermore, perfusion of *ZIP8*, *ZIP14*, and *ZnT10*-defective placental tissue with mixed metal solutions would contribute to the knowledge of TE homeostasis in conditions of impaired transport systems.

Since data obtained in the Mn and Fe transfer study is inconclusive a non-targeted approach, RNA sequencing can help to further clarify Mn and Fe interactions and to find pathways, which are predominantly targeted by Mn and/or Fe exposure in BeWo b30 cells. To date, considering measurements of RONS induction via Carboxy-DCFH-DA assay and qPCR analysis of oxidative stress-associated genes, Fe-, or Mn-induced oxidative stress is not a present concern in BeWo b30 cells. However, as protein expression and post-translational protein modifications of oxidative stress-associated proteins in BeWo b30 cells upon Mn and Fe treatment have not been investigated so far experiments such as western blot and MALDI-ToF-MS analysis may

rather hint at potentially involved pathways. Therefore, protein expression and modification need to be investigated in future studies to identify the role of oxidative stress responses. This can further be addressed by measuring protein carbonyls, the result of oxidatively damaged proteins among others via enzyme-linked immunosorbent assay (ELISA). In order to distinguish primarily formed protein carbonyls from those derived during lipid peroxidation, the subsequent measurement of malondialdehyde and 4-hydroxy-2-nonenal via an HPLC-FLD method is necessary [605,606]. Conceivably, quantification of the GSH/GSSH ratio via LC-MS/MS may reveal the antioxidative capacity of BeWo b30 cells, which may is presumably high as we observed no cytotoxic effects upon high Mn and Fe loads [547].

7.3.1. Future directions for placenta studies

Despite the enhancement of the BeWo b30 *in vitro* system already discussed in 7.2 and 7.3, another approach would be the investigation of changes in metal transfer and transfer kinetics across a layer of primary human trophoblasts, since they show other expression patterns of macro- and micronutrient transfer compared to BeWo b30 cells [346]. Primary human trophoblasts can be isolated from term placentae collected subsequently after delivery and therefore represent non-invasive trophoblasts of late gestation. They spontaneously fuse to syncytiotrophoblasts, which can be both an advantage and disadvantage regarding the modeling of the cytotrophoblast or syncytiotrophoblast layer, respectively. Additionally, a recent study by Karahoda *et al.* has also shown that among five key proteins of Fe transfer (SLC11A2 – DMT1, SLC40A1 – FPN1, SLC39A8 – ZIP8, SLC39A14 – ZIP14, and TfR1), *FPN1* and *TfR1* mRNA were significantly downregulated upon differentiation of primary cytotrophoblasts to syncytiotrophoblasts [347]. Aside from primary human trophoblasts, using induced pluripotent stem cells can be helpful to investigate different placental cellular structures (villous and extravillous trophoblasts) without elaborate isolation protocols as their development can be induced by following different differentiation procedures. Induced pluripotent stem cells from mothers suffering from pregnancy disorders such as PE can further be advantageous as these cells are already exhibiting PE phenotypes and therefore display a suitable model without further manipulation [209,607].

The pathogenesis of PE, in general, may also be an interesting objective, as *in silico* studies of the human placenta showed the disturbance in nutrient transporter genes in cases of intrauterine growth restriction and PE [608]. These findings could be verified in a mice study, where deletion of specific transporters of amino acid, lipid, and carbohydrate metabolism

showed impaired fetal growth. In this study transporters involved in macro- and micronutrient transport were investigated but regarding transport studies in this thesis, only ZIP8 and DMT1 were covered [208,609-611]. Women, which developed early onset PE and/ or fetal growth restriction also showed reductions in the mitochondrial respiratory capacity, which may be attributed to a secondary effect due to suppressed PI3K-AKT and mTOR (mammalian target of rapamycin) signaling in the placenta. In regard to nutrient acquisition, activation of PI3K is involved in the regulation of DMT1 via the IRP2 pathway and Zn deficiency has shown to disrupt AKT signaling [9,138,491]. Therefore, PE-induced suppression of these signaling proteins may also influence micronutrient distribution. With oxidative stress as a discussed hallmark of the PE pathology and reduced mitochondrial respiratory capacity in PE placentae, these may be particularly susceptible to metal-induced oxidative stress. Several studies have shown an involvement of Zn, magnesium (Mg), Fe, Ca, and Cu in PE, all of which are also involved in antioxidative defense as important co-factors or structural components. In a prospective pre-birth cohort study Mn levels in red blood cells were inversely correlated with PE showing that higher Mn levels are associated with decreased risk of PE. This may be assumed since enhanced Mn levels may lead to increased levels of MnSOD scavenging excess ROS present in the circulation. However, associations of Mn overexposure with PE pathology and exact underlying pathways have not been elucidated so far [440,446,612].

Regarding metal transfer studies, the comparison of *in vitro* with *ex vivo* placental perfusion data would further enhance the knowledge of nutrient transfer across the placenta and placental barrier-building cells. Besides the measurement of the transferred metal amounts, it would be interesting to investigate mRNA as well as protein expression of transporters associated with nutrient transfer isolated from freshly perfused tissue. For this, it would also be of particular interest to separate the maternal basal plate from the fetal chorionic plate beforehand. Additionally, laser ablation-inductively coupled plasma-spectrometry measurements in a perfused placental lobule would potentially reveal the localization and accumulation sites of different TEs like Mn and Fe in the treated lobule. This has already been done in a proof-of-principle study, visualizing multi-metal mixtures via LA-ICP-MS and colocalization with inflammation markers in human placental tissue [613].

In a recent study in cooperation with the working group of Prof. Dr. Uwe Karst and his co-workers Helena Friedrich, Catharina Erbacher, Alexander Köhrer, and Matthias Elinkmann from the University of Münster, we investigated the uptake of inorganic and organic mercury

(Hg) species, (inorganic Hg, methyl Hg (MeHg), ethyl Hg (EtHg)) in BeWo b30 cells measured in a single cell ICP-MS/MS (SC-ICP-MS/MS) approach. The analysis of the metal content in individual cells considers overall cell variances among others due to their heterogeneity in size, metabolic activity, and physiological status, which may lead to differences in metal uptake rates and cellular concentrations. This metal uptake distribution across the investigated cell population, which can be determined via SC-ICP-MS/MS is not covered in the conventional bulk metal analysis [614]. Furthermore, the underlying research interest regarding Hg treatment in BeWo b30 cells is based on the increased risk of perturbed fetal (neuro)development due to increased Hg transferred from maternal to fetal circulations and its direct effect on the trophoblast cells since pregnant women are exposed to environmental Hg pollution among others due to coal combustion or consumption of MeHg-contaminated seafood. EtHg is mainly formed in the metabolism of thiomersal, which is still added as a preservative in vaccines like a meningococcal or tetanus-toxoid vaccine in the USA and childhood-administered vaccines in developing countries [615-619]. To date, we were able to develop a suitable SC-ICP-MS/MS method to detect alterations in the uptake of all three Hg species in BeWo b30 cells and could show comparable Hg amounts in BeWo b30 cells quantified from the most abundant Hg concentration from single cell measurements and bulk Hg determination (data not shown but described elsewhere [620]). In a further approach via TIMS-ToF-MS (trapped ion mobility spectrometry-time of flight mass spectrometry) analysis we try to detect proteins, which are the main target for Hg in the BeWo b30 cells but this is still under evaluation. Recently, Ganapathy *et al.* investigated the transport and toxicity of cysteine-bound MeHg in BeWo cells and found that MeHg may predominantly be transported by sodium-dependent amino acid and organic anion transporters. Additionally, MeHg perturbed mitochondrial function, and viability and was involved in the induction of oxidative stress. The main limitation of this study is the use of culture dishes instead of Transwell® inserts, which limits the cells to follow their physiological, polarized phenotype. Regarding the induction of oxidative stress, measuring the GSH/GSSG ratio in Hg treated BeWo b30 cells would be interesting since glutathione is one main target for Hg because of its thiol groups. It has also been shown to negatively affect GPx and thioredoxin reductase (TrxR) activity since it has a very high Se affinity. Hg binding Se can also lead to the disruption of Se homeostasis. As already mentioned before, the determination of nuclear Nrf2 translocation would further represent another oxidative stress response pathway. Potential neurotoxicity due to Hg-dependent alterations in neurotransmitter metabolism may also be of interest in BeWo b30

cells since they are expressing enzymes and receptors important in neurotransmitter metabolism such as 5-hydroxytryptamine (5-HT), a serotonin receptor, and L-dopa decarboxylase, converting the precursor L-dopa into dopamine [621-625]. 5-HT has been shown to play a critical role in a variety of neurodevelopmental processes. Thus, alterations in the 5-HT system may have detrimental effects on fetal development and brain function, which may result in the development of neuropsychiatric disorders later in life. However, the effects of Mn on the serotonergic system are inconsistent. While adverse effects of Mn on the 5-HT levels could be observed in children, this was not the case *in utero* [626-628]. The effect of Mn on the serotonergic system in BeWo b30 cells can therefore be determined by analyzing the mRNA and protein expression of the 5-HT receptor and serotonin transporter as well as its activity including recaptured and titrated 5-HT [629]. Moreover, as Maccani *et al.* suggest altered DNA methylation patterns in the placenta, which can be associated with prenatal Mn exposure it would be of particular interest to investigate Mn-induced methylation patterns in BeWo b30 cells by determining cytosine methylation (5-methylcytosine, 5-hydroxymethylcytosine) via an established LC-MS/MS approach using isotopic dilution analysis. Since Fogarty *et al.* revealed epigenetic changes between cytotrophoblasts and syncytiotrophoblasts, DNA methylation analysis can be performed additionally in differentiated BeWo b30 cells [630,631]. To further concentrate on regulatory mechanisms involved in epigenetic changes, small non-coding RNA can be determined. Small non-coding RNA is involved in the regulation of epigenetic mechanisms of gene expression control [632].

7.4. Effects of Zn on Mn cytotoxicity and bioavailability in human hepatoma cells (HepG2)

The liver is predominantly involved in TE distribution, storage, and excretion and therefore serves as one of the main regulatory organs of TE homeostasis and metabolism in the human body. Besides gastrointestinal regulation, where TE uptake into the systemic circulation is tightly controlled, this efficient homeostasis can also be bypassed in case of administration of PN. However, PN formulations do rarely contain single TEs but mixtures, where present TEs potentially interact in terms of hepatocellular uptake, and distribution to other organs as well as systemic TE enrichment [8,34,108,172]. While interactions of Mn and Zn with Fe are investigated in more detail, the role of Mn on Zn homeostasis and vice versa is rarely characterized in liver tissue [10,633]. As already discussed in the introduction, Mn and Zn share a variety of transporters, and Zn is also involved in the regulation of TfR1 and DMT1, which generally do not have a high Zn binding affinity. Therefore, the study conducted in this thesis

should reveal the potential interrelation of Mn and Zn transport as well as its effects on Mn-induced cytotoxicity in human hepatoma (HepG2) cells. HepG2 cells resemble several characteristics of human hepatocytes and additionally express transporters involved in both Mn and Zn transport [188,494,506,508]. Surprisingly, comparing Mn-induced cytotoxicity across different cell types, and cell lines introduced in this thesis, HepG2 cells showed a significant reduction in cell number after treatment of 200 µM $MnCl_2$ for 24 h, while BeWo b30 cells were not affected by Mn in concentrations up to 1500 µM $MnCl_2$ (fig. S6 vs. fig. S2). Both organs are involved in TE metabolism and the main target of several xenobiotics and substances. However, even if the activities of xenobiotic metabolizing enzymes in the liver are higher compared to the placenta, BeWo b30 cells are more robust upon Mn exposure than HepG2 cells. This may potentially be attributed to the confluent monolayer, whereby the distribution of high metal loads is higher compared to HepG2 cells. As Mn treatment did not result in the induction of RONS, determined via Carboxy-DCFH-DA assay in either BeWo b30 and HepG2 cells (BeWo b30: fig. 27A, B, HepG2: data not shown, described elsewhere [634]), acute RONS formation leading to unbalanced antioxidative defense homeostasis does not appear to play a major role. Furthermore, $MnCl_2$ treatment also resulted in caspase-3 activation in HepG2 cells, which was only observed, after cells were incubated 48 h after seeding compared to 24 h (fig. 33D). This has been discussed in the context of senescence (see 5.4), which is associated with the induction of persistent DNA damage and the involvement of p53. However, after performing the alkaline unwinding assay in HepG2 cells, no DNA strand breaks could be observed upon Mn exposure, though not clarified if HepG2 cells exhibit efficient DNA damage response and DNA repair mechanisms (data not shown, described elsewhere [635]). A potential contribution of p53 in the mechanism of Mn-induced cytotoxicity in HepG2 cells cannot be ruled out completely, since it also plays a role in the regulation of ZIP14 protein expression. Induction of p53 has been shown to depress ZIP14 protein expression, while a lack of p53 resulted in ZIP14 upregulation. Activation of p53 in turn might be associated with DNA damage, which would contribute to the induction of cellular senescence. Therefore, it would be interesting to determine p53 mRNA and protein and ZIP14 protein expression, to reveal a potential involvement of p53 in the regulation of ZIP14 due to Mn treatment. However, this translational regulation may not correlate with alterations in *ZIP14* mRNA expression [468,469,512,513,636].

Moreover, combined exposure of HepG2 cells with Mn and Zn resulted in increased cellular viability and reduction of apoptosis and necrosis markers such as caspase-3 and LDH. This was

associated with decreased Mn bioavailability in HepG2 cells, after combined Zn exposure in both incubation scenarios. However, alterations in mRNA expression due to combined Mn and Zn exposure could not be attributed to one single TE affecting the homeostasis of the respective other. In a study regarding TE concentrations in plasma and tissue of Zn-fed rats, a semi-quantitative metallomics approach via ICP-MS measurements revealed a reduction of liver Mn in a concentration-dependent manner upon single dietary Zn exposure and significantly reduced liver *ZIP8* mRNA expression. Despite this, we observed significant induction of *ZIP8* upon single Zn treatment in HepG2 cells (fig. 36C), but results obtained in both studies are difficult to compare, since exposure dimensions may differ and therefore show different *ZIP8* responses upon Zn treatment [633]. As already mentioned in 5.4 upregulation of *ZIP8* has shown to be potentially induced by NF-κB, a transcription factor involved in acute phase response to inflammation [522]. This was in line with the induction of MTs, which was observed after single Mn, Zn, and combined Mn and Zn exposure in HepG2 cells (fig. 37E, F). Contradictory to this, several studies have reported *ZIP14* upregulation in case of inflammation, to facilitate Zn influx and therefore the induction of an anti-inflammatory response. It would be of particular interest to investigate the role of inflammation in the context of attenuated Mn cytotoxicity due to additional Zn exposure.

Using the fluorescence probe FluoZin™-3 allows us to sensitively measure the labile Zn fraction apart from total Zn levels after single Mn, Zn, or combined Mn and Zn exposure in HepG2 cells. Among other fluorescence probes, such as ZinPyr-1, using FluoZin™-3 is more advantageous, since single Mn exposure resulted in ZinPyr-1 quenching and therefore interfering with labile Zn measurements (data not shown, described elsewhere [637]), which may be attributed to a higher dissociation constant of the Mn-ZinPyr-1 complex compared to Zn, even if this was not observed in human serum [498,638]. Interestingly, decreased labile Zn levels are in accordance with the transcriptional upregulation of *MT1A* and *MT2A* after single Mn exposure (fig. 35, 37E, F), indicative of MTs binding available labile Zn as a response to Mn-induced radicals. This may also suggest, that the Carboxy-DCFH-DA assay was not able to show any induction of RONS, since the cellular antioxidant system was already able to scavenge RONS present in the cytosol. Since MTs can bind up to 7 Zn ions and not all MTs are occurring in a saturated state, it would be interesting to investigate if the number of Zn ions bound to MT would increase due to single Mn treatment in HepG2 cells. This might be realized by using ion mobility mass spectrometry [639,640]. Furthermore, determining oxidative stress-associated genes and proteins, GSH/GSSH ratios as well as isoprostanes as additional oxidative

stress markers may reveal alterations in the antioxidant system, potentially shifting to an increased response to present RONS.

Compared to the transcriptional regulation of Mn transfer in BeWo b30 cells, HepG2 cells showed clear responses to Mn treatment in *DMT1*, *ZIP8*, *ZIP14*, and *MT1A/ MT2A* mRNA expression. This may suggest, that Mn transfer is more tightly regulated in terms of active transport processes in HepG2 cells compared to placental BeWo b30 trophoblasts. However, this can also be attributed to the confluent monolayer, where higher metal yields potentially result in transcriptional transporter regulation. However, another possible assumption is that transcriptional regulation is already adapted to the present circumstances in BeWo b30 cells and therefore, alterations are rather observed on the translational level. Since translational transporter expression, as well as TE export, has not been determined in HepG2 cells this cannot be elucidated further, yet. In general, determining translational transporter expression as well as investigations on metal exporters such as ZnT10 and FPN1 would further support broadening the understanding of potential mechanisms of Mn and Zn interaction in HepG2 cells and potential regulatory targets.

7.5. Alterations of genome integrity and neurite outgrowth in LUHMES cells upon Mn overexposure

Mn is an important co-factor involved in neurodevelopment and neuronal antioxidative defense. However, Mn has also been discussed as a neurotoxicant and its role in dopaminergic neurotoxicity, one of the hallmarks of PD [5,190]. Several studies have shown preferential Mn accumulation in dopamine-rich areas of the *basal ganglia* and especially in the *substantia nigra* of PD patients, leading to persistent oxidative stress due to increased generation of RONS, which could be identified in various *in vitro* and *in vivo* studies [534-536,548,557]. RONS in turn can interact with macromolecules like DNA resulting in oxidative DNA damage with 8-oxodG as one of the most prominent lesions. However, the exact mechanisms of Mn-induced DNA damage, underlying DNA damage response, and effects on neurite outgrowth are still not clarified [548,573]. Utilizing post-mitotic LUHMES cells, resembling dopaminergic neurons upon differentiation, should therefore serve to investigate underlying mechanisms, which were further presented and discussed in [641]. Besides alterations in DNA damage, DNA damage response, and neurite outgrowth (fig. 41 – 44), Mn cytotoxicity regarding cell number, metabolic activity, and mitochondrial membrane potential was addressed (fig. 39, 40). Total cell number significantly decreased concentration- but not time-dependently upon $MnCl_2$

treatment (fig. 39B). Moreover, the significant concentration-dependent decrease of metabolic activity could be explained by a decrease in the mitochondrial membrane potential observed in the present study (fig. 39A, 40). The impairment of the mitochondrial membrane potential can be associated with the induction or as a result of oxidative stress and the increased generation of RONS, corroborated by previous *in vitro* and *in vivo* studies [547,548,557]. In comparison to HepG2 cells, resembling human hepatocytes and BeWo b30 cells, resembling placental trophoblasts, differentiated LUHMES cells showed higher sensitivity upon $MnCl_2$ treatment with 25 µM $MnCl_2$ sufficient to significantly reduce cell viability followed by HepG2 cells (significantly decreased cell viability at 200 µM $MnCl_2$) and BeWo b30 cells, which did not show any cytotoxic effects up to 1000 µM $MnCl_2$ (fig. 39B, 32, S2). While disturbed mitochondrial membrane potential may be one underlying pathway of Mn-induced LUHMES cell death, RONS induction could not be observed in HepG2 cells and BeWo b30 trophoblasts (HepG2: data not shown, BeWo b30: fig. 27). However, as many pathways are involved in antioxidative defense mechanisms, the role of RONS in Mn-induced cytotoxicity in HepG2 cells needs still to be elucidated. Regarding localization and function of these cells within the respective organs, hepatocytes and placental trophoblasts are mainly involved in nutrient transfer and are the initial targets of micronutrients, while neurons are protected by the epithelial cell layer, pericytes, and astrocytes of the BBB. Therefore, in healthy individuals with balanced metal homeostasis neurons are exposed to micronutrients only at physiological levels. Studies by Bornhorst *et al.* revealed that astrocytes showed incipient cytotoxic effects upon treatment of 1000 µM $MnCl_2$, which may be explained by their role in controlling ion balance within the BBB [8,199,226,453,642]. Nevertheless, differences in Mn-induced cytotoxicity can potentially be explained by focusing on Mn bioavailability.

Comparing cellular Mn uptake in differentiated LUHMES cells with HepG2 cells utilized in this thesis, Mn uptake was highest in differentiated LUHMES cells with 1812 µM Mn compared to 1439 µM Mn in HepG2 cells after 24 h of exposure (fig. 34 A, B, data for LUHMES not shown). Treatment of BeWo b30 cells with 100 µM $MnCl_2$ for 48 h resulted in cellular uptake of 0.171 µg Mn/ mg protein (fig. 24A). However, since bioavailability measurements of 100 µM $MnCl_2$ after 48 h of exposure were not realized in differentiated LUHMES cells, following the indicated almost direct proportional Mn uptake to incubation time observed for 50 µM $MnCl_2$, differentiated LUHMES cells are expected to take up about twice as much Mn as BeWo b30 cells. Interestingly, exposing differentiated LUHMES cells to 100 µM $MnCl_2$ for 24 h can directly be compared to Mn amount in BeWo b30 cells after 48 h of exposure (0.178 µg Mn/ mg

protein in LUHMES cells (fig. 38A) vs. 0.171 µg Mn/ mg protein in BeWo b30 cells (fig. 24A)). In consideration of Mn cytotoxicity, differentiated LUHMES are most sensitive towards Mn exposure potentially due to a higher bioavailability compared to HepG2 and BeWo b30 cells and potential differences in homeostatic Mn regulation by transport proteins. It would therefore be of particular interest to investigate alterations in transcriptional and translational transporter expression, to reveal if the higher sensitivity is leading to decreased Mn influx and increased efflux or to which extent regulatory processes are induced or depressed compared to Mn transporter expression in HepG2 and BeWo b30 cells. While dopaminergic neurons do also express TE-associated transporters, such as DMT1, TfR1, and FPN, studies have shown the main role of the citrate transporter and PARK9 contributing to neuronal Mn homeostasis. Furthermore, PARK9 expression is highest in the dopamine-rich *substantia nigra*, hinting at a potential correlation with Mn-induced neurotoxicity [643-646]. Furthermore, as differentiated LUHMES cells showed an increased number of DNA strand breaks upon $MnCl_2$ treatment a potential involvement of p53 seems likely. This in turn can affect ZIP14 protein expression and lead to potential alterations in Mn homeostasis [469]. Since the study in HepG2 cells showed *MT1A* and *MT2A* mRNA transcription response upon Mn treatment, it would be interesting to include *MT3*, which is brain-specifically expressed [647]. Discussed adverse effects due to inherited mutations in *SLC30A14* (ZIP14), *SLC30A10* (ZnT10), and *ATP13A2* (PARK9) showed clearly, that these transporters are needed to maintain brain Mn homeostasis, avoiding metal accumulation and resulting neurodegeneration [43,46,132]. Michalke *et. al* identified an Mn carrier switch from TfR-bound Mn to citrate-bound Mn in human serum at concentrations between 1.5 µg/mL – 1.7 µg/mL. Further accompanied by a positive linear association of CSF Mn and serum Mn levels to Mn-citrate levels (at serum Mn levels higher than 1.6 µg/L). In concentrations ranges lower than 1.6 µg/L this positive correlation was rather associated with serum Mn-TfR levels. Since CSF sampling is highly invasive, measuring Mn-citrate levels in serum can be used to reveal an increased risk of higher internal Mn exposure in the brain [648]. Therefore, it would be of particular interest to perform Mn speciation analysis in LUHMEs cells and the cell culture medium to investigate if the carrier switch is also relevant to cellular Mn bioavailability, and can be associated with increased neurotoxicity. Comparison with the other cell lines utilized in this thesis would further contribute to reveal organ-specific preferred Mn species.

Studies conducted in PARK9-deficient hOHS cells (termed olfactory neurosphere-derived cells) showed increased extracellular Zn sensitivity and altered Zn transporter expression [649].

Therefore, besides Mn-induced neurotoxicity, excess extracellular Zn may lead to the induction of oxidative stress in dopaminergic neurons by activation of NADPH oxidase and depletion of GSH, which has been shown in a rat study by Kumar *et al.* in patterns comparable to the neurotoxicant paraquat [650,651]. Chronic Zn treatment in rats did result in dopaminergic neurodegeneration accompanied by the induction of inflammatory mediators such as TNF-α and interleukins [651,652]. Neuroinflammation has also been discussed in the context of Mn-induced neurotoxicity, which might contribute to the demise of dopaminergic neurons [5,189]. It would be interesting to try concurrent Mn and Zn treatment in differentiated LUHMES cells, to reveal, if underlying mechanisms can be compared to results obtained in HepG2 cells. The role of Mn and Zn interactions in neuronal cells, especially in terms of increased cell viability due to concurrent Mn and Zn treatment, would contribute to understanding fundamentals in neuronal metal homeostasis, which are largely unknown yet.

Maintaining TE homeostasis is important for the immature brain to sustain further development. Regarding fetal neurodevelopment, epidemiological studies could associate TE overexposure with neurological effects in children [66,303]. Adverse effects on neurodevelopment due to Mn, Fe, and Zn overexposure are rarely clarified. Therefore, it would be interesting to investigate the effect of transferred metal yields across placental barrier-building cells on neuronal cells to reveal potential adverse effects on neurodevelopment. For this, Nishiguchi *et al.* established a 3D-vascularized placental barrier *in vitro* model including primary cytotrophoblasts and fibroblasts to model the maternal interface and fetal capillaries. After treatment with the respective substance basolateral medium was collected and incubated on rat cerebral cortices to assess damage signaling in neurons [337]. In consideration of the used cell types applied in this thesis, the basolateral medium from Mn, Fe, and Zn as well as concurrent exposures in the BeWo b30 Transwell® model can be collected and subsequently incubated in differentiated LUHMES cells to investigate alterations in neuronal integrity and neurite outgrowth. However, a suitable protocol has to be established beforehand, since medium change can also lead to impaired neuron development *in vitro*. Due to Mn-induced dopaminergic neurotoxicity, the measurement of neurotransmitters in BeWo b30 cells as well as exposed differentiated LUHMES cells would be promising to reveal fundamental TE-induced alterations in neurodevelopment. Additionally, it would be of particular interest to investigate Mn speciation across the BeWo b30 trophoblast layer to reveal if the conversion of Mn-transferrin to Mn-citrate is taking place at the placental barrier and if the increased formation

of Mn-citrate would result in an increased risk of perturbed neurodevelopment since Mn-citrate is presumed to be the predominant Mn-transport form in the brain [653].

Appendix - Supplementary Material

Supplementary Material Chapter 3

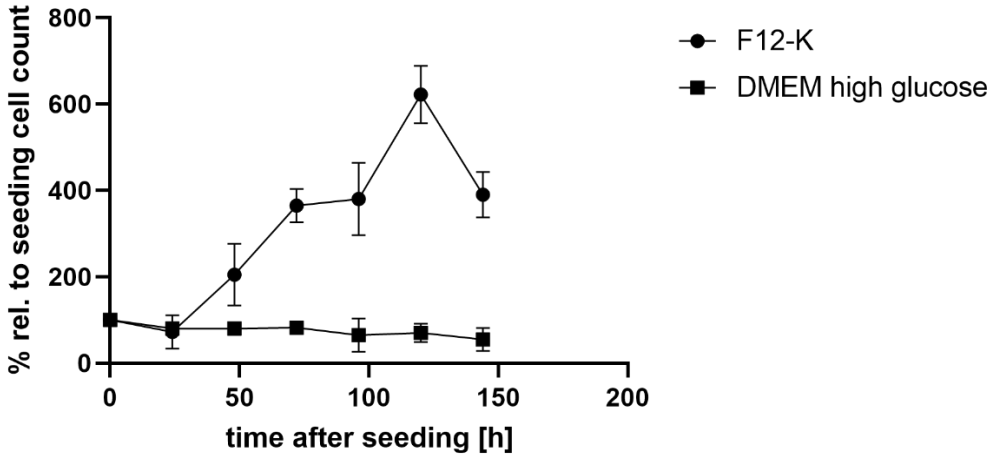

Figure S1: Growth curve of BeWo b30 cells cultivated in F-12K and DMEM high glucose, respectively. Cells were seeded at a density of 100,000 cells/ well in a 6-well cell culture dish in either F-12K or DMEM high glucose medium. Cell count was assessed every other day via the Neubauer counting chamber, and related to the starting cell count of 100,000 cells.

Supplementary Material Chapter 4

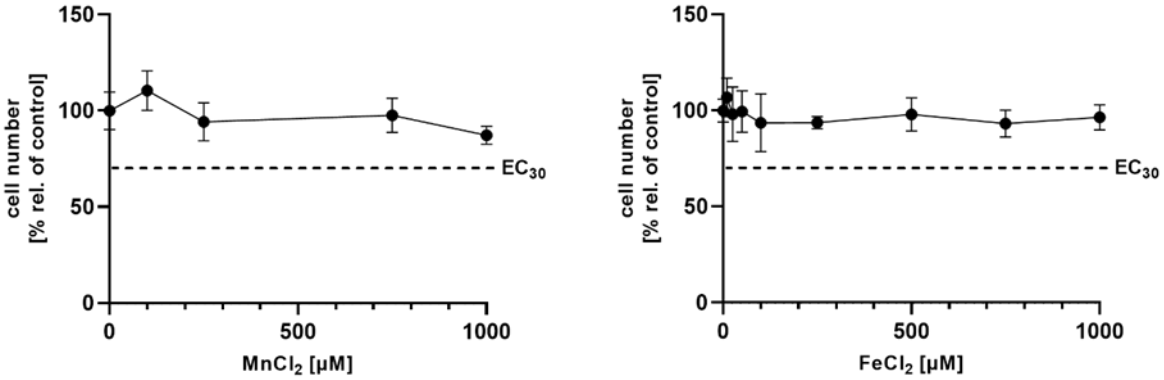

Figure S2: $MnCl_2$ and $FeCl_2$ cytotoxicity in confluent BeWo b30 cells after 24 h assessed using Hoechst Assay. Shown is the mean ± SD of three independent experiments.

Table S1: Bioavailability of $MnCl_2$ after 24 and 48 h in BeWo b30 cells. Data show the mean ± SD of at least three independent experiments with two replicates each.

Incubated $MnCl_2$ [µM]	Mn bioavailability [pg/ µg protein]	
	24 h	48 h
0	29.2 ± 9.5	63.4 ± 6.1
100	121.0 ± 33.7	143.7 ± 48.9
500	-	343.7 ± 50.9
750	-	541.2 ± 130.8
1000	-	705.0 ± 280.4

Table S2: Bioavailability of $FeCl_2$ after 48 h in BeWo b30 cells. Data show the mean ± SD of at least three independent experiments with two replicates each.

Incubated $FeCl_2$ [µM]	Fe bioavailability [pg/ µg protein]
	48 h
0	64.1 ± 12.0
10	82.5 ± 23.4
50	185.1 ± 67.2
100	290.4 ± 29.4
500	1092.6 ± 180.6

Table S3: ICP-OES parameters.

Parameter	Working conditions
Plasma power [W]	1400
Cooling gas flow [L/min]	12.00
Auxiliary gas flow [L/min]	1.00
Nebulizer flow [L/min]	1.00
Nebulizer type	MicroMist®
Torch alignment	Axial Basic settings: 0.2 mm horizontal 3.8 mm vertical 3.0 mm distance
Element wavelengths	Mn: 257.611 / 259.373 Fe: 259.940 / 238.204 Cu: 324.754 / 224.700 Zn: 202.548 / 213.856

Table S4: ICP-MS/MS parameters.

Parameter	Working conditions
Plasma power [W]	1550
Cooling gas flow [L/min]	15.00
Auxiliary gas flow [L/min]	0.90
Nebulizer flow [L/min]	1.00
Nebulizer type	MicroMist®
Spray chamber	Scott-type
Spray chamber temperature [°C]	2
Makeup Gas flow [L/min]	0.26
Torch alignment	Axial
Gas mode	He (CRC-mode)
He gas flow [mL/min]	3
Transitions	Mn: 55 → 55 Fe: 56 → 56 Cu: 63 → 63 Zn: 66 → 66 Internal Standard (IS) Ge: 72 → 72 Rh: 103 → 103

Table S5: Primer sequences of human metal transport- and storage-associated genes.

Gene name	Association	Primer sequences (5' → 3')	Amplicon length (bp)	Efficiency [%]
ACTB	β-actin	Forw.: CATCCGCAAAGACCTGTACG Rev.: TCTCCTTCTGCATCCTGTCG	86	103.4
DMT1	divalent metal transporter 1	Forw.: AGTTGGCTATCATCGGCTCA Rev.: TCTGCAATGGTGATGAGAACG	115	106.8
TfR1	transferrin receptor 1	Forw.: TGAGAGGTACAACAGCCAACT Rev.: CACGAGCAGAATACAGCCAC	107	108.1
SLC40A1 (FPN1)	ferroportin 1	Forw.: TCGCCTAGTGTCATGACCAG Rev.: TTGCAGAGGTCAGGTAGTCG	85	104.6
SLC39A14 (ZIP14)	zrt-, irt-related protein 14	Forw.: CAGTCACCATGAAGCTGCTG Rev.: GGTTCTCCATAAGCCAAGCAG	80	113.3

Continuation table S5

MT1A	metallothionein 1A	Forw.: GCAAAGGGGCATCAGAGAAG Rev.: TGGGTCAGGGTTGTATGGAA	119	118.9
MT2A	metallothionein 2A	Forw.: GTTGCCTCCTCAGTGATCCT Rev.: GGCGGCAGAGATGAGTACTA	77	105.3
FTH1	ferritin heavy chain 1	Forw.: CATCAACCGCCAGATCAACC Rev.: CACATCATCGCGGTCAAAGT	82	111.7
FTL	ferritin light chain	Forw.: ATCTTCTCGGCCATCTCCTG Rev.: TGGTTGGCAAGAAGGAGCTA	70	103.2
GSTP1	glutathione S-transferase pi 1	Forw.: CCCAAGTTCCAGGACGGAGA Rev.: GCCCGCCTCATAGTTGGTGT	186	101.0
GSTA1	glutathione S-transferase alpha 1	Forw.: GGCTGACATTCATCTGGTGG Rev.: CTGCCAGGCTGTAGAAACTTC	141	115.5
NFE2L2 (Nrf2)	nuclear factor erythroid 2-related factor 2	Forw.: ACATCGAGAGCCCAGTCTTC Rev.: TAGCTCCTCCCAAACTTGCT	125	111.9
SOD1 (Cu/ZnSOD)	superoxide dismutase 1	Forw.: GGAGACTTGGGCAATGTGAC Rev.: TCCACCTTTGCCCAAGTCAT	147	108.0
SOD2 (MnSOD)	superoxide dismutase 2	Forw.: CTGGAACCTCACATCAACGC Rev.: CCTGGTACTTCTCCTCGGTG	100	117.1
HMOX1	heme oxidase 1	Forw.: CAGGGCCATGAACTTTGTCC Rev.: CCAGAGAGAGGGACACAGTG	128	110.6
JUN	Jun proto-oncogene	Forw.: GAGTGACCGCGACTTTTCAA Rev.: AGGGAGCGCAGGGTTAATTA	88	119.2

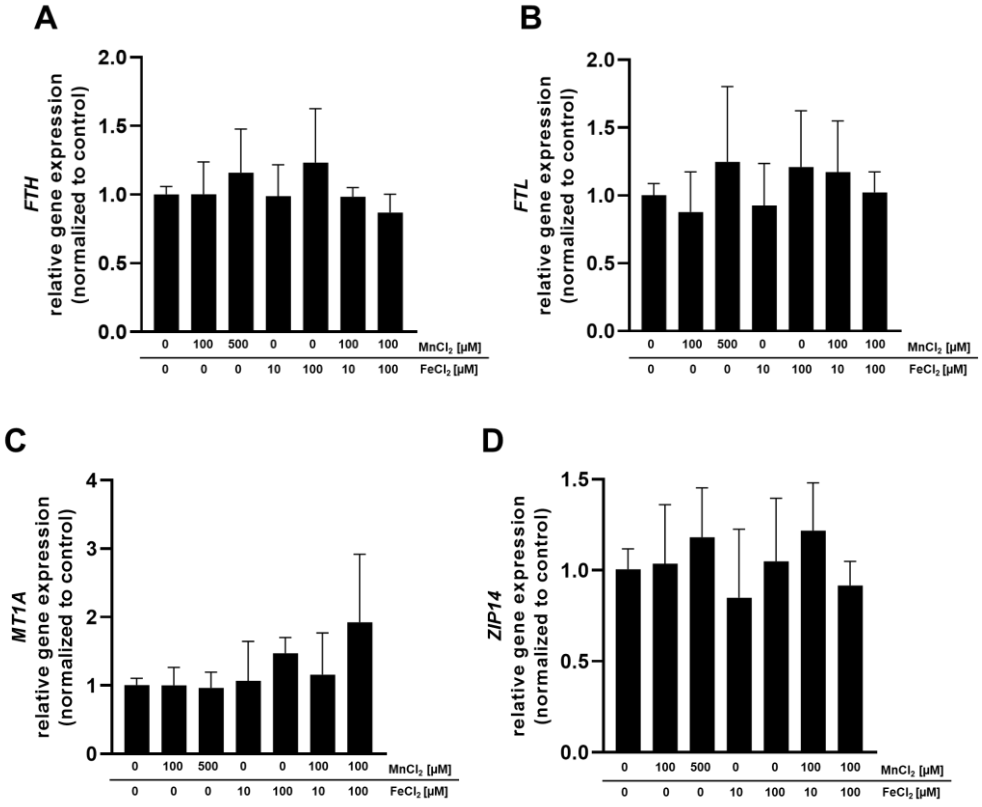

Figure S3: Relative mRNA levels of (A) *FTH*, (B) *FTL*, (C) *MT1A*, (D) *ZIP14*. Confluent BeWo b30 cells were incubated with $MnCl_2$ and/ or $FeCl_2$ for 24 h. Relative gene expression was determined using RT-qPCR and normalized to *ACTB* (β-actin) as the housekeeping gene. Shown is the mean + SD of at least three biological replicates.

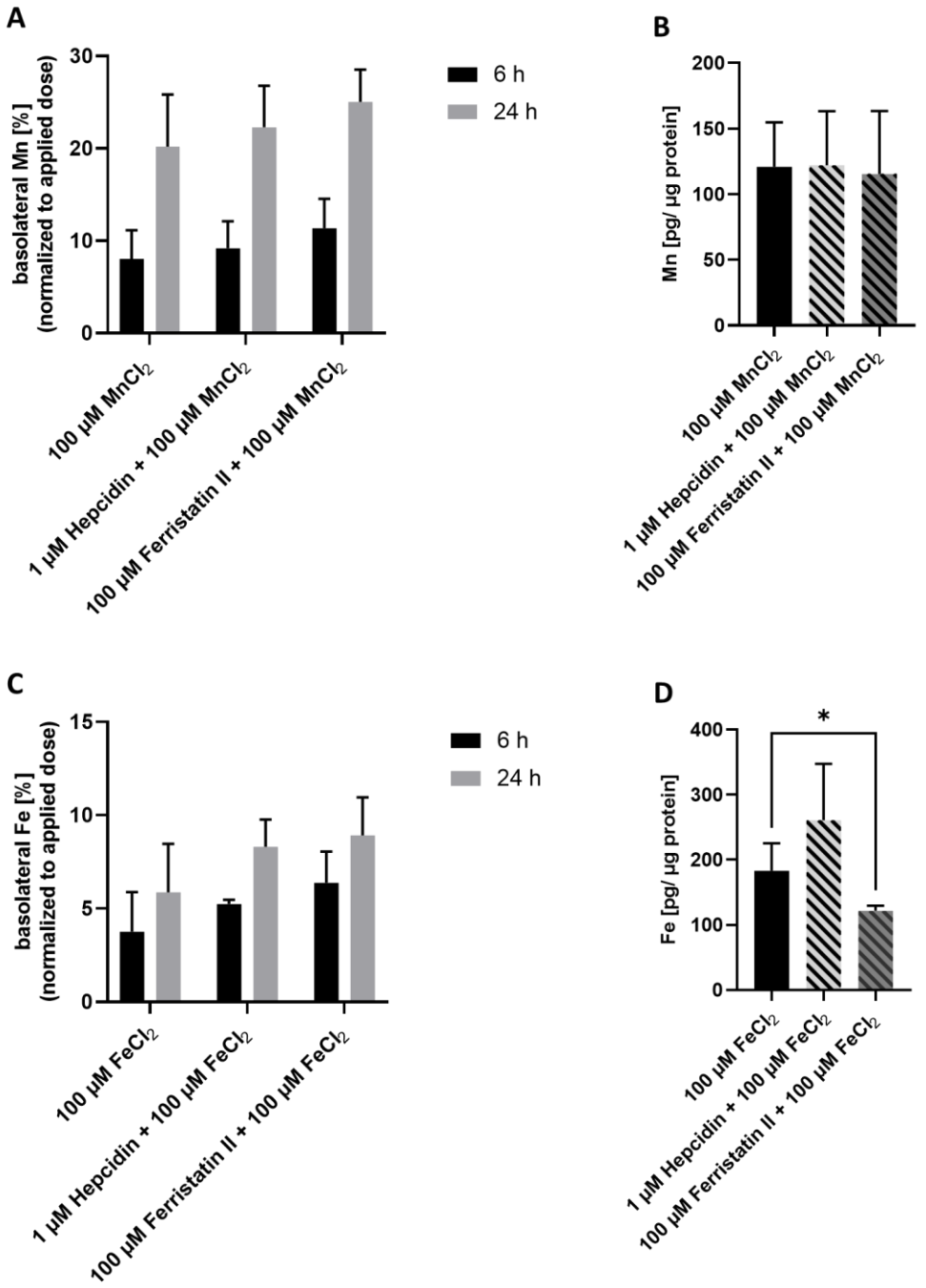

Figure S4: Basolateral (A) Mn or (C) Fe amount after 6 and 24 h and cellular (B) Mn or (D) Fe amount after 24 h of BeWo b30 cells incubated with inhibitors for DMT1 and TfR (Ferristatin II) and FPN (Hepcidin) in combination with $MnCl_2$ or $FeCl_2$. Shown is the mean + SD of at least three independent experiments with two biological replicates each. Statistical analysis based on an unpaired t test with Welch's correction is depicted as followed: *: compared to untreated control.

Supplementary Material Chapter 5

Materials and Methods – Cytotoxicity testing

Dehydrogenase activity

Dehydrogenase activity was determined by the Resazurin reduction assay, which is based on the reduction of the non-fluorescent resazurin to the fluorescent resorufin by intracellular dehydrogenases using NADH as a co-factor [654]. Briefly, after removal of the medium, cells were incubated with a 5 µg/ mL solution of resazurin (7-Hydroxy-3H-phenoxazin-3-one-10-oxide sodium salt, Sigma Aldrich) for 3 h at 37 °C and 5 % CO_2. Subsequently, fluorescence was detected using a microplate reader (Tecan® Infinite Pro M200; Ex: 530 nm; Em: 590 nm).

Results

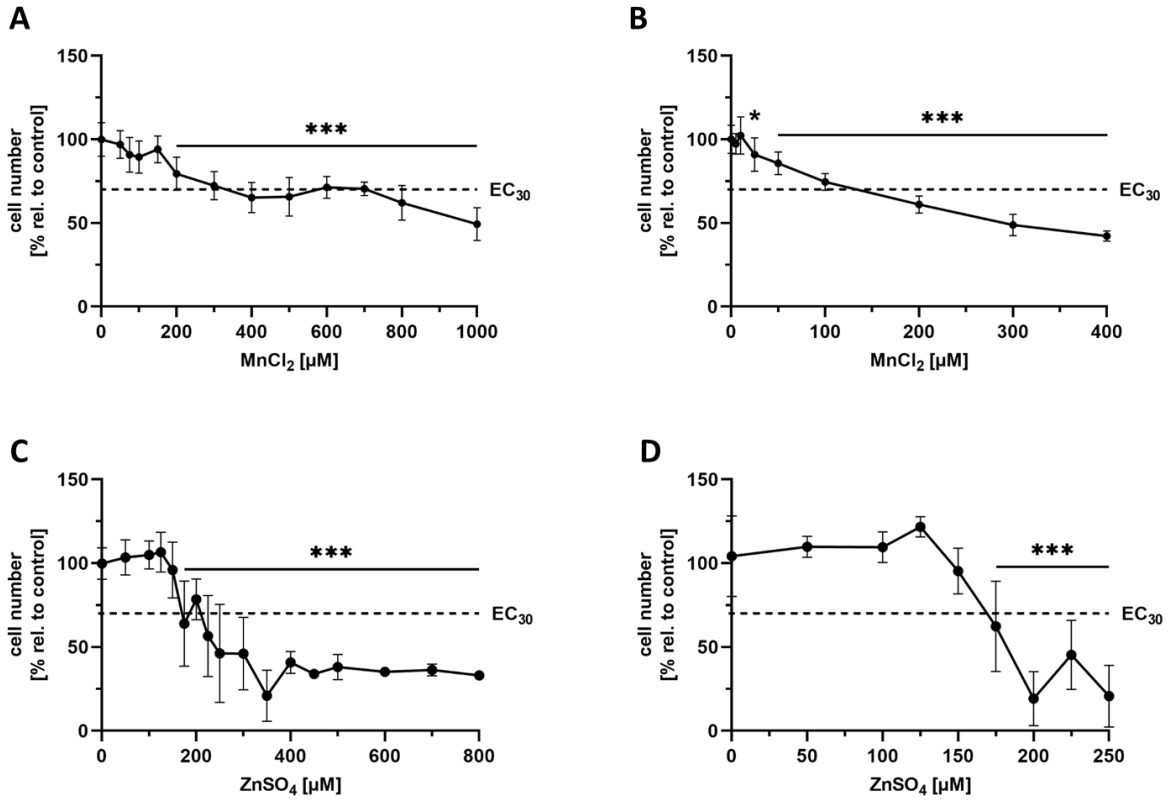

Figure S5: Mn and Zn cytotoxicity regarding cell number in HepG2 cells. Cytotoxicity was determined via Hoechst assay after 24 h or 48 h of incubation. (A) $MnCl_2$ treatment for 24 h, (B) $MnCl_2$ treatment for 48 h, (C) $ZnSO_4$ treatment for 24 h. (D) $ZnSO_4$ treatment for 48 h. Shown are the means ± SD of at least two independent experiments each. Significance values provided by one-way ANOVA with Tukey's multiple comparisons are depicted as ***p< 0.005: compared to untreated control.

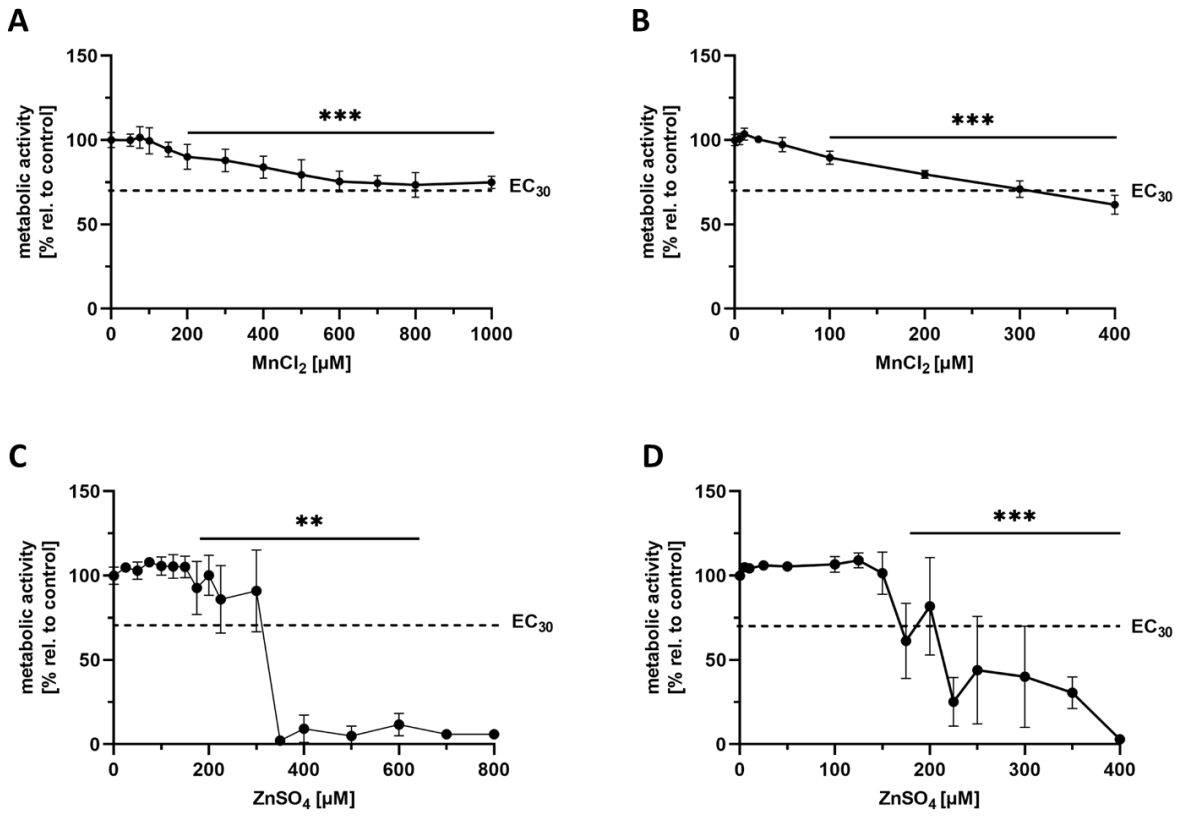

Figure S6: Mn and Zn cytotoxicity regarding metabolic activity in HepG2 cells. Cytotoxicity was determined via Resazurin Assay after 24 h or 48 h of incubation. (A) $MnCl_2$ treatment for 24 h, (B) $MnCl_2$ treatment for 48 h, (C) $ZnSO_4$ treatment for 24 h. (D) $ZnSO_4$ treatment for 48 h. Shown are the means ± SD of at least three independent experiments. Significance values provided by one-way ANOVA with Tukey's multiple comparisons are depicted as $^{**}p< 0.01$, $^{***}p< 0.005$: compared to untreated control.

Table S6: ICP-OES parameters.

Parameter	Working conditions
Plasma power [W]	1400
Cooling gas flow [L/min]	12.00
Auxiliary gas flow [L/min]	1.00
Nebulizer flow [L/min]	1.00
Nebulizer type	MicroMist®
Torch alignment	Axial Basic settings: 0.2 mm horizontal 3.8 mm vertical 3.0 mm distance
Element wavelengths	Mn: 257.611 / 259.373 Fe: 259.940 / 238.204 Cu: 324.754 / 224.700 Zn: 202.548 / 213.856

Table S7: ICP-MS/MS parameters.

Parameter	Working conditions
Plasma power [W]	1550
Cooling gas flow [L/min]	15.00
Auxiliary gas flow [L/min]	0.90
Nebulizer flow [L/min]	1.00
Nebulizer type	MicroMist®
Spray chamber	Scott-type
Torch alignment	Axial
Gas mode	He (CRC-mode)
He gas flow [L/min]	3
Transitions	Mn: 55 → 55 Fe: 56 → 56 Cu: 63 → 63 Zn: 66 → 66 Internal Standard (IS) Rh: 103 → 103

Table S8: Primer sequences of human metal transport- and storage-associated genes.

Gene name	Association	Primer sequences (5' → 3')	Amplicon length (bp)	Efficiency [%]
ACTB	β-actin	Forw.: CATCCGCAAAGACCTGTACG Rev.: TCTCCTTCTGCATCCTGTCG	86	112.6
DMT1	divalent metal transporter 1	Forw.: AGTTGGCTATCATCGGCTCA Rev.: TCTGCAATGGTGATGAGAACG	115	101.4
TfR1	transferrin receptor 1	Forw.: TGAGAGGTACAACAGCCAACT Rev.: CACGAGCAGAATACAGCCAC	107	110.6
SLC39A8 (ZIP8)	zrt-, irt-related protein 8	Forw.: TCCTGCACCTTGTCTCTCCT Rev.: AGGCTTGTCGAGTGCTCATC	124	104.7
SLC39A14 (ZIP14)	zrt-, irt-related protein 14	Forw.: CAGTCACCATGAAGCTGCTG Rev.: GGTTCTCCATAAGCCAAGCAG	80	111.5
MT1A	metallothionein 1A	Forw.: GCAAAGGGGCATCAGAGAAG Rev.: TGGGTCAGGGTTGTATGGAA	119	102.1

Continuation table S8

MT2A	metallothionein 2A	Forw.: GTTGCCTCCTCAGTGATCCT Rev.: GGCGGCAGAGATGAGTACTA	77	113.4
MTF1	metal transcription factor 1	Forw.: TCAGTCAGTGATGTTCCGCC Rev.: AGGTAGTAGAGGCTGGGGTG	87	103.2

Supplementary Material Chapter 6

Table S9: Overview of the m/z transitions used for molecule identification and quantification in MRM modus of the HPLC-MS/MS method.

Analyte	m/z		rt [min]
	Q1	Q2	
8oxodG	284	168*	6.6
		139	
		112	
8oxodG-^{13}C,-$^{15}N_2$	287	171*	6.6
		142	
		115	
dC	128	112*	5.5
		95	
dC-$^{15}N_3$	131	115*	5.5
		98	
*used as quantifier			

Table S10: MS method parameters for the analytical quantification of 8oxodG/ dC via HPLC-MS/MS method.

Parameter		Parameter	
CUR	35	CAD	Medium
IS	5500	DP	70
TEM	450	EP	10
GAS1	50	CXP	10
GAS2	50		

Table S11: HPLC gradient flow used for the separation of 8oxodG/ dC.

time [min]	A [%]	B [%]	flow [L/ min]	Max pressure [bar]
0	95	5	0.3	400
5	40	60	0.3	400
6.9	30	70	0.3	400
7	20	80	0.3	400
8	20	80	0.3	400
11.2	95	5	0.3	400
14.3	95	5	0.3	400

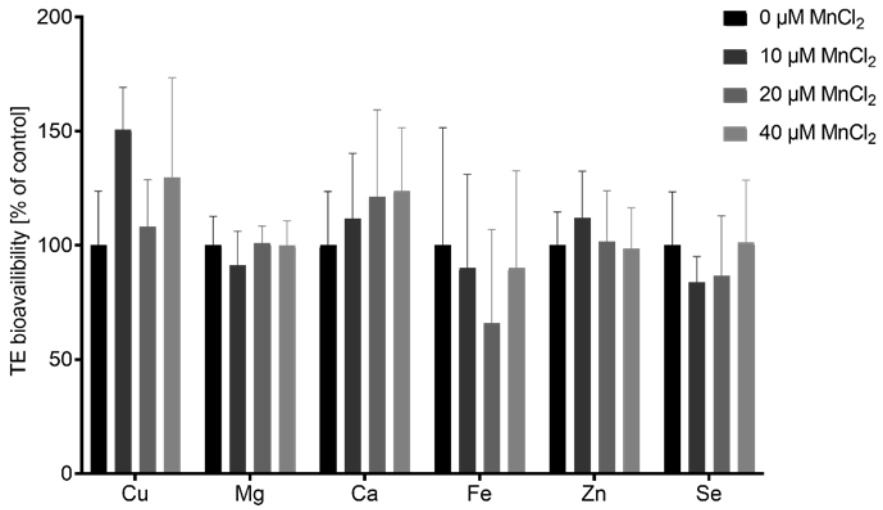

Figure S7: Comparison of the TE bioavailability after Mn exposure in differentiated LUHMES cells. Results indicate no changes in the bioavailability of copper, magnesium, calcium, iron, zinc, or selenium after 48 h exposure to 10 µM, 20 µM, or 40 µM $MnCl_2$. Data are expressed as means ± SD of at least two independent experiments.

References

1. Society, G.N. Reference values for nutrient intake. Available online: https://www.dge.de/wissenschaft/referenzwerte/?L=0 (accessed on 06.05.2022).
2. EFSA Panel on Dietetic Products, N.; Allergies. Scientific Opinion on Dietary Reference Values for iron. *EFSA Journal* **2015**, *13*, 4254, doi:https://doi.org/10.2903/j.efsa.2015.4254.
3. EFSA Panel on Dietetic Products, N.; Allergies. Scientific Opinion on Dietary Reference Values for manganese. *EFSA Journal* **2013**, *11*, 3419, doi:https://doi.org/10.2903/j.efsa.2013.3419.
4. EFSA Panel on Dietetic Products, N.; Allergies. Scientific Opinion on Dietary Reference Values for zinc. *EFSA Journal* **2014**, *12*, 3844, doi:https://doi.org/10.2903/j.efsa.2014.3844.
5. Mezzaroba, L.; Alfieri, D.F.; Colado Simão, A.N.; Vissoci Reiche, E.M. The role of zinc, copper, manganese and iron in neurodegenerative diseases. *Neurotoxicology* **2019**, *74*, 230-241, doi:10.1016/j.neuro.2019.07.007.
6. Zaugg, J.; Solenthaler, F.; Albrecht, C. Materno-fetal iron transfer and the emerging role of ferroptosis pathways. *Biochem Pharmacol* **2022**, *202*, 115141, doi:10.1016/j.bcp.2022.115141.
7. Smith, E.R.; He, S.; Klatt, K.C.; Barberio, M.D.; Rahnavard, A.; Azad, N.; Brandt, C.; Harker, B.; Hogan, E.; Kucherlapaty, P.; et al. Limited data exist to inform our basic understanding of micronutrient requirements in pregnancy. *Sci Adv* **2021**, *7*, eabj8016, doi:10.1126/sciadv.abj8016.
8. Chen, P.; Bornhorst, J.; Aschner, M. Manganese metabolism in humans. *Front Biosci (Landmark Ed)* **2018**, *23*, 1655-1679, doi:10.2741/4665.
9. Kondaiah, P.; Aslam, M.F.; Mashurabad, P.C.; Sharp, P.A.; Pullakhandam, R. Zinc induces iron uptake and DMT1 expression in Caco-2 cells via a PI3K/IRP2 dependent mechanism. *Biochem J* **2019**, *476*, 1573-1583, doi:10.1042/bcj20180939.
10. Bjørklund, G.; Aaseth, J.; Skalny, A.V.; Suliburska, J.; Skalnaya, M.G.; Nikonorov, A.A.; Tinkov, A.A. Interactions of iron with manganese, zinc, chromium, and selenium as related to prophylaxis and treatment of iron deficiency. *J Trace Elem Med Biol* **2017**, *41*, 41-53, doi:10.1016/j.jtemb.2017.02.005.
11. Freeland-Graves, J.H.; Sanjeevi, N.; Lee, J.J. Global perspectives on trace element requirements. *J Trace Elem Med Biol* **2015**, *31*, 135-141, doi:10.1016/j.jtemb.2014.04.006.
12. Chojnacka, K. Introduction. In *Recent Advances in Trace Elements*; 2018; pp. 1-10.
13. Post, J.E. Manganese oxide minerals: crystal structures and economic and environmental significance. *Proc Natl Acad Sci U S A* **1999**, *96*, 3447-3454, doi:10.1073/pnas.96.7.3447.
14. Au, C.; Benedetto, A.; Aschner, M. Manganese transport in eukaryotes: the role of DMT1. *Neurotoxicology* **2008**, *29*, 569-576, doi:10.1016/j.neuro.2008.04.022.
15. Williams, M.; Todd, G.D.; Roney, N.; Crawford, J.; Coles, C.; McClure, P.R.; Garey, J.D.; Zaccaria, K.; Citra, M. Agency for Toxic Substances and Disease Registry (ATSDR) Toxicological Profiles. In *Toxicological Profile for Manganese*; Agency for Toxic Substances and Disease Registry (US): Atlanta (GA), 2012.
16. Crowley, J.D.; Traynor, D.A.; Weatherburn, D.C. Enzymes and proteins containing manganese: an overview. *Met Ions Biol Syst* **2000**, *37*, 209-278.
17. Ljung, K.; Palm, B.; Grandér, M.; Vahter, M. High concentrations of essential and toxic elements in infant formula and infant foods - A matter of concern. *Food Chem* **2011**, *127*, 943-951, doi:10.1016/j.foodchem.2011.01.062.
18. Davidsson, L.; Cederblad, A.; Lönnerdal, B.; Sandström, B. Manganese retention in man: a method for estimating manganese absorption in man. *Am J Clin Nutr* **1989**, *49*, 170-179, doi:10.1093/ajcn/49.1.170.
19. Erikson, K.M.; Thompson, K.; Aschner, J.; Aschner, M. Manganese neurotoxicity: a focus on the neonate. *Pharmacol Ther* **2007**, *113*, 369-377, doi:10.1016/j.pharmthera.2006.09.002.
20. Shawki, A.; Anthony, S.R.; Nose, Y.; Engevik, M.A.; Niespodzany, E.J.; Barrientos, T.; Öhrvik, H.; Worrell, R.T.; Thiele, D.J.; Mackenzie, B. Intestinal DMT1 is critical for iron absorption in the mouse but is not required for the absorption of copper or manganese. *Am J Physiol Gastrointest Liver Physiol* **2015**, *309*, G635-647, doi:10.1152/ajpgi.00160.2015.

21. Aydemir, T.B.; Kim, M.H.; Kim, J.; Colon-Perez, L.M.; Banan, G.; Mareci, T.H.; Febo, M.; Cousins, R.J. Metal Transporter Zip14 (Slc39a14) Deletion in Mice Increases Manganese Deposition and Produces Neurotoxic Signatures and Diminished Motor Activity. *J Neurosci* **2017**, *37*, 5996-6006, doi:10.1523/jneurosci.0285-17.2017.
22. Bowman, A.B.; Kwakye, G.F.; Herrero Hernández, E.; Aschner, M. Role of manganese in neurodegenerative diseases. *J Trace Elem Med Biol* **2011**, *25*, 191-203, doi:10.1016/j.jtemb.2011.08.144.
23. Tripathi, A.K.; Haldar, S.; Qian, J.; Beserra, A.; Suda, S.; Singh, A.; Hopfer, U.; Chen, S.G.; Garrick, M.D.; Turner, J.R.; et al. Prion protein functions as a ferrireductase partner for ZIP14 and DMT1. *Free Radic Biol Med* **2015**, *84*, 322-330, doi:10.1016/j.freeradbiomed.2015.03.037.
24. Lin, W.; Vann, D.R.; Doulias, P.T.; Wang, T.; Landesberg, G.; Li, X.; Ricciotti, E.; Scalia, R.; He, M.; Hand, N.J.; et al. Hepatic metal ion transporter ZIP8 regulates manganese homeostasis and manganese-dependent enzyme activity. *J Clin Invest* **2017**, *127*, 2407-2417, doi:10.1172/jci90896.
25. Chua, A.C.; Herbison, C.E.; Drake, S.F.; Graham, R.M.; Olynyk, J.K.; Trinder, D. The role of Hfe in transferrin-bound iron uptake by hepatocytes. *Hepatology* **2008**, *47*, 1737-1744, doi:10.1002/hep.22180.
26. Mukhopadhyay, S. Familial manganese-induced neurotoxicity due to mutations in SLC30A10 or SLC39A14. *Neurotoxicology* **2018**, *64*, 278-283, doi:10.1016/j.neuro.2017.07.030.
27. Ye, Q.; Park, J.E.; Gugnani, K.; Betharia, S.; Pino-Figueroa, A.; Kim, J. Influence of iron metabolism on manganese transport and toxicity. *Metallomics* **2017**, *9*, 1028-1046, doi:10.1039/c7mt00079k.
28. Balachandran, R.C.; Mukhopadhyay, S.; McBride, D.; Veevers, J.; Harrison, F.E.; Aschner, M.; Haynes, E.N.; Bowman, A.B. Brain manganese and the balance between essential roles and neurotoxicity. *J Biol Chem* **2020**, *295*, 6312-6329, doi:10.1074/jbc.REV119.009453.
29. Frisbie, S.H.; Mitchell, E.J.; Dustin, H.; Maynard, D.M.; Sarkar, B. World Health Organization discontinues its drinking-water guideline for manganese. *Environ Health Perspect* **2012**, *120*, 775-778, doi:10.1289/ehp.1104693.
30. Rahman, S.M.; Kippler, M.; Tofail, F.; Bölte, S.; Hamadani, J.D.; Vahter, M. Manganese in Drinking Water and Cognitive Abilities and Behavior at 10 Years of Age: A Prospective Cohort Study. *Environ Health Perspect* **2017**, *125*, 057003, doi:10.1289/ehp631.
31. Lin, Y.Y.; Hwang, Y.H.; Chen, P.C.; Chen, B.Y.; Wen, H.J.; Liu, J.H.; Guo, Y.L. Contribution of gestational exposure to ambient traffic air pollutants to fetal cord blood manganese. *Environ Res* **2012**, *112*, 1-7, doi:10.1016/j.envres.2011.11.006.
32. Hassani, H.; Golbabaei, F.; Shirkhanloo, H.; Tehrani-Doust, M. Relations of biomarkers of manganese exposure and neuropsychological effects among welders and ferroalloy smelters. *Ind Health* **2016**, *54*, 79-86, doi:10.2486/indhealth.2014-0250.
33. Crossgrove, J.; Zheng, W. Manganese toxicity upon overexposure. *NMR Biomed* **2004**, *17*, 544-553, doi:10.1002/nbm.931.
34. Livingstone, C. Manganese Provision in Parenteral Nutrition: An Update. *Nutr Clin Pract* **2018**, *33*, 404-418, doi:10.1177/0884533617702837.
35. Peres, T.V.; Schettinger, M.R.; Chen, P.; Carvalho, F.; Avila, D.S.; Bowman, A.B.; Aschner, M. "Manganese-induced neurotoxicity: a review of its behavioral consequences and neuroprotective strategies". *BMC Pharmacol Toxicol* **2016**, *17*, 57, doi:10.1186/s40360-016-0099-0.
36. Kwakye, G.F.; Paoliello, M.M.; Mukhopadhyay, S.; Bowman, A.B.; Aschner, M. Manganese-Induced Parkinsonism and Parkinson's Disease: Shared and Distinguishable Features. *Int J Environ Res Public Health* **2015**, *12*, 7519-7540, doi:10.3390/ijerph120707519.
37. Guilarte, T.R.; Gonzales, K.K. Manganese-Induced Parkinsonism Is Not Idiopathic Parkinson's Disease: Environmental and Genetic Evidence. *Toxicol Sci* **2015**, *146*, 204-212, doi:10.1093/toxsci/kfv099.
38. Ellingsen, D.G.; Shvartsman, G.; Bast-Pettersen, R.; Chashchin, M.; Thomassen, Y.; Chashchin, V. Neurobehavioral performance of patients diagnosed with manganism and idiopathic

Parkinson disease. *Int Arch Occup Environ Health* **2019**, *92*, 383-394, doi:10.1007/s00420-019-01415-6.
39. Roth, J.A. Chapter 9 Mutual Neurotoxic Mechanisms Controlling Manganism and Parkisonism. In *Manganese in Health and Disease*; The Royal Society of Chemistry: 2015; pp. 221-257.
40. Tinkov, A.A.; Paoliello, M.M.B.; Mazilina, A.N.; Skalny, A.V.; Martins, A.C.; Voskresenskaya, O.N.; Aaseth, J.; Santamaria, A.; Notova, S.V.; Tsatsakis, A.; et al. Molecular Targets of Manganese-Induced Neurotoxicity: A Five-Year Update. *Int J Mol Sci* **2021**, *22*, doi:10.3390/ijms22094646.
41. Stephenson, A.P.; Schneider, J.A.; Nelson, B.C.; Atha, D.H.; Jain, A.; Soliman, K.F.; Aschner, M.; Mazzio, E.; Renee Reams, R. Manganese-induced oxidative DNA damage in neuronal SH-SY5Y cells: attenuation of thymine base lesions by glutathione and N-acetylcysteine. *Toxicol Lett* **2013**, *218*, 299-307, doi:10.1016/j.toxlet.2012.12.024.
42. Park, J.H.; Hogrebe, M.; Grüneberg, M.; DuChesne, I.; von der Heiden, A.L.; Reunert, J.; Schlingmann, K.P.; Boycott, K.M.; Beaulieu, C.L.; Mhanni, A.A.; et al. SLC39A8 Deficiency: A Disorder of Manganese Transport and Glycosylation. *Am J Hum Genet* **2015**, *97*, 894-903, doi:10.1016/j.ajhg.2015.11.003.
43. Tuschl, K.; Meyer, E.; Valdivia, L.E.; Zhao, N.; Dadswell, C.; Abdul-Sada, A.; Hung, C.Y.; Simpson, M.A.; Chong, W.K.; Jacques, T.S.; et al. Mutations in SLC39A14 disrupt manganese homeostasis and cause childhood-onset parkinsonism-dystonia. *Nat Commun* **2016**, *7*, 11601, doi:10.1038/ncomms11601.
44. Aydemir, T.B.; Thorn, T.L.; Ruggiero, C.H.; Pompilus, M.; Febo, M.; Cousins, R.J. Intestine-specific deletion of metal transporter Zip14 (Slc39a14) causes brain manganese overload and locomotor defects of manganism. *Am J Physiol Gastrointest Liver Physiol* **2020**, *318*, G673-g681, doi:10.1152/ajpgi.00301.2019.
45. Xin, Y.; Gao, H.; Wang, J.; Qiang, Y.; Imam, M.U.; Li, Y.; Wang, J.; Zhang, R.; Zhang, H.; Yu, Y.; et al. Manganese transporter Slc39a14 deficiency revealed its key role in maintaining manganese homeostasis in mice. *Cell Discov* **2017**, *3*, 17025, doi:10.1038/celldisc.2017.25.
46. Quadri, M.; Federico, A.; Zhao, T.; Breedveld, G.J.; Battisti, C.; Delnooz, C.; Severijnen, L.A.; Di Toro Mammarella, L.; Mignarri, A.; Monti, L.; et al. Mutations in SLC30A10 cause parkinsonism and dystonia with hypermanganesemia, polycythemia, and chronic liver disease. *Am J Hum Genet* **2012**, *90*, 467-477, doi:10.1016/j.ajhg.2012.01.017.
47. Mercadante, C.J.; Prajapati, M.; Conboy, H.L.; Dash, M.E.; Herrera, C.; Pettiglio, M.A.; Cintron-Rivera, L.; Salesky, M.A.; Rao, D.B.; Bartnikas, T.B. Manganese transporter Slc30a10 controls physiological manganese excretion and toxicity. *J Clin Invest* **2019**, *129*, 5442-5461, doi:10.1172/jci129710.
48. Group, F.-N.B.W. BEST (Biomarkers, EndpointS, and other Tools) Resource. Food and Drug Administration (US) National Institutes of Health (US): Silver Spring (MD) Bethesda (MD), 2016.
49. Silins, I.; Högberg, J. Combined toxic exposures and human health: biomarkers of exposure and effect. *Int J Environ Res Public Health* **2011**, *8*, 629-647, doi:10.3390/ijerph8030629.
50. Rolle-McFarland, D.; Liu, Y.; Zhou, J.; Mostafaei, F.; Zhou, Y.; Li, Y.; Fan, Q.; Zheng, W.; Nie, L.H.; Wells, E.M. Development of a Cumulative Exposure Index (CEI) for Manganese and Comparison with Bone Manganese and Other Biomarkers of Manganese Exposure. *Int J Environ Res Public Health* **2018**, *15*, doi:10.3390/ijerph15071341.
51. Smith, D.; Gwiazda, R.; Bowler, R.; Roels, H.; Park, R.; Taicher, C.; Lucchini, R. Biomarkers of Mn exposure in humans. *Am J Ind Med* **2007**, *50*, 801-811, doi:10.1002/ajim.20506.
52. Zheng, W.; Fu, S.X.; Dydak, U.; Cowan, D.M. Biomarkers of manganese intoxication. *Neurotoxicology* **2011**, *32*, 1-8, doi:10.1016/j.neuro.2010.10.002.
53. Greger, J.L. Nutrition versus toxicology of manganese in humans: evaluation of potential biomarkers. *Neurotoxicology* **1999**, *20*, 205-212.

54. Wang, D.; Du, X.; Zheng, W. Alteration of saliva and serum concentrations of manganese, copper, zinc, cadmium and lead among career welders. *Toxicol Lett* **2008**, *176*, 40-47, doi:10.1016/j.toxlet.2007.10.003.
55. Arora, M.; Bradman, A.; Austin, C.; Vedar, M.; Holland, N.; Eskenazi, B.; Smith, D.R. Determining fetal manganese exposure from mantle dentine of deciduous teeth. *Environ Sci Technol* **2012**, *46*, 5118-5125, doi:10.1021/es203569f.
56. Liu, W.; Xin, Y.; Li, Q.; Shang, Y.; Ping, Z.; Min, J.; Cahill, C.M.; Rogers, J.T.; Wang, F. Biomarkers of environmental manganese exposure and associations with childhood neurodevelopment: a systematic review and meta-analysis. *Environ Health* **2020**, *19*, 104, doi:10.1186/s12940-020-00659-x.
57. Bauer, J.A.; Claus Henn, B.; Austin, C.; Zoni, S.; Fedrighi, C.; Cagna, G.; Placidi, D.; White, R.F.; Yang, Q.; Coull, B.A.; et al. Manganese in teeth and neurobehavior: Sex-specific windows of susceptibility. *Environ Int* **2017**, *108*, 299-308, doi:10.1016/j.envint.2017.08.013.
58. Skröder, H.; Kippler, M.; Nermell, B.; Tofail, F.; Levi, M.; Rahman, S.M.; Raqib, R.; Vahter, M. Major Limitations in Using Element Concentrations in Hair as Biomarkers of Exposure to Toxic and Essential Trace Elements in Children. *Environ Health Perspect* **2017**, *125*, 067021, doi:10.1289/ehp1239.
59. Ward, E.J.; Edmondson, D.A.; Nour, M.M.; Snyder, S.; Rosenthal, F.S.; Dydak, U. Toenail Manganese: A Sensitive and Specific Biomarker of Exposure to Manganese in Career Welders. *Ann Work Expo Health* **2017**, *62*, 101-111, doi:10.1093/annweh/wxx091.
60. Ryde, S.J.S. In Vivo Neutron Activation Analysis. In Proceedings of the Quality of the Body Cell Mass, New York, NY, 2000//, 2000; pp. 103-118.
61. Jiang, Y.; Zheng, W.; Long, L.; Zhao, W.; Li, X.; Mo, X.; Lu, J.; Fu, X.; Li, W.; Liu, S.; et al. Brain magnetic resonance imaging and manganese concentrations in red blood cells of smelting workers: search for biomarkers of manganese exposure. *Neurotoxicology* **2007**, *28*, 126-135, doi:10.1016/j.neuro.2006.08.005.
62. Lucchini, R.; Albini, E.; Placidi, D.; Gasparotti, R.; Pigozzi, M.G.; Montani, G.; Alessio, L. Brain magnetic resonance imaging and manganese exposure. *Neurotoxicology* **2000**, *21*, 769-775.
63. Pejović-Milić, A.; Chettle, D.R.; Oudyk, J.; Pysklywec, M.W.; Haines, T. Bone manganese as a biomarker of manganese exposure: a feasibility study. *Am J Ind Med* **2009**, *52*, 742-750, doi:10.1002/ajim.20737.
64. Baker, M.G.; Simpson, C.D.; Stover, B.; Sheppard, L.; Checkoway, H.; Racette, B.A.; Seixas, N.S. Blood manganese as an exposure biomarker: state of the evidence. *J Occup Environ Hyg* **2014**, *11*, 210-217, doi:10.1080/15459624.2013.852280.
65. Laohaudomchok, W.; Lin, X.; Herrick, R.F.; Fang, S.C.; Cavallari, J.M.; Christiani, D.C.; Weisskopf, M.G. Toenail, blood, and urine as biomarkers of manganese exposure. *J Occup Environ Med* **2011**, *53*, 506-510, doi:10.1097/JOM.0b013e31821854da.
66. Claus Henn, B.; Bellinger, D.C.; Hopkins, M.R.; Coull, B.A.; Ettinger, A.S.; Jim, R.; Hatley, E.; Christiani, D.C.; Wright, R.O. Maternal and Cord Blood Manganese Concentrations and Early Childhood Neurodevelopment among Residents near a Mining-Impacted Superfund Site. *Environ Health Perspect* **2017**, *125*, 067020, doi:10.1289/ehp925.
67. Kornberg, T.G.; Stueckle, T.A.; Antonini, J.A.; Rojanasakul, Y.; Castranova, V.; Yang, Y.; Wang, L. Potential Toxicity and Underlying Mechanisms Associated with Pulmonary Exposure to Iron Oxide Nanoparticles: Conflicting Literature and Unclear Risk. *Nanomaterials (Basel)* **2017**, *7*, doi:10.3390/nano7100307.
68. Duck, K.A.; Connor, J.R. Iron uptake and transport across physiological barriers. *Biometals* **2016**, *29*, 573-591, doi:10.1007/s10534-016-9952-2.
69. Galaris, D.; Barbouti, A.; Pantopoulos, K. Iron homeostasis and oxidative stress: An intimate relationship. *Biochim Biophys Acta Mol Cell Res* **2019**, *1866*, 118535, doi:10.1016/j.bbamcr.2019.118535.
70. Chevion, M. A site-specific mechanism for free radical induced biological damage: the essential role of redox-active transition metals. *Free Radic Biol Med* **1988**, *5*, 27-37, doi:10.1016/0891-5849(88)90059-7.

71. Brissot, P.; Ropert, M.; Le Lan, C.; Loréal, O. Non-transferrin bound iron: a key role in iron overload and iron toxicity. *Biochim Biophys Acta* **2012**, *1820*, 403-410, doi:10.1016/j.bbagen.2011.07.014.
72. Donovan, A.; Lima, C.A.; Pinkus, J.L.; Pinkus, G.S.; Zon, L.I.; Robine, S.; Andrews, N.C. The iron exporter ferroportin/Slc40a1 is essential for iron homeostasis. *Cell Metab* **2005**, *1*, 191-200, doi:10.1016/j.cmet.2005.01.003.
73. Himeno, S.; Yanagiya, T.; Fujishiro, H. The role of zinc transporters in cadmium and manganese transport in mammalian cells. *Biochimie* **2009**, *91*, 1218-1222, doi:10.1016/j.biochi.2009.04.002.
74. Vesey, D.A. Transport pathways for cadmium in the intestine and kidney proximal tubule: focus on the interaction with essential metals. *Toxicol Lett* **2010**, *198*, 13-19, doi:10.1016/j.toxlet.2010.05.004.
75. Wang, C.Y.; Jenkitkasemwong, S.; Duarte, S.; Sparkman, B.K.; Shawki, A.; Mackenzie, B.; Knutson, M.D. ZIP8 is an iron and zinc transporter whose cell-surface expression is up-regulated by cellular iron loading. *J Biol Chem* **2012**, *287*, 34032-34043, doi:10.1074/jbc.M112.367284.
76. Jenkitkasemwong, S.; Wang, C.Y.; Mackenzie, B.; Knutson, M.D. Physiologic implications of metal-ion transport by ZIP14 and ZIP8. *Biometals* **2012**, *25*, 643-655, doi:10.1007/s10534-012-9526-x.
77. Chen, A.C.; Donovan, A.; Ned-Sykes, R.; Andrews, N.C. Noncanonical role of transferrin receptor 1 is essential for intestinal homeostasis. *Proc Natl Acad Sci U S A* **2015**, *112*, 11714-11719, doi:10.1073/pnas.1511701112.
78. Nemeth, E.; Tuttle, M.S.; Powelson, J.; Vaughn, M.B.; Donovan, A.; Ward, D.M.; Ganz, T.; Kaplan, J. Hepcidin regulates cellular iron efflux by binding to ferroportin and inducing its internalization. *Science* **2004**, *306*, 2090-2093, doi:10.1126/science.1104742.
79. Aschemeyer, S.; Qiao, B.; Stefanova, D.; Valore, E.V.; Sek, A.C.; Ruwe, T.A.; Vieth, K.R.; Jung, G.; Casu, C.; Rivella, S.; et al. Structure-function analysis of ferroportin defines the binding site and an alternative mechanism of action of hepcidin. *Blood* **2018**, *131*, 899-910, doi:10.1182/blood-2017-05-786590.
80. Qiao, B.; Sugianto, P.; Fung, E.; Del-Castillo-Rueda, A.; Moran-Jimenez, M.J.; Ganz, T.; Nemeth, E. Hepcidin-induced endocytosis of ferroportin is dependent on ferroportin ubiquitination. *Cell Metab* **2012**, *15*, 918-924, doi:10.1016/j.cmet.2012.03.018.
81. Gao, G.; Li, J.; Zhang, Y.; Chang, Y.Z. Cellular Iron Metabolism and Regulation. *Adv Exp Med Biol* **2019**, *1173*, 21-32, doi:10.1007/978-981-13-9589-5_2.
82. Knez, M.; Graham, R.D.; Welch, R.M.; Stangoulis, J.C. New perspectives on the regulation of iron absorption via cellular zinc concentrations in humans. *Crit Rev Food Sci Nutr* **2017**, *57*, 2128-2143, doi:10.1080/10408398.2015.1050483.
83. Marro, S.; Chiabrando, D.; Messana, E.; Stolte, J.; Turco, E.; Tolosano, E.; Muckenthaler, M.U. Heme controls ferroportin1 (FPN1) transcription involving Bach1, Nrf2 and a MARE/ARE sequence motif at position -7007 of the FPN1 promoter. *Haematologica* **2010**, *95*, 1261-1268, doi:10.3324/haematol.2009.020123.
84. Taher, A.T. Thalassemia. *Hematol Oncol Clin North Am* **2018**, *32*, xv-xvi, doi:10.1016/j.hoc.2017.12.003.
85. Pasricha, S.R.; Tye-Din, J.; Muckenthaler, M.U.; Swinkels, D.W. Iron deficiency. *Lancet* **2021**, *397*, 233-248, doi:10.1016/s0140-6736(20)32594-0.
86. Ginzburg, Y.; Rivella, S. β-thalassemia: a model for elucidating the dynamic regulation of ineffective erythropoiesis and iron metabolism. *Blood* **2011**, *118*, 4321-4330, doi:10.1182/blood-2011-03-283614.
87. Huang, X.; Atwood, C.S.; Moir, R.D.; Hartshorn, M.A.; Tanzi, R.E.; Bush, A.I. Trace metal contamination initiates the apparent auto-aggregation, amyloidosis, and oligomerization of Alzheimer's Abeta peptides. *J Biol Inorg Chem* **2004**, *9*, 954-960, doi:10.1007/s00775-004-0602-8.

88. Liu, B.; Moloney, A.; Meehan, S.; Morris, K.; Thomas, S.E.; Serpell, L.C.; Hider, R.; Marciniak, S.J.; Lomas, D.A.; Crowther, D.C. Iron promotes the toxicity of amyloid beta peptide by impeding its ordered aggregation. *J Biol Chem* **2011**, *286*, 4248-4256, doi:10.1074/jbc.M110.158980.
89. Belaidi, A.A.; Bush, A.I. Iron neurochemistry in Alzheimer's disease and Parkinson's disease: targets for therapeutics. *J Neurochem* **2016**, *139 Suppl 1*, 179-197, doi:10.1111/jnc.13425.
90. Rogers, J.T.; Randall, J.D.; Cahill, C.M.; Eder, P.S.; Huang, X.; Gunshin, H.; Leiter, L.; McPhee, J.; Sarang, S.S.; Utsuki, T.; et al. An iron-responsive element type II in the 5'-untranslated region of the Alzheimer's amyloid precursor protein transcript. *J Biol Chem* **2002**, *277*, 45518-45528, doi:10.1074/jbc.M207435200.
91. Febbraro, F.; Giorgi, M.; Caldarola, S.; Loreni, F.; Romero-Ramos, M. α-Synuclein expression is modulated at the translational level by iron. *Neuroreport* **2012**, *23*, 576-580, doi:10.1097/WNR.0b013e328354a1f0.
92. Costain, G.; Ghosh, M.C.; Maio, N.; Carnevale, A.; Si, Y.C.; Rouault, T.A.; Yoon, G. Absence of iron-responsive element-binding protein 2 causes a novel neurodegenerative syndrome. *Brain* **2019**, *142*, 1195-1202, doi:10.1093/brain/awz072.
93. Cooperman, S.S.; Meyron-Holtz, E.G.; Olivierre-Wilson, H.; Ghosh, M.C.; McConnell, J.P.; Rouault, T.A. Microcytic anemia, erythropoietic protoporphyria, and neurodegeneration in mice with targeted deletion of iron-regulatory protein 2. *Blood* **2005**, *106*, 1084-1091, doi:10.1182/blood-2004-12-4703.
94. LaVaute, T.; Smith, S.; Cooperman, S.; Iwai, K.; Land, W.; Meyron-Holtz, E.; Drake, S.K.; Miller, G.; Abu-Asab, M.; Tsokos, M.; et al. Targeted deletion of the gene encoding iron regulatory protein-2 causes misregulation of iron metabolism and neurodegenerative disease in mice. *Nat Genet* **2001**, *27*, 209-214, doi:10.1038/84859.
95. Pantopoulos, K. Inherited Disorders of Iron Overload. *Front Nutr* **2018**, *5*, 103, doi:10.3389/fnut.2018.00103.
96. Simon, M.; Alexandre, J.L.; Bourel, M.; Le Marec, B.; Scordia, C. Heredity of idiopathic haemochromatosis: a study of 106 families. *Clin Genet* **1977**, *11*, 327-341, doi:10.1111/j.1399-0004.1977.tb01324.x.
97. Brissot, P.; Loréal, O. Hemochromatoses. *J Hepatol* **2021**, *75*, 723-724, doi:10.1016/j.jhep.2021.04.001.
98. Drakesmith, H. Next-Generation Biomarkers for Iron Status. *Nestle Nutr Inst Workshop Ser* **2016**, *84*, 59-69, doi:10.1159/000436955.
99. Zimmermann, M.B. Methods to assess iron and iodine status. *Br J Nutr* **2008**, *99 Suppl 3*, S2-9, doi:10.1017/s000711450800679x.
100. Pfeiffer, C.M.; Looker, A.C. Laboratory methodologies for indicators of iron status: strengths, limitations, and analytical challenges. *Am J Clin Nutr* **2017**, *106*, 1606s-1614s, doi:10.3945/ajcn.117.155887.
101. Karakochuk, C.D.; Hess, S.Y.; Moorthy, D.; Namaste, S.; Parker, M.E.; Rappaport, A.I.; Wegmüller, R.; Dary, O. Measurement and interpretation of hemoglobin concentration in clinical and field settings: a narrative review. *Ann N Y Acad Sci* **2019**, *1450*, 126-146, doi:10.1111/nyas.14003.
102. World Health, O. *Serum ferritin concentrations for the assessment of iron status and iron deficiency in populations*; World Health Organization: Geneva, 2011 2011.
103. Hare, D.J. Hepcidin: a real-time biomarker of iron need. *Metallomics* **2017**, *9*, 606-618, doi:10.1039/c7mt00047b.
104. Roney, N.; Osier, M.; Paikoff, S.J.; Smith, C.V.; Williams, M.; De Rosa, C.T. ATSDR evaluation of potential for human exposure to zinc. *Toxicology and Industrial Health* **2007**, *23*, 247-308, doi:10.1177/0748233707083761.
105. Skalny, A.V.; Aschner, M.; Tinkov, A.A. Zinc. *Adv Food Nutr Res* **2021**, *96*, 251-310, doi:10.1016/bs.afnr.2021.01.003.
106. Kambe, T.; Tsuji, T.; Hashimoto, A.; Itsumura, N. The Physiological, Biochemical, and Molecular Roles of Zinc Transporters in Zinc Homeostasis and Metabolism. *Physiol Rev* **2015**, *95*, 749-784, doi:10.1152/physrev.00035.2014.

107. Cassandri, M.; Smirnov, A.; Novelli, F.; Pitolli, C.; Agostini, M.; Malewicz, M.; Melino, G.; Raschellà, G. Zinc-finger proteins in health and disease. *Cell Death Discov* **2017**, *3*, 17071, doi:10.1038/cddiscovery.2017.71.
108. Livingstone, C. Zinc: physiology, deficiency, and parenteral nutrition. *Nutr Clin Pract* **2015**, *30*, 371-382, doi:10.1177/0884533615570376.
109. Haase, H.; Ellinger, S.; Linseisen, J.; Neuhäuser-Berthold, M.; Richter, M. Revised D-A-CH-reference values for the intake of zinc. *J Trace Elem Med Biol* **2020**, *61*, 126536, doi:10.1016/j.jtemb.2020.126536.
110. Ford, D. Intestinal and placental zinc transport pathways. *Proc Nutr Soc* **2004**, *63*, 21-29, doi:10.1079/pns2003320.
111. Wang, X.; Zhou, B. Dietary zinc absorption: A play of Zips and ZnTs in the gut. *IUBMB Life* **2010**, *62*, 176-182, doi:10.1002/iub.291.
112. Krebs, N.F. Overview of zinc absorption and excretion in the human gastrointestinal tract. *J Nutr* **2000**, *130*, 1374s-1377s, doi:10.1093/jn/130.5.1374S.
113. Maret, W. Zinc in Cellular Regulation: The Nature and Significance of "Zinc Signals". *Int J Mol Sci* **2017**, *18*, doi:10.3390/ijms18112285.
114. Yasuno, T.; Okamoto, H.; Nagai, M.; Kimura, S.; Yamamoto, T.; Nagano, K.; Furubayashi, T.; Yoshikawa, Y.; Yasui, H.; Katsumi, H.; et al. In vitro study on the transport of zinc across intestinal epithelial cells using Caco-2 monolayers and isolated rat intestinal membranes. *Biol Pharm Bull* **2012**, *35*, 588-593, doi:10.1248/bpb.35.588.
115. Maares, M.; Haase, H. A Guide to Human Zinc Absorption: General Overview and Recent Advances of In Vitro Intestinal Models. *Nutrients* **2020**, *12*, doi:10.3390/nu12030762.
116. Gunshin, H.; Mackenzie, B.; Berger, U.V.; Gunshin, Y.; Romero, M.F.; Boron, W.F.; Nussberger, S.; Gollan, J.L.; Hediger, M.A. Cloning and characterization of a mammalian proton-coupled metal-ion transporter. *Nature* **1997**, *388*, 482-488, doi:10.1038/41343.
117. Illing, A.C.; Shawki, A.; Cunningham, C.L.; Mackenzie, B. Substrate profile and metal-ion selectivity of human divalent metal-ion transporter-1. *J Biol Chem* **2012**, *287*, 30485-30496, doi:10.1074/jbc.M112.364208.
118. King, J.C.; Shames, D.M.; Woodhouse, L.R. Zinc homeostasis in humans. *J Nutr* **2000**, *130*, 1360s-1366s, doi:10.1093/jn/130.5.1360S.
119. Grzeszczak, K.; Kwiatkowski, S.; Kosik-Bogacka, D. The Role of Fe, Zn, and Cu in Pregnancy. *Biomolecules* **2020**, *10*, doi:10.3390/biom10081176.
120. Hoeger, J.; Simon, T.P.; Doemming, S.; Thiele, C.; Marx, G.; Schuerholz, T.; Haase, H. Alterations in zinc binding capacity, free zinc levels and total serum zinc in a porcine model of sepsis. *Biometals* **2015**, *28*, 693-700, doi:10.1007/s10534-015-9858-4.
121. Ling, X.B.; Wei, H.W.; Wang, J.; Kong, Y.Q.; Wu, Y.Y.; Guo, J.L.; Li, T.F.; Li, J.K. Mammalian Metallothionein-2A and Oxidative Stress. *Int J Mol Sci* **2016**, *17*, doi:10.3390/ijms17091483.
122. Kimura, T.; Kambe, T. The Functions of Metallothionein and ZIP and ZnT Transporters: An Overview and Perspective. *Int J Mol Sci* **2016**, *17*, 336, doi:10.3390/ijms17030336.
123. Potter, B.M.; Feng, L.S.; Parasuram, P.; Matskevich, V.A.; Wilson, J.A.; Andrews, G.K.; Laity, J.H. The six zinc fingers of metal-responsive element binding transcription factor-1 form stable and quasi-ordered structures with relatively small differences in zinc affinities. *J Biol Chem* **2005**, *280*, 28529-28540, doi:10.1074/jbc.M505217200.
124. Foster, M.; Samman, S. Vegetarian diets across the lifecycle: impact on zinc intake and status. *Adv Food Nutr Res* **2015**, *74*, 93-131, doi:10.1016/bs.afnr.2014.11.003.
125. Uciechowski, P.; Rink, L. Chapter 39 - Zinc: An Essential Trace Element for the Elderly. In *Molecular Basis of Nutrition and Aging*, Malavolta, M., Mocchegiani, E., Eds.; Academic Press: San Diego, 2016; pp. 551-566.
126. Hussain, A.; Jiang, W.; Wang, X.; Shahid, S.; Saba, N.; Ahmad, M.; Dar, A.; Masood, S.U.; Imran, M.; Mustafa, A. Mechanistic Impact of Zinc Deficiency in Human Development. *Front Nutr* **2022**, *9*, 717064, doi:10.3389/fnut.2022.717064.
127. Wang, K.; Zhou, B.; Kuo, Y.M.; Zemansky, J.; Gitschier, J. A novel member of a zinc transporter family is defective in acrodermatitis enteropathica. *Am J Hum Genet* **2002**, *71*, 66-73, doi:10.1086/341125.

128. Plum, L.M.; Rink, L.; Haase, H. The essential toxin: impact of zinc on human health. *Int J Environ Res Public Health* **2010**, *7*, 1342-1365, doi:10.3390/ijerph7041342.
129. Prasad, A.S. Clinical manifestations of zinc deficiency. *Annu Rev Nutr* **1985**, *5*, 341-363, doi:10.1146/annurev.nu.05.070185.002013.
130. Homma, S.; Jones, R.; Qvist, J.; Zapol, W.M.; Reid, L. Pulmonary vascular lesions in the adult respiratory distress syndrome caused by inhalation of zinc chloride smoke: a morphometric study. *Hum Pathol* **1992**, *23*, 45-50, doi:10.1016/0046-8177(92)90010-z.
131. Brown, J.J. Zinc fume fever. *Br J Radiol* **1988**, *61*, 327-329, doi:10.1259/0007-1285-61-724-327.
132. Tsunemi, T.; Krainc, D. Zn^{2+} dyshomeostasis caused by loss of ATP13A2/PARK9 leads to lysosomal dysfunction and alpha-synuclein accumulation. *Hum Mol Genet* **2014**, *23*, 2791-2801, doi:10.1093/hmg/ddt572.
133. Lowe, N.M.; Fekete, K.; Decsi, T. Methods of assessment of zinc status in humans: a systematic review. *Am J Clin Nutr* **2009**, *89*, 2040s-2051s, doi:10.3945/ajcn.2009.27230G.
134. Bornhorst, J.; Kipp, A.P.; Haase, H.; Meyer, S.; Schwerdtle, T. The crux of inept biomarkers for risks and benefits of trace elements. *TrAC Trends in Analytical Chemistry* **2018**, *104*, 183-190, doi:https://doi.org/10.1016/j.trac.2017.11.007.
135. Wieringa, F.T.; Dijkhuizen, M.A.; Fiorentino, M.; Laillou, A.; Berger, J. Determination of zinc status in humans: which indicator should we use? *Nutrients* **2015**, *7*, 3252-3263, doi:10.3390/nu7053252.
136. King, J.C.; Brown, K.H.; Gibson, R.S.; Krebs, N.F.; Lowe, N.M.; Siekmann, J.H.; Raiten, D.J. Biomarkers of Nutrition for Development (BOND)-Zinc Review. *J Nutr* **2015**, *146*, 858s-885s, doi:10.3945/jn.115.220079.
137. King, J.C. Zinc: an essential but elusive nutrient. *Am J Clin Nutr* **2011**, *94*, 679s-684s, doi:10.3945/ajcn.110.005744.
138. de Benoist, B.; Darnton-Hill, I.; Davidsson, L.; Fontaine, O.; Hotz, C. Conclusions of the Joint WHO/UNICEF/IAEA/IZiNCG Interagency Meeting on Zinc Status Indicators. *Food and Nutrition Bulletin* **2007**, *28*, S480-S484, doi:10.1177/15648265070283s306.
139. King, J.C.; Shames, D.M.; Lowe, N.M.; Woodhouse, L.R.; Sutherland, B.; Abrams, S.A.; Turnlund, J.R.; Jackson, M.J. Effect of acute zinc depletion on zinc homeostasis and plasma zinc kinetics in men. *Am J Clin Nutr* **2001**, *74*, 116-124, doi:10.1093/ajcn/74.1.116.
140. Wessells, K.R.; Brown, K.H. Estimating the global prevalence of zinc deficiency: results based on zinc availability in national food supplies and the prevalence of stunting. *PLoS One* **2012**, *7*, e50568, doi:10.1371/journal.pone.0050568.
141. Brown, K.H.; Peerson, J.M.; Baker, S.K.; Hess, S.Y. Preventive zinc supplementation among infants, preschoolers, and older prepubertal children. *Food Nutr Bull* **2009**, *30*, S12-40, doi:10.1177/15648265090301s103.
142. Alker, W.; Schwerdtle, T.; Schomburg, L.; Haase, H. A Zinpyr-1-based Fluorimetric Microassay for Free Zinc in Human Serum. *Int J Mol Sci* **2019**, *20*, doi:10.3390/ijms20164006.
143. Hennigar, S.R.; Kelley, A.M.; McClung, J.P. Metallothionein and Zinc Transporter Expression in Circulating Human Blood Cells as Biomarkers of Zinc Status: a Systematic Review. *Adv Nutr* **2016**, *7*, 735-746, doi:10.3945/an.116.012518.
144. Reed, S.; Qin, X.; Ran-Ressler, R.; Brenna, J.T.; Glahn, R.P.; Tako, E. Dietary zinc deficiency affects blood linoleic acid: dihomo-ɣ-linolenic acid (LA:DGLA) ratio; a sensitive physiological marker of zinc status in vivo (Gallus gallus). *Nutrients* **2014**, *6*, 1164-1180, doi:10.3390/nu6031164.
145. Cheng, J.; Bar, H.; Tako, E. Zinc Status Index (ZSI) for Quantification of Zinc Physiological Status. *Nutrients* **2021**, *13*, doi:10.3390/nu13103399.
146. Reed, S.; Knez, M.; Uzan, A.; Stangoulis, J.C.R.; Glahn, R.P.; Koren, O.; Tako, E. Alterations in the Gut (Gallus gallus) Microbiota Following the Consumption of Zinc Biofortified Wheat (Triticum aestivum)-Based Diet. *J Agric Food Chem* **2018**, *66*, 6291-6299, doi:10.1021/acs.jafc.8b01481.
147. Finley, J.W.; Johnson, P.E.; Johnson, L.K. Sex affects manganese absorption and retention by humans from a diet adequate in manganese. *Am J Clin Nutr* **1994**, *60*, 949-955, doi:10.1093/ajcn/60.6.949.

148. Vincent, J.B.; Love, S. The binding and transport of alternative metals by transferrin. *Biochim Biophys Acta* **2012**, *1820*, 362-378, doi:10.1016/j.bbagen.2011.07.003.
149. Harris, W.R.; Chen, Y. Electron paramagnetic resonance and difference ultraviolet studies of Mn2+ binding to serum transferrin. *J Inorg Biochem* **1994**, *54*, 1-19, doi:10.1016/0162-0134(94)85119-0.
150. Anderson, J.G.; Fordahl, S.C.; Cooney, P.T.; Weaver, T.L.; Colyer, C.L.; Erikson, K.M. Extracellular norepinephrine, norepinephrine receptor and transporter protein and mRNA levels are differentially altered in the developing rat brain due to dietary iron deficiency and manganese exposure. *Brain Res* **2009**, *1281*, 1-14, doi:10.1016/j.brainres.2009.05.050.
151. Li, G.J.; Zhao, Q.; Zheng, W. Alteration at translational but not transcriptional level of transferrin receptor expression following manganese exposure at the blood-CSF barrier in vitro. *Toxicol Appl Pharmacol* **2005**, *205*, 188-200, doi:10.1016/j.taap.2004.10.003.
152. Suárez, N.; Eriksson, H. Receptor-mediated endocytosis of a manganese complex of transferrin into neuroblastoma (SHSY5Y) cells in culture. *J Neurochem* **1993**, *61*, 127-131, doi:10.1111/j.1471-4159.1993.tb03546.x.
153. Bjørklund, G.; Dadar, M.; Peana, M.; Rahaman, M.S.; Aaseth, J. Interactions between iron and manganese in neurotoxicity. *Arch Toxicol* **2020**, *94*, 725-734, doi:10.1007/s00204-020-02652-2.
154. Pang, L.; Wang, J.; Huang, W.; Guo, S. [A study of divalent metal transporter 1 and ferroportin 1 in brain of rats with manganese-induced parkinsonism]. *Zhonghua Lao Dong Wei Sheng Zhi Ye Bing Za Zhi* **2015**, *33*, 250-254.
155. Park, S.; Sim, C.S.; Lee, H.; Kim, Y. Blood manganese concentration is elevated in infants with iron deficiency. *Biol Trace Elem Res* **2013**, *155*, 184-189, doi:10.1007/s12011-013-9782-9.
156. Cowan, D.M.; Fan, Q.; Zou, Y.; Shi, X.; Chen, J.; Aschner, M.; Rosenthal, F.S.; Zheng, W. Manganese exposure among smelting workers: blood manganese-iron ratio as a novel tool for manganese exposure assessment. *Biomarkers* **2009**, *14*, 3-16, doi:10.1080/13547500902730672.
157. Venkataramani, V.; Doeppner, T.R.; Willkommen, D.; Cahill, C.M.; Xin, Y.; Ye, G.; Liu, Y.; Southon, A.; Aron, A.; Au-Yeung, H.Y.; et al. Manganese causes neurotoxic iron accumulation via translational repression of amyloid precursor protein and H-Ferritin. *J Neurochem* **2018**, *147*, 831-848, doi:10.1111/jnc.14580.
158. Olivares, M.; Pizarro, F.; Ruz, M.; de Romaña, D.L. Acute inhibition of iron bioavailability by zinc: studies in humans. *Biometals* **2012**, *25*, 657-664, doi:10.1007/s10534-012-9524-z.
159. Solomons, N.W. Competitive interaction of iron and zinc in the diet: consequences for human nutrition. *J Nutr* **1986**, *116*, 927-935, doi:10.1093/jn/116.6.927.
160. Tandy, S.; Williams, M.; Leggett, A.; Lopez-Jimenez, M.; Dedes, M.; Ramesh, B.; Srai, S.K.; Sharp, P. Nramp2 expression is associated with pH-dependent iron uptake across the apical membrane of human intestinal Caco-2 cells. *J Biol Chem* **2000**, *275*, 1023-1029, doi:10.1074/jbc.275.2.1023.
161. Yamaji, S.; Tennant, J.; Tandy, S.; Williams, M.; Singh Srai, S.K.; Sharp, P. Zinc regulates the function and expression of the iron transporters DMT1 and IREG1 in human intestinal Caco-2 cells. *FEBS Lett* **2001**, *507*, 137-141, doi:10.1016/s0014-5793(01)02953-2.
162. Iyengar, V.; Pullakhandam, R.; Nair, K.M. Coordinate expression and localization of iron and zinc transporters explain iron-zinc interactions during uptake in Caco-2 cells: implications for iron uptake at the enterocyte. *J Nutr Biochem* **2012**, *23*, 1146-1154, doi:10.1016/j.jnutbio.2011.06.008.
163. Frazer, D.M.; Wilkins, S.J.; Becker, E.M.; Murphy, T.L.; Vulpe, C.D.; McKie, A.T.; Anderson, G.J. A rapid decrease in the expression of DMT1 and Dcytb but not Ireg1 or hephaestin explains the mucosal block phenomenon of iron absorption. *Gut* **2003**, *52*, 340-346, doi:10.1136/gut.52.3.340.
164. Sharp, P.; Tandy, S.; Yamaji, S.; Tennant, J.; Williams, M.; Singh Srai, S.K. Rapid regulation of divalent metal transporter (DMT1) protein but not mRNA expression by non-haem iron in human intestinal Caco-2 cells. *FEBS Lett* **2002**, *510*, 71-76, doi:10.1016/s0014-5793(01)03225-2.
165. Nemeth, E.; Preza, G.C.; Jung, C.L.; Kaplan, J.; Waring, A.J.; Ganz, T. The N-terminus of hepcidin is essential for its interaction with ferroportin: structure-function study. *Blood* **2006**, *107*, 328-333, doi:10.1182/blood-2005-05-2049.

166. Knutson, M.D. Into the matrix: regulation of the iron regulatory hormone hepcidin by matriptase-2. *Nutr Rev* **2009**, *67*, 284-288, doi:10.1111/j.1753-4887.2009.00200.x.
167. Kondaiah, P.; Yaduvanshi, P.S.; Sharp, P.A.; Pullakhandam, R. Iron and Zinc Homeostasis and Interactions: Does Enteric Zinc Excretion Cross-Talk with Intestinal Iron Absorption? *Nutrients* **2019**, *11*, doi:10.3390/nu11081885.
168. Liu, Z.; Li, H.; Soleimani, M.; Girijashanker, K.; Reed, J.M.; He, L.; Dalton, T.P.; Nebert, D.W. Cd2+ versus Zn2+ uptake by the ZIP8 HCO3--dependent symporter: kinetics, electrogenicity and trafficking. *Biochem Biophys Res Commun* **2008**, *365*, 814-820, doi:10.1016/j.bbrc.2007.11.067.
169. Kambe, T.; Taylor, K.M.; Fu, D. Zinc transporters and their functional integration in mammalian cells. *J Biol Chem* **2021**, *296*, 100320, doi:10.1016/j.jbc.2021.100320.
170. Girijashanker, K.; He, L.; Soleimani, M.; Reed, J.M.; Li, H.; Liu, Z.; Wang, B.; Dalton, T.P.; Nebert, D.W. Slc39a14 gene encodes ZIP14, a metal/bicarbonate symporter: similarities to the ZIP8 transporter. *Mol Pharmacol* **2008**, *73*, 1413-1423, doi:10.1124/mol.107.043588.
171. Scheiber, I.F.; Wu, Y.; Morgan, S.E.; Zhao, N. The intestinal metal transporter ZIP14 maintains systemic manganese homeostasis. *J Biol Chem* **2019**, *294*, 9147-9160, doi:10.1074/jbc.RA119.008762.
172. Grüngreiff, K.; Reinhold, D.; Wedemeyer, H. The role of zinc in liver cirrhosis. *Ann Hepatol* **2016**, *15*, 7-16, doi:10.5604/16652681.1184191.
173. Stamoulis, I.; Kouraklis, G.; Theocharis, S. Zinc and the liver: an active interaction. *Dig Dis Sci* **2007**, *52*, 1595-1612, doi:10.1007/s10620-006-9462-0.
174. Rahil-Khazen, R.; Bolann, B.J.; Myking, A.; Ulvik, R.J. Multi-element analysis of trace element levels in human autopsy tissues by using inductively coupled atomic emission spectrometry technique (ICP-AES). *J Trace Elem Med Biol* **2002**, *16*, 15-25, doi:10.1016/s0946-672x(02)80004-9.
175. Kollmeier, H.; Seemann, J.; Wittig, P.; Rothe, G.; Witting, C. Zinc concentrations in human tissues. Liver zinc in carcinoma and severe liver disease. *Pathol Res Pract* **1992**, *188*, 942-945, doi:10.1016/s0344-0338(11)80255-4.
176. Sirlin, C.B.; Reeder, S.B. Magnetic resonance imaging quantification of liver iron. *Magn Reson Imaging Clin N Am* **2010**, *18*, 359-381, ix, doi:10.1016/j.mric.2010.08.014.
177. Meynard, D.; Babitt, J.L.; Lin, H.Y. The liver: conductor of systemic iron balance. *Blood* **2014**, *123*, 168-176, doi:10.1182/blood-2013-06-427757.
178. Wang, C.Y.; Knutson, M.D. Hepatocyte divalent metal-ion transporter-1 is dispensable for hepatic iron accumulation and non-transferrin-bound iron uptake in mice. *Hepatology* **2013**, *58*, 788-798, doi:10.1002/hep.26401.
179. Knutson, M.D. Iron transport proteins: Gateways of cellular and systemic iron homeostasis. *J Biol Chem* **2017**, *292*, 12735-12743, doi:10.1074/jbc.R117.786632.
180. Petering, D.H.; Zhu, J.; Krezoski, S.; Meeusen, J.; Kiekenbush, C.; Krull, S.; Specher, T.; Dughish, M. Apo-metallothionein emerging as a major player in the cellular activities of metallothionein. *Exp Biol Med (Maywood)* **2006**, *231*, 1528-1534, doi:10.1177/153537020623100912.
181. Zhang, Z.; Zhang, F.; Guo, X.; An, P.; Tao, Y.; Wang, F. Ferroportin1 in hepatocytes and macrophages is required for the efficient mobilization of body iron stores in mice. *Hepatology* **2012**, *56*, 961-971, doi:10.1002/hep.25746.
182. Seidelin, A.S.; Nordestgaard, B.G.; Tybjærg-Hansen, A.; Yaghootkar, H.; Stender, S. A rare genetic variant in the manganese transporter SLC30A10 and elevated liver enzymes in the general population. *Hepatol Int* **2022**, *16*, 702-711, doi:10.1007/s12072-022-10331-w.
183. Gandhi, D.; Rudrashetti, A.P.; Rajasekaran, S. The impact of environmental and occupational exposures of manganese on pulmonary, hepatic, and renal functions. *J Appl Toxicol* **2022**, *42*, 103-129, doi:10.1002/jat.4214.
184. Andrews, G.K. Cellular zinc sensors: MTF-1 regulation of gene expression. *Biometals* **2001**, *14*, 223-237, doi:10.1023/a:1012932712483.
185. Grüngreiff, K. Zinc in liver disease. *The Journal of Trace Elements in Experimental Medicine* **2002**, *15*, 67-78, doi:https://doi.org/10.1002/jtra.10002.

186. Arzumanian, V.A.; Kiseleva, O.I.; Poverennaya, E.V. The Curious Case of the HepG2 Cell Line: 40 Years of Expertise. *Int J Mol Sci* **2021**, *22*, doi:10.3390/ijms222313135.
187. López-Terrada, D.; Cheung, S.W.; Finegold, M.J.; Knowles, B.B. Hep G2 is a hepatoblastoma-derived cell line. *Hum Pathol* **2009**, *40*, 1512-1515, doi:10.1016/j.humpath.2009.07.003.
188. Donato, M.T.; Tolosa, L.; Gómez-Lechón, M.J. Culture and Functional Characterization of Human Hepatoma HepG2 Cells. *Methods Mol Biol* **2015**, *1250*, 77-93, doi:10.1007/978-1-4939-2074-7_5.
189. Garza-Lombó, C.; Posadas, Y.; Quintanar, L.; Gonsebatt, M.E.; Franco, R. Neurotoxicity Linked to Dysfunctional Metal Ion Homeostasis and Xenobiotic Metal Exposure: Redox Signaling and Oxidative Stress. *Antioxid Redox Signal* **2018**, *28*, 1669-1703, doi:10.1089/ars.2017.7272.
190. Kovacs, G.G. Molecular Pathological Classification of Neurodegenerative Diseases: Turning towards Precision Medicine. *Int J Mol Sci* **2016**, *17*, doi:10.3390/ijms17020189.
191. Islam, M.T. Oxidative stress and mitochondrial dysfunction-linked neurodegenerative disorders. *Neurol Res* **2017**, *39*, 73-82, doi:10.1080/01616412.2016.1251711.
192. Piloni, N.E.; Fermandez, V.; Videla, L.A.; Puntarulo, S. Acute iron overload and oxidative stress in brain. *Toxicology* **2013**, *314*, 174-182, doi:10.1016/j.tox.2013.09.015.
193. Portbury, S.D.; Adlard, P.A. Zinc Signal in Brain Diseases. *Int J Mol Sci* **2017**, *18*, doi:10.3390/ijms18122506.
194. Bredholt, M.; Frederiksen, J.L. Zinc in Multiple Sclerosis: A Systematic Review and Meta-Analysis. *ASN Neuro* **2016**, *8*, doi:10.1177/1759091416651511.
195. Ward, R.J.; Zucca, F.A.; Duyn, J.H.; Crichton, R.R.; Zecca, L. The role of iron in brain ageing and neurodegenerative disorders. *Lancet Neurol* **2014**, *13*, 1045-1060, doi:10.1016/s1474-4422(14)70117-6.
196. Mills, E.; Dong, X.P.; Wang, F.; Xu, H. Mechanisms of brain iron transport: insight into neurodegeneration and CNS disorders. *Future Med Chem* **2010**, *2*, 51-64, doi:10.4155/fmc.09.140.
197. Bowman, A.B.; Aschner, M. Considerations on manganese (Mn) treatments for in vitro studies. *Neurotoxicology* **2014**, *41*, 141-142, doi:10.1016/j.neuro.2014.01.010.
198. Steimle, B.L.; Smith, F.M.; Kosman, D.J. The solute carriers ZIP8 and ZIP14 regulate manganese accumulation in brain microvascular endothelial cells and control brain manganese levels. *J Biol Chem* **2019**, *294*, 19197-19208, doi:10.1074/jbc.RA119.009371.
199. Bornhorst, J.; Wehe, C.A.; Hüwel, S.; Karst, U.; Galla, H.J.; Schwerdtle, T. Impact of manganese on and transfer across blood-brain and blood-cerebrospinal fluid barrier in vitro. *J Biol Chem* **2012**, *287*, 17140-17151, doi:10.1074/jbc.M112.344093.
200. Takeda, A. Zinc homeostasis and functions of zinc in the brain. *Biometals* **2001**, *14*, 343-351, doi:10.1023/a:1012982123386.
201. Qian, Z.M.; Ke, Y. Brain iron transport. *Biol Rev Camb Philos Soc* **2019**, *94*, 1672-1684, doi:10.1111/brv.12521.
202. Cristóvão, J.S.; Santos, R.; Gomes, C.M. Metals and Neuronal Metal Binding Proteins Implicated in Alzheimer's Disease. *Oxid Med Cell Longev* **2016**, *2016*, 9812178, doi:10.1155/2016/9812178.
203. Du, K.; Liu, M.; Pan, Y.; Zhong, X.; Wei, M. Association of Serum Manganese Levels with Alzheimer's Disease and Mild Cognitive Impair ment: A Systematic Review and Meta-Analysis. *Nutrients* **2017**, *9*, doi:10.3390/nu9030231.
204. Zhang, X.M.; Yin, M.; Zhang, M.H. Cell-based assays for Parkinson's disease using differentiated human LUHMES cells. *Acta Pharmacol Sin* **2014**, *35*, 945-956, doi:10.1038/aps.2014.36.
205. Lotharius, J.; Falsig, J.; van Beek, J.; Payne, S.; Dringen, R.; Brundin, P.; Leist, M. Progressive degeneration of human mesencephalic neuron-derived cells triggered by dopamine-dependent oxidative stress is dependent on the mixed-lineage kinase pathway. *J Neurosci* **2005**, *25*, 6329-6342, doi:10.1523/jneurosci.1746-05.2005.
206. Burton, G.J.; Fowden, A.L.; Thornburg, K.L. Placental Origins of Chronic Disease. *Physiol Rev* **2016**, *96*, 1509-1565, doi:10.1152/physrev.00029.2015.

207. Gude, N.M.; Roberts, C.T.; Kalionis, B.; King, R.G. Growth and function of the normal human placenta. *Thromb Res* **2004**, *114*, 397-407, doi:10.1016/j.thromres.2004.06.038.
208. Cindrova-Davies, T.; Sferruzzi-Perri, A.N. Human placental development and function. *Semin Cell Dev Biol* **2022**, doi:10.1016/j.semcdb.2022.03.039.
209. Cherubini, M.; Erickson, S.; Haase, K. Modelling the Human Placental Interface In Vitro-A Review. *Micromachines (Basel)* **2021**, *12*, doi:10.3390/mi12080884.
210. Turco, M.Y.; Moffett, A. Development of the human placenta. *Development* **2019**, *146*, doi:10.1242/dev.163428.
211. Schlafke, S.; Enders, A.C. Cellular basis of interaction between trophoblast and uterus at implantation. *Biol Reprod* **1975**, *12*, 41-65, doi:10.1095/biolreprod12.1.41.
212. Rodeck, C.H.; Whittle, M.J.; Queenan, J.T. *Fetal Medicine: Basic Science and Clinical Practice*; Elsevier Health Sciences: 2008.
213. Tetro, N.; Moushaev, S.; Rubinchik-Stern, M.; Eyal, S. The Placental Barrier: the Gate and the Fate in Drug Distribution. *Pharm Res* **2018**, *35*, 71, doi:10.1007/s11095-017-2286-0.
214. Jaremek, A.; Jeyarajah, M.J.; Jaju Bhattad, G.; Renaud, S.J. Omics Approaches to Study Formation and Function of Human Placental Syncytiotrophoblast. *Frontiers in Cell and Developmental Biology* **2021**, *9*, doi:10.3389/fcell.2021.674162.
215. Jones, C.J.; Harris, L.K.; Whittingham, J.; Aplin, J.D.; Mayhew, T.M. A re-appraisal of the morphophenotype and basal lamina coverage of cytotrophoblasts in human term placenta. *Placenta* **2008**, *29*, 215-219, doi:10.1016/j.placenta.2007.11.004.
216. Kurt Benirschke, G.J.B., Rebecca N Baergen. *Pathology of the Human Placenta*, 6 ed.; Springer Berlin, Heidelberg: 2012.
217. Fuchs, R.; Ellinger, I. Endocytic and transcytotic processes in villous syncytiotrophoblast: role in nutrient transport to the human fetus. *Traffic* **2004**, *5*, 725-738, doi:10.1111/j.1600-0854.2004.00221.x.
218. Aplin, J.D.; Jones, C.J.P. Cell dynamics in human villous trophoblast. *Hum Reprod Update* **2021**, *27*, 904-922, doi:10.1093/humupd/dmab015.
219. Knöfler, M.; Haider, S.; Saleh, L.; Pollheimer, J.; Gamage, T.; James, J. Human placenta and trophoblast development: key molecular mechanisms and model systems. *Cell Mol Life Sci* **2019**, *76*, 3479-3496, doi:10.1007/s00018-019-03104-6.
220. Rothbauer, M.; Patel, N.; Gondola, H.; Siwetz, M.; Huppertz, B.; Ertl, P. A comparative study of five physiological key parameters between four different human trophoblast-derived cell lines. *Sci Rep* **2017**, *7*, 5892, doi:10.1038/s41598-017-06364-z.
221. Walker, N.; Filis, P.; Soffientini, U.; Bellingham, M.; O'Shaughnessy, P.J.; Fowler, P.A. Placental transporter localization and expression in the Human: the importance of species, sex, and gestational age differences†. *Biol Reprod* **2017**, *96*, 733-742, doi:10.1093/biolre/iox012.
222. Aengenheister, L.; Keevend, K.; Muoth, C.; Schönenberger, R.; Diener, L.; Wick, P.; Buerki-Thurnherr, T. An advanced human in vitro co-culture model for translocation studies across the placental barrier. *Sci Rep* **2018**, *8*, 5388, doi:10.1038/s41598-018-23410-6.
223. Feneley, M.R.; Burton, G.J. Villous composition and membrane thickness in the human placenta at term: a stereological study using unbiased estimators and optimal fixation techniques. *Placenta* **1991**, *12*, 131-142, doi:10.1016/0143-4004(91)90017-a.
224. Rubinchik-Stern, M.; Eyal, S. Drug Interactions at the Human Placenta: What is the Evidence? *Front Pharmacol* **2012**, *3*, 126, doi:10.3389/fphar.2012.00126.
225. Syme, M.R.; Paxton, J.W.; Keelan, J.A. Drug transfer and metabolism by the human placenta. *Clin Pharmacokinet* **2004**, *43*, 487-514, doi:10.2165/00003088-200443080-00001.
226. Poulsen, M.S.; Rytting, E.; Mose, T.; Knudsen, L.E. Modeling placental transport: correlation of in vitro BeWo cell permeability and ex vivo human placental perfusion. *Toxicol In Vitro* **2009**, *23*, 1380-1386, doi:10.1016/j.tiv.2009.07.028.
227. Khanal, R.C.; Nemere, I. Endocrine regulation of calcium transport in epithelia. *Clin Exp Pharmacol Physiol* **2008**, *35*, 1277-1287, doi:10.1111/j.1440-1681.2008.05053.x.
228. Tabuchi, M.; Tanaka, N.; Nishida-Kitayama, J.; Ohno, H.; Kishi, F. Alternative splicing regulates the subcellular localization of divalent metal transporter 1 isoforms. *Mol Biol Cell* **2002**, *13*, 4371-4387, doi:10.1091/mbc.e02-03-0165.

229. Connor, K.L.; Kibschull, M.; Matysiak-Zablocki, E.; Nguyen, T.T.N.; Matthews, S.G.; Lye, S.J.; Bloise, E. Maternal malnutrition impacts placental morphology and transporter expression: an origin for poor offspring growth. *J Nutr Biochem* **2020**, *78*, 108329, doi:10.1016/j.jnutbio.2019.108329.
230. Koren, G.; Ornoy, A. The role of the placenta in drug transport and fetal drug exposure. *Expert Rev Clin Pharmacol* **2018**, *11*, 373-385, doi:10.1080/17512433.2018.1425615.
231. Elad, D.; Levkovitz, R.; Jaffa, A.J.; Desoye, G.; Hod, M. Have we neglected the role of fetal endothelium in transplacental transport? *Traffic* **2014**, *15*, 122-126, doi:10.1111/tra.12130.
232. Jauniaux, E.; Gulbis, B.; Burton, G.J. The human first trimester gestational sac limits rather than facilitates oxygen transfer to the foetus--a review. *Placenta* **2003**, *24 Suppl A*, S86-93, doi:10.1053/plac.2002.0932.
233. Roberts, V.H.J.; Morgan, T.K.; Bednarek, P.; Morita, M.; Burton, G.J.; Lo, J.O.; Frias, A.E. Early first trimester uteroplacental flow and the progressive disintegration of spiral artery plugs: new insights from contrast-enhanced ultrasound and tissue histopathology. *Hum Reprod* **2017**, *32*, 2382-2393, doi:10.1093/humrep/dex301.
234. Georgiades, P.; Ferguson-Smith, A.C.; Burton, G.J. Comparative developmental anatomy of the murine and human definitive placentae. *Placenta* **2002**, *23*, 3-19, doi:10.1053/plac.2001.0738.
235. Burton, G.J.; Watson, A.L.; Hempstock, J.; Skepper, J.N.; Jauniaux, E. Uterine glands provide histiotrophic nutrition for the human fetus during the first trimester of pregnancy. *J Clin Endocrinol Metab* **2002**, *87*, 2954-2959, doi:10.1210/jcem.87.6.8563.
236. Kundu, G.C.; Mantile, G.; Miele, L.; Cordella-Miele, E.; Mukherjee, A.B. Recombinant human uteroglobin suppresses cellular invasiveness via a novel class of high-affinity cell surface binding site. *Proc Natl Acad Sci U S A* **1996**, *93*, 2915-2919, doi:10.1073/pnas.93.7.2915.
237. Lala, P.K.; Hamilton, G.S.; Athanassiades, A. Role of growth factors and other placental signals in extravillous trophoblast cell function: A review. *Placenta* **1998**, *19*, 327-339, doi:https://doi.org/10.1016/S0143-4004(98)80052-0.
238. Sawyer, L. β-Lactoglobulin and Glycodelin: Two Sides of the Same Coin? *Front Physiol* **2021**, *12*, 678080, doi:10.3389/fphys.2021.678080.
239. Lee, C.L.; Lam, K.K.; Koistinen, H.; Seppala, M.; Kurpisz, M.; Fernandez, N.; Pang, R.T.; Yeung, W.S.; Chiu, P.C. Glycodelin-A as a paracrine regulator in early pregnancy. *J Reprod Immunol* **2011**, *90*, 29-34, doi:10.1016/j.jri.2011.04.007.
240. Gaccioli, F.; Lager, S.; Powell, T.L.; Jansson, T. Placental transport in response to altered maternal nutrition. *J Dev Orig Health Dis* **2013**, *4*, 101-115, doi:10.1017/s2040174412000529.
241. Desforges, M.; Sibley, C.P. Placental nutrient supply and fetal growth. *Int J Dev Biol* **2010**, *54*, 377-390, doi:10.1387/ijdb.082765md.
242. Burton, G.J.; Fowden, A.L. The placenta: a multifaceted, transient organ. *Philos Trans R Soc Lond B Biol Sci* **2015**, *370*, 20140066, doi:10.1098/rstb.2014.0066.
243. Stulc, J.; Svihovec, J.; Drábková, J.; Stríbrný, J.; Kobilková, J.; Vido, I.; Dolezal, A. Electrical potential difference across the mid-term human placenta. *Acta Obstet Gynecol Scand* **1978**, *57*, 125-126, doi:10.3109/00016347809155889.
244. Mellor, D.J.; Cockburn, F.; Lees, M.M.; Blagden, A. Distribution of ions and electrical potential differences between mother and fetus in the human at term. *J Obstet Gynaecol Br Commonw* **1969**, *76*, 993-998, doi:10.1111/j.1471-0528.1969.tb09465.x.
245. Dobson, P.D.; Kell, D.B. Carrier-mediated cellular uptake of pharmaceutical drugs: an exception or the rule? *Nat Rev Drug Discov* **2008**, *7*, 205-220, doi:10.1038/nrd2438.
246. Bain, M.D.; Copas, D.K.; Taylor, A.; Landon, M.J.; Stacey, T.E. Permeability of the human placenta in vivo to four non-metabolized hydrophilic molecules. *J Physiol* **1990**, *431*, 505-513, doi:10.1113/jphysiol.1990.sp018343.
247. Brownbill, P.; Mahendran, D.; Owen, D.; Swanson, P.; Thornburg, K.L.; Nelson, D.M.; Sibley, C.P. Denudations as paracellular routes for alphafetoprotein and creatinine across the human syncytiotrophoblast. *Am J Physiol Regul Integr Comp Physiol* **2000**, *278*, R677-683, doi:10.1152/ajpregu.2000.278.3.R677.

248. Brownbill, P.; Edwards, D.; Jones, C.; Mahendran, D.; Owen, D.; Sibley, C.; Johnson, R.; Swanson, P.; Nelson, D.M. Mechanisms of alphafetoprotein transfer in the perfused human placental cotyledon from uncomplicated pregnancy. *J Clin Invest* **1995**, *96*, 2220-2226, doi:10.1172/jci118277.
249. Lewis, R.M.; Baskaran, H.; Green, J.; Tashev, S.; Paleologou, E.; Lofthouse, E.M.; Cleal, J.K.; Page, A.; Chatelet, D.S.; Goggin, P.; et al. 3D Visualisation of trans-syncytial nanopores provides a pathway for paracellular diffusion across the human placental syncytiotrophoblast. *bioRxiv* **2022**, 2022.2001.2026.477815, doi:10.1101/2022.01.26.477815.
250. Tashev, S.A.; Parsons, D.; Hillman, C.; Harris, S.; Lofthouse, E.M.; Goggin, P.; Chatelet, D.S.; Cleal, J.K.; Smyth, N.; Palaiologou, H.; et al. Folding of the syncytiotrophoblast basal plasma membrane increases the surface area available for exchange in human placenta. *Placenta* **2022**, *117*, 57-63, doi:10.1016/j.placenta.2021.11.002.
251. Bastin, J.; Drakesmith, H.; Rees, M.; Sargent, I.; Townsend, A. Localisation of proteins of iron metabolism in the human placenta and liver. *Br J Haematol* **2006**, *134*, 532-543, doi:10.1111/j.1365-2141.2006.06216.x.
252. Sangkhae, V.; Nemeth, E. Placental iron transport: The mechanism and regulatory circuits. *Free Radic Biol Med* **2019**, *133*, 254-261, doi:10.1016/j.freeradbiomed.2018.07.001.
253. Wada, H.G.; Hass, P.E.; Sussman, H.H. Transferrin receptor in human placental brush border membranes. Studies on the binding of transferrin to placental membrane vesicles and the identification of a placental brush border glycoprotein with high affinity for transferrin. *J Biol Chem* **1979**, *254*, 12629-12635.
254. Seligman, P.A.; Schleicher, R.B.; Allen, R.H. Isolation and characterization of the transferrin receptor from human placenta. *J Biol Chem* **1979**, *254*, 9943-9946.
255. Georgieff, M.K.; Wobken, J.K.; Welle, J.; Burdo, J.R.; Connor, J.R. Identification and localization of divalent metal transporter-1 (DMT-1) in term human placenta. *Placenta* **2000**, *21*, 799-804, doi:10.1053/plac.2000.0566.
256. Zaugg, J.; Melhem, H.; Huang, X.; Wegner, M.; Baumann, M.; Surbek, D.; Körner, M.; Albrecht, C. Gestational diabetes mellitus affects placental iron homeostasis: Mechanism and clinical implications. *Faseb j* **2020**, *34*, 7311-7329, doi:10.1096/fj.201903054R.
257. Mackenzie, B.; Ujwal, M.L.; Chang, M.H.; Romero, M.F.; Hediger, M.A. Divalent metal-ion transporter DMT1 mediates both H+ -coupled Fe2+ transport and uncoupled fluxes. *Pflugers Arch* **2006**, *451*, 544-558, doi:10.1007/s00424-005-1494-3.
258. Cooke, L.D.F.; Tumbarello, D.A.; Harvey, N.C.; Sethi, J.K.; Lewis, R.M.; Cleal, J.K. Endocytosis in the placenta: An undervalued mediator of placental transfer. *Placenta* **2021**, *113*, 67-73, doi:10.1016/j.placenta.2021.04.014.
259. Parmley, R.T.; Barton, J.C.; Conrad, M.E. Ultrastructural localization of transferrin, transferrin receptor, and iron-binding sites on human placental and duodenal microvilli. *Br J Haematol* **1985**, *60*, 81-89, doi:10.1111/j.1365-2141.1985.tb07388.x.
260. King, B.F. Localization of transferrin on the surface of the human placenta by electron microscopic immunocytochemistry. *Anat Rec* **1976**, *186*, 151-159, doi:10.1002/ar.1091860203.
261. Cao, C.; Fleming, M.D. The placenta: the forgotten essential organ of iron transport. *Nutr Rev* **2016**, *74*, 421-431, doi:10.1093/nutrit/nuw009.
262. Wang, M.; Tian, Y.; Yu, P.; Li, N.; Deng, Y.; Li, L.; Kang, H.; Chen, D.; Wang, H.; Liu, Z.; et al. Association between congenital heart defects and maternal manganese and iron concentrations: a case-control study in China. *Environ Sci Pollut Res Int* **2022**, *29*, 26950-26959, doi:10.1007/s11356-021-17054-9.
263. Catov, J.M.; Bodnar, L.M.; Olsen, J.; Olsen, S.; Nohr, E.A. Periconceptional multivitamin use and risk of preterm or small-for-gestational-age births in the Danish National Birth Cohort. *Am J Clin Nutr* **2011**, *94*, 906-912, doi:10.3945/ajcn.111.012393.
264. Richard, K.; Holland, O.; Landers, K.; Vanderlelie, J.J.; Hofstee, P.; Cuffe, J.S.M.; Perkins, A.V. Review: Effects of maternal micronutrient supplementation on placental function. *Placenta* **2017**, *54*, 38-44, doi:10.1016/j.placenta.2016.12.022.

265. Perkins, A.V.; Vanderlelie, J.J. Multiple micronutrient supplementation and birth outcomes: The potential importance of selenium. *Placenta* **2016**, *48 Suppl 1*, S61-s65, doi:10.1016/j.placenta.2016.02.007.
266. Schmidt, A.; Morales-Prieto, D.M.; Pastuschek, J.; Fröhlich, K.; Markert, U.R. Only humans have human placentas: molecular differences between mice and humans. *J Reprod Immunol* **2015**, *108*, 65-71, doi:10.1016/j.jri.2015.03.001.
267. Institute of Medicine Panel on, M. Dietary Reference Intakes for Vitamin A, Vitamin K, Arsenic, Boron, Chromium, Copper, Iodine, Iron, Manganese, Molybdenum, Nickel, Silicon, Vanadium, and Zinc. In *Dietary Reference Intakes for Vitamin A, Vitamin K, Arsenic, Boron, Chromium, Copper, Iodine, Iron, Manganese, Molybdenum, Nickel, Silicon, Vanadium, and Zinc*; Washington (DC), 2001.
268. Institute of Medicine Committee on the Prevention, D.; Management of Iron Deficiency Anemia Among, U.S.C.; Women of Childbearing, A. In *Iron Deficiency Anemia: Recommended Guidelines for the Prevention, Detection, and Management Among U.S. Children and Women of Childbearing Age*, Earl, R., Woteki, C.E., Eds.; National Academies Press (US) Copyright 1993 by the National Academy of Sciences. All rights reserved.: Washington (DC), 1993.
269. King, J.C. Physiology of pregnancy and nutrient metabolism. *Am J Clin Nutr* **2000**, *71*, 1218s-1225s, doi:10.1093/ajcn/71.5.1218s.
270. Stern, C.; Schwarz, S.; Moser, G.; Cvitic, S.; Jantscher-Krenn, E.; Gauster, M.; Hiden, U. Placental Endocrine Activity: Adaptation and Disruption of Maternal Glucose Metabolism in Pregnancy and the Influence of Fetal Sex. *Int J Mol Sci* **2021**, *22*, doi:10.3390/ijms222312722.
271. Vaughan, O.R.; Rosario, F.J.; Powell, T.L.; Jansson, T. Regulation of Placental Amino Acid Transport and Fetal Growth. *Prog Mol Biol Transl Sci* **2017**, *145*, 217-251, doi:10.1016/bs.pmbts.2016.12.008.
272. Mégier, C.; Peoc'h, K.; Puy, V.; Cordier, A.G. Iron Metabolism in Normal and Pathological Pregnancies and Fetal Consequences. *Metabolites* **2022**, *12*, doi:10.3390/metabo12020129.
273. Georgieff, M.K. Long-term brain and behavioral consequences of early iron deficiency. *Nutr Rev* **2011**, *69 Suppl 1*, S43-48, doi:10.1111/j.1753-4887.2011.00432.x.
274. Fisher, A.L.; Nemeth, E. Iron homeostasis during pregnancy. *Am J Clin Nutr* **2017**, *106*, 1567s-1574s, doi:10.3945/ajcn.117.155812.
275. Gernand, A.D.; Schulze, K.J.; Stewart, C.P.; West, K.P., Jr.; Christian, P. Micronutrient deficiencies in pregnancy worldwide: health effects and prevention. *Nat Rev Endocrinol* **2016**, *12*, 274-289, doi:10.1038/nrendo.2016.37.
276. Best, C.M.; Pressman, E.K.; Cao, C.; Cooper, E.; Guillet, R.; Yost, O.L.; Galati, J.; Kent, T.R.; O'Brien, K.O. Maternal iron status during pregnancy compared with neonatal iron status better predicts placental iron transporter expression in humans. *Faseb j* **2016**, *30*, 3541-3550, doi:10.1096/fj.201600069R.
277. Sangkhae, V.; Fisher, A.L.; Wong, S.; Koenig, M.D.; Tussing-Humphreys, L.; Chu, A.; Lelić, M.; Ganz, T.; Nemeth, E. Effects of maternal iron status on placental and fetal iron homeostasis. *J Clin Invest* **2020**, *130*, 625-640, doi:10.1172/jci127341.
278. Scholl, T.O.; Reilly, T. Anemia, iron and pregnancy outcome. *J Nutr* **2000**, *130*, 443s-447s, doi:10.1093/jn/130.2.443S.
279. WHO Guidelines Approved by the Guidelines Review Committee. In *Guideline: Daily Iron and Folic Acid Supplementation in Pregnant Women*; World Health Organization Copyright © 2012, World Health Organization.: Geneva, 2012.
280. Siu, A.L. Screening for Iron Deficiency Anemia and Iron Supplementation in Pregnant Women to Improve Maternal Health and Birth Outcomes: U.S. Preventive Services Task Force Recommendation Statement. *Ann Intern Med* **2015**, *163*, 529-536, doi:10.7326/m15-1707.
281. Fisher, A.L.; Sangkhae, V.; Balušíková, K.; Palaskas, N.J.; Ganz, T.; Nemeth, E. Iron-dependent apoptosis causes embryotoxicity in inflamed and obese pregnancy. *Nat Commun* **2021**, *12*, 4026, doi:10.1038/s41467-021-24333-z.

282. Wang, Y.; Wu, Y.; Li, T.; Wang, X.; Zhu, C. Iron Metabolism and Brain Development in Premature Infants. *Front Physiol* **2019**, *10*, 463, doi:10.3389/fphys.2019.00463.
283. Perrone, S.; Tataranno, L.M.; Stazzoni, G.; Ramenghi, L.; Buonocore, G. Brain susceptibility to oxidative stress in the perinatal period. *J Matern Fetal Neonatal Med* **2015**, *28 Suppl 1*, 2291-2295, doi:10.3109/14767058.2013.796170.
284. Baud, O.; Greene, A.E.; Li, J.; Wang, H.; Volpe, J.J.; Rosenberg, P.A. Glutathione peroxidase-catalase cooperativity is required for resistance to hydrogen peroxide by mature rat oligodendrocytes. *J Neurosci* **2004**, *24*, 1531-1540, doi:10.1523/jneurosci.3989-03.2004.
285. Panfoli, I.; Candiano, G.; Malova, M.; De Angelis, L.; Cardiello, V.; Buonocore, G.; Ramenghi, L.A. Oxidative Stress as a Primary Risk Factor for Brain Damage in Preterm Newborns. *Front Pediatr* **2018**, *6*, 369, doi:10.3389/fped.2018.00369.
286. Lönnerdal, B.; Georgieff, M.K.; Hernell, O. Developmental Physiology of Iron Absorption, Homeostasis, and Metabolism in the Healthy Term Infant. *J Pediatr* **2015**, *167*, S8-14, doi:10.1016/j.jpeds.2015.07.014.
287. Falchuk, K.H. The molecular basis for the role of zinc in developmental biology. *Mol Cell Biochem* **1998**, *188*, 41-48.
288. Terrin, G.; Berni Canani, R.; Di Chiara, M.; Pietravalle, A.; Aleandri, V.; Conte, F.; De Curtis, M. Zinc in Early Life: A Key Element in the Fetus and Preterm Neonate. *Nutrients* **2015**, *7*, 10427-10446, doi:10.3390/nu7125542.
289. Brion, L.P.; Heyne, R.; Lair, C.S. Role of zinc in neonatal growth and brain growth: review and scoping review. *Pediatr Res* **2021**, *89*, 1627-1640, doi:10.1038/s41390-020-01181-z.
290. Tomat, A.L.; Juriol, L.V.; Gobetto, M.N.; Veiras, L.C.; Mendes Garrido Abregú, F.; Zilberman, J.; Fasoli, H.; Elesgaray, R.; Costa, M.; Arranz, C.T. Morphological and functional effects on cardiac tissue induced by moderate zinc deficiency during prenatal and postnatal life in male and female rats. *Am J Physiol Heart Circ Physiol* **2013**, *305*, H1574-1583, doi:10.1152/ajpheart.00578.2013.
291. Wilson, R.L.; Leemaqz, S.Y.; Goh, Z.; McAninch, D.; Jankovic-Karasoulos, T.; Leghi, G.E.; Phillips, J.A.; Colafella, K.M.; Tran, C.; O'Leary, S.; et al. Zinc is a critical regulator of placental morphogenesis and maternal hemodynamics during pregnancy in mice. *Sci Rep* **2017**, *7*, 15137, doi:10.1038/s41598-017-15085-2.
292. Widdowson EM, D.J. *Mineral Metabolism. An Advanced Treatise Vol. II. The Elements. Part A*; Comar CL, B.F., Ed.; Academic Press, New York, USA: 1964; Volume II.
293. Shaw, J.C. Trace elements in the fetus and young infant. I. Zinc. *Am J Dis Child* **1979**, *133*, 1260-1268, doi:10.1001/archpedi.1979.02130120052011.
294. Donangelo, C.M.; King, J.C. Maternal zinc intakes and homeostatic adjustments during pregnancy and lactation. *Nutrients* **2012**, *4*, 782-798, doi:10.3390/nu4070782.
295. Vargas Zapata, C.L.; Trugo, N.M.; Donangelo, C.M. Zinc uptake by human placental microvillous membrane vesicles: effects of gestational age and maternal serum zinc levels. *Biol Trace Elem Res* **2000**, *73*, 127-137, doi:10.1385/bter:73:2:127.
296. Dey, A.C.; Shahidullah, M.; Mannan, M.A.; Noor, M.K.; Saha, L.; Rahman, S.A. Maternal and neonatal serum zinc level and its relationship with neural tube defects. *J Health Popul Nutr* **2010**, *28*, 343-350, doi:10.3329/jhpn.v28i4.6040.
297. Solomons, N.W.; Pineda, O.; Viteri, F.; Sandstead, H.H. Studies on the bioavailability of zinc in humans: mechanism of the intestinal interaction of nonheme iron and zinc. *J Nutr* **1983**, *113*, 337-349, doi:10.1093/jn/113.2.337.
298. Spencer, A. Whole blood manganese levels in pregnancy and the neonate. *Nutrition* **1999**, *15*, 731-734, doi:10.1016/s0899-9007(99)00144-6.
299. Liu, J.; Jin, L.; Zhang, L.; Li, Z.; Wang, L.; Ye, R.; Zhang, Y.; Ren, A. Placental concentrations of manganese and the risk of fetal neural tube defects. *J Trace Elem Med Biol* **2013**, *27*, 322-325, doi:10.1016/j.jtemb.2013.04.001.
300. Mistry, H.D.; Williams, P.J. The importance of antioxidant micronutrients in pregnancy. *Oxid Med Cell Longev* **2011**, *2011*, 841749, doi:10.1155/2011/841749.
301. Wood, R.J. Manganese and birth outcome. *Nutr Rev* **2009**, *67*, 416-420, doi:10.1111/j.1753-4887.2009.00214.x.

302. Takser, L.; Mergler, D.; Hellier, G.; Sahuquillo, J.; Huel, G. Manganese, monoamine metabolite levels at birth, and child psychomotor development. *Neurotoxicology* **2003**, *24*, 667-674, doi:10.1016/s0161-813x(03)00058-5.
303. Claus Henn, B.; Ettinger, A.S.; Schwartz, J.; Téllez-Rojo, M.M.; Lamadrid-Figueroa, H.; Hernández-Avila, M.; Schnaas, L.; Amarasiriwardena, C.; Bellinger, D.C.; Hu, H.; et al. Early postnatal blood manganese levels and children's neurodevelopment. *Epidemiology* **2010**, *21*, 433-439, doi:10.1097/ede.0b013e3181df8e52.
304. Miller, R.K.; Mattison, D.R.; Panigel, M.; Ceckler, T.; Bryant, R.; Thomford, P. Kinetic assessment of manganese using magnetic resonance imaging in the dually perfused human placenta in vitro. *Environ Health Perspect* **1987**, *74*, 81-91, doi:10.1289/ehp.877481.
305. Maccani, J.Z.; Koestler, D.C.; Houseman, E.A.; Armstrong, D.A.; Marsit, C.J.; Kelsey, K.T. DNA methylation changes in the placenta are associated with fetal manganese exposure. *Reprod Toxicol* **2015**, *57*, 43-49, doi:10.1016/j.reprotox.2015.05.002.
306. Nandakumaran, M.; Al-Sannan, B.; Al-Sarraf, H.; Al-Shammari, M. Maternal-fetal transport kinetics of manganese in perfused human placental lobule in vitro. *J Matern Fetal Neonatal Med* **2016**, *29*, 274-278, doi:10.3109/14767058.2014.998193.
307. Krachler, M.; Rossipal, E.; Micetic-Turk, D. Trace element transfer from the mother to the newborn--investigations on triplets of colostrum, maternal and umbilical cord sera. *Eur J Clin Nutr* **1999**, *53*, 486-494, doi:10.1038/sj.ejcn.1600781.
308. Michaelis, V.; Aengenheister, L.; Tuchtenhagen, M.; Rinklebe, J.; Ebert, F.; Schwerdtle, T.; Buerki-Thurnherr, T.; Bornhorst, J. Differences and Interactions in Placental Manganese and Iron Transfer across an In Vitro Model of Human Villous Trophoblasts. *Int J Mol Sci* **2022**, *23*, doi:10.3390/ijms23063296.
309. Panigel, M. Placental perfusion experiments. *American Journal of Obstetrics and Gynecology* **1962**, *84*, 1664-1683, doi:https://doi.org/10.1016/0002-9378(62)90009-1.
310. Schneider, H.; Panigel, M.; Dancis, J. Transfer across the perfused human placenta of antipyrine, sodium and leucine. *Am J Obstet Gynecol* **1972**, *114*, 822-828, doi:10.1016/0002-9378(72)90909-x.
311. Miller, R.K.; Wier, P.J.; Shah, Y.; di Sant'Agnese, P.A.; D'Gregorio, R.P. Criteria for In Vitro Dual Perfusions in the Human Placental Lobule: Perfusions in Excess of 12 Hours. In *Placenta as a Model and a Source*, Genbačev, O., Klopper, A., Beaconsfield, R., Eds.; Springer US: Boston, MA, 1989; pp. 27-38.
312. Myllynen, P.; Vähäkangas, K. Placental transfer and metabolism: an overview of the experimental models utilizing human placental tissue. *Toxicol In Vitro* **2013**, *27*, 507-512, doi:10.1016/j.tiv.2012.08.027.
313. Mose, T.; Mathiesen, L.; Karttunen, V.; Nielsen, J.K.; Sieppi, E.; Kummu, M.; Mørck, T.A.; Myöhänen, K.; Partanen, H.; Vähäkangas, K.; et al. Meta-analysis of data from human ex vivo placental perfusion studies on genotoxic and immunotoxic agents within the integrated European project NewGeneris. *Placenta* **2012**, *33*, 433-439, doi:10.1016/j.placenta.2012.02.004.
314. Correia Carreira, S.; Cartwright, L.; Mathiesen, L.; Knudsen, L.E.; Saunders, M. Studying placental transfer of highly purified non-dioxin-like PCBs in two models of the placental barrier. *Placenta* **2011**, *32*, 283-291, doi:10.1016/j.placenta.2010.12.024.
315. Hutson, J.R.; Garcia-Bournissen, F.; Davis, A.; Koren, G. The human placental perfusion model: a systematic review and development of a model to predict in vivo transfer of therapeutic drugs. *Clin Pharmacol Ther* **2011**, *90*, 67-76, doi:10.1038/clpt.2011.66.
316. Grafmüller, S.; Manser, P.; Krug, H.F.; Wick, P.; von Mandach, U. Determination of the transport rate of xenobiotics and nanomaterials across the placenta using the ex vivo human placental perfusion model. *J Vis Exp* **2013**, doi:10.3791/50401.
317. Dilworth, M.R.; Sibley, C.P. Review: Transport across the placenta of mice and women. *Placenta* **2013**, *34 Suppl*, S34-39, doi:10.1016/j.placenta.2012.10.011.
318. Abbas, Y.; Turco, M.Y.; Burton, G.J.; Moffett, A. Investigation of human trophoblast invasion in vitro. *Hum Reprod Update* **2020**, *26*, 501-513, doi:10.1093/humupd/dmaa017.

319. Holson, J.F.; Stump, D.G.; Pearce, L.B.; Watson, R.E.; DeSesso, J.M. Mode of action: yolk sac poisoning and impeded histiotrophic nutrition--HBOC-related congenital malformations. *Crit Rev Toxicol* **2005**, *35*, 739-745, doi:10.1080/10408440591007412.
320. Enders, A.C.; Blankenship, T.N. Comparative placental structure. *Adv Drug Deliv Rev* **1999**, *38*, 3-15, doi:10.1016/s0169-409x(99)00003-4.
321. Ruane, P.T.; Garner, T.; Parsons, L.; Babbington, P.A.; Wangsaputra, I.; Kimber, S.J.; Stevens, A.; Westwood, M.; Brison, D.R.; Aplin, J.D. Trophectoderm differentiation to invasive syncytiotrophoblast is promoted by endometrial epithelial cells during human embryo implantation. *Hum Reprod* **2022**, *37*, 777-792, doi:10.1093/humrep/deac008.
322. Haider, S.; Meinhardt, G.; Saleh, L.; Kunihs, V.; Gamperl, M.; Kaindl, U.; Ellinger, A.; Burkard, T.R.; Fiala, C.; Pollheimer, J.; et al. Self-Renewing Trophoblast Organoids Recapitulate the Developmental Program of the Early Human Placenta. *Stem Cell Reports* **2018**, *11*, 537-551, doi:10.1016/j.stemcr.2018.07.004.
323. Turco, M.Y.; Gardner, L.; Hughes, J.; Cindrova-Davies, T.; Gomez, M.J.; Farrell, L.; Hollinshead, M.; Marsh, S.G.E.; Brosens, J.J.; Critchley, H.O.; et al. Long-term, hormone-responsive organoid cultures of human endometrium in a chemically defined medium. *Nat Cell Biol* **2017**, *19*, 568-577, doi:10.1038/ncb3516.
324. Turco, M.Y.; Gardner, L.; Kay, R.G.; Hamilton, R.S.; Prater, M.; Hollinshead, M.S.; McWhinnie, A.; Esposito, L.; Fernando, R.; Skelton, H.; et al. Trophoblast organoids as a model for maternal-fetal interactions during human placentation. *Nature* **2018**, *564*, 263-267, doi:10.1038/s41586-018-0753-3.
325. King, A.; Thomas, L.; Bischof, P. Cell culture models of trophoblast II: trophoblast cell lines--a workshop report. *Placenta* **2000**, *21 Suppl A*, S113-119, doi:10.1053/plac.1999.0526.
326. Hiden, U.; Wadsack, C.; Prutsch, N.; Gauster, M.; Weiss, U.; Frank, H.G.; Schmitz, U.; Fast-Hirsch, C.; Hengstschläger, M.; Pötgens, A.; et al. The first trimester human trophoblast cell line ACH-3P: a novel tool to study autocrine/paracrine regulatory loops of human trophoblast subpopulations--TNF-alpha stimulates MMP15 expression. *BMC Dev Biol* **2007**, *7*, 137, doi:10.1186/1471-213x-7-137.
327. Abou-Kheir, W.; Barrak, J.; Hadadeh, O.; Daoud, G. HTR-8/SVneo cell line contains a mixed population of cells. *Placenta* **2017**, *50*, 1-7, doi:10.1016/j.placenta.2016.12.007.
328. Straszewski-Chavez, S.L.; Abrahams, V.M.; Alvero, A.B.; Aldo, P.B.; Ma, Y.; Guller, S.; Romero, R.; Mor, G. The isolation and characterization of a novel telomerase immortalized first trimester trophoblast cell line, Swan 71. *Placenta* **2009**, *30*, 939-948, doi:10.1016/j.placenta.2009.08.007.
329. Steinberg, M.L.; Robins, J.C. Cellular Models of Trophoblast Differentiation. *Semin Reprod Med* **2016**, *34*, 50-56, doi:10.1055/s-0035-1570026.
330. Orendi, K.; Kivity, V.; Sammar, M.; Grimpel, Y.; Gonen, R.; Meiri, H.; Lubzens, E.; Huppertz, B. Placental and trophoblastic in vitro models to study preventive and therapeutic agents for preeclampsia. *Placenta* **2011**, *32 Suppl*, S49-54, doi:10.1016/j.placenta.2010.11.023.
331. Bode, C.J.; Jin, H.; Rytting, E.; Silverstein, P.S.; Young, A.M.; Audus, K.L. In vitro models for studying trophoblast transcellular transport. *Methods Mol Med* **2006**, *122*, 225-239, doi:10.1385/1-59259-989-3:225.
332. Graham, C.H.; Hawley, T.S.; Hawley, R.G.; MacDougall, J.R.; Kerbel, R.S.; Khoo, N.; Lala, P.K. Establishment and characterization of first trimester human trophoblast cells with extended lifespan. *Exp Cell Res* **1993**, *206*, 204-211, doi:10.1006/excr.1993.1139.
333. Bischof, P.; Irminger-Finger, I. The human cytotrophoblastic cell, a mononuclear chameleon. *Int J Biochem Cell Biol* **2005**, *37*, 1-16, doi:10.1016/j.biocel.2004.05.014.
334. Kliman, H.J.; Nestler, J.E.; Sermasi, E.; Sanger, J.M.; Strauss, J.F., 3rd. Purification, characterization, and in vitro differentiation of cytotrophoblasts from human term placentae. *Endocrinology* **1986**, *118*, 1567-1582, doi:10.1210/endo-118-4-1567.
335. Robins, J.C.; Morgan, J.R.; Krueger, P.; Carson, S.A. Bioengineering anembryonic human trophoblast vesicles. *Reprod Sci* **2011**, *18*, 128-135, doi:10.1177/1933719110381923.

336. Kreuder, A.E.; Bolaños-Rosales, A.; Palmer, C.; Thomas, A.; Geiger, M.A.; Lam, T.; Amler, A.K.; Markert, U.R.; Lauster, R.; Kloke, L. Inspired by the human placenta: a novel 3D bioprinted membrane system to create barrier models. *Sci Rep* **2020**, *10*, 15606, doi:10.1038/s41598-020-72559-6.
337. Nishiguchi, A.; Gilmore, C.; Sood, A.; Matsusaki, M.; Collett, G.; Tannetta, D.; Sargent, I.L.; McGarvey, J.; Halemani, N.D.; Hanley, J.; et al. In vitro placenta barrier model using primary human trophoblasts, underlying connective tissue and vascular endothelium. *Biomaterials* **2019**, *192*, 140-148, doi:10.1016/j.biomaterials.2018.08.025.
338. Miura, S.; Sato, K.; Kato-Negishi, M.; Teshima, T.; Takeuchi, S. Fluid shear triggers microvilli formation via mechanosensitive activation of TRPV6. *Nat Commun* **2015**, *6*, 8871, doi:10.1038/ncomms9871.
339. Blundell, C.; Tess, E.R.; Schanzer, A.S.; Coutifaris, C.; Su, E.J.; Parry, S.; Huh, D. A microphysiological model of the human placental barrier. *Lab Chip* **2016**, *16*, 3065-3073, doi:10.1039/c6lc00259e.
340. Illsley, N.P. Glucose transporters in the human placenta. *Placenta* **2000**, *21*, 14-22, doi:10.1053/plac.1999.0448.
341. Friedman, S.J.; Skehan, P. Morphological differentiation of human choriocarcinoma cells induced by methotrexate. *Cancer Res* **1979**, *39*, 1960-1967.
342. Wice, B.; Menton, D.; Geuze, H.; Schwartz, A.L. Modulators of cyclic AMP metabolism induce syncytiotrophoblast formation in vitro. *Exp Cell Res* **1990**, *186*, 306-316, doi:10.1016/0014-4827(90)90310-7.
343. Seamon, K.B.; Padgett, W.; Daly, J.W. Forskolin: unique diterpene activator of adenylate cyclase in membranes and in intact cells. *Proc Natl Acad Sci U S A* **1981**, *78*, 3363-3367, doi:10.1073/pnas.78.6.3363.
344. Borges, M.; Bose, P.; Frank, H.G.; Kaufmann, P.; Pötgens, A.J. A two-colour fluorescence assay for the measurement of syncytial fusion between trophoblast-derived cell lines. *Placenta* **2003**, *24*, 959-964, doi:10.1016/s0143-4004(03)00173-5.
345. Hertz, R. Choriocarcinoma of women maintained in serial passage in hamster and rat. *Proc Soc Exp Biol Med* **1959**, *102*, 77-81, doi:10.3181/00379727-102-25149.
346. Kallol, S.; Moser-Haessig, R.; Ontsouka, C.E.; Albrecht, C. Comparative expression patterns of selected membrane transporters in differentiated BeWo and human primary trophoblast cells. *Placenta* **2018**, *72-73*, 48-52, doi:10.1016/j.placenta.2018.10.008.
347. Karahoda, R.; Zaugg, J.; Fuenzalida, B.; Kallol, S.; Moser-Haessig, R.; Staud, F.; Albrecht, C. Trophoblast Differentiation Affects Crucial Nutritive Functions of Placental Membrane Transporters. *Front Cell Dev Biol* **2022**, *10*, 820286, doi:10.3389/fcell.2022.820286.
348. Liu, F.; Soares, M.J.; Audus, K.L. Permeability properties of monolayers of the human trophoblast cell line BeWo. *Am J Physiol* **1997**, *273*, C1596-1604, doi:10.1152/ajpcell.1997.273.5.C1596.
349. Zhao, H.; Hundal, H.S. Identification and biochemical localization of a Na-K-Cl cotransporter in the human placental cell line BeWo. *Biochem Biophys Res Commun* **2000**, *274*, 43-48, doi:10.1006/bbrc.2000.3099.
350. Cerneus, D.P.; van der Ende, A. Apical and basolateral transferrin receptors in polarized BeWo cells recycle through separate endosomes. *J Cell Biol* **1991**, *114*, 1149-1158, doi:10.1083/jcb.114.6.1149.
351. Li, H.; van Ravenzwaay, B.; Rietjens, I.M.; Louisse, J. Assessment of an in vitro transport model using BeWo b30 cells to predict placental transfer of compounds. *Arch Toxicol* **2013**, *87*, 1661-1669, doi:10.1007/s00204-013-1074-9.
352. Heaton, S.J.; Eady, J.J.; Parker, M.L.; Gotts, K.L.; Dainty, J.R.; Fairweather-Tait, S.J.; McArdle, H.J.; Srai, K.S.; Elliott, R.M. The use of BeWo cells as an in vitro model for placental iron transport. *Am J Physiol Cell Physiol* **2008**, *295*, C1445-1453, doi:10.1152/ajpcell.00286.2008.
353. Puliafito, A.; Hufnagel, L.; Neveu, P.; Streichan, S.; Sigal, A.; Fygenson, D.K.; Shraiman, B.I. Collective and single cell behavior in epithelial contact inhibition. *Proc Natl Acad Sci U S A* **2012**, *109*, 739-744, doi:10.1073/pnas.1007809109.

354. Vargesson, N. Thalidomide-induced teratogenesis: history and mechanisms. *Birth Defects Res C Embryo Today* **2015**, *105*, 140-156, doi:10.1002/bdrc.21096.
355. Beekhuijzen, M. The era of 3Rs implementation in developmental and reproductive toxicity (DART) testing: Current overview and future perspectives. *Reprod Toxicol* **2017**, *72*, 86-96, doi:10.1016/j.reprotox.2017.05.006.
356. W. M. S. Russel, R.L.B. The Principles of Humane Experimental Technique. *Medical Journal of Australia* **1960**, *1*, 500-500, doi:https://doi.org/10.5694/j.1326-5377.1960.tb73127.x.
357. Sokolov, D.I.; Furaeva, K.N.; Stepanova, O.I.; Ovchinnikova, O.M.; Viazmina, L.P.; Kozonov, G.R.; Kuzminykh, T.U.; Selkov, S.A. Changes in Functional Activity of JEG-3 Trophoblast Cell Line in the Presence of Factors Secreted by Placenta. *Arch Med Res* **2015**, *46*, 245-256, doi:10.1016/j.arcmed.2015.05.004.
358. Stenqvist, A.C.; Chen, T.; Hedlund, M.; Dimova, T.; Nagaeva, O.; Kjellberg, L.; Innala, E.; Mincheva-Nilsson, L. An efficient optimized method for isolation of villous trophoblast cells from human early pregnancy placenta suitable for functional and molecular studies. *Am J Reprod Immunol* **2008**, *60*, 33-42, doi:10.1111/j.1600-0897.2008.00588.x.
359. Dallmann, A.; Liu, X.I.; Burckart, G.J.; van den Anker, J. Drug Transporters Expressed in the Human Placenta and Models for Studying Maternal-Fetal Drug Transfer. *J Clin Pharmacol* **2019**, *59 Suppl 1*, S70-s81, doi:10.1002/jcph.1491.
360. Panigel, M.; Pascaud, M.; Brun, J.L. [Radioangiographic study of circulation in the villi and intervillous space of isolated human placental cotyledon kept viable by perfusion]. *J Physiol (Paris)* **1967**, *59*, 277.
361. Schneider, H.; Huch, A. Dual in vitro perfusion of an isolated lobe of human placenta: method and instrumentation. *Contrib Gynecol Obstet* **1985**, *13*, 40-47.
362. Dwyer, J.T.; Coates, P.M.; Smith, M.J. Dietary Supplements: Regulatory Challenges and Research Resources. *Nutrients* **2018**, *10*, doi:10.3390/nu10010041.
363. Brown, B.; Wright, C. Safety and efficacy of supplements in pregnancy. *Nutr Rev* **2020**, *78*, 813-826, doi:10.1093/nutrit/nuz101.
364. Vardhana, P.A.; Illsley, N.P. Transepithelial glucose transport and metabolism in BeWo choriocarcinoma cells. *Placenta* **2002**, *23*, 653-660, doi:10.1053/plac.2002.0857.
365. Kallol, S.; Albrecht, C. Materno-fetal cholesterol transport during pregnancy. *Biochem Soc Trans* **2020**, *48*, 775-786, doi:10.1042/bst20190129.
366. Srinivasan, B.; Kolli, A.R.; Esch, M.B.; Abaci, H.E.; Shuler, M.L.; Hickman, J.J. TEER measurement techniques for in vitro barrier model systems. *J Lab Autom* **2015**, *20*, 107-126, doi:10.1177/2211068214561025.
367. Benson, K.; Cramer, S.; Galla, H.J. Impedance-based cell monitoring: barrier properties and beyond. *Fluids Barriers CNS* **2013**, *10*, 5, doi:10.1186/2045-8118-10-5.
368. Rohn, I.; Kroepfl, N.; Bornhorst, J.; Kuehnelt, D.; Schwerdtle, T. Side-Directed Transfer and Presystemic Metabolism of Selenoneine in a Human Intestinal Barrier Model. *Mol Nutr Food Res* **2019**, *63*, e1900080, doi:10.1002/mnfr.201900080.
369. Crowe, A.; Keelan, J.A. Development of a model for functional studies of ABCG2 (breast cancer resistance protein) efflux employing a standard BeWo clone (B24). *Assay Drug Dev Technol* **2012**, *10*, 476-484, doi:10.1089/adt.2011.441.
370. Szaraz, P.; Librach, M.; Mander, P.; Hoseini, B.; Librach, M.; Iqbal, F.; Librach, C. A solution to prevent secondary flow in adherent cell cultures. *Biol Open* **2019**, *8*, doi:10.1242/bio.045294.
371. Cartwright, L.; Poulsen, M.S.; Nielsen, H.M.; Pojana, G.; Knudsen, L.E.; Saunders, M.; Rytting, E. In vitro placental model optimization for nanoparticle transport studies. *Int J Nanomedicine* **2012**, *7*, 497-510, doi:10.2147/ijn.S26601.
372. Lang, I.; Pabst, M.A.; Hiden, U.; Blaschitz, A.; Dohr, G.; Hahn, T.; Desoye, G. Heterogeneity of microvascular endothelial cells isolated from human term placenta and macrovascular umbilical vein endothelial cells. *Eur J Cell Biol* **2003**, *82*, 163-173, doi:10.1078/0171-9335-00306.
373. GmbH, P. Product description Endothelial Cell Growth Medium supplement. Available online: https://promocell.com/product/endothelial-cell-growth-medium/#tab-description (accessed on

374. Forbes, K.; Westwood, M.; Baker, P.N.; Aplin, J.D. Insulin-like growth factor I and II regulate the life cycle of trophoblast in the developing human placenta. *Am J Physiol Cell Physiol* **2008**, *294*, C1313-1322, doi:10.1152/ajpcell.00035.2008.
375. Stevenson, B.R.; Siliciano, J.D.; Mooseker, M.S.; Goodenough, D.A. Identification of ZO-1: a high molecular weight polypeptide associated with the tight junction (zonula occludens) in a variety of epithelia. *J Cell Biol* **1986**, *103*, 755-766, doi:10.1083/jcb.103.3.755.
376. Bhabra, G.; Sood, A.; Fisher, B.; Cartwright, L.; Saunders, M.; Evans, W.H.; Surprenant, A.; Lopez-Castejon, G.; Mann, S.; Davis, S.A.; et al. Nanoparticles can cause DNA damage across a cellular barrier. *Nat Nanotechnol* **2009**, *4*, 876-883, doi:10.1038/nnano.2009.313.
377. Kaufmann, P.; Mayhew, T.M.; Charnock-Jones, D.S. Aspects of human fetoplacental vasculogenesis and angiogenesis. II. Changes during normal pregnancy. *Placenta* **2004**, *25*, 114-126, doi:10.1016/j.placenta.2003.10.009.
378. Leach, L.; Badet, J.; Brownbill, P.; Harris, L.; Keogh, R.; Kalionis, B.; Whitley, G. Endothelium, blood vessels and angiogenesis -- a workshop report. *Placenta* **2006**, *27 Suppl A*, S26-29, doi:10.1016/j.placenta.2006.01.022.
379. Levkovitz, R.; Zaretsky, U.; Gordon, Z.; Jaffa, A.J.; Elad, D. In vitro simulation of placental transport: part I. Biological model of the placental barrier. *Placenta* **2013**, *34*, 699-707, doi:10.1016/j.placenta.2013.03.014.
380. Lee, J.S.; Romero, R.; Han, Y.M.; Kim, H.C.; Kim, C.J.; Hong, J.S.; Huh, D. Placenta-on-a-chip: a novel platform to study the biology of the human placenta. *J Matern Fetal Neonatal Med* **2016**, *29*, 1046-1054, doi:10.3109/14767058.2015.1038518.
381. Wong, M.K.; Li, E.W.; Adam, M.; Selvaganapathy, P.R.; Raha, S. Establishment of an in vitro placental barrier model cultured under physiologically relevant oxygen levels. *Mol Hum Reprod* **2020**, *26*, 353-365, doi:10.1093/molehr/gaaa018.
382. Huang, X.; Jia, L.; Qian, Z.; Jia, Y.; Chen, X.; Xu, X.; Chang, X.; Liu, M.; Wang, K. Diversity in human placental microvascular endothelial cells and macrovascular endothelial cells. *Cytokine* **2018**, *111*, 287-294, doi:10.1016/j.cyto.2018.09.009.
383. Mirbod, P. Analytical model of the feto-placental vascular system: consideration of placental oxygen transport. *R Soc Open Sci* **2018**, *5*, 180219, doi:10.1098/rsos.180219.
384. Wang, W.; Zhao, F.; Ma, X.; Perry, G.; Zhu, X. Mitochondria dysfunction in the pathogenesis of Alzheimer's disease: recent advances. *Mol Neurodegener* **2020**, *15*, 30, doi:10.1186/s13024-020-00376-6.
385. Farina, M.; Avila, D.S.; da Rocha, J.B.; Aschner, M. Metals, oxidative stress and neurodegeneration: a focus on iron, manganese and mercury. *Neurochem Int* **2013**, *62*, 575-594, doi:10.1016/j.neuint.2012.12.006.
386. Rock, K.D.; Patisaul, H.B. Environmental Mechanisms of Neurodevelopmental Toxicity. *Curr Environ Health Rep* **2018**, *5*, 145-157, doi:10.1007/s40572-018-0185-0.
387. Ek, C.J.; Dziegielewska, K.M.; Habgood, M.D.; Saunders, N.R. Barriers in the developing brain and Neurotoxicology. *Neurotoxicology* **2012**, *33*, 586-604, doi:10.1016/j.neuro.2011.12.009.
388. Hurley, L.S. The roles of trace elements in foetal and neonatal development. *Philos Trans R Soc Lond B Biol Sci* **1981**, *294*, 145-152, doi:10.1098/rstb.1981.0095.
389. Kupsco, A.; Estrada-Gutierrez, G.; Cantoral, A.; Schnaas, L.; Pantic, I.; Amarasiriwardena, C.; Svensson, K.; Bellinger, D.C.; Téllez-Rojo, M.M.; Baccarelli, A.A.; et al. Modification of the effects of prenatal manganese exposure on child neurodevelopment by maternal anemia and iron deficiency. *Pediatr Res* **2020**, *88*, 325-333, doi:10.1038/s41390-020-0754-4.
390. de Water, E.; Papazaharias, D.M.; Ambrosi, C.; Mascaro, L.; Iannilli, E.; Gasparotti, R.; Lucchini, R.G.; Austin, C.; Arora, M.; Tang, C.Y.; et al. Early-life dentine manganese concentrations and intrinsic functional brain connectivity in adolescents: A pilot study. *PLoS One* **2019**, *14*, e0220790, doi:10.1371/journal.pone.0220790.
391. Witt, B.; Meyer, S.; Ebert, F.; Francesconi, K.A.; Schwerdtle, T. Toxicity of two classes of arsenolipids and their water-soluble metabolites in human differentiated neurons. *Arch Toxicol* **2017**, *91*, 3121-3134, doi:10.1007/s00204-017-1933-x.

392. Nikulin, S.V.; Knyazev, E.N.; Gerasimenko, T.N.; Shilin, S.A.; Gazizov, I.N.; Zakharova, G.S.; Poloznikov, A.A.; Sakharov, D.A. [Impedance Spectroscopy and Transcriptome Analysis of Choriocarcinoma BeWo b30 as a Model of Human Placenta]. *Mol Biol (Mosk)* **2019**, *53*, 467-475, doi:10.1134/s0026898419030133.
393. Widhalm, R.; Ellinger, I.; Granitzer, S.; Forsthuber, M.; Bajtela, R.; Gelles, K.; Hartig, P.Y.; Hengstschläger, M.; Zeisler, H.; Salzer, H.; et al. Human placental cell line HTR-8/SVneo accumulates cadmium by divalent metal transporters DMT1 and ZIP14. *Metallomics* **2020**, *12*, 1822-1833, doi:10.1039/d0mt00199f.
394. Prouillac, C.; Lecoeur, S. The role of the placenta in fetal exposure to xenobiotics: importance of membrane transporters and human models for transfer studies. *Drug Metab Dispos* **2010**, *38*, 1623-1635, doi:10.1124/dmd.110.033571.
395. Faust, J.J.; Zhang, W.; Chen, Y.; Capco, D.G. Alpha-Fe(2)O(3) elicits diameter-dependent effects during exposure to an in vitro model of the human placenta. *Cell Biol Toxicol* **2014**, *30*, 31-53, doi:10.1007/s10565-013-9267-9.
396. Li, X.; Xie, J.; Lu, L.; Zhang, L.; Zhang, L.; Zou, Y.; Wang, Q.; Luo, X.; Li, S. Kinetics of manganese transport and gene expressions of manganese transport carriers in Caco-2 cell monolayers. *Biometals* **2013**, *26*, 941-953, doi:10.1007/s10534-013-9670-y.
397. Aschner, M. The transport of manganese across the blood-brain barrier. *Neurotoxicology* **2006**, *27*, 311-314, doi:10.1016/j.neuro.2005.09.002.
398. Chen, P.; Chakraborty, S.; Mukhopadhyay, S.; Lee, E.; Paoliello, M.M.; Bowman, A.B.; Aschner, M. Manganese homeostasis in the nervous system. *J Neurochem* **2015**, *134*, 601-610, doi:10.1111/jnc.13170.
399. Yoon, M.; Nong, A.; Clewell, H.J., 3rd; Taylor, M.D.; Dorman, D.C.; Andersen, M.E. Evaluating placental transfer and tissue concentrations of manganese in the pregnant rat and fetuses after inhalation exposures with a PBPK model. *Toxicol Sci* **2009**, *112*, 44-58, doi:10.1093/toxsci/kfp198.
400. Natoli, M.; Felsani, A.; Ferruzza, S.; Sambuy, Y.; Canali, R.; Scarino, M.L. Mechanisms of defence from Fe(II) toxicity in human intestinal Caco-2 cells. *Toxicol In Vitro* **2009**, *23*, 1510-1515, doi:10.1016/j.tiv.2009.06.016.
401. Casanueva, E.; Viteri, F.E. Iron and oxidative stress in pregnancy. *J Nutr* **2003**, *133*, 1700s-1708s, doi:10.1093/jn/133.5.1700S.
402. Walker, O.S.; Ragos, R.; Wong, M.K.; Adam, M.; Cheung, A.; Raha, S. Reactive oxygen species from mitochondria impacts trophoblast fusion and the production of endocrine hormones by syncytiotrophoblasts. *PLoS One* **2020**, *15*, e0229332, doi:10.1371/journal.pone.0229332.
403. Mikelson, C.K.; Troisi, J.; LaLonde, A.; Symes, S.J.K.; Thurston, S.W.; DiRe, L.M.; David Adair, C.; Miller, R.K.; Richards, S.M. Placental concentrations of essential, toxic, and understudied metals and relationships with birth outcomes in Chattanooga, TN. *Environ Res* **2019**, *168*, 118-129, doi:10.1016/j.envres.2018.09.006.
404. Yin, S.; Wang, C.; Wei, J.; Wang, D.; Jin, L.; Liu, J.; Wang, L.; Li, Z.; Ren, A.; Yin, C. Essential trace elements in placental tissue and risk for fetal neural tube defects. *Environ Int* **2020**, *139*, 105688, doi:10.1016/j.envint.2020.105688.
405. Callan, A.C.; Hinwood, A.L.; Ramalingam, M.; Boyce, M.; Heyworth, J.; McCafferty, P.; Odland, J. Maternal exposure to metals--concentrations and predictors of exposure. *Environ Res* **2013**, *126*, 111-117, doi:10.1016/j.envres.2013.07.004.
406. Freire, C.; Amaya, E.; Gil, F.; Murcia, M.; S, L.L.; Casas, M.; Vrijheid, M.; Lertxundi, A.; Irizar, A.; Fernández-Tardón, G.; et al. Placental metal concentrations and birth outcomes: The Environment and Childhood (INMA) project. *Int J Hyg Environ Health* **2019**, *222*, 468-478, doi:10.1016/j.ijheh.2018.12.014.
407. de Angelis, P.; Miller, R.K.; Darrah, T.H.; Katzman, P.J.; Pressman, E.K.; Kent, T.R.; O'Brien, K.O. Elemental content of the placenta: A comparison between two high-risk obstetrical populations, adult women carrying multiples and adolescents carrying singletons. *Environ Res* **2017**, *158*, 553-565, doi:10.1016/j.envres.2017.07.008.

408. Union, T.E.P.a.t.C.o.t.E. DIRECTIVE 2002/46/EC OF TH EUROPEAN PARLIAMENT AND OF THE COUNCIL of 10 June 2002 on the approximation of the laws of the Member States relating to food supplements. *Official Journal of the European Communitites* **2002**.
409. Rabin, O.; Hegedus, L.; Bourre, J.M.; Smith, Q.R. Rapid brain uptake of manganese(II) across the blood-brain barrier. *J Neurochem* **1993**, *61*, 509-517, doi:10.1111/j.1471-4159.1993.tb02153.x.
410. Yoon, M.; Schroeter, J.D.; Nong, A.; Taylor, M.D.; Dorman, D.C.; Andersen, M.E.; Clewell, H.J., 3rd. Physiologically based pharmacokinetic modeling of fetal and neonatal manganese exposure in humans: describing manganese homeostasis during development. *Toxicol Sci* **2011**, *122*, 297-316, doi:10.1093/toxsci/kfr141.
411. Byrne, S.L.; Buckett, P.D.; Kim, J.; Luo, F.; Sanford, J.; Chen, J.; Enns, C.; Wessling-Resnick, M. Ferristatin II promotes degradation of transferrin receptor-1 in vitro and in vivo. *PLoS One* **2013**, *8*, e70199, doi:10.1371/journal.pone.0070199.
412. Yanatori, I.; Yasui, Y.; Noguchi, Y.; Kishi, F. Inhibition of iron uptake by ferristatin II is exerted through internalization of DMT1 at the plasma membrane. *Cell Biol Int* **2015**, *39*, 427-434, doi:10.1002/cbin.10403.
413. Arumugasaamy, N.; Rock, K.D.; Kuo, C.Y.; Bale, T.L.; Fisher, J.P. Microphysiological systems of the placental barrier. *Adv Drug Deliv Rev* **2020**, *161-162*, 161-175, doi:10.1016/j.addr.2020.08.010.
414. Gambling, L.; Lang, C.; McArdle, H.J. Fetal regulation of iron transport during pregnancy. *Am J Clin Nutr* **2011**, *94*, 1903s-1907s, doi:10.3945/ajcn.110.000885.
415. Michalke, B.; Willkommen, D.; Venkataramani, V. Iron Redox Speciation Analysis Using Capillary Electrophoresis Coupled to Inductively Coupled Plasma Mass Spectrometry (CE-ICP-MS). *Front Chem* **2019**, *7*, 136, doi:10.3389/fchem.2019.00136.
416. Aschner, J.L.; Aschner, M. Nutritional aspects of manganese homeostasis. *Mol Aspects Med* **2005**, *26*, 353-362, doi:10.1016/j.mam.2005.07.003.
417. Miyazawa, M.; Bogdan, A.R.; Hashimoto, K.; Tsuji, Y. Regulation of transferrin receptor-1 mRNA by the interplay between IRE-binding proteins and miR-7/miR-141 in the 3'-IRE stem-loops. *Rna* **2018**, *24*, 468-479, doi:10.1261/rna.063941.117.
418. Klausner, R.D.; Rouault, T.A.; Harford, J.B. Regulating the fate of mRNA: the control of cellular iron metabolism. *Cell* **1993**, *72*, 19-28, doi:10.1016/0092-8674(93)90046-s.
419. Mazgaj, R.; Lipiński, P.; Edison, E.S.; Bednarz, A.; Staroń, R.; Haberkiewicz, O.; Lenartowicz, M.; Smuda, E.; Jończy, A.; Starzyński, R.R. Marginally reduced maternal hepatic and splenic ferroportin under severe nutritional iron deficiency in pregnancy maintains systemic iron supply. *Am J Hematol* **2021**, *96*, 659-670, doi:10.1002/ajh.26152.
420. Li, Y.Q.; Bai, B.; Cao, X.X.; Yan, H.; Zhuang, G.H. Ferroportin 1 and hephaestin expression in BeWo cell line with different iron treatment. *Cell Biochem Funct* **2012**, *30*, 249-255, doi:10.1002/cbf.1843.
421. Bogdan, A.R.; Miyazawa, M.; Hashimoto, K.; Tsuji, Y. Regulators of Iron Homeostasis: New Players in Metabolism, Cell Death, and Disease. *Trends Biochem Sci* **2016**, *41*, 274-286, doi:10.1016/j.tibs.2015.11.012.
422. Yang, A.; Zhao, J.; Lu, M.; Gu, Y.; Zhu, Y.; Chen, D.; Fu, J. Expression of Hepcidin and Ferroportin in the Placenta, and Ferritin and Transferrin Receptor 1 Levels in Maternal and Umbilical Cord Blood in Pregnant Women with and without Gestational Diabetes. *Int J Environ Res Public Health* **2016**, *13*, doi:10.3390/ijerph13080766.
423. Tai, Y.K.; Chew, K.C.M.; Tan, B.W.Q.; Lim, K.L.; Soong, T.W. Iron mitigates DMT1-mediated manganese cytotoxicity via the ASK1-JNK signaling axis: Implications of iron supplementation for manganese toxicity. *Sci Rep* **2016**, *6*, 21113, doi:10.1038/srep21113.
424. Zheng, W.; Zhao, Q. Iron overload following manganese exposure in cultured neuronal, but not neuroglial cells. *Brain Res* **2001**, *897*, 175-179, doi:10.1016/s0006-8993(01)02049-2.
425. Wu, F.; Tian, F.J.; Lin, Y.; Xu, W.M. Oxidative Stress: Placenta Function and Dysfunction. *Am J Reprod Immunol* **2016**, *76*, 258-271, doi:10.1111/aji.12454.

426. Burton, G.J.; Jauniaux, E.; Watson, A.L. Maternal arterial connections to the placental intervillous space during the first trimester of human pregnancy: the Boyd collection revisited. *Am J Obstet Gynecol* **1999**, *181*, 718-724, doi:10.1016/s0002-9378(99)70518-1.
427. Cindrova-Davies, T.; van Patot, M.T.; Gardner, L.; Jauniaux, E.; Burton, G.J.; Charnock-Jones, D.S. Energy status and HIF signalling in chorionic villi show no evidence of hypoxic stress during human early placental development. *Mol Hum Reprod* **2015**, *21*, 296-308, doi:10.1093/molehr/gau105.
428. Lees, J.G.; Gardner, D.K.; Harvey, A.J. Pluripotent Stem Cell Metabolism and Mitochondria: Beyond ATP. *Stem Cells Int* **2017**, *2017*, 2874283, doi:10.1155/2017/2874283.
429. Burton, G.J.; Hempstock, J.; Jauniaux, E. Oxygen, early embryonic metabolism and free radical-mediated embryopathies. *Reprod Biomed Online* **2003**, *6*, 84-96, doi:10.1016/s1472-6483(10)62060-3.
430. Burton, G.J.; Jauniaux, E. Placental oxidative stress: from miscarriage to preeclampsia. *J Soc Gynecol Investig* **2004**, *11*, 342-352, doi:10.1016/j.jsgi.2004.03.003.
431. Chiarello, D.I.; Abad, C.; Rojas, D.; Toledo, F.; Vázquez, C.M.; Mate, A.; Sobrevia, L.; Marín, R. Oxidative stress: Normal pregnancy versus preeclampsia. *Biochim Biophys Acta Mol Basis Dis* **2020**, *1866*, 165354, doi:10.1016/j.bbadis.2018.12.005.
432. Watson, A.L.; Skepper, J.N.; Jauniaux, E.; Burton, G.J. Susceptibility of human placental syncytiotrophoblastic mitochondria to oxygen-mediated damage in relation to gestational age. *J Clin Endocrinol Metab* **1998**, *83*, 1697-1705, doi:10.1210/jcem.83.5.4830.
433. Manna, S.; Ruano, C.S.M.; Hegenbarth, J.C.; Vaiman, D.; Gupta, S.; McCarthy, F.P.; Méhats, C.; McCarthy, C.; Apicella, C.; Scheel, J. Computational Models on Pathological Redox Signalling Driven by Pregnancy: A Review. *Antioxidants (Basel)* **2022**, *11*, doi:10.3390/antiox11030585.
434. Perrone, S.; Laschi, E.; Buonocore, G. Biomarkers of oxidative stress in the fetus and in the newborn. *Free Radic Biol Med* **2019**, *142*, 23-31, doi:10.1016/j.freeradbiomed.2019.03.034.
435. Mistry, H.D.; Kurlak, L.O.; Williams, P.J.; Ramsay, M.M.; Symonds, M.E.; Broughton Pipkin, F. Differential expression and distribution of placental glutathione peroxidases 1, 3 and 4 in normal and preeclamptic pregnancy. *Placenta* **2010**, *31*, 401-408, doi:10.1016/j.placenta.2010.02.011.
436. Endler, M.; Saltvedt, S.; Eweida, M.; Åkerud, H. Oxidative stress and inflammation in retained placenta: a pilot study of protein and gene expression of GPX1 and NFκB. *BMC Pregnancy Childbirth* **2016**, *16*, 384, doi:10.1186/s12884-016-1135-1.
437. Zusterzeel, P.L.; Peters, W.H.; De Bruyn, M.A.; Knapen, M.F.; Merkus, H.M.; Steegers, E.A. Glutathione S-transferase isoenzymes in decidua and placenta of preeclamptic pregnancies. *Obstet Gynecol* **1999**, *94*, 1033-1038, doi:10.1016/s0029-7844(99)00433-0.
438. Guller, S.; Buhimschi, C.S.; Ma, Y.Y.; Huang, S.T.; Yang, L.; Kuczynski, E.; Zambrano, E.; Lockwood, C.J.; Buhimschi, I.A. Placental expression of ceruloplasmin in pregnancies complicated by severe preeclampsia. *Lab Invest* **2008**, *88*, 1057-1067, doi:10.1038/labinvest.2008.74.
439. McAleer, M.F.; Tuan, R.S. Cytotoxicant-induced trophoblast dysfunction and abnormal pregnancy outcomes: role of zinc and metallothionein. *Birth Defects Res C Embryo Today* **2004**, *72*, 361-370, doi:10.1002/bdrc.20024.
440. Aouache, R.; Biquard, L.; Vaiman, D.; Miralles, F. Oxidative Stress in Preeclampsia and Placental Diseases. *Int J Mol Sci* **2018**, *19*, doi:10.3390/ijms19051496.
441. Vaka, R.; Deer, E.; LaMarca, B. Is Mitochondrial Oxidative Stress a Viable Therapeutic Target in Preeclampsia? *Antioxidants (Basel)* **2022**, *11*, doi:10.3390/antiox11020210.
442. Walsh, S.W.; Vaughan, J.E.; Wang, Y.; Roberts, L.J., 2nd. Placental isoprostane is significantly increased in preeclampsia. *Faseb j* **2000**, *14*, 1289-1296, doi:10.1096/fj.14.10.1289.
443. Wang, Y.; Walsh, S.W. Increased superoxide generation is associated with decreased superoxide dismutase activity and mRNA expression in placental trophoblast cells in pre-eclampsia. *Placenta* **2001**, *22*, 206-212, doi:10.1053/plac.2000.0608.
444. Goulopoulou, S.; Davidge, S.T. Molecular mechanisms of maternal vascular dysfunction in preeclampsia. *Trends Mol Med* **2015**, *21*, 88-97, doi:10.1016/j.molmed.2014.11.009.

445. Sarwar, M.S.; Ahmed, S.; Ullah, M.S.; Kabir, H.; Rahman, G.K.; Hasnat, A.; Islam, M.S. Comparative study of serum zinc, copper, manganese, and iron in preeclamptic pregnant women. *Biol Trace Elem Res* **2013**, *154*, 14-20, doi:10.1007/s12011-013-9721-9.
446. Liu, T.; Hivert, M.F.; Rifas-Shiman, S.L.; Rahman, M.L.; Oken, E.; Cardenas, A.; Mueller, N.T. Prospective Association Between Manganese in Early Pregnancy and the Risk of Preeclampsia. *Epidemiology* **2020**, *31*, 677-680, doi:10.1097/ede.0000000000001227.
447. Beharier, O.; Kajiwara, K.; Sadovsky, Y. Ferroptosis, trophoblast lipotoxic damage, and adverse pregnancy outcome. *Placenta* **2021**, *108*, 32-38, doi:10.1016/j.placenta.2021.03.007.
448. Li, H.; Wu, S.; Shi, N.; Lian, S.; Lin, W. Nrf2/HO-1 pathway activation by manganese is associated with reactive oxygen species and ubiquitin-proteasome pathway, not MAPKs signaling. *J Appl Toxicol* **2011**, *31*, 690-697, doi:10.1002/jat.1654.
449. Zhang, H.; He, Y.; Wang, J.X.; Chen, M.H.; Xu, J.J.; Jiang, M.H.; Feng, Y.L.; Gu, Y.F. miR-30-5p-mediated ferroptosis of trophoblasts is implicated in the pathogenesis of preeclampsia. *Redox Biol* **2020**, *29*, 101402, doi:10.1016/j.redox.2019.101402.
450. Hirata, Y. Manganese-induced apoptosis in PC12 cells. *Neurotoxicol Teratol* **2002**, *24*, 639-653, doi:10.1016/s0892-0362(02)00215-5.
451. Crittenden, P.L.; Filipov, N.M. Manganese-induced potentiation of in vitro proinflammatory cytokine production by activated microglial cells is associated with persistent activation of p38 MAPK. *Toxicol In Vitro* **2008**, *22*, 18-27, doi:10.1016/j.tiv.2007.07.004.
452. Crittenden, P.L.; Filipov, N.M. Manganese modulation of MAPK pathways: effects on upstream mitogen activated protein kinase kinases and mitogen activated kinase phosphatase-1 in microglial cells. *J Appl Toxicol* **2011**, *31*, 1-10, doi:10.1002/jat.1552.
453. Bornhorst, J.; Meyer, S.; Weber, T.; Böker, C.; Marschall, T.; Mangerich, A.; Beneke, S.; Bürkle, A.; Schwerdtle, T. Molecular mechanisms of Mn induced neurotoxicity: RONS generation, genotoxicity, and DNA-damage response. *Mol Nutr Food Res* **2013**, *57*, 1255-1269, doi:10.1002/mnfr.201200758.
454. Hempel, S.L.; Buettner, G.R.; O'Malley, Y.Q.; Wessels, D.A.; Flaherty, D.M. Dihydrofluorescein diacetate is superior for detecting intracellular oxidants: comparison with 2',7'-dichlorodihydrofluorescein diacetate, 5(and 6)-carboxy-2',7'-dichlorodihydrofluorescein diacetate, and dihydrorhodamine 123. *Free Radic Biol Med* **1999**, *27*, 146-159, doi:10.1016/s0891-5849(99)00061-1.
455. Raijmakers, M.T.; Bruggeman, S.W.; Steegers, E.A.; Peters, W.H. Distribution of components of the glutathione detoxification system across the human placenta after uncomplicated vaginal deliveries. *Placenta* **2002**, *23*, 490-496, doi:10.1053/plac.2002.0832.
456. Gundacker, C.; Hengstschläger, M. The role of the placenta in fetal exposure to heavy metals. *Wien Med Wochenschr* **2012**, *162*, 201-206, doi:10.1007/s10354-012-0074-3.
457. Yuan, Y.; Qian, Z.R.; Sano, T.; Asa, S.L.; Yamada, S.; Kagawa, N.; Kudo, E. Reduction of GSTP1 expression by DNA methylation correlates with clinicopathological features in pituitary adenomas. *Mod Pathol* **2008**, *21*, 856-865, doi:10.1038/modpathol.2008.60.
458. Shilpa, V.; Bhagat, R.; Premalata, C.; Pallavi, V.; Krishnamoorthy, L. GSTP1 expression and promoter methylation in epithelial ovarian carcinoma. *Clinical Cancer Investigation Journal* **2014**, *3*, 487-492.
459. Taylor, S.C.; Nadeau, K.; Abbasi, M.; Lachance, C.; Nguyen, M.; Fenrich, J. The Ultimate qPCR Experiment: Producing Publication Quality, Reproducible Data the First Time. *Trends Biotechnol* **2019**, *37*, 761-774, doi:10.1016/j.tibtech.2018.12.002.
460. Troy, C.M.; Derossi, D.; Prochiantz, A.; Greene, L.A.; Shelanski, M.L. Downregulation of Cu/Zn superoxide dismutase leads to cell death via the nitric oxide-peroxynitrite pathway. *J Neurosci* **1996**, *16*, 253-261, doi:10.1523/jneurosci.16-01-00253.1996.
461. Lim, L.; Song, J. A novel SOD1-dependent mechanism for the iron-induced production of toxic SOD1 and oxidative stress that initiates ALS. *bioRxiv* **2015**, 018846, doi:10.1101/018846.
462. Danzeisen, R.; Achsel, T.; Bederke, U.; Cozzolino, M.; Crosio, C.; Ferri, A.; Frenzel, M.; Gralla, E.B.; Huber, L.; Ludolph, A.; et al. Superoxide dismutase 1 modulates expression of transferrin receptor. *J Biol Inorg Chem* **2006**, *11*, 489-498, doi:10.1007/s00775-006-0099-4.

463. Milczarek, A.; Starzyński, R.R.; Styś, A.; Jończy, A.; Staroń, R.; Grzelak, A.; Lipiński, P. A drastic superoxide-dependent oxidative stress is prerequisite for the down-regulation of IRP1: Insights from studies on SOD1-deficient mice and macrophages treated with paraquat. *PLoS One* **2017**, *12*, e0176800, doi:10.1371/journal.pone.0176800.
464. Jouihan, H.A.; Cobine, P.A.; Cooksey, R.C.; Hoagland, E.A.; Boudina, S.; Abel, E.D.; Winge, D.R.; McClain, D.A. Iron-mediated inhibition of mitochondrial manganese uptake mediates mitochondrial dysfunction in a mouse model of hemochromatosis. *Mol Med* **2008**, *14*, 98-108, doi:10.2119/2007-00114.Jouihan.
465. Lee, S.H.; Jouihan, H.A.; Cooksey, R.C.; Jones, D.; Kim, H.J.; Winge, D.R.; McClain, D.A. Manganese supplementation protects against diet-induced diabetes in wild type mice by enhancing insulin secretion. *Endocrinology* **2013**, *154*, 1029-1038, doi:10.1210/en.2012-1445.
466. Nikinmaa, M.; Waser, W. Molecular and cellular studies in evolutionary physiology of natural vertebrate populations: influences of individual variation and genetic components on sampling and measurements. *J Exp Biol* **2007**, *210*, 1847-1857, doi:10.1242/jeb.002717.
467. Dhar, S.K.; Xu, Y.; St Clair, D.K. Nuclear factor kappaB- and specificity protein 1-dependent p53-mediated bi-directional regulation of the human manganese superoxide dismutase gene. *J Biol Chem* **2010**, *285*, 9835-9846, doi:10.1074/jbc.M109.060715.
468. Wan, C.; Ma, X.; Shi, S.; Zhao, J.; Nie, X.; Han, J.; Xiao, J.; Wang, X.; Jiang, S.; Jiang, J. Pivotal roles of p53 transcription-dependent and -independent pathways in manganese-induced mitochondrial dysfunction and neuronal apoptosis. *Toxicol Appl Pharmacol* **2014**, *281*, 294-302, doi:10.1016/j.taap.2014.10.013.
469. Zhao, N.; Zhang, A.S.; Wortham, A.M.; Jue, S.; Knutson, M.D.; Enns, C.A. The Tumor Suppressor, P53, Decreases the Metal Transporter, ZIP14. *Nutrients* **2017**, *9*, doi:10.3390/nu9121335.
470. Casalino, E.; Calzaretti, G.; Landriscina, M.; Sblano, C.; Fabiano, A.; Landriscina, C. The Nrf2 transcription factor contributes to the induction of alpha-class GST isoenzymes in liver of acute cadmium or manganese intoxicated rats: comparison with the toxic effect on NAD(P)H:quinone reductase. *Toxicology* **2007**, *237*, 24-34, doi:10.1016/j.tox.2007.04.020.
471. Kerins, M.J.; Ooi, A. The Roles of NRF2 in Modulating Cellular Iron Homeostasis. *Antioxid Redox Signal* **2018**, *29*, 1756-1773, doi:10.1089/ars.2017.7176.
472. Dong, J.; Sulik, K.K.; Chen, S.Y. Nrf2-mediated transcriptional induction of antioxidant response in mouse embryos exposed to ethanol in vivo: implications for the prevention of fetal alcohol spectrum disorders. *Antioxid Redox Signal* **2008**, *10*, 2023-2033, doi:10.1089/ars.2007.2019.
473. Huang, B.W.; Ray, P.D.; Iwasaki, K.; Tsuji, Y. Transcriptional regulation of the human ferritin gene by coordinated regulation of Nrf2 and protein arginine methyltransferases PRMT1 and PRMT4. *Faseb j* **2013**, *27*, 3763-3774, doi:10.1096/fj.12-226043.
474. Poganik, J.R.; Long, M.J.C.; Disare, M.T.; Liu, X.; Chang, S.H.; Hla, T.; Aye, Y. Post-transcriptional regulation of Nrf2-mRNA by the mRNA-binding proteins HuR and AUF1. *Faseb j* **2019**, *33*, 14636-14652, doi:10.1096/fj.201901930R.
475. Nguyen, T.; Sherratt, P.J.; Huang, H.C.; Yang, C.S.; Pickett, C.B. Increased protein stability as a mechanism that enhances Nrf2-mediated transcriptional activation of the antioxidant response element. Degradation of Nrf2 by the 26 S proteasome. *J Biol Chem* **2003**, *278*, 4536-4541, doi:10.1074/jbc.M207293200.
476. Imhoff, B.R.; Hansen, J.M. Tert-butylhydroquinone induces mitochondrial oxidative stress causing Nrf2 activation. *Cell Biol Toxicol* **2010**, *26*, 541-551, doi:10.1007/s10565-010-9162-6.
477. Biswas, C.; Shah, N.; Muthu, M.; La, P.; Fernando, A.P.; Sengupta, S.; Yang, G.; Dennery, P.A. Nuclear heme oxygenase-1 (HO-1) modulates subcellular distribution and activation of Nrf2, impacting metabolic and anti-oxidant defenses. *J Biol Chem* **2014**, *289*, 26882-26894, doi:10.1074/jbc.M114.567685.
478. Seiwert, N.; Wecklein, S.; Demuth, P.; Hasselwander, S.; Kemper, T.A.; Schwerdtle, T.; Brunner, T.; Fahrer, J. Heme oxygenase 1 protects human colonocytes against ROS formation, oxidative DNA damage and cytotoxicity induced by heme iron, but not inorganic iron. *Cell Death Dis* **2020**, *11*, 787, doi:10.1038/s41419-020-02950-8.

479. Kwon, M.Y.; Park, E.; Lee, S.J.; Chung, S.W. Heme oxygenase-1 accelerates erastin-induced ferroptotic cell death. *Oncotarget* **2015**, *6*, 24393-24403, doi:10.18632/oncotarget.5162.
480. Costa, D.L.; Amaral, E.P.; Andrade, B.B.; Sher, A. Modulation of Inflammation and Immune Responses by Heme Oxygenase-1: Implications for Infection with Intracellular Pathogens. *Antioxidants (Basel)* **2020**, *9*, doi:10.3390/antiox9121205.
481. Meng, Q.; Xia, Y. c-Jun, at the crossroad of the signaling network. *Protein Cell* **2011**, *2*, 889-898, doi:10.1007/s13238-011-1113-3.
482. Moens, U.; Kostenko, S.; Sveinbjørnsson, B. The Role of Mitogen-Activated Protein Kinase-Activated Protein Kinases (MAPKAPKs) in Inflammation. *Genes (Basel)* **2013**, *4*, 101-133, doi:10.3390/genes4020101.
483. Faniello, M.C.; Chirico, G.; Quaresima, B.; Cuda, G.; Allevato, G.; Bevilacqua, M.A.; Baudi, F.; Colantuoni, V.; Cimino, F.; Venuta, S.; et al. An alternative model of H ferritin promoter transactivation by c-Jun. *Biochem J* **2002**, *363*, 53-58, doi:10.1042/0264-6021:3630053.
484. Lee, Y.S.; Kim, Y.H.; Jung, Y.S.; Kim, K.S.; Kim, D.K.; Na, S.Y.; Lee, J.M.; Lee, C.H.; Choi, H.S. Hepatocyte toll-like receptor 4 mediates lipopolysaccharide-induced hepcidin expression. *Exp Mol Med* **2017**, *49*, e408, doi:10.1038/emm.2017.207.
485. Biesalski, H.K.; Tinz, J. Multivitamin/mineral supplements: Rationale and safety - A systematic review. *Nutrition* **2017**, *33*, 76-82, doi:10.1016/j.nut.2016.02.013.
486. Engelken, J.; Altmeyer, M.; Franklin, R. The disruption of trace element homeostasis due to aneuploidy as a unifying theme in the etiology of cancer. *bioRxiv* **2014**, 002105, doi:10.1101/002105.
487. Wang, L.; Yin, Y.L.; Liu, X.Z.; Shen, P.; Zheng, Y.G.; Lan, X.R.; Lu, C.B.; Wang, J.Z. Current understanding of metal ions in the pathogenesis of Alzheimer's disease. *Transl Neurodegener* **2020**, *9*, 10, doi:10.1186/s40035-020-00189-z.
488. Maret, W. The redox biology of redox-inert zinc ions. *Free Radic Biol Med* **2019**, *134*, 311-326, doi:10.1016/j.freeradbiomed.2019.01.006.
489. Maret, W. Molecular aspects of human cellular zinc homeostasis: redox control of zinc potentials and zinc signals. *Biometals* **2009**, *22*, 149-157, doi:10.1007/s10534-008-9186-z.
490. Ogiso, T.; Ogawa, N.; Miura, T. Inhibitory effect of high dietary zinc on copper absorption in rats. II. Binding of copper and zinc to cytosol proteins in the intestinal mucosa. *Chem Pharm Bull (Tokyo)* **1979**, *27*, 515-521, doi:10.1248/cpb.27.515.
491. Clegg, M.S.; Hanna, L.A.; Niles, B.J.; Momma, T.Y.; Keen, C.L. Zinc deficiency-induced cell death. *IUBMB Life* **2005**, *57*, 661-669, doi:10.1080/15216540500264554.
492. Finley, J.W. Manganese uptake and release by cultured human hepato-carcinoma (Hep-G2) cells. *Biol Trace Elem Res* **1998**, *64*, 101-118.
493. Jenkitkasemwong, S.; Akinyode, A.; Paulus, E.; Weiskirchen, R.; Hojyo, S.; Fukada, T.; Giraldo, G.; Schrier, J.; Garcia, A.; Janus, C.; et al. SLC39A14 deficiency alters manganese homeostasis and excretion resulting in brain manganese accumulation and motor deficits in mice. *Proc Natl Acad Sci U S A* **2018**, *115*, E1769-e1778, doi:10.1073/pnas.1720739115.
494. Gong, W.; Liu, Y.; Qu, H.; Liu, A.; Sun, P.; Wang, X. The effect of CTCF binding sites destruction by CRISPR/Cas9 on transcription of metallothionein gene family in liver hepatocellular carcinoma. *Biochem Biophys Res Commun* **2019**, *510*, 530-538, doi:10.1016/j.bbrc.2019.01.107.
495. Bannon, D.I.; Abounader, R.; Lees, P.S.; Bressler, J.P. Effect of DMT1 knockdown on iron, cadmium, and lead uptake in Caco-2 cells. *Am J Physiol Cell Physiol* **2003**, *284*, C44-50, doi:10.1152/ajpcell.00184.2002.
496. Finke, H.; Wandt, V.K.; Ebert, F.; Guttenberger, N.; Glabonjat, R.A.; Stiboller, M.; Francesconi, K.A.; Raber, G.; Schwerdtle, T. Toxicological assessment of arsenic-containing phosphatidylcholines in HepG2 cells. *Metallomics* **2020**, *12*, 1159-1170, doi:10.1039/d0mt00073f.
497. Li, Y.; Maret, W. Transient fluctuations of intracellular zinc ions in cell proliferation. *Exp Cell Res* **2009**, *315*, 2463-2470, doi:10.1016/j.yexcr.2009.05.016.

498. Alker, W.; Haase, H. Comparison of Free Zinc Levels Determined by Fluorescent Probes in THP1 Cells Using Microplate Reader and Flow Cytometer. *Biol Trace Elem Res* **2021**, *199*, 2414-2419, doi:10.1007/s12011-020-02355-w.
499. Matsuura, K.; Canfield, K.; Feng, W.; Kurokawa, M. Metabolic Regulation of Apoptosis in Cancer. *Int Rev Cell Mol Biol* **2016**, *327*, 43-87, doi:10.1016/bs.ircmb.2016.06.006.
500. Chan, F.K.; Moriwaki, K.; De Rosa, M.J. Detection of necrosis by release of lactate dehydrogenase activity. *Methods Mol Biol* **2013**, *979*, 65-70, doi:10.1007/978-1-62703-290-2_7.
501. Ding, Y.; Wang, B.; Chen, X.; Zhou, Y.; Ge, J. Staurosporine suppresses survival of HepG2 cancer cells through Omi/HtrA2-mediated inhibition of PI3K/Akt signaling pathway. *Tumour Biol* **2017**, *39*, 1010428317694317, doi:10.1177/1010428317694317.
502. Fotakis, G.; Timbrell, J.A. In vitro cytotoxicity assays: comparison of LDH, neutral red, MTT and protein assay in hepatoma cell lines following exposure to cadmium chloride. *Toxicol Lett* **2006**, *160*, 171-177, doi:10.1016/j.toxlet.2005.07.001.
503. Smith, P.K.; Krohn, R.I.; Hermanson, G.T.; Mallia, A.K.; Gartner, F.H.; Provenzano, M.D.; Fujimoto, E.K.; Goeke, N.M.; Olson, B.J.; Klenk, D.C. Measurement of protein using bicinchoninic acid. *Anal Biochem* **1985**, *150*, 76-85, doi:10.1016/0003-2697(85)90442-7.
504. Maret, W. Analyzing free zinc(II) ion concentrations in cell biology with fluorescent chelating molecules. *Metallomics* **2015**, *7*, 202-211, doi:10.1039/c4mt00230j.
505. Tapiero, H.; Tew, K.D. Trace elements in human physiology and pathology: zinc and metallothioneins. *Biomed Pharmacother* **2003**, *57*, 399-411, doi:10.1016/s0753-3322(03)00081-7.
506. Di Bella, L.M.; Alampi, R.; Biundo, F.; Toscano, G.; Felice, M.R. Copper chelation and interleukin-6 proinflammatory cytokine effects on expression of different proteins involved in iron metabolism in HepG2 cell line. *BMC Biochem* **2017**, *18*, 1, doi:10.1186/s12858-017-0076-2.
507. Gao, J.; Zhao, N.; Knutson, M.D.; Enns, C.A. The hereditary hemochromatosis protein, HFE, inhibits iron uptake via down-regulation of Zip14 in HepG2 cells. *J Biol Chem* **2008**, *283*, 21462-21468, doi:10.1074/jbc.M803150200.
508. Bowers, K.; Srai, S.K.S. The trafficking of metal ion transporters of the Zrt- and Irt-like protein family. *Traffic* **2018**, *19*, 813-822, doi:10.1111/tra.12602.
509. Fujishiro, H.; Kambe, T. Manganese transport in mammals by zinc transporter family proteins, ZNT and ZIP. *J Pharmacol Sci* **2022**, *148*, 125-133, doi:10.1016/j.jphs.2021.10.011.
510. Howard, L.; Ashley, C.; Lyon, D.; Shenkin, A. Autopsy tissue trace elements in 8 long-term parenteral nutrition patients who received the current U.S. Food and Drug Administration formulation. *JPEN J Parenter Enteral Nutr* **2007**, *31*, 388-396, doi:10.1177/0148607107031005388.
511. Porte Alcon, S.; Gorojod, R.M.; Kotler, M.L. Regulated Necrosis Orchestrates Microglial Cell Death in Manganese-Induced Toxicity. *Neuroscience* **2018**, *393*, 206-225, doi:10.1016/j.neuroscience.2018.10.006.
512. Rodier, F.; Campisi, J. Four faces of cellular senescence. *J Cell Biol* **2011**, *192*, 547-556, doi:10.1083/jcb.201009094.
513. Nicolai, M.M.; Witt, B.; Friese, S.; Michaelis, V.; Hölz-Armstrong, L.; Martin, M.; Ebert, F.; Schwerdtle, T.; Bornhorst, J. Mechanistic studies on the adverse effects of manganese overexposure in differentiated LUHMES cells. *Food Chem Toxicol* **2022**, *161*, 112822, doi:10.1016/j.fct.2022.112822.
514. Prasad, A.S.; Bao, B. Molecular Mechanisms of Zinc as a Pro-Antioxidant Mediator: Clinical Therapeutic Implications. *Antioxidants (Basel)* **2019**, *8*, doi:10.3390/antiox8060164.
515. Zhu, L.; Huang, C.; Yang, X.; Zhang, B.; He, X.; Xu, W.; Huang, K. Proteomics reveals the alleviation of zinc towards aflatoxin B1-induced cytotoxicity in human hepatocyes (HepG2 cells). *Ecotoxicol Environ Saf* **2020**, *198*, 110596, doi:10.1016/j.ecoenv.2020.110596.
516. Liu, J.; Kershaw, W.C.; Klaassen, C.D. Protective effects of zinc on cultured rat primary hepatocytes to metals with low affinity for metallothionein. *J Toxicol Environ Health* **1992**, *35*, 51-62, doi:10.1080/15287399209531593.
517. Fujishiro, H.; Yano, Y.; Takada, Y.; Tanihara, M.; Himeno, S. Roles of ZIP8, ZIP14, and DMT1 in transport of cadmium and manganese in mouse kidney proximal tubule cells. *Metallomics* **2012**, *4*, 700-708, doi:10.1039/c2mt20024d.

518. Wolff, N.A.; Garrick, M.D.; Zhao, L.; Garrick, L.M.; Ghio, A.J.; Thévenod, F. A role for divalent metal transporter (DMT1) in mitochondrial uptake of iron and manganese. *Sci Rep* **2018**, *8*, 211, doi:10.1038/s41598-017-18584-4.
519. Martelli, A.; Moulis, J.M. Zinc and cadmium specifically interfere with RNA-binding activity of human iron regulatory protein 1. *J Inorg Biochem* **2004**, *98*, 1413-1420, doi:10.1016/j.jinorgbio.2004.04.011.
520. Jensen, L.T.; Carroll, M.C.; Hall, M.D.; Harvey, C.J.; Beese, S.E.; Culotta, V.C. Down-regulation of a manganese transporter in the face of metal toxicity. *Mol Biol Cell* **2009**, *20*, 2810-2819, doi:10.1091/mbc.e08-10-1084.
521. Herbison, C.E.; Thorstensen, K.; Chua, A.C.; Graham, R.M.; Leedman, P.; Olynyk, J.K.; Trinder, D. The role of transferrin receptor 1 and 2 in transferrin-bound iron uptake in human hepatoma cells. *Am J Physiol Cell Physiol* **2009**, *297*, C1567-1575, doi:10.1152/ajpcell.00649.2008.
522. Jarosz, M.; Olbert, M.; Wyszogrodzka, G.; Młyniec, K.; Librowski, T. Antioxidant and anti-inflammatory effects of zinc. Zinc-dependent NF-κB signaling. *Inflammopharmacology* **2017**, *25*, 11-24, doi:10.1007/s10787-017-0309-4.
523. Foligné, B.; George, F.; Standaert, A.; Garat, A.; Poiret, S.; Peucelle, V.; Ferreira, S.; Sobry, H.; Muharram, G.; Lucau-Danila, A.; et al. High-dose dietary supplementation with zinc prevents gut inflammation: Investigation of the role of metallothioneins and beyond by transcriptomic and metagenomic studies. *Faseb j* **2020**, *34*, 12615-12633, doi:10.1096/fj.202000562RR.
524. Waalkes, M.P.; Harvey, M.J.; Klaassen, C.D. Relative in vitro affinity of hepatic metallothionein for metals. *Toxicol Lett* **1984**, *20*, 33-39, doi:10.1016/0378-4274(84)90179-6.
525. Kobayashi, K.; Kuroda, J.; Shibata, N.; Hasegawa, T.; Seko, Y.; Satoh, M.; Tohyama, C.; Takano, H.; Imura, N.; Sakabe, K.; et al. Induction of metallothionein by manganese is completely dependent on interleukin-6 production. *J Pharmacol Exp Ther* **2007**, *320*, 721-727, doi:10.1124/jpet.106.112912.
526. Yosef, R.; Pilpel, N.; Papismadov, N.; Gal, H.; Ovadya, Y.; Vadai, E.; Miller, S.; Porat, Z.; Ben-Dor, S.; Krizhanovsky, V. p21 maintains senescent cell viability under persistent DNA damage response by restraining JNK and caspase signaling. *Embo j* **2017**, *36*, 2280-2295, doi:10.15252/embj.201695553.
527. Mattison, D.R.; Milton, B.; Krewski, D.; Levy, L.; Dorman, D.C.; Aggett, P.J.; Roels, H.A.; Andersen, M.E.; Karyakina, N.A.; Shilnikova, N.; et al. Severity scoring of manganese health effects for categorical regression. *Neurotoxicology* **2017**, *58*, 203-216, doi:10.1016/j.neuro.2016.09.001.
528. Martins, A.C., Jr.; Gubert, P.; Villas Boas, G.R.; Meirelles Paes, M.; Santamaría, A.; Lee, E.; Tinkov, A.A.; Bowman, A.B.; Aschner, M. Manganese-induced neurodegenerative diseases and possible therapeutic approaches. *Expert Rev Neurother* **2020**, *20*, 1109-1121, doi:10.1080/14737175.2020.1807330.
529. Rollin, H.B.; Nogueira, C.M.C.A. Manganese: Environmental Pollution and Health Effects. 2011.
530. Dlamini, W.W.; Nelson, G.; Nielsen, S.S.; Racette, B.A. Manganese exposure, parkinsonian signs, and quality of life in South African mine workers. *Am J Ind Med* **2020**, *63*, 36-43, doi:10.1002/ajim.23060.
531. Racette, B.A.; Searles Nielsen, S.; Criswell, S.R.; Sheppard, L.; Seixas, N.; Warden, M.N.; Checkoway, H. Dose-dependent progression of parkinsonism in manganese-exposed welders. *Neurology* **2017**, *88*, 344-351, doi:10.1212/wnl.0000000000003533.
532. Bjørklund, G.; Chartrand, M.S.; Aaseth, J. Manganese exposure and neurotoxic effects in children. *Environ Res* **2017**, *155*, 380-384, doi:10.1016/j.envres.2017.03.003.
533. Michalke, B.; Berthele, A.; Venkataramani, V. Simultaneous Quantification and Speciation of Trace Metals in Paired Serum and CSF Samples by Size Exclusion Chromatography-Inductively Coupled Plasma-Dynamic Reaction Cell-Mass Spectrometry (SEC-DRC-ICP-MS). *Int J Mol Sci* **2021**, *22*, doi:10.3390/ijms22168892.
534. Prohaska, J.R. Functions of trace elements in brain metabolism. *Physiol Rev* **1987**, *67*, 858-901, doi:10.1152/physrev.1987.67.3.858.

535. Morello, M.; Canini, A.; Mattioli, P.; Sorge, R.P.; Alimonti, A.; Bocca, B.; Forte, G.; Martorana, A.; Bernardi, G.; Sancesario, G. Sub-cellular localization of manganese in the basal ganglia of normal and manganese-treated rats An electron spectroscopy imaging and electron energy-loss spectroscopy study. *Neurotoxicology* **2008**, *29*, 60-72, doi:10.1016/j.neuro.2007.09.001.
536. Lin, M.; Colon-Perez, L.M.; Sambo, D.O.; Miller, D.R.; Lebowitz, J.J.; Jimenez-Rondan, F.; Cousins, R.J.; Horenstein, N.; Aydemir, T.B.; Febo, M.; et al. Mechanism of Manganese Dysregulation of Dopamine Neuronal Activity. *J Neurosci* **2020**, *40*, 5871-5891, doi:10.1523/jneurosci.2830-19.2020.
537. Sengupta, A.; Mense, S.M.; Lan, C.; Zhou, M.; Mauro, R.E.; Kellerman, L.; Bentsman, G.; Volsky, D.J.; Louis, E.D.; Graziano, J.H.; et al. Gene expression profiling of human primary astrocytes exposed to manganese chloride indicates selective effects on several functions of the cells. *Neurotoxicology* **2007**, *28*, 478-489, doi:10.1016/j.neuro.2006.10.005.
538. Giordano, G.; Pizzurro, D.; VanDeMark, K.; Guizzetti, M.; Costa, L.G. Manganese inhibits the ability of astrocytes to promote neuronal differentiation. *Toxicol Appl Pharmacol* **2009**, *240*, 226-235, doi:10.1016/j.taap.2009.06.004.
539. Roth, J.A. Correlation between the biochemical pathways altered by mutated parkinson-related genes and chronic exposure to manganese. *Neurotoxicology* **2014**, *44*, 314-325, doi:10.1016/j.neuro.2014.08.006.
540. WHO. Manganese in Drinking Water. . *WHO Guidelines for Drinking-water Quality* **2011**.
541. Dobson, A.W.; Weber, S.; Dorman, D.C.; Lash, L.K.; Erikson, K.M.; Aschner, M. Oxidative stress is induced in the rat brain following repeated inhalation exposure to manganese sulfate. *Biol Trace Elem Res* **2003**, *93*, 113-126, doi:10.1385/bter:93:1-3:113.
542. Aschner, M.; Guilarte, T.R.; Schneider, J.S.; Zheng, W. Manganese: recent advances in understanding its transport and neurotoxicity. *Toxicol Appl Pharmacol* **2007**, *221*, 131-147, doi:10.1016/j.taap.2007.03.001.
543. Zhang, S.; Zhou, Z.; Fu, J. Effect of manganese chloride exposure on liver and brain mitochondria function in rats. *Environ Res* **2003**, *93*, 149-157, doi:10.1016/s0013-9351(03)00109-9.
544. Malecki, E.A. Manganese toxicity is associated with mitochondrial dysfunction and DNA fragmentation in rat primary striatal neurons. *Brain Res Bull* **2001**, *55*, 225-228, doi:10.1016/s0361-9230(01)00456-7.
545. Galvani, P.; Fumagalli, P.; Santagostino, A. Vulnerability of mitochondrial complex I in PC12 cells exposed to manganese. *Eur J Pharmacol* **1995**, *293*, 377-383, doi:10.1016/0926-6917(95)90058-6.
546. Cooke, M.S.; Evans, M.D.; Dizdaroglu, M.; Lunec, J. Oxidative DNA damage: mechanisms, mutation, and disease. *Faseb j* **2003**, *17*, 1195-1214, doi:10.1096/fj.02-0752rev.
547. Neumann, C.; Baesler, J.; Steffen, G.; Nicolai, M.M.; Zubel, T.; Aschner, M.; Bürkle, A.; Mangerich, A.; Schwerdtle, T.; Bornhorst, J. The role of poly(ADP-ribose) polymerases in manganese exposed Caenorhabditis elegans. *J Trace Elem Med Biol* **2020**, *57*, 21-27, doi:10.1016/j.jtemb.2019.09.001.
548. Bornhorst, J.; Schwerdtle, T. Chapter 24 DNA Damage Induced by Manganese. In *Manganese in Health and Disease*; The Royal Society of Chemistry: 2015; pp. 604-620.
549. Wandt, V.K.; Winkelbeiner, N.; Bornhorst, J.; Witt, B.; Raschke, S.; Simon, L.; Ebert, F.; Kipp, A.P.; Schwerdtle, T. A matter of concern - Trace element dyshomeostasis and genomic stability in neurons. *Redox Biol* **2021**, *41*, 101877, doi:10.1016/j.redox.2021.101877.
550. Lohren, H.; Blagojevic, L.; Fitkau, R.; Ebert, F.; Schildknecht, S.; Leist, M.; Schwerdtle, T. Toxicity of organic and inorganic mercury species in differentiated human neurons and human astrocytes. *J Trace Elem Med Biol* **2015**, *32*, 200-208, doi:10.1016/j.jtemb.2015.06.008.
551. Schildknecht, S.; Pöltl, D.; Nagel, D.M.; Matt, F.; Scholz, D.; Lotharius, J.; Schmieg, N.; Salvo-Vargas, A.; Leist, M. Requirement of a dopaminergic neuronal phenotype for toxicity of low concentrations of 1-methyl-4-phenylpyridinium to human cells. *Toxicol Appl Pharmacol* **2009**, *241*, 23-35, doi:10.1016/j.taap.2009.07.027.

552. Chazotte, B. Labeling mitochondria with MitoTracker dyes. *Cold Spring Harb Protoc* **2011**, *2011*, 990-992, doi:10.1101/pdb.prot5648.
553. Perry, S.W.; Norman, J.P.; Barbieri, J.; Brown, E.B.; Gelbard, H.A. Mitochondrial membrane potential probes and the proton gradient: a practical usage guide. *Biotechniques* **2011**, *50*, 98-115, doi:10.2144/000113610.
554. Brunk, C.F.; Jones, K.C.; James, T.W. Assay for nanogram quantities of DNA in cellular homogenates. *Anal Biochem* **1979**, *92*, 497-500, doi:10.1016/0003-2697(79)90690-0.
555. Greer, E.L.; Blanco, M.A.; Gu, L.; Sendinc, E.; Liu, J.; Aristizábal-Corrales, D.; Hsu, C.H.; Aravind, L.; He, C.; Shi, Y. DNA Methylation on N6-Adenine in C. elegans. *Cell* **2015**, *161*, 868-878, doi:10.1016/j.cell.2015.04.005.
556. Finke, H.; Winkelbeiner, N.; Lossow, K.; Hertel, B.; Wandt, V.K.; Schwarz, M.; Pohl, G.; Kopp, J.F.; Ebert, F.; Kipp, A.P.; et al. Effects of a Cumulative, Suboptimal Supply of Multiple Trace Elements in Mice: Trace Element Status, Genomic Stability, Inflammation, and Epigenetics. *Mol Nutr Food Res* **2020**, *64*, e2000325, doi:10.1002/mnfr.202000325.
557. Bornhorst, J.; Ebert, F.; Hartwig, A.; Michalke, B.; Schwerdtle, T. Manganese inhibits poly(ADP-ribosyl)ation in human cells: a possible mechanism behind manganese-induced toxicity? *J Environ Monit* **2010**, *12*, 2062-2069, doi:10.1039/c0em00252f.
558. Schwerdtle, T.; Hamann, I.; Jahnke, G.; Walter, I.; Richter, C.; Parsons, J.L.; Dianov, G.L.; Hartwig, A. Impact of copper on the induction and repair of oxidative DNA damage, poly(ADP-ribosyl)ation and PARP-1 activity. *Mol Nutr Food Res* **2007**, *51*, 201-210, doi:10.1002/mnfr.200600107.
559. Hartwig, A.; Groblinghoff, U.D.; Beyersmann, D.; Natarajan, A.T.; Filon, R.; Mullenders, L.H. Interaction of arsenic(III) with nucleotide excision repair in UV-irradiated human fibroblasts. *Carcinogenesis* **1997**, *18*, 399-405, doi:10.1093/carcin/18.2.399.
560. Zubel, T.; Martello, R.; Bürkle, A.; Mangerich, A. Quantitation of Poly(ADP-Ribose) by Isotope Dilution Mass Spectrometry. *Methods Mol Biol* **2017**, *1608*, 3-18, doi:10.1007/978-1-4939-6993-7_1.
561. Martello, R.; Mangerich, A.; Sass, S.; Dedon, P.C.; Bürkle, A. Quantification of cellular poly(ADP-ribosyl)ation by stable isotope dilution mass spectrometry reveals tissue- and drug-dependent stress response dynamics. *ACS Chem Biol* **2013**, *8*, 1567-1575, doi:10.1021/cb400170b.
562. Ebert, F.; Thomann, M.; Witt, B.; Müller, S.M.; Meyer, S.; Weber, T.; Christmann, M.; Schwerdtle, T. Evaluating long-term cellular effects of the arsenic species thio-DMA(V): qPCR-based gene expression as screening tool. *J Trace Elem Med Biol* **2016**, *37*, 78-84, doi:10.1016/j.jtemb.2016.06.004.
563. Witt, B.; Ebert, F.; Meyer, S.; Francesconi, K.A.; Schwerdtle, T. Assessing neurodevelopmental effects of arsenolipids in pre-differentiated human neurons. *Mol Nutr Food Res* **2017**, *61*, doi:10.1002/mnfr.201700199.
564. Bornhorst, J.; Ebert, F.; Lohren, H.; Humpf, H.U.; Karst, U.; Schwerdtle, T. Effects of manganese and arsenic species on the level of energy related nucleotides in human cells. *Metallomics* **2012**, *4*, 297-306, doi:10.1039/c2mt00164k.
565. Witt, B.; Stiboller, M.; Raschke, S.; Friese, S.; Ebert, F.; Schwerdtle, T. Characterizing effects of excess copper levels in a human astrocytic cell line with focus on oxidative stress markers. *J Trace Elem Med Biol* **2021**, *65*, 126711, doi:10.1016/j.jtemb.2021.126711.
566. Bonke, E.; Zwicker, K.; Dröse, S. Manganese ions induce H2O2 generation at the ubiquinone binding site of mitochondrial complex II. *Arch Biochem Biophys* **2015**, *580*, 75-83, doi:10.1016/j.abb.2015.06.011.
567. Lindahl, T. Instability and decay of the primary structure of DNA. *Nature* **1993**, *362*, 709-715, doi:10.1038/362709a0.
568. Poetsch, A.R. The genomics of oxidative DNA damage, repair, and resulting mutagenesis. *Comput Struct Biotechnol J* **2020**, *18*, 207-219, doi:10.1016/j.csbj.2019.12.013.
569. Fortini, P.; Dogliotti, E. Mechanisms of dealing with DNA damage in terminally differentiated cells. *Mutat Res* **2010**, *685*, 38-44, doi:10.1016/j.mrfmmm.2009.11.003.

570. Fishel, M.L.; Vasko, M.R.; Kelley, M.R. DNA repair in neurons: so if they don't divide what's to repair? *Mutat Res* **2007**, *614*, 24-36, doi:10.1016/j.mrfmmm.2006.06.007.
571. Brooks, P.J. DNA repair in neural cells: basic science and clinical implications. *Mutat Res* **2002**, *509*, 93-108, doi:10.1016/s0027-5107(02)00222-1.
572. Lu, T.; Pan, Y.; Kao, S.Y.; Li, C.; Kohane, I.; Chan, J.; Yankner, B.A. Gene regulation and DNA damage in the ageing human brain. *Nature* **2004**, *429*, 883-891, doi:10.1038/nature02661.
573. Kino, K.; Hirao-Suzuki, M.; Morikawa, M.; Sakaga, A.; Miyazawa, H. Generation, repair and replication of guanine oxidation products. *Genes Environ* **2017**, *39*, 21, doi:10.1186/s41021-017-0081-0.
574. Valavanidis, A.; Vlachogianni, T.; Fiotakis, C. 8-hydroxy-2' -deoxyguanosine (8-OHdG): A critical biomarker of oxidative stress and carcinogenesis. *J Environ Sci Health C Environ Carcinog Ecotoxicol Rev* **2009**, *27*, 120-139, doi:10.1080/10590500902885684.
575. Di Mascio, P.; Martinez, G.R.; Miyamoto, S.; Ronsein, G.E.; Medeiros, M.H.G.; Cadet, J. Singlet Molecular Oxygen Reactions with Nucleic Acids, Lipids, and Proteins. *Chem Rev* **2019**, *119*, 2043-2086, doi:10.1021/acs.chemrev.8b00554.
576. Margolin, Y.; Cloutier, J.F.; Shafirovich, V.; Geacintov, N.E.; Dedon, P.C. Paradoxical hotspots for guanine oxidation by a chemical mediator of inflammation. *Nat Chem Biol* **2006**, *2*, 365-366, doi:10.1038/nchembio796.
577. Hegde, M.L.; Hazra, T.K.; Mitra, S. Early steps in the DNA base excision/single-strand interruption repair pathway in mammalian cells. *Cell Res* **2008**, *18*, 27-47, doi:10.1038/cr.2008.8.
578. Papaluca, A.; Wagner, J.R.; Saragovi, H.U.; Ramotar, D. UNG-1 and APN-1 are the major enzymes to efficiently repair 5-hydroxymethyluracil DNA lesions in C. elegans. *Sci Rep* **2018**, *8*, 6860, doi:10.1038/s41598-018-25124-1.
579. Elsakrmy, N.; Zhang-Akiyama, Q.M.; Ramotar, D. The Base Excision Repair Pathway in the Nematode Caenorhabditis elegans. *Front Cell Dev Biol* **2020**, *8*, 598860, doi:10.3389/fcell.2020.598860.
580. Dizdaroglu, M.; Coskun, E.; Jaruga, P. Repair of oxidatively induced DNA damage by DNA glycosylases: Mechanisms of action, substrate specificities and excision kinetics. *Mutat Res Rev Mutat Res* **2017**, *771*, 99-127, doi:10.1016/j.mrrev.2017.02.001.
581. Boiteux, S.; Guillet, M. Abasic sites in DNA: repair and biological consequences in Saccharomyces cerevisiae. *DNA Repair (Amst)* **2004**, *3*, 1-12, doi:10.1016/j.dnarep.2003.10.002.
582. Sczepanski, J.T.; Wong, R.S.; McKnight, J.N.; Bowman, G.D.; Greenberg, M.M. Rapid DNA-protein cross-linking and strand scission by an abasic site in a nucleosome core particle. *Proc Natl Acad Sci U S A* **2010**, *107*, 22475-22480, doi:10.1073/pnas.1012860108.
583. Allgayer, J.; Kitsera, N.; Bartelt, S.; Epe, B.; Khobta, A. Widespread transcriptional gene inactivation initiated by a repair intermediate of 8-oxoguanine. *Nucleic Acids Res* **2016**, *44*, 7267-7280, doi:10.1093/nar/gkw473.
584. Yang, X.; Yang, H.; Wu, F.; Qi, Z.; Li, J.; Xu, B.; Liu, W.; Xu, Z.; Deng, Y. Mn Inhibits GSH Synthesis via Downregulation of Neuronal EAAC1 and Astrocytic xCT to Cause Oxidative Damage in the Striatum of Mice. *Oxid Med Cell Longev* **2018**, *2018*, 4235695, doi:10.1155/2018/4235695.
585. Pilié, P.G.; Tang, C.; Mills, G.B.; Yap, T.A. State-of-the-art strategies for targeting the DNA damage response in cancer. *Nat Rev Clin Oncol* **2019**, *16*, 81-104, doi:10.1038/s41571-018-0114-z.
586. Smith, R.; Lebeaupin, T.; Juhász, S.; Chapuis, C.; D'Augustin, O.; Dutertre, S.; Burkovics, P.; Biertümpfel, C.; Timinszky, G.; Huet, S. Poly(ADP-ribose)-dependent chromatin unfolding facilitates the association of DNA-binding proteins with DNA at sites of damage. *Nucleic Acids Res* **2019**, *47*, 11250-11267, doi:10.1093/nar/gkz820.
587. Liu, C.; Vyas, A.; Kassab, M.A.; Singh, A.K.; Yu, X. The role of poly ADP-ribosylation in the first wave of DNA damage response. *Nucleic Acids Res* **2017**, *45*, 8129-8141, doi:10.1093/nar/gkx565.
588. Ohgushi, H.; Yoshihara, K.; Kamiya, T. Bovine thymus poly(adenosine diphosphate ribose) polymerase. Physical properties and binding to DNA. *J Biol Chem* **1980**, *255*, 6205-6211.

589. Langelier, M.F.; Planck, J.L.; Roy, S.; Pascal, J.M. Structural basis for DNA damage-dependent poly(ADP-ribosyl)ation by human PARP-1. *Science* **2012**, *336*, 728-732, doi:10.1126/science.1216338.
590. Gibbs-Seymour, I.; Fontana, P.; Rack, J.G.M.; Ahel, I. HPF1/C4orf27 Is a PARP-1-Interacting Protein that Regulates PARP-1 ADP-Ribosylation Activity. *Mol Cell* **2016**, *62*, 432-442, doi:10.1016/j.molcel.2016.03.008.
591. Kim, I.K.; Stegeman, R.A.; Brosey, C.A.; Ellenberger, T. A quantitative assay reveals ligand specificity of the DNA scaffold repair protein XRCC1 and efficient disassembly of complexes of XRCC1 and the poly(ADP-ribose) polymerase 1 by poly(ADP-ribose) glycohydrolase. *J Biol Chem* **2015**, *290*, 3775-3783, doi:10.1074/jbc.M114.624718.
592. Hazra, T.K.; Hill, J.W.; Izumi, T.; Mitra, S. Multiple DNA glycosylases for repair of 8-oxoguanine and their potential in vivo functions. *Prog Nucleic Acid Res Mol Biol* **2001**, *68*, 193-205, doi:10.1016/s0079-6603(01)68100-5.
593. Fukae, J.; Takanashi, M.; Kubo, S.; Nishioka, K.; Nakabeppu, Y.; Mori, H.; Mizuno, Y.; Hattori, N. Expression of 8-oxoguanine DNA glycosylase (OGG1) in Parkinson's disease and related neurodegenerative disorders. *Acta Neuropathol* **2005**, *109*, 256-262, doi:10.1007/s00401-004-0937-9.
594. Chu, C.T.; Plowey, E.D.; Dagda, R.K.; Hickey, R.W.; Cherra, S.J., 3rd; Clark, R.S. Autophagy in neurite injury and neurodegeneration: in vitro and in vivo models. *Methods Enzymol* **2009**, *453*, 217-249, doi:10.1016/s0076-6879(08)04011-1.
595. Machado-Salas, J.; Ibarra, O.; Martinez Fong, D.; Cornejo, A.; Aceves, J.; Kuri, J. Degenerative ultrastructural changes observed in the neuropil of caudate nuclei from Parkinson's disease patients. *Stereotact Funct Neurosurg* **1990**, *54-55*, 297-305, doi:10.1159/000100226.
596. Lach, B.; Grimes, D.; Benoit, B.; Minkiewicz-Janda, A. Caudate nucleus pathology in Parkinson's disease: ultrastructural and biochemical findings in biopsy material. *Acta Neuropathol* **1992**, *83*, 352-360, doi:10.1007/bf00713525.
597. Stanwood, G.D.; Leitch, D.B.; Savchenko, V.; Wu, J.; Fitsanakis, V.A.; Anderson, D.J.; Stankowski, J.N.; Aschner, M.; McLaughlin, B. Manganese exposure is cytotoxic and alters dopaminergic and GABAergic neurons within the basal ganglia. *J Neurochem* **2009**, *110*, 378-389, doi:10.1111/j.1471-4159.2009.06145.x.
598. Freyer, N.; Greuel, S.; Knöspel, F.; Strahl, N.; Amini, L.; Jacobs, F.; Monshouwer, M.; Zeilinger, K. Effects of Co-Culture Media on Hepatic Differentiation of hiPSC with or without HUVEC Co-Culture. *Int J Mol Sci* **2017**, *18*, doi:10.3390/ijms18081724.
599. Müller, E.K.; Gräfe, C.; Wiekhorst, F.; Bergemann, C.; Weidner, A.; Dutz, S.; Clement, J.H. Magnetic Nanoparticles Interact and Pass an In Vitro Co-Culture Blood-Placenta Barrier Model. *Nanomaterials (Basel)* **2018**, *8*, doi:10.3390/nano8020108.
600. Brugger, B.A.; Guettler, J.; Gauster, M. Go with the Flow-Trophoblasts in Flow Culture. *Int J Mol Sci* **2020**, *21*, doi:10.3390/ijms21134666.
601. Hennigar, S.R.; McClung, J.P. Homeostatic regulation of trace mineral transport by ubiquitination of membrane transporters. *Nutr Rev* **2016**, *74*, 59-67, doi:10.1093/nutrit/nuv060.
602. Liang, G.H.; Weber, C.R. Molecular aspects of tight junction barrier function. *Curr Opin Pharmacol* **2014**, *19*, 84-89, doi:10.1016/j.coph.2014.07.017.
603. Tinkov, A.A.; Martins, A.C.; Avila, D.S.; Gritsenko, V.A.; Skalny, A.V.; Santamaria, A.; Lee, E.; Bowman, A.B.; Aschner, M. Gut Microbiota as a Potential Player in Mn-Induced Neurotoxicity. *Biomolecules* **2021**, *11*, doi:10.3390/biom11091292.
604. Liévano, S.; Alarcón, L.; Chávez-Munguía, B.; González-Mariscal, L. Endothelia of term human placentae display diminished expression of tight junction proteins during preeclampsia. *Cell Tissue Res* **2006**, *324*, 433-448, doi:10.1007/s00441-005-0135-7.
605. Dalle-Donne, I.; Rossi, R.; Giustarini, D.; Milzani, A.; Colombo, R. Protein carbonyl groups as biomarkers of oxidative stress. *Clin Chim Acta* **2003**, *329*, 23-38, doi:10.1016/s0009-8981(03)00003-2.
606. Grintzalis, K.; Zisimopoulos, D.; Grune, T.; Weber, D.; Georgiou, C.D. Method for the simultaneous determination of free/protein malondialdehyde and lipid/protein hydroperoxides. *Free Radic Biol Med* **2013**, *59*, 27-35, doi:10.1016/j.freeradbiomed.2012.09.038.

607. Horii, M.; Bui, T.; Touma, O.; Cho, H.Y.; Parast, M.M. An Improved Two-Step Protocol for Trophoblast Differentiation of Human Pluripotent Stem Cells. *Curr Protoc Stem Cell Biol* **2019**, *50*, e96, doi:10.1002/cpsc.96.
608. Huang, X.; Anderle, P.; Hostettler, L.; Baumann, M.U.; Surbek, D.V.; Ontsouka, E.C.; Albrecht, C. Identification of placental nutrient transporters associated with intrauterine growth restriction and pre-eclampsia. *BMC Genomics* **2018**, *19*, 173, doi:10.1186/s12864-018-4518-z.
609. Herrmann, T.; van der Hoeven, F.; Grone, H.J.; Stewart, A.F.; Langbein, L.; Kaiser, I.; Liebisch, G.; Gosch, I.; Buchkremer, F.; Drobnik, W.; et al. Mice with targeted disruption of the fatty acid transport protein 4 (Fatp 4, Slc27a4) gene show features of lethal restrictive dermopathy. *J Cell Biol* **2003**, *161*, 1105-1115, doi:10.1083/jcb.200207080.
610. Ganguly, A.; McKnight, R.A.; Raychaudhuri, S.; Shin, B.C.; Ma, Z.; Moley, K.; Devaskar, S.U. Glucose transporter isoform-3 mutations cause early pregnancy loss and fetal growth restriction. *Am J Physiol Endocrinol Metab* **2007**, *292*, E1241-1255, doi:10.1152/ajpendo.00344.2006.
611. Vaughan, O.R.; Maksym, K.; Silva, E.; Barentsen, K.; Anthony, R.V.; Brown, T.L.; Hillman, S.L.; Spencer, R.; David, A.L.; Rosario, F.J.; et al. Placenta-specific Slc38a2/SNAT2 knockdown causes fetal growth restriction in mice. *Clin Sci (Lond)* **2021**, *135*, 2049-2066, doi:10.1042/cs20210575.
612. Chen, Y.; Ou, Q.X.; Chen, Y.; Zhu, Q.L.; Tan, M.H.; Zhang, M.M.; Wu, S.Z.; Xu, H.Y. Association between trace elements and preeclampsia: A retrospective cohort study. *J Trace Elem Med Biol* **2022**, *72*, 126971, doi:10.1016/j.jtemb.2022.126971.
613. Niedzwiecki, M.M.; Austin, C.; Remark, R.; Merad, M.; Gnjatic, S.; Estrada-Gutierrez, G.; Espejel-Nuñez, A.; Borboa-Olivares, H.; Guzman-Huerta, M.; Wright, R.J.; et al. A multimodal imaging workflow to visualize metal mixtures in the human placenta and explore colocalization with biological response markers. *Metallomics* **2016**, *8*, 444-452, doi:10.1039/c6mt00010j.
614. Michalke, B. Review about Powerful Combinations of Advanced and Hyphenated Sample Introduction Techniques with Inductively Coupled Plasma-Mass Spectrometry (ICP-MS) for Elucidating Trace Element Species in Pathologic Conditions on a Molecular Level. *Int J Mol Sci* **2022**, *23*, doi:10.3390/ijms23116109.
615. (ATSDR), A.o.T.S.a.D.R. Toxicological Profile for Mercury (Draft for Public Comment). Available online: https://wwwn.cdc.gov/TSP/ToxProfiles/ToxProfiles.aspx?id=115&tid=24#bookmark01 (accessed on 13.07.2022).
616. Dórea, J.G.; Farina, M.; Rocha, J.B. Toxicity of ethylmercury (and Thimerosal): a comparison with methylmercury. *J Appl Toxicol* **2013**, *33*, 700-711, doi:10.1002/jat.2855.
617. Barbosa, R.V.; Point, D.; Médieu, A.; Allain, V.; Gillikin, D.P.; Couturier, L.I.E.; Munaron, J.M.; Roupsard, F.; Lorrain, A. Mercury concentrations in tuna blood and muscle mirror seawater methylmercury in the Western and Central Pacific Ocean. *Mar Pollut Bull* **2022**, *180*, 113801, doi:10.1016/j.marpolbul.2022.113801.
618. Fitzgerald, W.F.; Engstrom, D.R.; Mason, R.P.; Nater, E.A. The Case for Atmospheric Mercury Contamination in Remote Areas. *Environmental Science & Technology* **1998**, *32*, 1-7, doi:10.1021/es970284w.
619. Hammerschmidt, C.R. Mercury and carbon dioxide emissions: uncoupling a toxic relationship. *Environ Toxicol Chem* **2011**, *30*, 2640-2646, doi:10.1002/etc.702.
620. Friedrich, H.K.J. Plasma mass spectrometry for the analyis of metals in single cells. Westfälische Wilhelms Universität Münster, 2022.
621. Ganapathy, S.; Farrell, E.R.; Vaghela, S.; Joshee, L.; Ford, E.G.t.; Uchakina, O.; McKallip, R.J.; Barkin, J.L.; Bridges, C.C. Transport and Toxicity of Methylmercury-Cysteine in Cultured BeWo Cells. *Int J Mol Sci* **2021**, *23*, doi:10.3390/ijms23010394.
622. Bjørklund, G.; Tinkov, A.A.; Dadar, M.; Rahman, M.M.; Chirumbolo, S.; Skalny, A.V.; Skalnaya, M.G.; Haley, B.E.; Ajsuvakova, O.P.; Aaseth, J. Insights into the Potential Role of Mercury in Alzheimer's Disease. *J Mol Neurosci* **2019**, *67*, 511-533, doi:10.1007/s12031-019-01274-3.

623. Gratz, M.J.; Stavrou, S.; Kuhn, C.; Hofmann, S.; Hermelink, K.; Heidegger, H.; Hutter, S.; Mayr, D.; Mahner, S.; Jeschke, U.; et al. Dopamine synthesis and dopamine receptor expression are disturbed in recurrent miscarriages. *Endocr Connect* **2018**, *7*, 727-738, doi:10.1530/ec-18-0126.
624. Klempan, T.; Hudon-Thibeault, A.A.; Oufkir, T.; Vaillancourt, C.; Sanderson, J.T. Stimulation of serotonergic 5-HT2A receptor signaling increases placental aromatase (CYP19) activity and expression in BeWo and JEG-3 human choriocarcinoma cells. *Placenta* **2011**, *32*, 651-656, doi:10.1016/j.placenta.2011.06.003.
625. Pan, J.; Li, X.; Wei, Y.; Ni, L.; Xu, B.; Deng, Y.; Yang, T.; Liu, W. Advances on the Influence of Methylmercury Exposure during Neurodevelopment. *Chem Res Toxicol* **2022**, *35*, 43-58, doi:10.1021/acs.chemrestox.1c00255.
626. Zhang, G.; Liu, D.; He, P. [Effects of manganese on learning abilities in school children]. *Zhonghua Yu Fang Yi Xue Za Zhi* **1995**, *29*, 156-158.
627. Velasquez, J.C.; Goeden, N.; Bonnin, A. Placental serotonin: implications for the developmental effects of SSRIs and maternal depression. *Front Cell Neurosci* **2013**, *7*, 47, doi:10.3389/fncel.2013.00047.
628. Sonier, B.; Lavigne, C.; Arseneault, M.; Ouellette, R.; Vaillancourt, C. Expression of the 5-HT2A serotoninergic receptor in human placenta and choriocarcinoma cells: mitogenic implications of serotonin. *Placenta* **2005**, *26*, 484-490, doi:10.1016/j.placenta.2004.08.003.
629. Fraser, M.; Viau, M.; Lafond, J.; Mergler, D.; Surette, C.; Vaillancourt, C. Effects of cadmium, lead and manganese on the serotonin system in human placenta. *Placenta* **2014**, *35*, A112, doi:https://doi.org/10.1016/j.placenta.2014.06.365.
630. Fogarty, N.M.; Burton, G.J.; Ferguson-Smith, A.C. Different epigenetic states define syncytiotrophoblast and cytotrophoblast nuclei in the trophoblast of the human placenta. *Placenta* **2015**, *36*, 796-802, doi:10.1016/j.placenta.2015.05.006.
631. Müller, S.M.; Finke, H.; Ebert, F.; Kopp, J.F.; Schumacher, F.; Kleuser, B.; Francesconi, K.A.; Raber, G.; Schwerdtle, T. Arsenic-containing hydrocarbons: effects on gene expression, epigenetics, and biotransformation in HepG2 cells. *Arch Toxicol* **2018**, *92*, 1751-1765, doi:10.1007/s00204-018-2194-z.
632. Costa, F.F. Non-coding RNAs, epigenetics and complexity. *Gene* **2008**, *410*, 9-17, doi:10.1016/j.gene.2007.12.008.
633. Fujimura, T.; Terachi, T.; Funaba, M.; Matsui, T. Reduction of liver manganese concentration in response to the ingestion of excess zinc: identification using metallomic analyses. *Metallomics* **2012**, *4*, 847-850, doi:10.1039/c2mt20100c.
634. Thiel, A. Metall-induzierter oxidativer Stress in Modellorganismen. University of Wuppertal, 2021.
635. Marutschke, J. Mechanismen der Mangan- und Zink-Interaktionen in humanen Zellinien. University of Wuppertal, 2021.
636. Meek, D.W. The p53 response to DNA damage. *DNA Repair (Amst)* **2004**, *3*, 1049-1056, doi:10.1016/j.dnarep.2004.03.027.
637. Kasper, S. Interaktionen von Spurenelementhomöostasen in Leberzellen. University of Wuppertal, 2022.
638. Zhao, J.; Bertoglio, B.A.; Devinney, M.J., Jr.; Dineley, K.E.; Kay, A.R. The interaction of biological and noxious transition metals with the zinc probes FluoZin-3 and Newport Green. *Anal Biochem* **2009**, *384*, 34-41, doi:10.1016/j.ab.2008.09.019.
639. Peris-Díaz, M.D.; Guran, R.; Domene, C.; de Los Rios, V.; Zitka, O.; Adam, V.; Krężel, A. An Integrated Mass Spectrometry and Molecular Dynamics Simulations Approach Reveals the Spatial Organization Impact of Metal-Binding Sites on the Stability of Metal-Depleted Metallothionein-2 Species. *J Am Chem Soc* **2021**, *143*, 16486-16501, doi:10.1021/jacs.1c05495.
640. Chen, S.H.; Chen, L.; Russell, D.H. Metal-induced conformational changes of human metallothionein-2A: a combined theoretical and experimental study of metal-free and partially metalated intermediates. *J Am Chem Soc* **2014**, *136*, 9499-9508, doi:10.1021/ja5047878.
641. Nicolai, M.M. The role of Genomic Integrity in Mn-induced Neurotoxicity Dissertation, Bergische Universität Wuppertal, 2022.

642. Michinaga, S.; Koyama, Y. Dual Roles of Astrocyte-Derived Factors in Regulation of Blood-Brain Barrier Function after Brain Damage. *Int J Mol Sci* **2019**, *20*, doi:10.3390/ijms20030571.
643. Liu, C.; Zhang, C.W.; Lo, S.Q.; Ang, S.T.; Chew, K.C.M.; Yu, D.; Chai, B.H.; Tan, B.; Tsang, F.; Tai, Y.K.; et al. S-Nitrosylation of Divalent Metal Transporter 1 Enhances Iron Uptake to Mediate Loss of Dopaminergic Neurons and Motoric Deficit. *J Neurosci* **2018**, *38*, 8364-8377, doi:10.1523/jneurosci.3262-17.2018.
644. Taylor, C.A.; Grant, S.; Jursa, T.; Aschner, M.; Smith, D.R.; Gonzales, R.; Mukhopadhyay, S. Activity of the manganese efflux transporter SLC30A10 in dopaminergic but not GABAergic neurons protects against neurotoxicity. *bioRxiv* **2022**, 2022.2002.2021.481385, doi:10.1101/2022.02.21.481385.
645. Tuschl, K.; Mills, P.B.; Clayton, P.T. Manganese and the brain. *Int Rev Neurobiol* **2013**, *110*, 277-312, doi:10.1016/b978-0-12-410502-7.00013-2.
646. Nyarko-Danquah, I.; Pajarillo, E.; Digman, A.; Soliman, K.F.A.; Aschner, M.; Lee, E. Manganese Accumulation in the Brain via Various Transporters and Its Neurotoxicity Mechanisms. *Molecules* **2020**, *25*, doi:10.3390/molecules25245880.
647. Atrian, S.; Capdevila, M. Metallothionein-protein interactions. *Biomol Concepts* **2013**, *4*, 143-160, doi:10.1515/bmc-2012-0049.
648. Michalke, B.; Aslanoglou, L.; Ochsenkühn-Petropoulou, M.; Bergström, B.; Berthele, A.; Vinceti, M.; Lucio, M.; Lidén, G. An approach for manganese biomonitoring using a manganese carrier switch in serum from transferrin to citrate at slightly elevated manganese concentration. *J Trace Elem Med Biol* **2015**, *32*, 145-154, doi:10.1016/j.jtemb.2015.07.006.
649. Park, J.S.; Koentjoro, B.; Veivers, D.; Mackay-Sim, A.; Sue, C.M. Parkinson's disease-associated human ATP13A2 (PARK9) deficiency causes zinc dyshomeostasis and mitochondrial dysfunction. *Hum Mol Genet* **2014**, *23*, 2802-2815, doi:10.1093/hmg/ddt623.
650. Kumar, A.; Singh, B.K.; Ahmad, I.; Shukla, S.; Patel, D.K.; Srivastava, G.; Kumar, V.; Pandey, H.P.; Singh, C. Involvement of NADPH oxidase and glutathione in zinc-induced dopaminergic neurodegeneration in rats: similarity with paraquat neurotoxicity. *Brain Res* **2012**, *1438*, 48-64, doi:10.1016/j.brainres.2011.12.028.
651. Sikora, J.; Ouagazzal, A.M. Synaptic Zinc: An Emerging Player in Parkinson's Disease. *Int J Mol Sci* **2021**, *22*, doi:10.3390/ijms22094724.
652. Chauhan, A.K.; Mittra, N.; Kumar, V.; Patel, D.K.; Singh, C. Inflammation and B-cell Lymphoma-2 Associated X Protein Regulate Zinc-Induced Apoptotic Degeneration of Rat Nigrostriatal Dopaminergic Neurons. *Mol Neurobiol* **2016**, *53*, 5782-5795, doi:10.1007/s12035-015-9478-6.
653. Yokel, R.A.; Crossgrove, J.S. Manganese toxicokinetics at the blood-brain barrier. *Res Rep Health Eff Inst* **2004**, 7-58; discussion 59-73.
654. O'Brien, J.; Wilson, I.; Orton, T.; Pognan, F. Investigation of the Alamar Blue (resazurin) fluorescent dye for the assessment of mammalian cell cytotoxicity. *Eur J Biochem* **2000**, *267*, 5421-5426, doi:10.1046/j.1432-1327.2000.01606.x.

Acknowledgments

Every part of this thesis would not have been possible without the help of many people who supported me during this exciting journey of my doctorate. I would therefore like to take the opportunity to thank everyone for their effort and support over the last few years.

First of all, a very special thanks goes to Julia Bornhorst my PhD supervisor for giving me the opportunity to work on a project, which was exciting new for both of us. Teil davon sein zu dürfen das Labor in Wuppertal aufzubauen und die Gruppe wachsen zu sehen war eine sehr lehrreiche, aufregende aber auch sehr lustige Zeit. Ohne dein Vertrauen, Zuspruch, gute Laune, Motivation und Begeisterungsfähigkeit wäre das alles nicht möglich gewesen. Ich bin unheimlich dankbar dafür, dass du mir dein Vertrauen und die Möglichkeit gegeben hast an diesem Thema selbstständig zu arbeiten und Kooperationspartner besuchen dürfen, um viele neue Methoden kennenzulernen. Die Teilnahme an verschiedenen Tagungen hat mir ebenfalls geholfen, weiter in der Wissenschaft zu wachsen. Ich schätze sehr, dass du jederzeit ein offenes Ohr hattest und mich jederzeit ohne Wenn und Aber unterstützt und mir zur Seite gestanden hast.

I would also like to thank Tanja Schwerdtle and the whole AKS for their support in the last years. Vielen Dank Tanja, dass ich in deinem Labor die Welt der Zellkultur kennenlernen durfte und du mich immer unterstützt hast, wenn es Probleme gab, ein neuer Abstract, Poster oder Manuskript auf deinem Tisch lag. Ohne deine Unterstützung wäre vieles in dieser Arbeit nicht möglich gewesen.

Sehr danken möchte ich auch Franziska Ebert für die Unterstützung in der Zellkultur, der Vorbereitung der qPCR und Western Blot Studien. Danke Franzy, dass du jederzeit da warst, als ich gelernt habe in der Zellkultur zu arbeiten, wenn die Heps in Wuppertal nicht so wollten oder der Western Blot eher aussah wie ein großer schwarzer Fleck. Vielen Dank auch dir Max für deine Zeit meine gefühlt tausend Proben zu messen und einzuspringen wann auch immer es nötig war.

Ich möchte mich auch bei Jessi, Nici und Viki bedanken. Vielen Dank Jessi, dass du mir in der Masterarbeit schon gezeigt hast, wie viel Spaß Wissenschaft macht und du mich während meiner Promotion immer unterstützt und gut zugeredet hast. Danke euch auch Nici und Viki, für all eure Zeit während der Zellkultureinarbeitung und den wenigen aber sehr schönen Stunden mit euch allen außerhalb des Labors.

Furthermore, I would like to thank the many collaborators, who contributed to the work presented in this thesis whether in the form of lab capacity, use of equipment, expertise or advice. A special thanks goes to Tina Buerki-Thurnherr and Leonie Aengenheister who introduced me to the wonderful world of placenta research. Ich danke euch beiden sehr für eure Unterstützung in den letzten Jahren. Vielen Dank, dass ihr mir die wichtigsten Methoden im Labor nähergebracht habt und mich mit euren Ratschlägen und Vorschlägen unterstützt habt.

Another special thanks go to Jörg Rinklebe, Claus Vandenhirtz and Kail Matuszak. Ich danke euch für eure Unterstützung als unsere ICP ausgefallen ist und eure Zeit meine Proben zu messen.

Last but not least I would dearly thank Uwe Karst and his co-workers Helena Friedrich, Catharina Erbacher, Alexander Köhrer and Matthias Elinkmann. Ich danke euch für die Möglichkeit mit der „single cell-Hg-Analytik“ ein neues spannendes Projekt zu bearbeiten und mich mit euch durch einige lange Messtage mit verstopften Nebulizern, toten Zellen, wenig Signalen, einem besseren Steini als Autosampler und Hawaiihemd-Freitagen zu arbeiten. Es hat mir unheimlich viel Spaß gemacht und danke auch dir Catharina, dass du noch immer nicht aufgegeben hast ein Hg-gebundenes Protein zu finden. Von euch kann ich noch unheimlich viel lernen und hoffe, dass ich noch mal zu Besuch kommen darf.

Before appreciating the support of many people who accompanied me through lots of ups and downs during the course of my doctorate I have to take the opportunity for a somehow strange acknowledgement. A special thanks goes to Erna our 18-year-old retired ICP-OES. Without Erna my PhD studies would not have been possible. Dank Erna habe ich unheimlich viel über ICP-OES gelernt. Dadurch, dass ständig ein Bauteil aufgeschraubt werden musste hatte ich die Chance zu lernen wie dieses Gerät aufgebaut war und welche Bauteile für was zuständig sind. Dies war eine einzigartige Möglichkeit, die ich so schnell nicht wiederbekommen werden.

Besides the effort and work that goes into this thesis, many people made the entire PhD time a lot more extraordinary, funny, and beautiful.

Someone who accompanied almost the entire course of my doctorate was Merle Nicolai. I’m so grateful to share with you so many funny and exciting memories, which were made during our time at University. Merle, wir haben während unserer Promotion mehr Zeit miteinander als mit unseren Familien und Partnern verbracht und es war eine wirklich schöne und

unheimlich lustige Zeit für die ich sehr dankbar bin. Du warst immer an meiner Seite und hast mich bei allem unterstützt und mit deiner strukturellen Herangehensweise aufgebaut, wenn es mal nicht so geklappt hat oder wir einen „Hass im Ärmel“ hatten. Auch wenn ich kurzzeitig dank dir dachte, dass ich verrückt werde (Miau!) haben die vielen Schnäpse (natürlich nur Lemikaner), plötzlichen Aufsteh-Momente, selbst gedichtete und mitgesungene Lieder und Feiertags-Labor Partys die Zeit um vieles schöner gemacht.

A huge thank you goes to all my master students who supported my PhD and who became new PhD students in this working group. Danke euch Lisa, Jan, Jana und Silja für all eure Arbeit im HepG2-Projekt und für den Spaß den wir im Labor gemeinsam hatten. Ich danke auch Ann-Kathrin Weishaupt, Alicia „Alice“ Thiel und Anna Gremme. Euer Semester war das erste, welches ich als Doktorandin im Praktikum betreut habe und nun konnte ich euch auch beim Start eurer eigenen Promotion begleiten. Ihr habt nicht nur bei der Rudel-Korrektur dieses riesige Dokument gelesen, sondern habt mich immer mal wieder von meiner Schreibtischarbeit abgelenkt, aufgebaut und motiviert und dafür bin ich sehr dankbar. Ein riesiger Dank gilt auch Laura Kubens, welche mich seit meiner Zeit in der Lebensmittelchemie begleitet hat und auch die Zeit während der Masterarbeit und Einarbeitung in Potsdam durchlebt hat. Danke dir Laura, dass du immer ein offenes Ohr für mich hast, mich immer wieder aufmunterst, aufbaust und motivierst.

A special thanks go to a variety of people on the 11th floor and former colleagues, namely Elli, Nadja, Nicole, Katharina R., Katharina M., Gürbüz, Diana, Rebecca, Nuno, Richard, and the other people of the working groups. Thank you so much for all the great moments in and out of University. Lots of fun at carnival parties, beers in pubs, Kneipentours, board game parties, and waffle dates. I appreciate being part of all this and having so many great people around me during my PhD.

I would also like to thank the AG Simon and the PTC for using their laboratories and equipment and appreciate the pleasant atmosphere and fun there. Vielen lieben Dank Martin, Franzi und Marcello für eure Hilfe bei vielen Fragen rund um RNA, Gele, Western Blot und und und. Danke, dass ich so viel Equipment mitverwenden durfte und immer willkommen war.

Ganz besonders danken möchte ich meiner besten Freundin Sammy, dafür, dass sie immer an meiner Seite war, mich in meinem gesamten Leben unterstützt hat und auch während der Promotion immer Verständnis hatte. Unsere Essens-Dates, Singstar-Abende und Quatsch-Momente haben mich von stressigen Zeiten ablenken können.

Ohne die Unterstützung von dir Dominik, wäre das alles nicht möglich gewesen. Du warst immer an meiner Seite, hast mich aufgebaut, wenn ich schlechte Tage hatte, hast mich bedingungslos unterstützt und hast meist auch meine Verzweiflungsanfälle abbekommen. Trotzdem warst du immer für mich da und hast mich dazu motiviert nicht aufzugeben.

Mein größter Dank gilt meinen Eltern und meiner Schwester Angelina. Ohne eure Unterstützung hätte ich weder überhaupt studieren können noch hätte ich die Möglichkeit gehabt den Weg zu gehen, den ich gegangen bin. Ihr habt mich schon immer bei allem Unterstützt was ich getan habe und auch bei der Promotion mir immer gut zugesprochen. Ihr wart immer an meiner Seite und seid es auch noch immer dafür bin ich unendlich dankbar.

Declaration

The presented semi-cumulative constituted doctoral thesis comprises four independent chapters. Chapters 4 and 6 are published in international peer-reviewed scientific journals, chapter 5 is submitted and in the peer-reviewing process. The published and submitted articles include suggestions from co-authors, editors, and reviewers obtained during the peer-reviewing process. Chapter 3 is based on unpublished data on the method development.

As the leading author of chapters 4 and 5, the studies were conceptualized together with my PhD supervisor Julia Bornhorst and the majority of experiments conducted in chapters 3 and 4 were carried out by myself as well as data analysis and data interpretation. Experiments in chapter 5 were realized with the help of all master's students who were supervised by Julia Bornhorst and me throughout the time of my PhD studies. All work by the co-authors was additionally highlighted in the "Author contribution" section at the end of each article chapter. As a co-author of chapter 6, I contributed with intellectual input.

Published data, methods, statements, and data interpretations provided by other researchers are indicated by the appropriate references in the respective articles, as well as in all other chapters of this thesis.

_____

Vivien Michaelis

(Doctoral candidate)